CRITICAL GAS-PHASE AND SURFACE REACTIONS INVOLVED IN THE CHEMICAL VAPOR DEPOSITION OF DIAMOND FILMS

by

COLIN ANDREW WOLDEN

M. S. Chemical Engineering Practice
Massachusetts Institute of Technology
February 1992

B. S. Chemical Engineering
The University of Minnesota
June 1990

Submitted to the Department of Chemical Engineering in Partial Fulfillment of the Requirements for the Degree of

DOCTOR OF PHILOSOPHY

in

CHEMICAL ENGINEERING

at the
Massachusetts Institute of Technology
June, 1995

© 1995 Massachusetts Institute of Technology
All rights Reserved.

Signature of Author

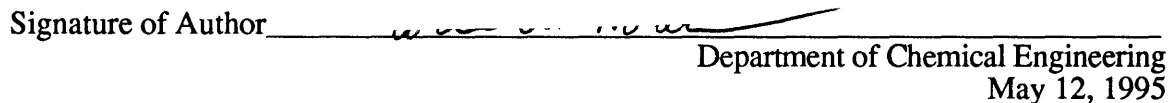

Department of Chemical Engineering
May 12, 1995

Certified by

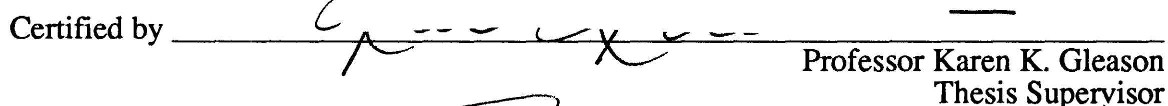

Professor Karen K. Gleason
Thesis Supervisor

Accepted by ______________________
Professor Robert E. Cohen
Graduate Committee Chairman
Department of Chemical Engineering

MASSACHUSETTS INSTITUTE

JUL 12 1995

Science

CRITICAL GAS-PHASE AND SURFACE REACTIONS INVOLVED IN THE CHEMICAL VAPOR DEPOSITION OF DIAMOND FILMS

by

COLIN ANDREW WOLDEN

Submitted to the Department of Chemical Engineering on May 12, 1995 in partial fulfillment of the requirements for the Degree of Doctor of Philosophy in Chemical Engineering

Abstract

The past five years have seen the successful commercialization of diamond films and the introduction of products as protective coatings and thermal management devices. Widespread use of these films is limited by manufacturing cost and improved quality is required to exploit diamond's potential in optoelectronics. To this end an improved understanding of the kinetics of nucleation and growth is required. A combined approach of experimentation and detailed kinetic modeling has been used to identify and quantify the critical reactions in the low pressure chemical vapor deposition of diamond films.

Although diamond a pure form of carbon, the important reactions in diamond CVD synthesis are dominated by atomic hydrogen. A three dimensional heat transfer model which included radiation and conduction was developed that successfully predicts substrate temperatures. A major finding of this work was the discovery that exothermic recombination of atomic hydrogen on the growing surface is an important mechanism of heat transfer to the substrate.

Further studies of the hot-filament system using finite element techniques showed that the atomic hydrogen distribution is controlled by heterogeneous production at the filament and recombination on the growing surface. Simulations also identified the presence of natural convection in the reactors, but the impact on film growth is negligible due to high diffusivities and the filament substrate proximity.

Analysis of gas-phase chemistry identified a set of six hydrogen abstraction and radical recombination reactions that successfully predicts the thermal hydrocarbon chemistry and identified the major pathways for methane to acetylene conversion.

A novel molecular beam was constructed which produced beams of atomic hydrogen and hydrocarbon species which could be varied independently to probe diamond surface chemistry without gas-phase scrambling. A novel microwave source produces a hydrogen discharge inside the reactor, eliminating surface recombination to provide relatively high fluxes at the reduced pressure. Growth rates attained are slow and deposited material is not high quality diamond. The surface chemistry was modeled and revealed two regimes of growth control. At normal operating pressures growth rate is limited by hydrogen abstraction reactions, however as the pressure is reduced below one torr desorption of surface methyl groups becomes rate limiting, thus causing a dramatic fall-off in growth rates. The predicted behavior has been observed in hot-filament systems and explains the results of the molecular beam reactor.

Finally, an analytical model of H atom chemistry and transport in a hot filament system is developed to analyze atomic hydrogen recombination on the surface. Maximum H concentrations and the profile near the surface are very sensitive to the value of γ, the probability of reaction between H and the diamond surface. By comparing predictions with recently measured atomic hydrogen profiles the value of γ is estimated to be ≈ 0.04. Kinetic parameters of current surface models yield much larger values (>0.2) which are in conflict with thermodynamics and energy balance considerations.

Thesis Supervisors: Dr. Karen K. Gleason, Associate Professor of Chemical Engineering
Dr. Jack B. Howard, Professor of Chemical Engineering

Acknowledgements

First, I would like to thank Professor Karen Gleason, for her innumerable and invaluable contributions to this thesis. I am very grateful for her guidance, friendship, and for being a most excellent triathalon partner. I am also grateful to the members of my committee, Professors Jack Howard, Herb Sawin, and Klavs Jensen. I would like to especially thank Profs. Howard and Sawin for many valuable discussions and the opportunity to work with their research groups. Funding for this work was provided by the National Science Foundation and the Office of Naval Research.

During this thesis I had the unique opportunity to work in three dynamic laboratories and I thank all the members of the Gleason, Sawin, and Howard research groups. Specifically, I would like to acknowledge Joe Marr and Rich Shandross for their efforts in getting me up to speed with detailed kinetic modeling. A great deal of experimental work was performed in the Sawin lab and I would like to thank Bill Conner, Gavin Zau, and Gerald Gibson for their contributions to the molecular beam reactor. I am in debt to the dynamic team of Bruce Scruggs, Dave Levy, and Karen McNamara for "breaking me in". I want to thank Mike Kwan for discussions of diamond chemistry and withstanding copious amounts of abuse. I want to acknowledge the rest of the Gleason group: Scott, Kit, Cathy, and Leslie - hopefully I haven't been too bad an influence. I also want to thank Janet Fischer, Elaine Aufiero-Peters, Kathy Brownell and Craig Abernathy for taking care of a ll the little things.

Life in Cambridge has been enjoyable thanks to a terrific group of friends. First, I thank Rick Batycky and Lloyd Johnston for heightening my awareness of Canada and hanging with me for five years despite a bad first impression. With the risk of forgetting someone, I want to thank the people I've lived with, played with, and had a hell of a lot of fun with over the last five tears: Kim Pacheco, Eric Hamby, M.J. Belanger (may I have this dance), Cathy Ford, Paul Nealey's awful backhand, Diane and her "Dekkerisms", Andrena Batycky (TMI), all my teammates from IMs (ChemE Rules), Caroline Fitzpatrick, Sam Gerritz + Ivan Lorkovic = 26.2 miles and too many beers, Bill Stockton ('MBR Rules), and Yoky Matsuoka.

Lastly, I would like to thank my parents, Chuck and Jan Wolden, whom I love very much, and who instilled my love for learning that has taken me here today.

Table of Contents

ABSTRACT.......... 2

ACKNOWLEDGEMENTS.......... 4

TABLE OF CONTENTS.......... 5

CHAPTER ONE
Important Reactions in Chemical Vapor Deposition.......... 9

CHAPTER TWO
Review of Diamond Chemical Vapor Deposition Literature.......... 15

CHAPTER THREE
Heat Transfer in Hot-filament Diamond Deposition.......... 33

CHAPTER FOUR
Mass Transport Phenomena in Diamond Reactors.......... 58

CHAPTER FIVE
Heterogeneous Reactions of Atomic Hydrogen.......... 65

CHAPTER SIX
Gas-Phase Chemistry.......... 76

CHAPTER SEVEN
Molecular Beam Reactor for the Study of Diamond Surface Chemistry.......... 86

CHAPTER EIGHT
Modeling of Surface Kinetics.......... 99

APPENDIX I
Radiative Heat Transfer Codes.......... 120

APPENDIX II
FIDAP Codes for Mass Transport and Atomic Hydrogen Production.......... 127

APPENDIX III
Molecular Beam Reactor Drawings.......... 145

APPENDIX IV
Fortran Program to Evaluate Surface Kinetics.......... 171

List of Figures

1-1 Elements of diamond chemical vapor deposition.................................. 10
1-2 Atomic C-H-O phase diagram.. 11
1-3 Gas-phase reaction in diamond growth environments............................. 12
1-4 Reactions of atomic hydrogen with the diamond surface.......................... 13
2-1 Common diamond CVD systems... 17
2-2 Hydrogen terminated 111 Surface.. 26
2-3 Mechanism for homoepitaxial growth via methyl radicals proposed by Harris.. 28
3-1 A schematic diagram of the hot-filament CVD used in experiments............... 36
3-2 A schematic of a simple filament geometry.. 38
3-3 A comparison between normalized calculated temperature profiles................ 41
3-4 Temperature profiles for a single straight filament.................................. 43
3-5 Comparison between calculated temperature contours(K) in vacuum............ 44
3-6 Comparison between calculated temperature contours(K) in hydrogen.......... 45
3-7 The dependence of calculated maximum substrate temperature on (a) filament emissivity ε_f, (b) filament temperature T_f, (c) filament diameter d_f, and (d) filament-substrate separation h_f.. 47
3-8 Comparison of calculated temperature profiles for different geometries.......... 49
3-9 Comparison of calculated temperature profiles for a novel geometry............. 51
3-10 Comparison of calculated temperature profiles for an optimized geometry....... 52
3-11 Comparison of calculated temperature profiles for (a) stationary, and (b) rotating substrates... 54
3-12 A comparison between the normalized growth profiles and normalized radiation flux profiles.. 55
4-1 Predicted streamlines for (a) a vertical reactor with gas inlet at the bottom and flowing upward, (b) a vertical reactor with inlet at the top and flowing downward, and (c) a horizontal reactor... 62
4-2 The impact of pressure and flowrate on predicted streamlines..................... 62
5-1 Cross section of the reactor that was modeled...................................... 68
5-2 Top: Temperature profiles between filament and substrate. Bottom: Atomic hydrogen profiles between filament and substrate as a function of γ............ 69
5-3 Comparison of calculated [H]fil (squares), and equilibrium values

(solid lines) as a function of filament temperature................................ 72

5-4 Arrhenius plot of atomic hydrogen REMPI signal as a function of methane concentration.. 73

6-1 Concentrations of atomic hydrogen, methyl radical, and acetylene calculated from the reduced mechanism versus the values from the complete mechanisms.. 81

6-2 Concentrations of atomic hydrogen, methyl radical, and acetylene calculated from the Harris mechanism and from the Frenklach mechanism............... 82

7-1 Diagram of molecular beam reactor... 89

7-2 Substrate temperature calibration of thermocouple using optical pyrometry..... 90

7-3 Detail of microwave discharge source... 91

7-4 Lock-in mass spectrometer signal for amu 15, 43 as a function of quartz....... temperature for 2 sccm DTBP.. 94

7-5 SEM of material deposited in molecular beam reactor............................. 95

7-6 Micro-raman spectra of material deposited in molecular beam reactor........... 95

7-7 Bachmann triangle showing region of carbon deposition in beam system....... 97

8-1 Schematic drawing of the surface species considered............................ 101

8-2 Dependence of growth rate on a.) total pressure(flux), b.) atomic hydrogen mole fraction, and c.) methyl radical mole fraction............................... 105

8-3 Plot of number of collisions between atomic hydrogen and an absorbed methyl radical during it's lifetime as a function of atomic hydrogen partial pressure.. 107

8-4 Experimental observation of falloff in growth rate with pressure................ 107

8-5 Geometry used to solve for atomic hydrogen heterogeneous reaction - nonisothermal diffusion problem.. 109

8-6 Comparison of analytical solution and power law formulation used for temperature profile.. 110

8-7 Atomic hydrogen profiles as a function of sticking probability................. 112

8-8 Filament mole fraction as a function of γ for two substrate mole fractions..... 113

8-9 Comparison of data of Childs et. al. and 3 profiles controlled by different sticking probabilities, γ.. 114

8–10 Percentage of radical sites as a function of γ assuming $k_{2f} = 2 \times 10^{13}$.......... 117

List of Tables

2-1 Hot Filament CVD Operating Parameters.. 24

3-1 Emissivity of Common Refractory Materials.. 46

3-2 Characteristic diffusion lengths for several species................................ 50

6-1 Reduced reaction mechanism: Comparison of kinetic parameters............... 80

7-1 Summary of experimental conditons used in molecular beam reactor........... 93

8-1 Surface reaction mechanism, all reactions reversible.............................. 102

8-2 Summary of H atom and methyl radical concentration measurements. 103

8-3 Surface species fractions calculated for the base case conditions................ 104

8-4 A comparison of kinetics by evaluating γ, associated heat flux (Q/A), equivalent blackbody substrate temperature T_B, and the number of H atoms required per carbon atom incorporated................................ 116

CHAPTER ONE

IMPORTANT REACTIONS IN DIAMOND CHEMICAL VAPOR DEPOSITION

Diamond has always been a prized material due to its unsurpassed beauty and strength. In addition, diamond has high thermal conductivity, is optically transparent over a large range of wavelengths (300-2500 nm), and possesses a wide band gap(5.5 eV). The combination of intrinsic properties of diamond and the ability deposit it in the form of a film has created a unique engineering material unsurpassed for many applications. Films may be deposited from a wide array of chemical vapor deposition (CVD) techniques [1], which are considered in more detail in the next chapter. Regardless of method, the 4 basic elements shown in Figure 1-1 are central to all systems.

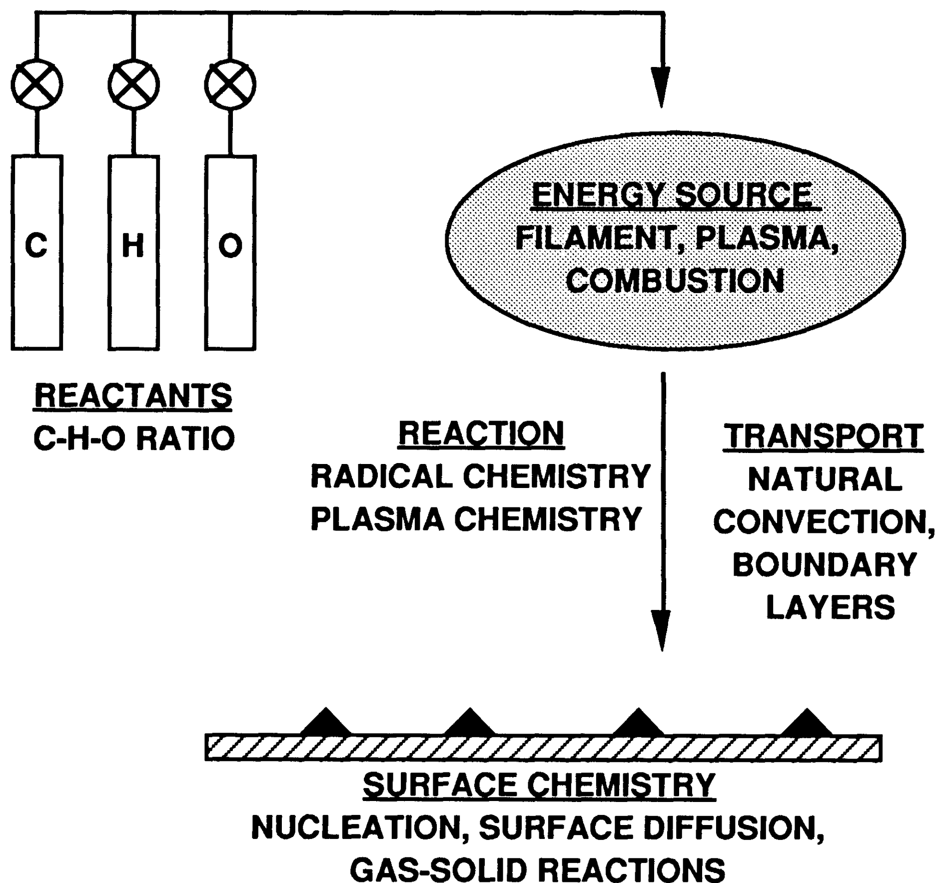

Figure 1-1: Essential elements involved in the chemical vapor deposition of diamond films.

First, the reactant composition that has been used successfully to deposit diamond falls into a narrow range. Bachmann et al. [2] examined the results of over 100 experiments in a variety of systems and plotted the composition of starting reactants on a ternary C-H-O atomic phase diagram which is reproduced as Figure 1-2. The C/H/O

combinations that successfully produced diamond films all fall into the banded region centered on the equimolar CO line. Above the band only amorphous and graphitic carbon has been formed, and below is a region of no growth. The boundary on the between high quality growth and no growth is very sharp [3]. In contrast, the border on the carbon-rich side is more ambiguous, depending on one's definition the definition of quality. Generally, as the carbon fraction increases quality declines and growth rates increase. The presence of noble gases such as argon or helium have not been shown to affect the C-H-O phase diagram [2].

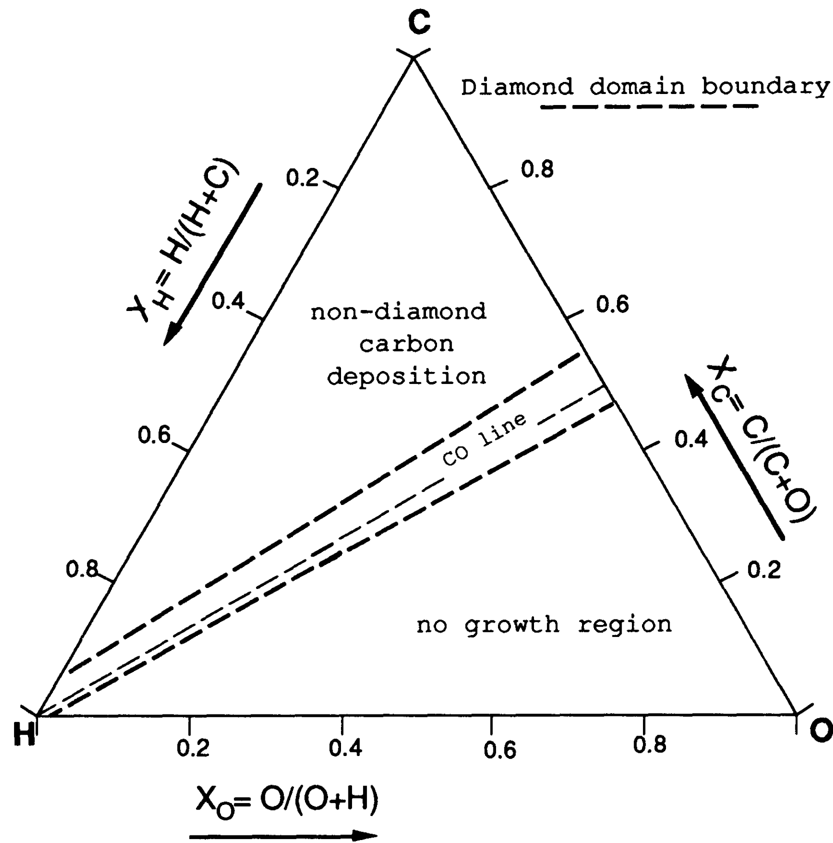

Figure 1-2: Atomic C-H-O phase diagram indicating regions of non-diamond deposition, diamond deposition, and no growth. From Bachmann et al. [2].

Second, an energy source is required to dissociate hydrogen and the hydrocarbon reactant. Energy may be supplied thermally (hot filament, combustion) or electrically (DC, rf, and microwave plasmas). The growth rate generally correlates with power density,

presumably due to an increase in atomic hydrogen production. Hydrogen atom supersaturation is a prerequisite for diamond growth [4-6]. Postulated roles include termination of surface carbons to maintain sp^3 hybridization, abstraction of surface hydrogen to create surface sites for carbon addition, and preferential etching of graphitic and sp^2 carbon [7]. The relative effectiveness of competing technologies is in part controlled by their efficiency in producing atomic hydrogen.

After activation, species undergo reactantion and transport to the growing sutrface. The gas-phase chemistry is dominated by rapid hydrogen abstraction reactions which govern the distribution of hydrocarbon fragments. The decomposition of methane, the most common carbon containing reactant, is shown in Figure 1-3. Since typical mixtures are >99% hydrogen, the H abstraction reactions are typically much faster than bimolecular reactions between 2 carbon containing species.

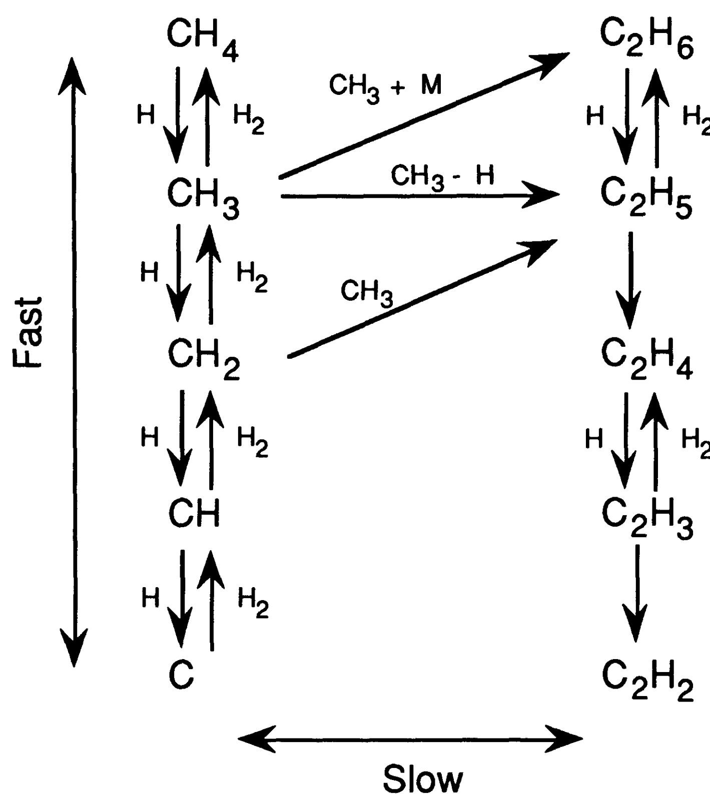

Figure 1-3: Gas-phase reaction in diamond growth environments.

These reactions are generally well-known due to research in the field of combustion [8]. In addition to thermal chemistry, electron impact dissociation reactions significantly

impact the gas-phase composition in plasma systems [9], although they are not considered in detail in this thesis. In low pressure systems transport is typically diffusion-controlled (Pe# < 10-3), although steep temperature gradients make natural convection a concern. In combustion and plasma jet synthesis convective transport is fast, but the critical step is diffusion through the finite boundary layer above the substrate.

The final component is surface reactions. First, it is important to note that although gas-phase temperatures can range from 1000 to > 5000 K, the substrate temperature must be maintained between 1000-1400 K [2]. Many mechanisms have been proposed for diamond growth [6,10-16]. The first two reactions in all of these mechanisms is the hydrogen abstraction to create a radical site followed by addition of another hydrogen atom to re-terminate the site as shown in Fig. 1-4.

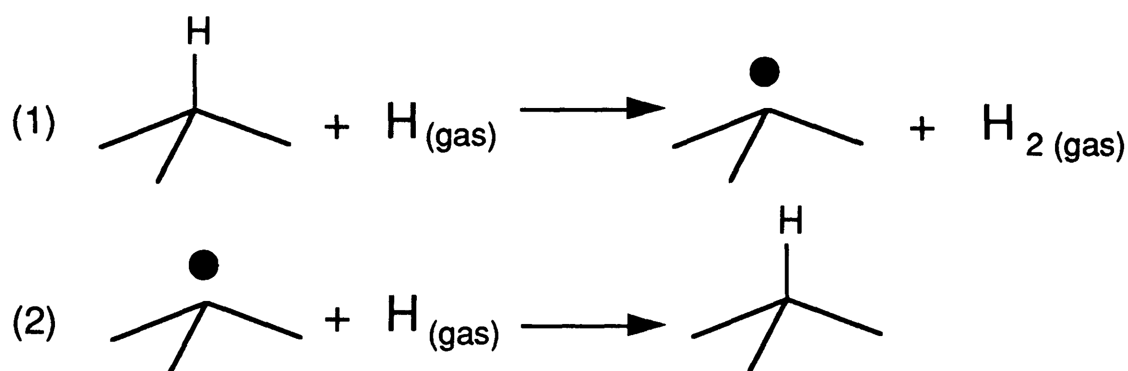

Figure 1-4: H abstraction and addition reactions with hydrogen terminated surface sites

These two reactions are expected to be the fastest gas-surface reaction, and the ratio of the two control the availability of surface radical sites for carbon addition [6]. The rates of surface reactions have been estimated using analogous gas-phase reactions [10] and monte-carlo simulations [15], but there is little direct experimental evidence [16].

The past five years have seen the successful commercialization of diamond films and the introduction of products as protective coatings and thermal management devices. Widespread use of these films is limited by manufacturing cost[17], and improved quality is required to exploit diamond's potential in optoelectronics. To this end an improved understanding of the kinetics of nucleation and growth is required. A combined approach of experimentation and detailed kinetic modeling has been used to identify and quantify the critical reactions in the low pressure chemical vapor deposition of diamond film.

The conclusion of this thesis is that diamond CVD is controlled by the reactions of atomic hydrogen. Analyzing the heat transfer in hot-filament reactors revealed that the reactions shown in Fig. 1-4 contribute significantly to substrate heating. Upon this discovery we developed a finite element reactor model and comparing simulations with experimental concentration measurements we were able to quantify atomic production and destruction in hot- filament reactors. A detailed analysis of gas-phase chemistry and sensitivity analysis revealed that the important aspects are controlled by hydrogen abstractions reactions as depicted in Fig. 1-3. A novel molecular beam reactor was developed to investigate the surface kinetics of diamond deposition where the flux of atomic hydrogen, flux of carbon precursors, and substrate temperature are controlled independently. A surface kinetic model was used to analyze experimental results and identify rate limiting steps. Proposed kinetic parameter are assessed and compared with measured concentration profiles.

REFERENCES

1. P. K. Bachmann and W. Van Enckevort, Diamond and Related Mater. **1**, 1021 (1992).
2. P. K. Bachmann, D. Leers and H. Lydtin, Diamond and Related Mater. **1**, 1 (1991).
3. G. Balestrino, M. Marinelli, E. Milani, A. Paoletti, I. Pinter, A. Tebano, P. Paroli, Appl. Phys Lett. **62**, 879 (1993).
4. J. C. Angus and C. C. Hayman, Science **241**, 913 (1988).
5. W. A. Yarbourgh and R. Messier, Science **247**, 688, (1990).
6. J. E. Butler and R. L. Woodin, Phil. Trans. R. Soc. Lond. **342**, 209, (1993).
7. M. Frenklach, J. Appl. Phys. **65**, 5142 (1989).
8. J. Warnatz, in *Combustion Chemistry*, ed. W. C. Gardiner Jr. , p.197, (Springer-Verlag, New York, 1984).
9. C. R. Koemtzopoulus, R. Pollard, and D. J. Economou, Diamond and Related Mater. **2**, 25 (1993).
10. S. J. Harris, Appl. Phys. Lett. **56**, 2298, (1990).
11. M. Frenklach and H. Wang, Phys. Rev. B **43**, 1520, (1991).
12. S. J. Harris and D. G. Goodwin, J. Phys. Chem. **97**, 23 (1993).
13. B. J. Garrison, E.J. Dawnkaski, D. Srivastava, and D. W. Brenner, Science **255**, 835, (1992).
14. M. E. Coltrin and D. S. Dandy, J. Appl. Phys. **74**, 5803, (1993).
15. S. Skokov, B. Weiner, and M. Frenklach, J. Phys. Chem. **98**, 7073 (1994).
16. L. N. Krasnoperov, I. J. Kalinovski, H-N. Chu, and D. Gutman, J. Phys. Chem. **97**, 11787, (1993).
17. J. V. Busch and J. P. Dismukes, Diamond and Related Mater. **3**, 295, (1994).

CHAPTER TWO

REVIEW OF DIAMOND CHEMICAL VAPOR DEPOSITION LITERATURE

INTRODUCTION

The mechanical properties of natural and man-made diamonds, such as hardness, strength, and corrosion resistance, have long been exploited in technological applications. In addition, diamond has high thermal conductivity, is optically transparent over a large range of wavelengths (300-2500 nm), and possesses a wide band gap(5.5 eV). The synthesis of diamond in film form by chemical vapor deposition (CVD) in the past decade has inspired numerous potential applications. Products featuring CVD diamonds are now commercially available, the most common being protective coatings [1] and thermal management devices [2]. Currently groups are attempting to harness diamond's potential in optics [3] and as a semiconductor [4].

HISTORY

Eversole first grew diamonds from the thermal decomposition of carbon monoxide in 1952, predating the development of high pressure high temperature synthesis by General Electric in 1955 [5]. Research in low pressure diamond continued through the 60's led by a group in the Soviet Union [6] and Angus in the United States [7]. However, skepticism greeted these early reports, mostly due to the relative stability of graphite and the relatively low growth rates (<0.01 μ/hr). The present interest in diamond films was stimulated in the early 80's by the discovery of Setaka and coworkers that quality diamond could be produced at reasonable growth rates (≈ 1 μm/hr) in the presence of excess hydrogen [8].

DEPOSITION SYSTEMS

Diamond CVD is synthesized in a wide variety of systems including hot - filament [8], microwave [9], DC arc jets [10], and oxy-acetylene torches [11]. The simplest system for diamond production is the hot-filament reactor shown in Figure 2-1a. A mixture of hydrogen and hydrocarbon are passed over a filament heated to ~2500 K and diamond is deposited on a substrate which is held between 3 and 15 mm away from the filament. Advantages of hot-filament CVD are its simplicity and its ability to be scaled to coat non-planar geometries. Most published experimental measurements of gas-phase concentrations have been measured in hot-filament reactors, providing an excellent comparison for models of nucleation and film growth.

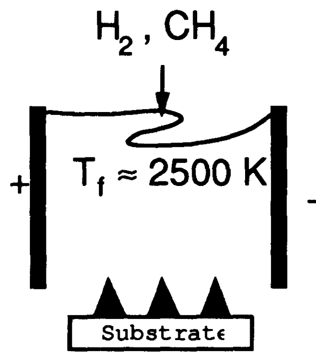

a.) Hot -Filament

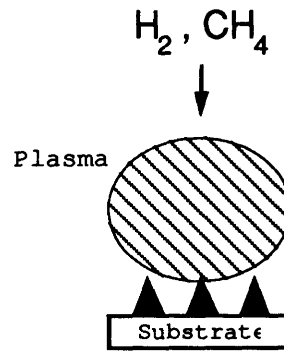

b.) Microwave Plasma

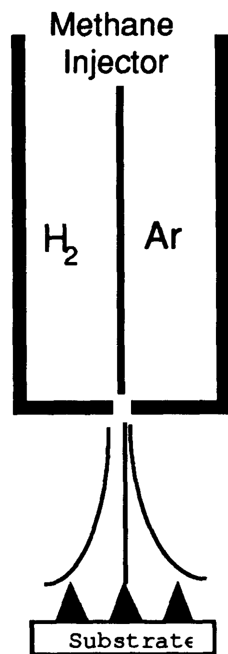

c.) DC Arc Jet

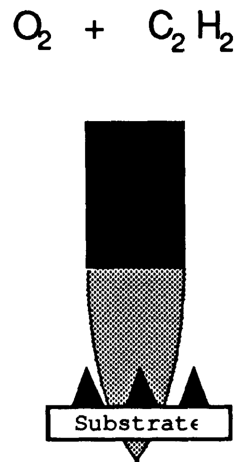

d.) Combustion Torch

Figure 2-1: Common diamond CVD systems.

In addition, by introducing boron trioxide (B_2O_3) and diphosphorous pentaoxide (P_2O_5) as doping sources, a hot-filament system was used recently to fabricate the first p-n junction diode from diamond films [12,13]. Drawbacks of the hot-filament systems have been lack of uniformity and the incorporation of filament material in the films.

Hot - filament systems are generally operated in the hydrogen rich sector of the C-H-O phase diagram (Fig. 1-3). In the absence of oxygen, diamond formation is limited to carbon contents < 3%. As oxygen is added to the system , the position on the phase diagram is shifted to the right and higher carbon concentrations may be used. A variety of carbon - containing have been used in hot-filament systems, including methane (CH_4), acetylene (C_2H_2), acetone (CH_3OCH_3), methanol (CH_3OH), ethanol (CH_3CH_2OH), diethyl ether ($C_2H_5OC_2H_5$) and trimethylamine ($(CH_3)_3N$) [14] Observed growth rates(~1 µm/hr) are generally independent of the carbon source, although slightly higher rates were attained with oxygen containing compounds [14] The same result was found by simply adding oxygen to a hydrogen/methane system [15]. These results have led to the proposal of a universal growth species, most notably methyl radical [16,17] and acetylene [18,19].

Microwave plasma has also been used extensively in CVD diamond synthesis [20]. Reactants used have spanned the diamond deposition region of phase diagram (Fig. 1-3). In this system a microwave source is used to produce up to 25% atomic hydrogen (Fig. 2-1b). A magnetic field is used as a wave guide to prevent the plasma from interacting with the reactor walls. Advantages of microwave CVD reactors are the absence of electrodes and relatively high growth rates (~10 µm/hr). Similar systems use capacitively coupled rf sources to generate the plasma, but these plasmas are less stable than those generated by microwave sources. In addition, operating at lower pressure (≈500 mTorr) the growth rates are extremely slow and the quality suffers due damage caused by ions accelerated across the sheath [21].

Growth rates of up to 900 µm/hr have been achieved in atmospheric arc jets CVD [22,23]. A typical system is shown in Fig. 2-1c. The plasma may be generated by a applying a DC voltage as depicted in Fig. 2-1c, or by inductively coupled rf energy supplied by coils wrapped around the exterior of the reactor chamber [24,25]. Reactants used are found in the hydrogen-rich section of the phase diagram (Fig. 1-3). Although this system yields the highest growth rates, the resulting films are highly nonuniform and incorporation of metal impurities from the electrodes are as high as 5% [23]. The inductively coupled rf plasmas do not suffer this drawback. High plasma temperatures (3000 to >5000 K) generated require an intricate substrate cooling system to maintain substrate temperature uniformity and reproducibility.

Combustion systems are typically operated near the equimolar conditions found in an acetylene torch ($R = C_2H_2/O_2 = 1$). It has been found that the substrate must be held in the hydrocarbon feather away from the flame front as shown in Fig. 2-1d for optimal

diamond growth [26]. Flame temperatures are ~3000-3400 K and growth rates up to 200 μm/hr have been achieved. Optimum results are attained with slightly fuel rich conditions(R = 1.1)[27], and the addition of hydrogen has been found to improve the quality of the films[26]. As with DC arc jets, it is difficult to deposit uniform, graphite-free films over large areas with this technique [27].

DIAMOND GROWTH - EXPERIMENTAL

There has been a substantial volume of experimental work in diamond synthesis. In subsequent paragraphs, the results of experiments performed in a variety of systems and operating conditions are summarized, in order to provide insight into the mechanism of diamond formation. Major areas of experimental work has focused on temperature dependence, gas-phase precursors, gas-phase concentration measurements, and nucleation.

Diamond has been deposited on substrates ranging from insulators to metals to semiconductors. The main requirement is mechanical and chemical stability at the temperatures involved. While diamond has been deposited at temperatures as low as 500 K [28], the rates were too slow to be practical. The temperature requirements may limit the practical applicability of diamond. In a hot-filament systems, apparent activation energies between 10 and 23 kcal/mol have been reported for substrate temperatures of 600-900° C [29, 30]. Similar values have been reported for combustion synthesis as well [31]. The activation energy decreases strongly to as low as 1 kcal/mol at substrate temperatures less than 700° C [28, 30]. Above 930°C growth rates and quality deteriorate in hot-filament systems [28]. In combustion and plasma jet synthesis, substrate temperatures are typically a few hundred degrees hotter, 1000-1300°C [30, 25]. The difference has been explained by the higher concentration of H atoms in the last 2 systems [32].

Methyl Radical v. Acetylene

There has been extensive debate over the identity of the most primary growth species, methyl radical or acetylene. Methyl radical and acetylene have been the focus of attention because along with methane they are the most abundant species measured in hot-filament systems [33-36]. In fact, upper-bound, diffusion limited calculations indicate that these are the only species in high enough concentrations to account for observed growth rates [37]. Due to its chemical stability it is doubtful that methane is significantly

incorporated in diamond films.

Experiments in hot-filament reactors using oxygen, which extends the region of diamond deposition, provided the first insight into this question. The addition of oxygen was found to correspond to a significant decrease in acetylene concentration, but only a slight decrease in methane (and indirectly, methyl radical) [38,39]. Further experiments have provided additional support for the importance of the methyl radical. In their hot-filament experiments, Chu et al. [40,41] used different mixtures of isotopically enriched acetylene and methane. The ^{13}C content of the films grown on diamond (100), (111), and (110) faces were determined by the shift in the first-order Raman frequency. The ^{13}C mole fractions of acetylene, methane and methyl radical (derived indirectly from the fractions of $H^{13}C^{13}CH$ and $H^{13}C^{12}CH$ using an assumption of partial equilibrium) were determined using matrix isolation IR spectroscopy. A comparison of all three films showed that the content in the films agreed with the value for the methyl radical, but differed significantly for both methane and acetylene.

Martin and Hill [42,43] alternately injected acetylene and methane into a flow of partially dissociated hydrogen created by a microwave source. They measured growth rates of 0.3 and 0.04 μm/hr for methane and acetylene, respectively, and the quality of the films was better in the case of methane injection. Additional kinetic analysis showed that only CH_3 or CH_4 could account for the observed growth in the first case, and only C_2H_2 in the second [44]. Therefore, both species could be diamond growth species, although CH_3 is an order of magnitude more effective. Frenklach has proposed that benzene and polyaromatic hydrocarbons(PAH) could inhibit diamond growth [45]. However, in additional experiments in which methane and varying amounts of benzene were injected into the flowtube showed that benzene did not effect either the growth rate or the quality of the films [46]. Furthermore, no species larger than C_{10} (probably naphthalene) has been detected in hot - filament systems, and the mole fractions of species $>C_4$ are all $<10^{-6}$ [47]. Lastly, Chen's group [48] grew diamond from supersonic beams of atomic hydrogen and methyl radical. Similar experiments with acetylene showed no growth. Additional support for a C1 precursor species comes from microwave systems where it has been observed that diamond growth is optimized when the CH emission (431 nm) is maximized and the C2 swan bands (505-515 nm) are minimized [49].

Other Precursors

Methyl radical appears to be the most important growth species in hot-filament and microwave systems, but it can not adequately explain growth rates greater than 200 μm/hr observed in high temperature DC plasmas [22] and acetylene torches [26]. Goodwin has attempted to explain growth rates of less than 100 μm/hr through simulations based on methyl as the growth species [50] The limitations of his modeling efforts are discussed in a later section.

First, in flame systems, detailed kinetic calculations indicate that CO, C_2H_2, CO_2, CH_3, and CH_4 are prominent in flames [51]. Matsui et al. [11] showed that the C_2 concentrations measured by laser-induced fluorescence (LIF), was in good agreement with growth rates for various positions in the flame. In addition, for a range of equivalence ratios ($1<R<1.2$), the normalized concentrations of C_2, CH and C_2H_2 were in agreement with calculated equilibrium values in the feather of the flame, while C_2 and CH were in good agreement with measured growth profiles but acetylene was not [11]. Additional LIF measurements by a Stanford group has confirmed that C_2 and C_2H profiles agreed qualitatively with the annular diamond deposition in their system [27].

The high concentration of CO in flames makes it worthy for consideration as a growth species. In addition, diamond films have been grown in microwave systems from CO/H_2 mixtures with CO fractions as high as 70% [52,53] At these conditions the concentrations of C_xH_y is insufficient to account for diamond growth. Raman spectra of films grown in a hot-filament system from acetone isotopically enriched at either the methyl or carbonyl carbon showed that both carbons were equally incorporated into the film, but this could be explained by heterogeneous exchange reactions with the tantalum filament [54]. In subsequent experiments with rhenium filaments, in which heterogeneous exchange does not occur, the amount of ^{13}C in the films grown from acetone enriched at the methyl site agreed with the gas -phase isotopic composition, but the shift in the raman spectra was five times less for films enriched at the carbonyl site [55]. Therefore CO may be incorporated into films, but at a significantly slower rate than hydrocarbon precursors.

In DC plasmas the gas reaches temperatures in excess of 5000 K as measured by emission spectroscopy [56]. Equilibrium calculations indicate that C, CH, C_2, C_2H and C_3 are the most abundant in DC arc jets [57]. The mole fraction of methyl radical is less than 10^{-7}. The strongest lines observed in optical emission spectra a typical plasma were

C_2 and CH [23]. Under these conditions more than 90% of the hydrogen will be disassociated. Kinetic calculations show that the composition is very dependent on the fraction dissociated [58]. The importance of atomic hydrogen and oxygen are addressed in the next section.

The majority of debate has focused on the idea of determining the diamond growth precursor. Alternatively, I will investigate the possibility that multiple C_xH_y species might act as a growth species through a four step process: (1) hydrogen or hydroxide abstraction creates a surface site; (2) a carbon - containing species adsorbs, (3) neighboring surface sites are created by additional abstractions, and (4) the adsorbed species incorporates into the diamond lattice. Of course each species would have different rates of adsorption and incorporation, which is manifested in the inability to grow a single crystal film. Anderson found for clean and hydrogen terminated surface that the adsorption energies are in order $C_2H > CH \approx CH_2 > CH_3$ [59]. There is no reason to doubt that a species and/or atomic carbon, and not methyl radical, is the dominant growth species in flames and DC arc jets. The role of atomic hydrogen may be more important than the concentration of a particular hydrocarbon. In fact, there is experimental evidence that growth proceeds through the conversion of amorphous carbon to diamond, and not through a homoepitaxial addition from the gas-phase. Work performed at Stanford [60,61], diamond was deposited from sequential exposures to sputtered carbon and atomic hydrogen. In the first step amorphous carbon is deposited, in the next a monolayer is converted to diamond while the rest is etched away. The results suggest that no particular hydrocarbon is required, any carbon containing species that absorbs will work

Impact of Hydrogen, Oxygen, and Noble Gases

Hydrogen is also incorporated into the diamond films themselves. It has been found that hydrogen incorporation increases at lower substrate temperatures [62] and at higher growth rates [63]. Hydrogen incorporation correlates to optical absorption in the IR region [63], which is detrimental for optical applications. Multiple quantum NMR experiments have shown that the majority of the hydrogen is located at grain boundaries [64].

It has been observed that the presence of small amounts of oxygen has increased the growth rates and expanded the regime of diamond deposition in both hot - filament [15,39] and microwave assisted [65,66] CVD reactors. Harris [39] proposed that the two

important effects of oxygen addition were the reduction of graphite-forming precursors and etching of non-diamond carbon by oxygen containing species. Calculations and measurements indicate that large amounts of methane and acetylene are converted to carbon monoxide. The O_2 and OH removal rates for non-diamond carbon can be estimated relatively well [67,68] while oxygen plasmas selectively etch sp and sp2 carbon [69]. Harris estimated an OH etching rate of 0.25 μm/h for pyrolytic carbon, which would significantly improve the quality of films. Two separate LIF measurements of flames have shown that the concentration profiles of OH are consistent with the annular deposition profile of diamond in their systems[11,27]. It is known that the H atom and OH radical have similar profiles in combustion systems [68]. Therefore, it is concluded that OH plays a role similar to hydrogen. Oxygen chemisorbs on the diamond surface in a range of states [70]. Being bound more strongly than hydrogen [71], oxygen may be incorporated in the diamond film creating a defects [72]. Indeed, repeated exposure of atomic oxygen have been shown to poison diamond film growth [73]. So although a small additions (< 0.25%) of oxygen seem to be beneficial [74], additional amounts are not.

The addition of argon also improves the growth rate of diamond films [75]. It is doubtful that the noble gas itself plays a role. Rather, the presence of argon increases the dissociated fraction of hydrogen [76], which is consistent with the postulate that atomic hydrogen is a limiting reagent in for diamond formation.

MODELING OF DIAMOND REACTORS

The two major limitations of all efforts are the omission of heterogenous chemistry and insufficient treatment of the fluid dynamics. To date, the majority of detailed modeling has been applied to hot-filament systems. The hot -filament reactor from our laboratory is shown schematically in Fig. 2-1a. Table 2-1 lists typical operating conditions and relevant physical parameters for two different operating pressures. The small values of the Peclet numbers indicate that mass and heat transfer are dominated by diffusion and conduction, respectively. High diffusivities (≈ 1000 cm^2/s) suggest that the reactor may be modeled as a perfectly-stirred reactor(PSR), however, the substrate/filament proximity imposes large thermal gradients(1000 K/cm), which strongly influence the kinetic parameters. In fact, large radial variations in film deposition rate and morphology are observed in hot-filament reactors. The value of the Rayleigh number indicates that natural convection will play an important role in this system. Thermal (Soret) diffusion is also important due to the high

TABLE 2-1: Hot Filament CVD Operating Parameters.

	P= 20 torr	P = 300 torr
Filament Temperature	2600 K	2600 K
Filament/Substrate Distance	1 cm	1 cm
Flow Rate (1% CH_4, H_2)	100 sccm	100 sccm
Inlet Velocity (U_∞)	0.3 cm/s	0.02 cm/s
Diffusivity (H_2)	2500 cm^2/s	150 cm^2/s
Reynolds # (Re)	~ $3x10^{-3}$	~$3x10^{-3}$
Thermal Peclet # (Pe_H)	~ $3x10^{-3}$	~$3x10^{-3}$
Mass Peclet # (Pe_M)	~ $1x10^{-3}$	~$1x10^{-3}$
Thermal Rayleigh # (Ra_H)	~5	~1000
Mass Rayleigh # (Ra_M)	~1	~100

temperature gradients.

The longest sustained modeling effort is by Harris and co-workers [77-79, 33,34,39]. Their original gas-phase mechanism considered 25 methane pyrolysis reactions that includes all the important reactions for C_1 and C_2 species[77]. The mechanism was extended to include 67 additional reactions for an oxidizing environment [39], with most of the kinetic parameters drawn from the combustion literature[80]. Harris models his system as a PSR [33] that evolves at near the filament temperature(2000 K) for a prescribed residence time, τ_{res}= 0.2 s, followed by a 1-dimensional plug flow reactor(PFR) to the substrate surface[34]. A major assumption in this work is that thermal diffusion depletes the hot filament zone of half of the hydrocarbons [39]. Harris handles this by simply entering only half of true concentration of hydrocarbon [34,39]. As a result, he finds that the model predicts the measured concentrations. Actually, the value of τ_{res} and the choice of T= 2000 K are fitting parameters. Residence times of ≈ 0.2 s are unreasonable considering the high diffusion velocities of the system (>100 cm/s). By integrating his equations one finds that the mole fractions are almost invariant after the PSR section of the model. In effect all the reactions occur in the PSR, are then quenched, and transported to the filament surface. Most recently, Harris has combined his surface mechanism [17] with another empirical parameter, α, to account for growth rate variations with pressure [78].

Frenklach [81] has developed an extensive model which includes 50 species and 158 reactions in the gas-phase, and 15 different surface sites and 52 surface reactions. The surface mechanism has pathways for both diamond and graphitic carbon deposition. The

gas-phase mechanism is similar to that offered by Harris, but his has been extended to include species as large as naphthalene($C_{10}H_8$). In modeling the gas-phase chemistry Frenklach used a 1-D PFR model. He used the measured temperature profile of Harris, fixing the temperature at 2600 K for the length of the filament. He then used the diameter of the filament as a fitting parameter. The best fit was found for a diameter of 1.5 cm, quite unreasonable when most filaments are ≈1 mm. As in Harris's model, the reactions are effectively quenched after the filament and transported to the substrate. Both of the authors ignore the presence of the substrate and its effect on the flow fields and gas-phase chemistry.

Goodwin and Gavillet[37] attempted to extend modeling efforts to three dimensions, using the model developed by Coltrin et al.[82] for a rotating disk silicon CVD reactor. For an infinite radius rotating disk, a similarity transformation may be used to convert the 3-dimensional equations for energy, mass, and momentum into ordinary differential equations [83]. Evans and Greif[84] solved the axisymmetric problem for a disk of finite radius, and showed that the infinite radius solution is valid when the effects of natural convection are eliminated(i.e. $\Omega > 1000$ rpm). In the case of Goodwin and Gavillet, the rotation rate is zero, and the infinite radius solution does not have a hot filament in the middle of the system. In order to account for the filament, the authors allow the system to evolve in a PSR for τ_{res}=0.1 s. Again τ_{res} is a fitting parameter as the concentration profiles after the PSR are flat lines. Goodwin [50] then applied the model to acetylene torches and DC arc-jets, with equal validity. Dandy and Coltrin [58] more appropriately modeled the DC-arc plasma gun shown in Fig. 2-1c with the same rotating disk formulation.

In all of the above efforts, the one-dimensional treatment of the fluid dynamics is obviously inadequate. As a result, none of the modeling has explained observed changes in growth rates that result from variations in operating temperature, pressure, or geometry. In addition, all of the models ignore heterogenous chemistry at the filament. This is one of the reasons that none of the modeling efforts predict the dramatic falloff in atomic hydrogen concentration with increasing methane production [35]. An accurate incorporation of these two phenomena is a primary objective of our modeling effort.

PROPOSED DIAMOND GROWTH MECHANISMS

The formation of solid carbon has been extensively studied by researchers in the combustion field [85] Whether diamond forms by an analogous or different mechanism has not been adequately explained by modeling efforts. Despite all the attention focused on diamond films, the growth mechanism remains unclear. A number of species have been discussed as possible growth species, including CH_3, C_2H_2, CH, CH_2, C, C_2, C_2H and CO. To date detailed mechanisms have been proposed for methyl radical [17,86], acetylene[18,87], and gas-phase carbon [88] as the gas-phase precursors. All of the proposals begin with a diamond surface terminated with hydrogen atoms as shown in Fig. 2-2 for the (111) plane. The presence of terminal hydrogen atoms has been experimentally verified for single crystal diamonds at atmospheric pressure using photon-stimulated desorption [89] and electron energy loss spectroscopy(EELS) [90]. In addition, infrared spectroscopy work in our lab has revealed the presence of CH and CH_2 groups in CVD diamonds [63].

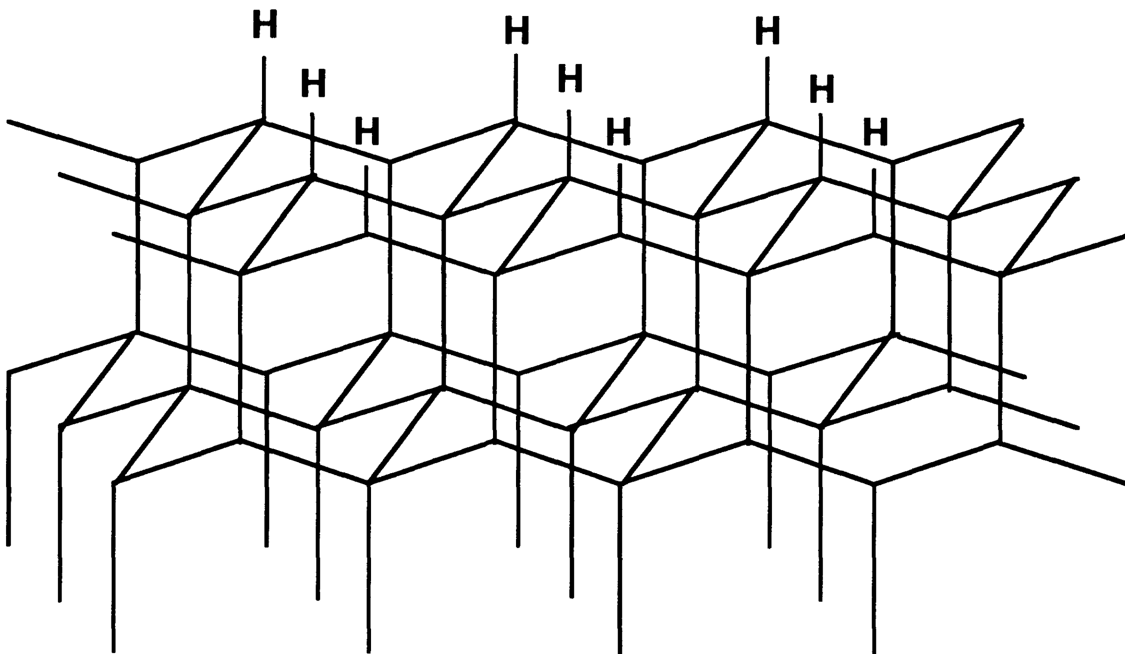

Figure 2-2: Hydrogen terminated 111 Surface.

Despite espousing different precursors and different reactions, all the proposed mechanisms have a number of similarities. First, a small carbon cluster is used as a model compound to simulate the diamond surface. Original models contained around 10 carbon atoms [17,91] while more recent simulations contain in excess of several hundred [92,93], but the approach is the same. Second, the models only predict homoepitaxial growth without the creation of defects or sp2 bonded carbon. A less elementary model tried to incorporate the effect of sp2 bonded carbon [58].

The original mechanism of Harris[17] is reproduced in Fig. 2-3. Although models have increased in complexity and refinement, they still consist of the simple reactions considered here. Harris' mechanism for epitaxial growth on the (100) surface via methyl radical addition using bicylco[3.3.1] nonane(BCN) as a model compound. The first step in this and all mechanisms is the abstraction of a surface hydrogen to create a surface radical (HH + $H_{(g)}$ -> H*) A methyl group then adds to the radical site to form HM (H*+ $CH_{3(g)}$ -> HM). Propagation of the diamond lattice is modelled as the formation of compound B(adamantine), which requires two additional hydrogen abstraction reactions. An H abstraction from the methyl group to form M*, when followed by a abstraction at the neighboring carbon the 2 radicals recombine irreversibly to form B.

Harris estimated the kinetic parameters using the method of analogy first proposed by Frenklach[45]. The underlying assumption of this method is that there are equal reaction probabilities for similar gas-phase and gas-surface reactions. This method has been used successfully to estimate the gas-phase kinetics of high molecular weight alkanes [80,94]. Whether it is appropriate or not to extend this reasoning to condensed species is debatable. Integrating the rate equations Harris calculated a growth rate of ~0.1µm/hr, which is within an order of magnitude of experimental measurements. The agreement may be fortuitous when considering the approximations taken into account. Reverse reactions are calculated from equilibrium considerations which have been estimated using group additivity methods [95], monte-carlo simulations [96], and development of empirical potentials[97].

The first mechanism proposed involved methyl radicals was proposed by Tsuda [86], but it required a methyl cation which would not be present in thermal systems. Frenklach and Spear [18] proposed that acetylene could propagate diamond growth as it does in soot production [98,99]. Semi-empirical calculations by Huang et al.[91] showed that this mechanism could proceed to complete the (111) diamond surface without any energy barriers.

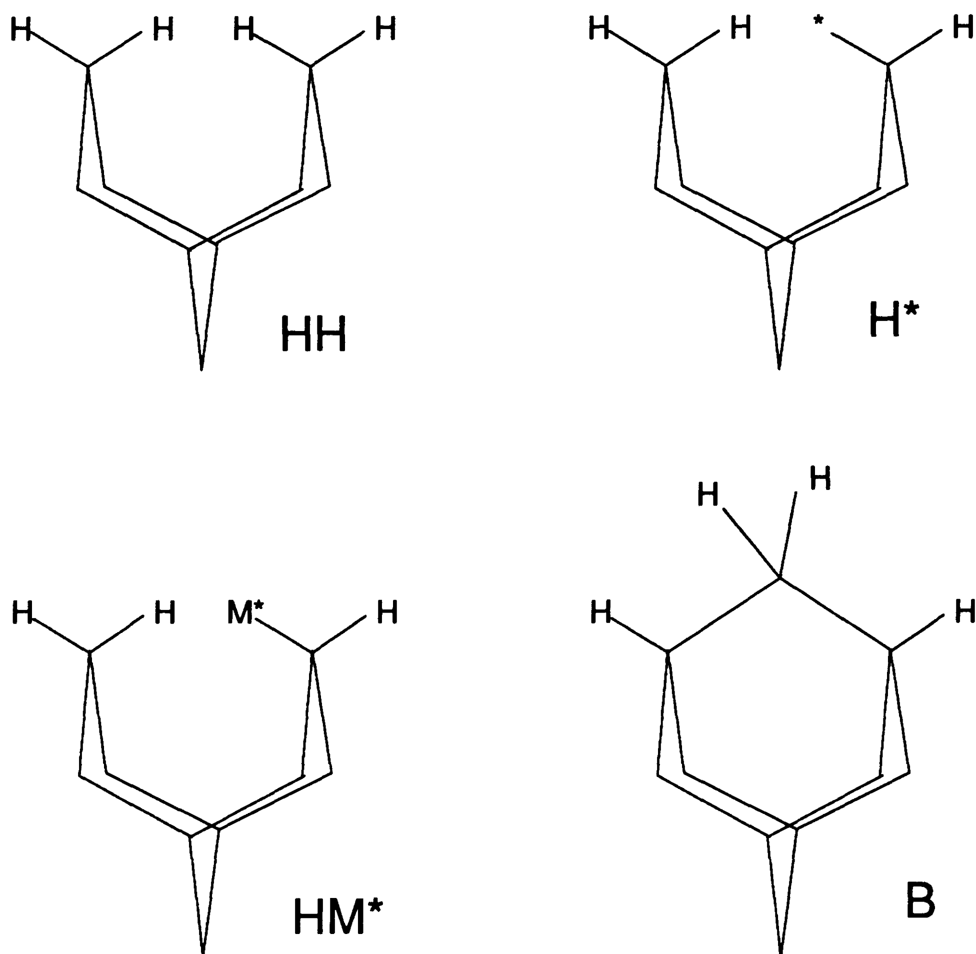

Figure 2-3: Mechanism for homoepitaxial growth via methyl radicals proposed by Harris [17].

However, a thermochemical analysis by Harris and Belton [100] indicated that acetylene would desorb faster than it could incorporate into the diamond lattice. One reason why all of these calculations are somewhat suspect is that the smaller model compounds to not capture the rigidity of the diamond lattice and the extreme steric repulsions that can occur on the surface[59]. In fact the nature of the growing diamond surface is not clear. The (100) dihydride surface mimicked in Fig. 2-3 probably does not exist, reconstructing to a monohyride phase to reduce steric barriers[101].

The current models that are being considered include growth by methyl radical [92,93] on the reconstructed (100) -(2x1) surface. Both mechanisms incorporate the beta - scission sequence proposed by Garrison [97], while Harris completes the mechanism with a step similar to his original mechanism [92]. Frenklach [93] invokes surface diffusion of

adsorbed methyl radicals to complete the growth sequence. Frenklach [102] has also proposed a mechanism for addition of acetylene to the same surface. Harris and Belton proposed an alternative mechanism for diamond growth from acetylene on the (110) surface [103], although the predicted growth rate is very slow.

Despite all the effort, the models are a long way from understanding the underlying chemistry. Most are only evaluated at a single temperature (1200 K), and haven't successfully explained observed Arrhenius behavior. In addition, the most work has focused on the (100) surface. No plausible mechanisms have been put forward for the (111) surface. There have been some work on the (110) surface [32,103], but the models do not predict observed growth rates.

The paper by Coltrin and Dandy[59] allows for growth of both diamond and non-diamond carbon from acetylene, methyl radical, and gaseous carbon. In their proposal they assign different reaction probabilities for the addition of the various species. It provides a qualitative tool for analyzing growth under different conditions. Similarly, Girshick and coworkers [88] extended the Harris mechanism to include growth from C, CH, and CH_2. These papers may be more appropriate for the plasma jet systems, but they still suffer from a lack fundamental understanding of the reactions at the surface.

REFERENCES

1. P. M. Stephen, C. D. Dean, and R. A. Hay, Diamond and Related Mat. **1**, 710, (1992).
2. R. C. Eden, Diamond and Related Mat. **2**, 1051, (1993).
3. M. C. Costello, D. M. Reece, J. A. Savage, D. A. Tossell, and C. J. Brierley, Diamond and Related Mat. **3**, 1137, (1993).
4. A. T. Collins, Phil. Trans. R. Soc. Lond. A, **342**, 233 (1993).
5. J. C. Angus and C. C. Hayman, Science **241**, 913 (1988).
6. B. V. Deryagin and D. V. Fedoseev, Russ. Chem. Rev. **39**, 783 (1970).
7. J. C. Angus, H. A. Hill, and W. S. Stanko, J. Appl. Phys. **39**, 2915, (1968).
8. S. Matsumoto, Y. Sato, M. Tsutsumi, and N. Setaka, J. Mat. Sci. **17**, 3106, (1982). see also S. Matsumoto, Y. Sato, M. Kamo and N. Setaka, Jpn. J. Appl. Phys. **21**, L183 (1982).
9. F. G. Celii, D. White, and A. J. Purdes, J. Appl. Phys., **70**, 5636, 1991.
10. K. Suzuki, A. Sawabe, H. Yasuda, T,. Inuzuka, Appl. Phys. Lett. **50**, 728, (1987).
11. Y. Matsui, A. Yukki, M. Sahara and Y. Hirose, Jpn. J. Appl. Phys. **28**, 1718, (1989).
12. K. Okano, H. Kiyota, T. Iwasaki, Y. Nakamura, Y. Akiba, T. Kurosu, M. Iida, and T. Nakamura, Appl. Phys. Lett. **51**, 344 (1990).
13. K. Okano, H. Kiyota, T. Iwasaki, T. Kurosu, M. Iida, and T. Nakamura, Appl. Phys. Lett. **58**, 840 (1991).
14. Y. Hirose and Y. Terasawa, Jap. J. Appl. Phys. **25**, L519, (1986).
15. T. Kawato and K.-I. Kondo, Jap. J. Appl. Phys. **26**, 1429, (1987).

16. M. Tsuda, M. Nakajma, and S. Oikawa, J. Am. Chem. Soc. **108**, 5780 (1986).
17. S. J. Harris, Appl. Phys. Lett. **56**, 2298 (1990).
18. M. Frenklach and K. Spear, J. Mater. Res. **3**, 133 (1988).
19. D. Huang, M. Frenklach, and M. Maroncelli, J. Phys. Chem. **92**, 6379, (1990).
20. P. K. Bachmann, D. Leers and H. Lydtin, Diamond and Related Materials **1**, 1, (1992).
21. R. B. Jackman, J. Beckman, and J. S. Foord, Appl. Phys. Lett. **66**, 1018 (1995).
22. F. Akamatsu, Y. Hirose, and K. Komaki, Jap. J. Appl. Phys. **27**, L1600, (1988).
23. K. R. Stadler and R. L. Sharpless, J. Appl. Phys. **68**, 6187, (1990).
24. R. A. Rudder, G. C. Hudson, J. B. Posthill, R. E. Thomas, R. C. Hendry, D. P. Malta, T. P. Humphreys, and R. J. Nemanich, Appl. Phys. Lett. **60**, 329, (1992).
25. T. G. Owano and C. H. Kruger, Plasma Chem. Plasma Process. **13**, 433 (1992).
26. D. B. Oakes, J. E. Butler, K. A. Snail, W. A. Carrington, and L.M. Hanssen, J. Appl. Phys. **69**, 2602, 1991.
27. M. A. Cappelli and P. H. Paul, J. Appl. Phys. **67**, 2596, (1990).
28. E. Kondoh, T. Ohta, T. Mitomo, and K. Ohtsuka, Appl. Phys. Lett. **59**, 488 (1991).
29. C. J. Chu, R. H. Hauge, J. L. Margrave, and M. P. D'Evelyn, Appl. Phys. Lett. **61**, 1393 (1992).
30. A. Yamaguchi, M. Ihara, and H. Komiyama, Appl. Phys. Lett. **64**, 1306, (1994).
31. K. A. Snail, and C. Marks, Appl. Phys. Lett. **60**, 3135, (1992).
32. J. E. Butler and R. L. Woodin, Phil. Trans. R. Soc. Lond. **342**, 209, (1993).
33. S. J. Harris, A. M. Weiner and T. A. Perry, Appl. Phys. Lett. **53**, 1605, (1988).
34. S. J. Harris and A. M. Weiner, J. Appl. Phys. **67**, 6520, (1990).
35. W. L. Hsu, Appl. Phys. Lett. **59**, 1427, (1991).
36. K. L. Menningen, M. A. Childs, P. Chevako, H. Toyoda, L. W. Anderson, J. E. Lawler, Chem. Phys. Lett. **204**, 573 (1993).
37. D. G. Goodwin and G. G. Gavillet, J. Appl. Phys. **68**, 6393, (1990).
38. T. Kawato and K. I. Kondo, Jap. J. Appl. Phys. **26**, 1429, (1987).
39. S. J. Harris and A. M. Weiner, Appl. Phys. Lett. **55**, 2179, (1989).
40. C. J. Chu, M. P. D'Evelyn, R. H. Hauge, and J. L. Margrave, J. Mater. Res. **5**, 2405, (1990).
41. C. J. Chu, M. P. D'Evelyn, R. H. Hauge, and J. L. Margrave, J. Appl. Phys. **70**, (1991).
42. L. R. Martin and M. W. Hill, Appl. Phys. Lett. **55**, 2248, (1989).
43. L. R. Martin and M. W. Hill, J. Mater. Sci. Lett. **9**, 621, (1990).
44. S. J. Harris and L. R. Martin, J. Mater. Res. **5**, 2313, (1990).
45. M. Frenklach, J. Appl. Phys. **65**, 5142 (1989).
46. L. R. Martin and S. J. Harris, Appl. Phys. Lett. **59**, 1911, (1991).
47. S. J. Harris, A. M. Weiner, D. N. Belton and S. J. Schmieg, J. Appl. Phys. **66**, 5353, (1989).
48. S. S. Lee, D. W. Minsk, D. J. Vestyck, and P. Chen, Science **263**, 1596, (1994).
49. G. Balestrino, M. Marinelli, E. Milani, A. Paoletti, I. Pinter, A. Tebano, P. Paroli, Appl. Phys. Lett. **62**, 879 (1993).
50. D. G. Goodwin, Appl. Phys, Lett. **59**, 277, (1991).
51. E. Meeks, R. J. Kee, D. S. Dandy, M. E. Coltrin, Combust. Flame **92**, 144 (1993).
52. K. Ito, T. Ito, and I. Hosya, Chem. Lett., p. 589, (1988).
53. Idemitsu Petrochemical, *Eur. Patent Appl. EP 0327110A1* , (1988).
54. K. M. McNamara and K. K. Gleason, J. Appl. Phys. **71**, 2885, (1992).
55. K.M. McNamara, private communication, (1992).
56. K. Suzuki, A. Sawabe, and T. Inuzuka, Appl. Phys. Ltt. **53**, 1818, (1988).

57. STANJAN, Version 3, © Stanford University, 1987.
58. M. E. Coltrin and D. S. Dandy, J. Appl. Phys. **74**, 5803, (1993).
59. S. P. Mehandru and A. B. Anderson, J. Mater. Res. **5**, 2286, (1990).
60. D. S. Olson, M. A. Kelly, S. Kapoor, and S. B. Hagstrom, Appl. Phys. Lett. **60**, 2502, (1992).
61. D. S. Olson, M. A. Kelly, S. Kapoor, and S. B. Hagstrom, J. Appl. Phys. **74**, 5167, (1993).
62. H. Kaneko, M. Kamada, R. Kuwae, A. Sawabe, and T. Inuzuka, Applied Surface Science **33/34**, 546, (1988).
63. K. M. McNamara, D. H. Levy, C. J. Robinson and K. K. Gleason, Appl. Phys. Lett. **60**, 580, (1992).
64. D. H. Levy and K. K. Gleason, J. Phys. Chem., *in press*, (1992).
65. Y. Liou, A. Inspektor, R. Weimer, D. Knight, and R. Messier, J. Mater. Res. **5**, 2305, (1990).
66. A. B. Harker and J. F. DeNatale, J. Mater. Res. **5**, 818, (1990).
67. K.G. Neoh, J. B. Howard, and A.F. Sarofim, in *Particulate Carbon Formation During Combustion*, eds. D. C. Siegla and G. W. Smith, (Plenum, New York, 1981).
68. B. G. Wicke and K. A. Grady, Combust. Flame **69**, 185 (1987).
69. A. Joshi and R. Nimmagadda, J. Mater. Res. **6**, 1484, (1991).
70. R. E. Thomas, R. A. Rudder, and R. J. Markunas, J. Vac. Sci. Tech. A **10**, 2451, (1992).
71. X. M. Zheng and P. V. Smith, Surf. Sci. **262**, 219 (1992).
72. J. Ruan, W. J. Choyke, and K. Kobashi, Appl. Phys. Lett. **62**, 1379 (1993).
73. W. N. Howard, K. E. Spear, and M. Frenklach, Appl. Phys. Lett. **63**, 2641 (1993).
74. R. E. Rawles, C. Kittrel, and M. P. D'Evelyn, *Proc. 3rd Int. Symp. Diamond Materials*, The Electrochemical Society (1993).
75. W. Zhu, A. Inspektor, A. R. Badzian, T. McKenna and R. Messier, J. Appl. Phys. **68**, 1489, (1990).
76. M. Bourene, O. Dutuit and J. Le Calve, J. Chem . Phys. **63**, 166, (1975).
77. S. J. Harris, A. M. Weiner, and R. J. Blint, Combust. Flame **72**, 91, (1988).
78. S. J. Harris, A. M. Weiner and T. A. Perry, J. Appl. Phys. **70**, 1385, (1991).
79. S. J. Harris and A. M. Weiner, J. Appl. Phys. **75**, 5026, (1994).
80. J. Warnatz, in *Combustion Chemistry*, ed. W. C. Gardiner Jr. , p.197, (Springer-Verlag, New York, 1984).
81. M. Frenklach and H. Wang, Physical Review B **43**, 1520, (1991).
82. M. E. Coltrin, R. J. Kee, and G.H. Evans, J. Electrochem. Soc. **136**, 819, (1989).
83. T. von Karman, A. Angew. Math. Mech., **1**, 233 (1921).
84. G. Evans and R. Greif, J. Heat Trans. **109**, 928, (1987).
85. D. C. Siegla and G. W. Smith, eds., Particulate Formation During Combustion (Plenum, New York) 1981.
86. M. Tsuda, M. Nakajma, and S. Oikawa, J. Am. Chem. Soc. **108**, 5780 (1986).
87. D. N. Belton and S. J. Harris, J. Chem. Phys. **96**, 2371 (1992).
88. B. W. Yu and S. L. Girshick, J. Appl. Phys. **75**, 3914 (1994),
89. B. B. Pate, Surf. Sci. **165**, 83 (1986).
90. W. S. Wang, J. Sokolov, F. Jona, and P. M. Marcus, Solid State Commun. **41**, 191, (1982).
91. D. Huang, M. Frenklach, and M. Maroncelli, J. Phys. Chem. **92**, 6379, (1988).
92. S. J. Harris and D. G. Goodwin, J. Phys. Chem. **97**, 23 (1993).
93. S. Skokov, B. Weiner, and M. Frenklach, J. Phys. Chem. **98**, 7073 (1994).
94. C. K. Westbrook, J. Warnatz, and W. J. Pritz, in 22nd Symposium (International)

on Combustion, p. 893, The Combustion Institute, (1988).
95. S. Benson, *Thermochemiical Kinetics* (Wiley, New York, 1976).
96. M. Frenklach, J. Chem. Phys. **97**, 5794, (1992).
97. B. J. Garrison, E.J. Dawnkaski, D. Srivastava, and D. W. Brenner, Science **255**, 835, (1992).
98. M. Frenklach, D. W. Clary, W. C. Gardiner, and S. T. Stein, 20th International Symposium on Combustion (The Combustion Institue, 1984), p.887.
99. S. J. Harris, A. M. Weiner and R. J. Blint, Combustion and Flame **72**, 91 (1988).
100. S. J. Harris and D. N. Belton, Jap. J. Appl. Phys. **30**, 2615, (1991).
101. Y. L. Yang, and M. P. D 'Evelyn, J. Vac. Sci. Tech. A **10**, 978 (1992).
102. S. Skokov, B. Weiner, and M. Frenklach, J. Phys. Chem. **98**, 98 (1994).
103. S. J. Harris and D. N. Belton, J. Phys. Chem. **96**, 2371 (1992).

CHAPTER THREE

HEAT TRANSFER IN HOT-FILAMENT DIAMOND DEPOSITION

(Published in Journal of Applied Physics, Volume **72**, p. 3750, (1992) as "Radiative Heat Transfer in Hot-filament Diamond Reactors", C. A. Wolden, S. Mitra, and K. K. Gleason)

Abstract

Hot-filament chemical vapor deposition is a common method employed for diamond deposition. Due to the filament-substrate proximity, large temperature variations across the substrate is often possible. Variations in substrate temperature need to be minimized in order to deposit polycrystalline diamond films of uniform thickness over large areas. Thus heat transfer calculations which consider radiation from the filament to the substrate, radiation from the substrate to the reactor walls, and finally conduction in the silicon wafer have been developed to predict substrate temperature profiles as a function of the filament shape and geometry. The calculated values are found to be in reasonable agreement with experimentally measured substrate temperatures. It was found that hydrogen atom recombination makes a significant contribution to the absolute substrate temperature, but that the normalized temperature profiles are determined primarily by the radiation flux distribution. The effects of the other deposition parameters are also discussed. Comparison with experimental results show an apparent correlation between growth rate profiles and radiation flux profiles from the filament as predicted by the calculations.

I. Introduction

In the past decade there has been considerable increase in the study of polycrystalline diamond films.[1-10] The impetus for these studies has been provided by the discovery that diamond films can be grown on a variety of substrates under metastable conditions.[2,3] Diamond films have now been grown using a variety of deposition techniques and under a wide range of conditions.[11] Since, in most of these methods diamond films are deposited in subatmospheric pressures and relatively low substrate temperatures, it is anticipated that many of the unique mechanical and opto-electronic properties of diamond can now be commercially exploited.

Hot-filament chemical vapor deposition (hot-filament CVD) has been used extensively to deposit diamond films. Typically in this method, a dilute mixture(0.5-3%) of a carbon containing gas such as methane or acetone in hydrogen is thermally activated at subatmospheric pressures (~ 25 - 300 torr) by a filament held at ~2500 K. A substrate is held between 0.5 and 1.5 cm from the filament, resulting in substrate temperatures of 900-1200 K and polycrystalline diamond is deposited at rates ~1 μ/hr. Advantages of this

method are its simplicity and potential for scale-up. However, the ability to grow films of uniform thickness and high quality over large areas and at acceptable growth rates demands a improved substrate temperature uniformity.[12]

Variations in the substrate temperature in hot-filament CVD are a result of high filament temperatures and a small filament-substrate distance. Thus the radiation flux from the filament induces temperature variations across the substrate even in the presence of external heating. In order to obtain a deeper insight into these effects, heat transfer in a hot-filament CVD reactor has been numerically modeled and the resulting predictions have been compared with experimental substrate temperature measurements. The calculations were used to determine the substrate temperature profiles as a function of filament temperature, material, and substrate separation. In addition this model was then used to compare different filament geometries and the effect of rotating the substrate with the goal of improving substrate temperature uniformity.

II. Experimental

A schematic diagram of the hot-filament CVD reactor used in this work is shown in Figure 3-1. A mixture of acetone vapor and hydrogen was introduced through the bottom of the reactor and heated by tantalum filaments held between 0.5 and 2.0 cms from a 4" diameter silicon wafer. The filaments were supported by zirconium rods to ensure a constant filament-substrate separation during operation. The operating conditions unless noted differently were 100 torr and $T_f = 2600$ K. For each condition a separate run in the absence of a substrate allowed the filament to be viewed directly. By matching its color to that of one internal to a pyrometer the filament's temperature was obtained. A copper plate with holes of diameter 1/16" drilled at 45 degree increments on circles of radii 0, 1, 2, 3, 4 and 5 cms was placed on top of the quartz plate external to the reactor. The temperature of the unpolished backside of the silicon wafer, which faces the quartz plate, was measured by a Raytek optical pyrometer model S3AHTCF4 operating at 2.2 mm with a spot size of 0.2 cm at its focus. The accuracy of the pyrometer was $\pm 1.0\%$ of the temperature reading. The temperature at various locations on the substrate was measured by aligning the pyrometer over the holes in the copper plate to ensure reproducible positioning. The introduction of the copper plate was not found to change the substrate temperature within experimental accuracy. Care was taken to hold the pyrometer perpendicular to the surface of the copper plate in order to ensure greater accuracy of the profiles. A one-dimensional

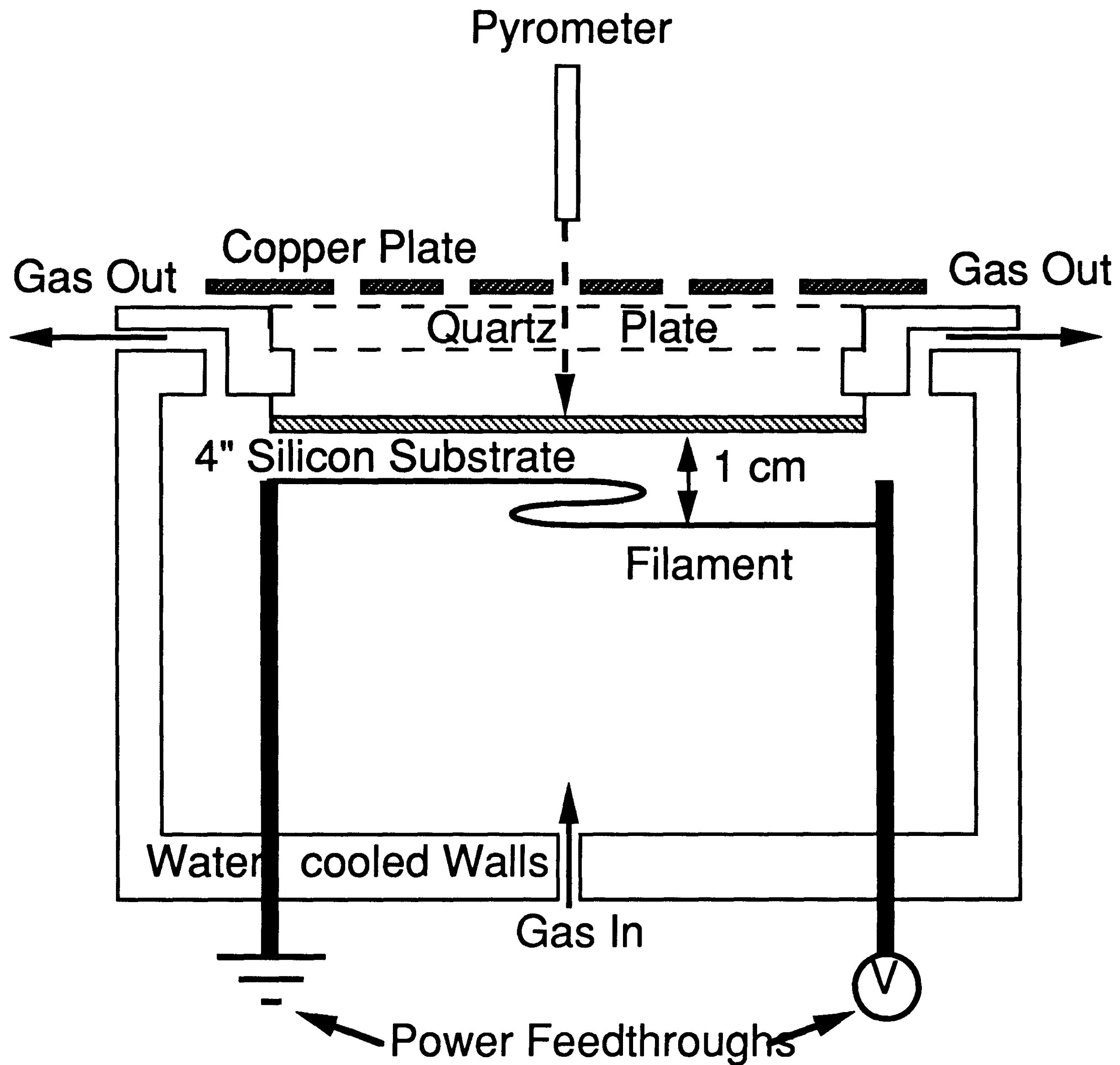

Figure 3-1. A schematic diagram of the hot-filament CVD reactor used in this work. For temperature profile measurements, a copper plate with holes drilled at regular intervals was placed on top of the quartz plate (see text for details).

steady-state energy balance calculation on the 500 μm thick silicon wafer indicates the difference in temperature between the front (growing) and the back surfaces is ≤1° C, which is smaller than the rated accuracy of the pyrometer. Consequently, the temperature indicated by the pyrometer is equal to that of the growing surface. The temperature profile measurements were taken after the reactor had attained steady state conditions for at least 1

hour. This ensured complete carburization of the tantalum filament and thus eliminated any changes in its emissivity with time. The temperature at the center of the substrate was monitored at regular intervals to monitor any long term drift of the operating conditions.

At each point, the substrate temperature was calculated from the pyrometer reading of black body temperature using the temperature-dependent grey body emissivity of the substrate. This temperature dependence cannot be ignored since the emissivity of silicon, the substrate used in this work, has a strong increase from 0.3 at 500 K to 0.85 at 900 K, beyond which it decreases slowly with temperature.[13] Measurements at each open position on the copper plate immediately yield temperature profiles which can be directly compared with those predicted by the heat transfer calculations.

III. Heat Transfer Calculations

Three possible mechanisms available for heat transfer from the filament to the substrate; radiation, conduction and convection. Since the filament temperatures are very high (typically around ~2500 K), radiative heat transfer dominates over both conduction and convection. The Peclet number, a measure of the relative importance of convection to conduction,[14] is estimated to be $\sim 10^{-4}$ and consequently the heat loss by convection can be safely neglected. The effect of conduction in the gas phase, though small, is not negligible. In addition, it has been observed that the recombination of hydrogen atoms on the surface increases the substrate temperature.[15] The contributions of these two effects were examined experimentally and are discussed later in the text. As both of these effects are minimized at low pressure, radiation is assumed to be the only mechanism in heat transfer from the filament to the substrate.

Consider the simple filament geometry as shown in Fig. 2-1 of a straight filament of length 2L, temperature T_f, centered at the coordinates (0, 0, h_f). In Fig. 2, d_f is the diameter of the filament and $\emptyset_1$ is the angle formed by the vector **r** joining dA_1 and dA_2 and the substrate normal, n_1. The position of the differential filament element dA_2 is defined by the distance from the filament center, x, and its surface normal, n_2. The angle α ($0 \leq \alpha \leq 2\pi$) is formed between n_2 and n_f, the normal vector in the plane containing **r** and the center of the filament. Likewise, the angle $\emptyset_2$ is formed between **r** and n_f. The shape factor between the two surfaces depends on **r**, α, $\emptyset_1$, and $\emptyset_2$. Since **r** is much greater

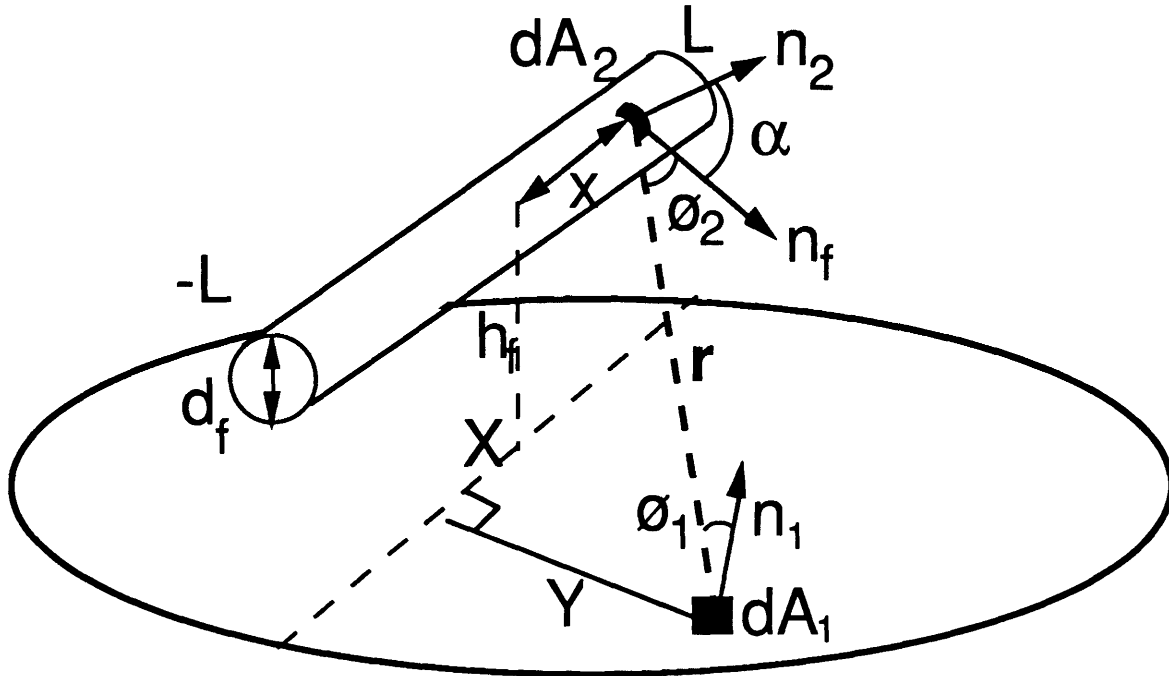

Figure 3-2: A schematic of a simple filament geometry. The radiation flux to a differential substrate area is proportional to the shape factor, the fraction of radiant energy leaving the filament that is incident on the substrate at that point.

than the filament radius, the magnitude of **r** is nearly independent of α. Thus, the dependence on the angle α can be treated by integrating over a cylindrical element of area $\pi d_f\,dx$ which yields an effective surface area $dA_f = d_f\,dx$, radiating in the direction n_f. The shape factor for diffuse radiation between the filament and a differential substrate area dA_1 simplifies to,[14]

$$F_{fs} = \int_{-L}^{L} \frac{\cos \varnothing_1 \cos \varnothing_2 \, d_f \, dx}{\pi \, \mathbf{r}^2} \tag{1}$$

For the substrate element dA_1 fixed at coordinates = (X,Y, 0) and a filament at (-L $\leq x \leq$ L, 0, h_f), the terms in Eq. 1 become:

$$\mathbf{r} = ((x-X)^2 + Y^2 + h_f^2)^{0.5} \quad (2)$$

$$\cos \varnothing_1 = \frac{h_f}{\mathbf{r}} \quad (3)$$

$$\cos \varnothing_2 = \frac{(h_f^2 + Y^2)^{0.5}}{\mathbf{r}} \quad (4)$$

Upon substitution into Eq. 1, one obtains an expression for F_{fs} that is only a function of x that can be evaluated analytically at each grid point, (X_n, Y_n, 0). When multiple filaments are used the shape factors of the individual filaments are simply superposed. For filaments that are not straight the shape factor must be computed numerically. Finally, the radiative heat absorbed by a differential substrate area dA_1 from the filament, Q_{fs}, is given by ,

$$Q_{fs} = F_{fs} \varepsilon_f \sigma T_f^4 \varepsilon_s dA_1 \qquad \text{[Watts]} \quad (5)$$

where ε_f and ε_s are the grey-body emissivities of the filament and substrate, σ is the Stefan-Boltzman constant (5.67 x 10^{-12} W/cm^2 K^4).

Three calculations were compared to illustrate the relative importance of various factors. In the first, only the radiation flux from the filament was considered, while radiation from the substrate to the reactor walls was ignored. It follows from Eqn. (5) that the radiation flux from the filament at any given point on the substrate is proportional to the shape factor at that point. Assuming a constant filament temperature, the problem in this case reduces to evaluation of the shape factor at different points on the substrate. It is assumed that the substrate temperature is proportional to Q_{fs} and thus, only normalized temperature profiles can be predicted which depends only on the filament shape and geometry through F_{fs}.

The second calculation improves upon the first by considering heat losses from the substrate to the reactor walls by radiation . The water-cooled walls of our reactor (Fig. 3-1) are assumed not to reflect incident radiation and hence are modelled as infinite heat sinks. Thus, the energy lost by the substrate to its surroundings Q_{sw} is given by,

$$Q_{sw} = 2\,\varepsilon_s(T_s)\,T_s^4\,dA_1 \qquad \text{[Watts]} \qquad (6)$$

where T_s is the substrate temperature and $\varepsilon_s(T_s)$ is the temperature dependent grey-body emissivity of the substrate[13] which was fitted to a third degree polynomial for 500 K < T_s < 1200 K,

$$\varepsilon_s(T_s) = -2.8324 + 1.0379\text{x}10^{-2}\,T_s - 9.653\text{x}10^{-6}\,T_s^2 + 2.963\text{x}10^{-9}\,T_s^3 \qquad (7)$$

The factor of 2 in Eqn. 3 accounts for heat loss by both surfaces of the substrate. At steady state conditions, Q_{fs} equals Q_{sw}, and T_s is determined from Eqns. (5) and (6). For each calculated temperature profile, the wafer surface was divided into a mesh of square grids of area 0.25 cm^2. Further grid refinement did not alter the results of the calculations. Initial guesses for the minimum and maximum substrate temperature provided the starting values, and successive substitution was used to solve for new temperature values, and the entire process was iterated until a convergence criteria of 0.25 K was met.

In the final calculation, the effect of lateral conduction of heat in the wafer was also included. The amount of heat Q_c conducted between a grid point on the surface and one of its four neighbors can be written as,

$$Q_c = k_s(T_s)t_s(T_s - T_n) \qquad \text{[Watts]} \qquad (8)$$

Here t_s[cm] and T_n are the thickness of the substrate and the temperature of a neighboring grid, respectively. The temperature dependence of the thermal conductivity of silicon, $k_s(T_s)$ [W/ cm K],[14] is accounted for by the polynomial,

$$k_s(T_s) = 2.4408 - 5.1269\text{x}10^{-2}\,T_s + 4.2304\text{x}10^{-6}\,T_s^2 - 1.2292\text{x}10^{-9}\,T_s^4 \qquad (9)$$

Temperature profiles were calculated as outlined previously, except now there are four additional terms of the form of Eqn. (8) - one for each neighboring grid - that must be included in the energy balance. The final calculation will be used throughout the final the results and discussion section unless otherwise indicated.

IV. Results and Discussion

A. Comparison of Heat Transfer Calculations

The temperature profiles as predicted by the three calculations were compared for the simplest case of a single, straight Ta filament of length 9 cm. The temperature variation on the centerline of the substrate perpendicular to the filament is shown in Fig. 3-3. It is clear that even when only radiation flux is taken into account, the predicted temperature profile is in reasonable agreement with the other two profiles representing the radiation balance and radiation plus conduction.

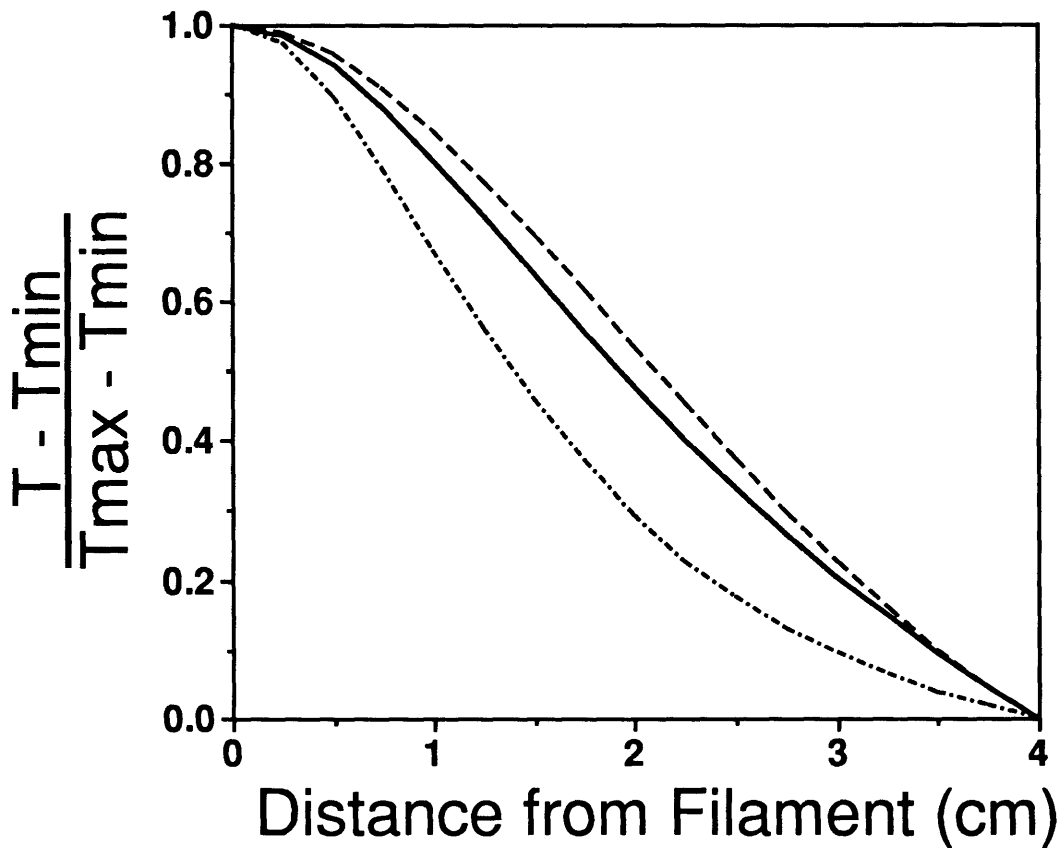

Figure 3-3: A comparison between normalized calculated temperature profiles for a single filament at y = 0 cm, length = 9 cm, d_f = 1.27 mm and h_f = 1.6 cm. Radiation flux from filament (-·-·-); radiation balance (—); radiation balance plus lateral conduction (- - -).

A consequence of lateral heat conduction in the wafer is that it reduces both the maximum substrate temperature and the gradients across the substrate. The predicted contour plots are drawn for a single straight filament of length 9 cm for the radiation balance with and without lateral heat conduction (Fig. 3-4). The maximum temperature (located at the center of the wafer) as predicted are 975 K and 790 K, respectively. The temperature gradients along the direction perpendicular to the filament axis are also smaller when the effect of lateral heat conduction along the wafer is also taken into account. For instance, the distance between 100° contours is ~0.5 cm for the radiation only calculation, but takes place over ~0.9 cm distance when conduction is included. Increasing the wafer thickness or mounting the wafer on a solid support would increase the effect of conduction and improve temperature uniformity. However, the general shape of the profile imposed by radiation will remain.

B. Calculation vs. Measurement

The substrate temperature profile predicted by the final calculation was compared to values measured under vacuum for the case of three parallel tantalum filaments (Fig. 3-5). Since the experiment was performed in vacuum, the calculation considers all means of heat transfer and contain no adjustable parameters. The experimental data agrees well considering the filaments tend to bend during operation.

The calculation neglects heat transfer due to conduction and hydrogen atom recombination. In order to estimate and distinguish the effect of these two contributions the temperature of the center of the substrate was monitored in a vacuum, and at 30 torr in helium and in hydrogen. Raising the pressure from vacuum to 30 torr in helium resulted in a 20°C increase in the center temperature. Repeating the experiment in hydrogen resulted in a 90°C increase. Based on the thermal conductivities of the two gases, approximately 60±5°C of the temperature rise is attributed to H atom recombination and 25±5°C to conduction. These findings are in good agreement with previous observations.[15] Further increasing the reactor pressure up to 300 torr did not effect the substrate temperature in either gas. No change in conduction is expected as the thermal conductivity of gases is nearly invariant to pressure. However, the insensitivity to pressure also indicates that the H atom recombination rate at the center of the substrate is limited by the surface reaction under these conditions. From the difference observed in substrate temperature between vacuum and a hydrogen atmosphere, it is calculated that the contribution by H atom

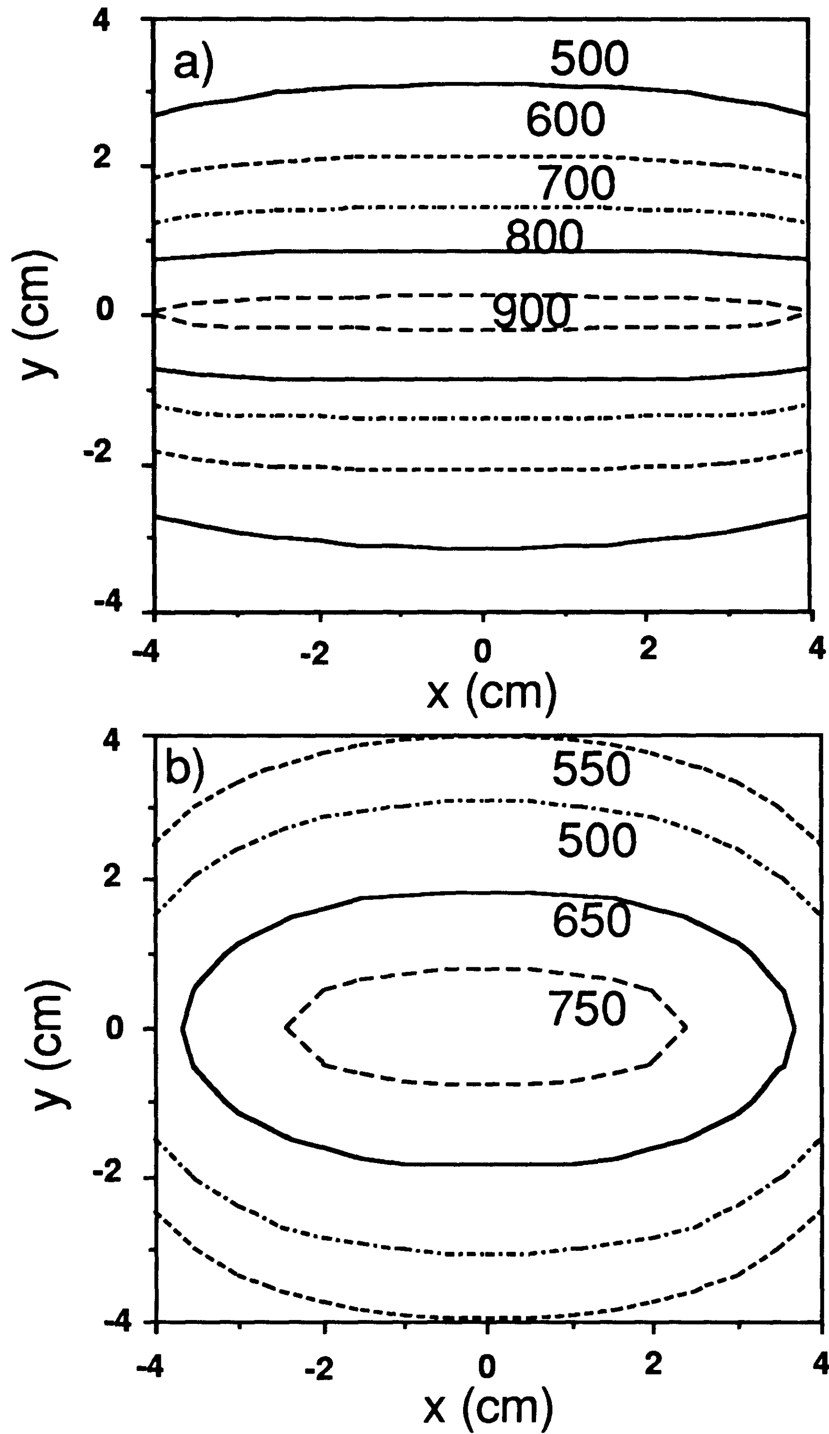

Figure 3-4. Temperature contours for a single filament of length 9 cm, diameter 1.27 mm $T_f = 2600$ K and $\varepsilon_f = 0.5$ as calculated from (a) a radiation balance, and (b) with lateral conduction.

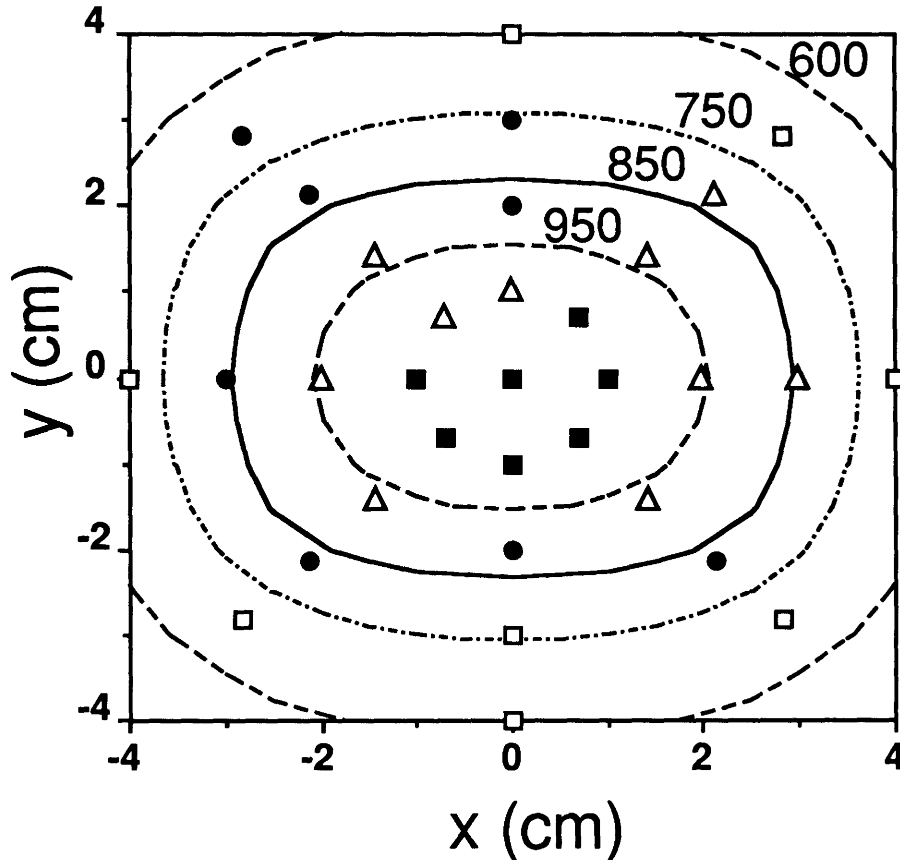

Figure 3-5: Comparison between calculated temperature contours(K) for three parallel tantalum filaments at $y = 0, \pm 1.5$ cm under vacuum and measured data. 950-1015 K: solid squares, 850-950 K: open triangles, 750-850 K: solid circles, 650-750 K: open squares. Filament parameters were $d_f = 1.6$ mm, $h_f = 0.9$ cm, length = 6.2 cm.

recombination and conduction to the energy flux from the filament to the substrate at deposition conditions is 33±5% of the flux due to radiation. The recombination of H atoms at substrate temperatures is a very exothermic reaction[16],

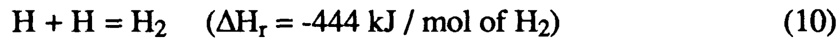

$$H + H = H_2 \quad (\Delta H_r = -444 \text{ kJ / mol of } H_2) \qquad (10)$$

From the heat of reaction and estimated energy flux, the H atom recombination rate was calculated to be 5×10^{-6} mol/ cm^2 s. Using recent measurements of the H atom concentration in a hot-filament CVD system by Hsu[17], it is calculated that H atoms bombard the substrate at a rate of 1×10^{-4} mol/ cm^2 s. Although these are rough estimates, the differences in magnitude indicate that the surface reaction is indeed rate limiting at the

center of the wafer.

Radiation-based calculations were compared to temperature profiles measured under diamond growth conditions (Fig. 3-6). The overall shape and gradients of the predicted contours show good agreement with measurements, but the actual temperatures were ~100°C greater than predicted, as can be accounted for by H atom recombination and conduction. The importance of atomic hydrogen in the deposition of diamond has been reviewed.[18] The concentration of atomic hydrogen in the gas phase depends the carbon concentration, filament diameter, and filament temperature.[17, 19, 20] Therefore, it is expected the number and shape of the filaments will have an effect on the quality of the film, perhaps in a complicated way. The agreement of experimental and calculated temperature gradients in Fig. 3-6, despite the omission of hydrogen chemistry, suggests that the H atom flux has a similar dependence on filament geometry as the radiation flux.

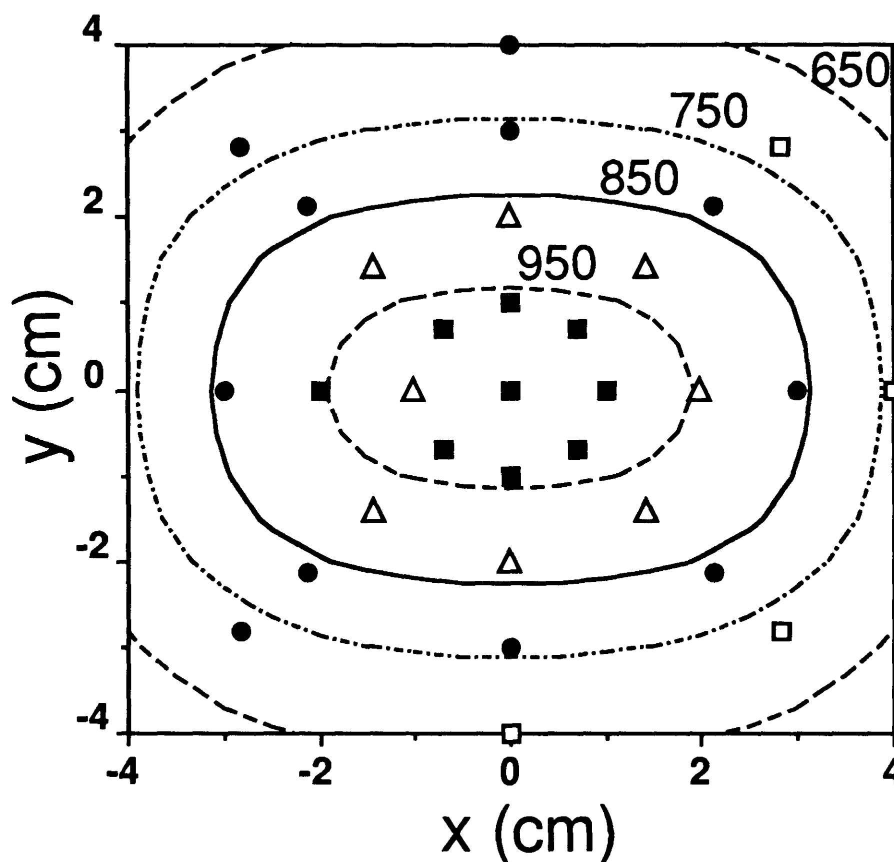

Figure 3-6. Comparison between calculated temperature contours(K) for three parallel tantalum filaments at y = 0, ±1.5 cm at 100 torr and measured data. 1050-1100 K: solid squares, 950-1050 K: open triangles, 850-950 K: solid circles, 750-850 K: open squares. Filament parameters were d_f = 1.27 mm, h_f = 1.2 cm, length = 7 cm.

C. Maximum Substrate Temperature

The effect of parameters like filament diameter (d_f), emissivity (ε_f), temperature (T_f), and the filament-substrate separation(h_f) has a profound effect on both the substrate and gas-phase temperatures, which influence both the growth rate and the quality of the film. Varying one of the first three variables does not appreciably change the substrate temperature profiles, but they influence the magnitude of the surface temperatures and thus can be examined through consideration of the maximum substrate temperature . The effect of these parameters are not independent of each other. Thus, the growth conditions are altered in a complex manner.

An experimental determination of the true filament temperature requires knowledge of the emissivity of the filament, which not only depends on the surface roughness but also on the filament material. Table 3-1 summarizes the emissivity data of refractory metals commonly used in hot-filament CVD[21].

Table 3-1: Emissivity of Common Refractory Materials[a]

λ	W	Re	Ta
0.66 µm	0.36	0.41	0.38
1.6 µm	0.29	0.30	n/a
2.6 µm	0.22	0.21	n/a

[a] See Ref. 21

Calculations with the same filament geometry show that the maximum substrate temperature is sensitive to ε_f (Fig. 3-7a). For example a change from 0.3 to 0.4 increases the temperature by 73 K. Note that both tungsten and tantalum form carbides during deposition, and variations in emissivity may significantly effect the substrate temperature during carburization.

Though radiation flux from the filament is proportional to T_f^4 , the maximum substrate temperature increases only linearly with T_f since this effect is balanced by increased radiation from the substrate to the wall (Fig. 3-7b). The substrate temperature only varies 10° with a 25° change in T_f. Therefore, errors in our optical determination of the filament temperature will not significantly effect the results of the calculations.

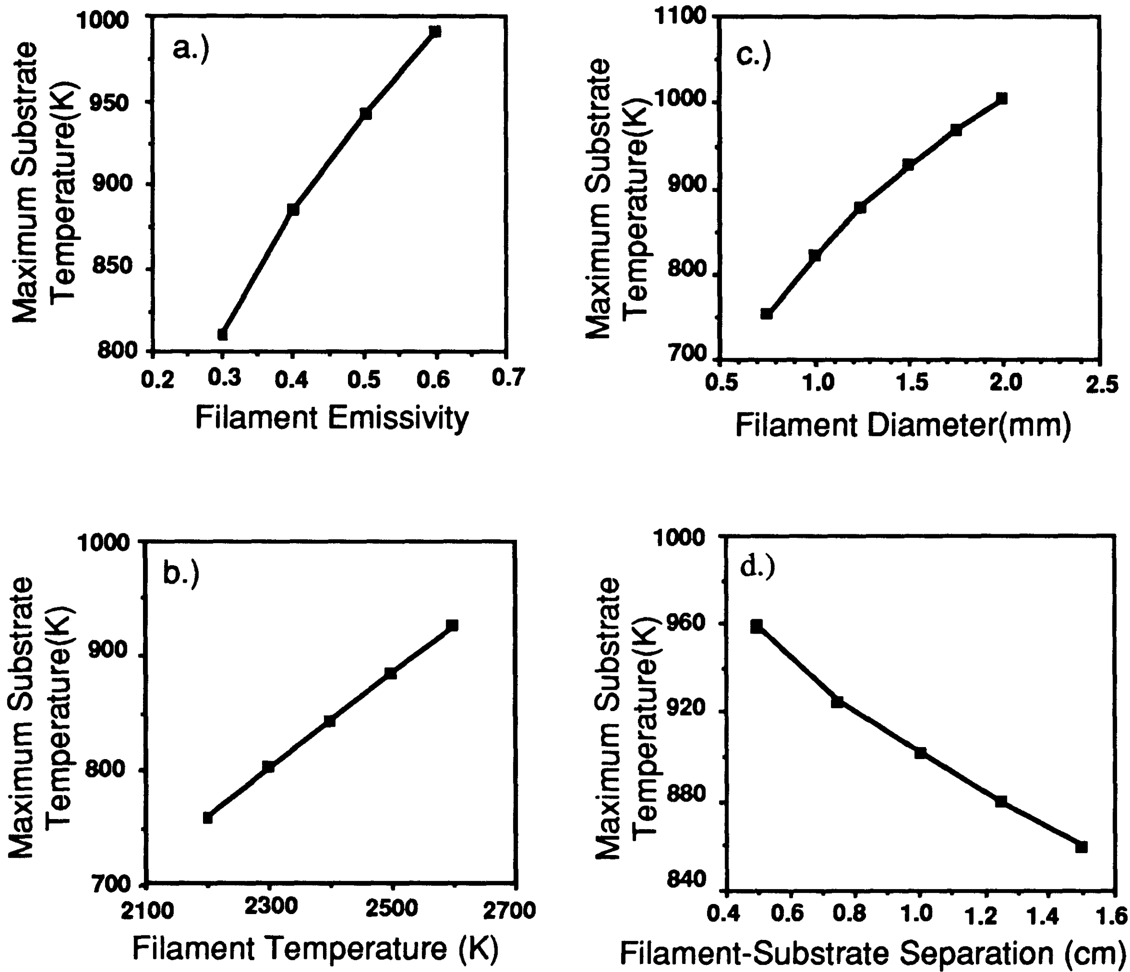

Figure 3-7. The dependence of calculated maximum substrate temperature on (a) filament emissivity ε_f, (b) filament temperature T_f, (c) filament diameter d_f, and (d) filament-substrate separation h_f. Calculations for three 10 cm parallel filaments at y =0, ±2 cm. The other parameters used are d_f = 1.25 mm, h_f = 1.2 cm, ε_f = 0.4, T_f = 2500 K.

For deposition of high quality material for optical and electronic applications, a more important concern is the strong temperature dependence of the vapor pressure (P_{vap}) of common filament materials such as Ta, W, and Re.[22] For example, P_{vap} for tantalum is almost five times greater at 2600 K than at 2500 K.[21] Thus, the concentration of impurities from the filament incorporated into the growing film depends strongly on temperature as demonstrated by Jansen and coworkers[22] for rhenium filaments. Thus the level of

acceptable impurity concentration would determine upper limit of the operating filament temperature. The lower limit appears to be 2400 K, the temperature required to thermally activate the necessary gas-phase chemistry.[15]

A better way to control the substrate temperature is through variation of the filament diameter. The maximum substrate temperature is strongly dependent on filament diameter as the radiation flux is directly proportional to the filament diameter (Fig. 3-7c). The substrate temperature increases by 105°C as d_f increases from 0.5 to 1 mm.

Increasing the filament-substrate separation, h_f, decreases the maximum substrate temperature because it decreases the view factor (Fig. 3-7d). However, the temperature drops only 10° for a 1 mm increase in h_f. However, the effect of h_f will be more pronounced for filaments close to the substrate (<5 mm). The effect of h_f on the temperature contours is discussed further in the next subsection.

D. Substrate Temperature Uniformity

The model provides a convenient tool to investigate novel filament geometries to improve temperature uniformity. First, the effect of the number of filaments and their spacing was examined. The temperature profiles for parallel filaments separated by 2 cm is shown in Fig. 3-8. Comparing contours for 1, 5, and 15 filaments demonstrate that temperature uniformity is significantly improved when the filament number is increased (Figs. 3-8a,b,c). The difference between minimum and maximum substrate temperature in the three cases is 225°C, 45°C, and 15°C, respectively. Hence, increasing the number of filaments improves temperature uniformity at the expense of simplicity and increased energy consumption.

In addition, temperature uniformity is improved as the filament-substrate separation, h_f, is increased while the distance between filaments is held constant. For an infinite number of long, parallel filaments, it was found that when h_f was 0.75 ± 0.05 of the filament spacing, the temperatures across a 4 inch silicon wafer varied by <10%. These calculations suggest that h_f should be as large as the separation between the filaments to ensure reasonable temperature uniformity. However, the transport of species from the hot filament to the substrate is dominated by diffusion.[23] Consequently, the maximum value of h_f is limited by the need to maintain a sufficient flux of H atoms and diamond precursors to the substrate. Characteristic diffusion lengths, the distance a species will diffuse before

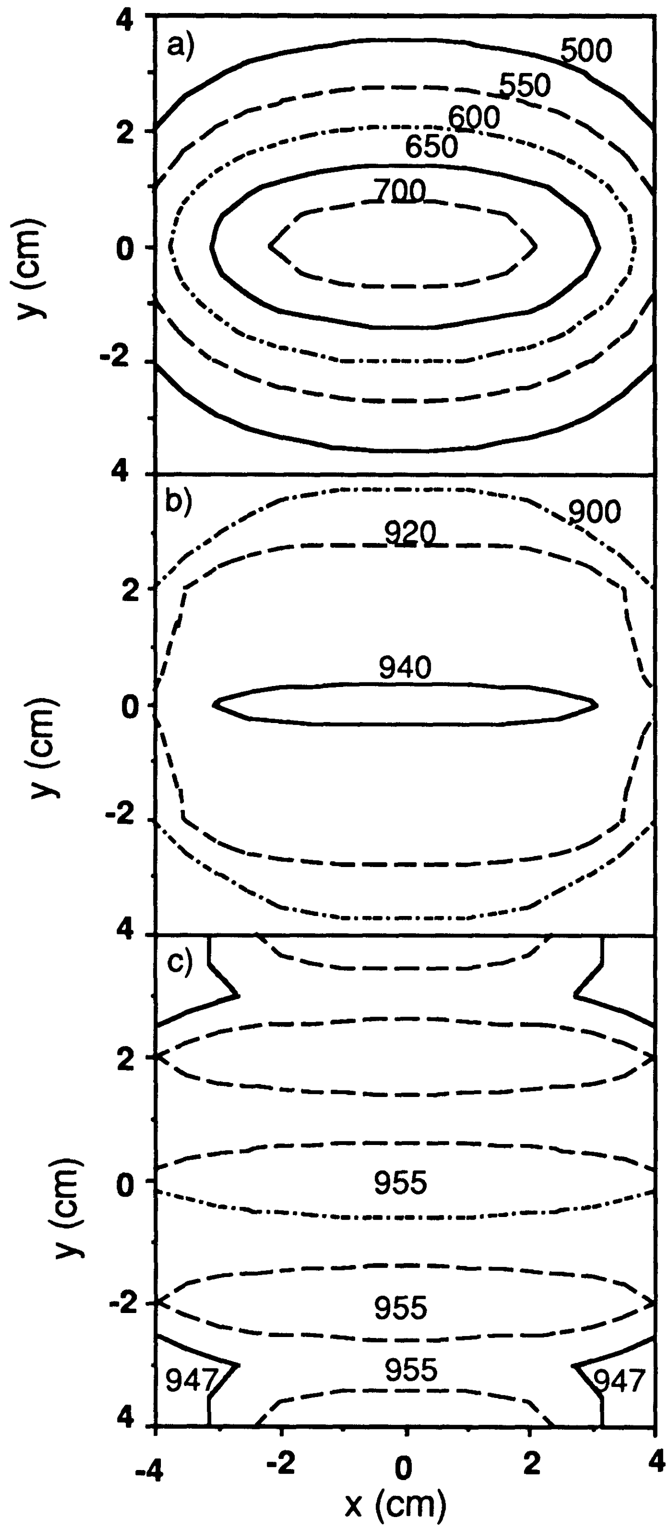

Figure 3-8. Comparison of calculated temperature profiles for (a) 1 filament at y = 0 cm; (b) 5 filaments at y = 0, ±2, ±4 cm; (c) 15 filaments at y = 0, ±2, ±4, ±6, ±8, ±10, ±12, ±14 cm. In each case length = 16 cm, d_f = 1 mm, h_f =1 cm, T_f = 2600 K.

being consumed chemically, were estimated for hot-filament CVD conditions by Goodwin and Gavillet[24]. These values are summarized for important species in Table 3-2.

Table 3-2: Characteristic diffusion lengths for several species[a]

Species	Diffusion lengths (cm)
C_2H_2	3.0
H	1.0
CH_4	0.2 - 0.8
C_2H_4	0.3
CH_3	0.2 - 0.007

[a] See Ref. 24

An alternative to increasing the number of filaments is using unique filament shapes. The calculations were used to design the filament shown in Fig. 3-9a. The solid line is the actual shape of the filament used and the dotted line is the straight filament approximation used for the calculations. The measured substrate temperature over the shaded 2 x 6 cm area was 1060±30 K, while the calculated contour which shows T=910±30 K over the same area (Fig. 3-9b). Note that for this filament geometry the difference between calculated and measured values is 150 K, which is accounted for by the H atom recombination and conduction and the approximation of the true filament geometry, but again it did not effect the gradients.

As mentioned previously, the effect of filament parameters are not independent. These interrelationships may be manipulated judiciously to design filament geometries for improved substrate temperature uniformity as shown in Fig. 3-10. Fig. 3-10a shows the temperature profiles for three parallel filaments of the same diameter and filament-substrate separation. The maximum substrate temperature is 958 K. By slightly decreasing d_f of the middle filament and h_f of the outer filaments, an 18 cm^2 area is obtained where T_s = 915±15 K (Fig. 3-10b).

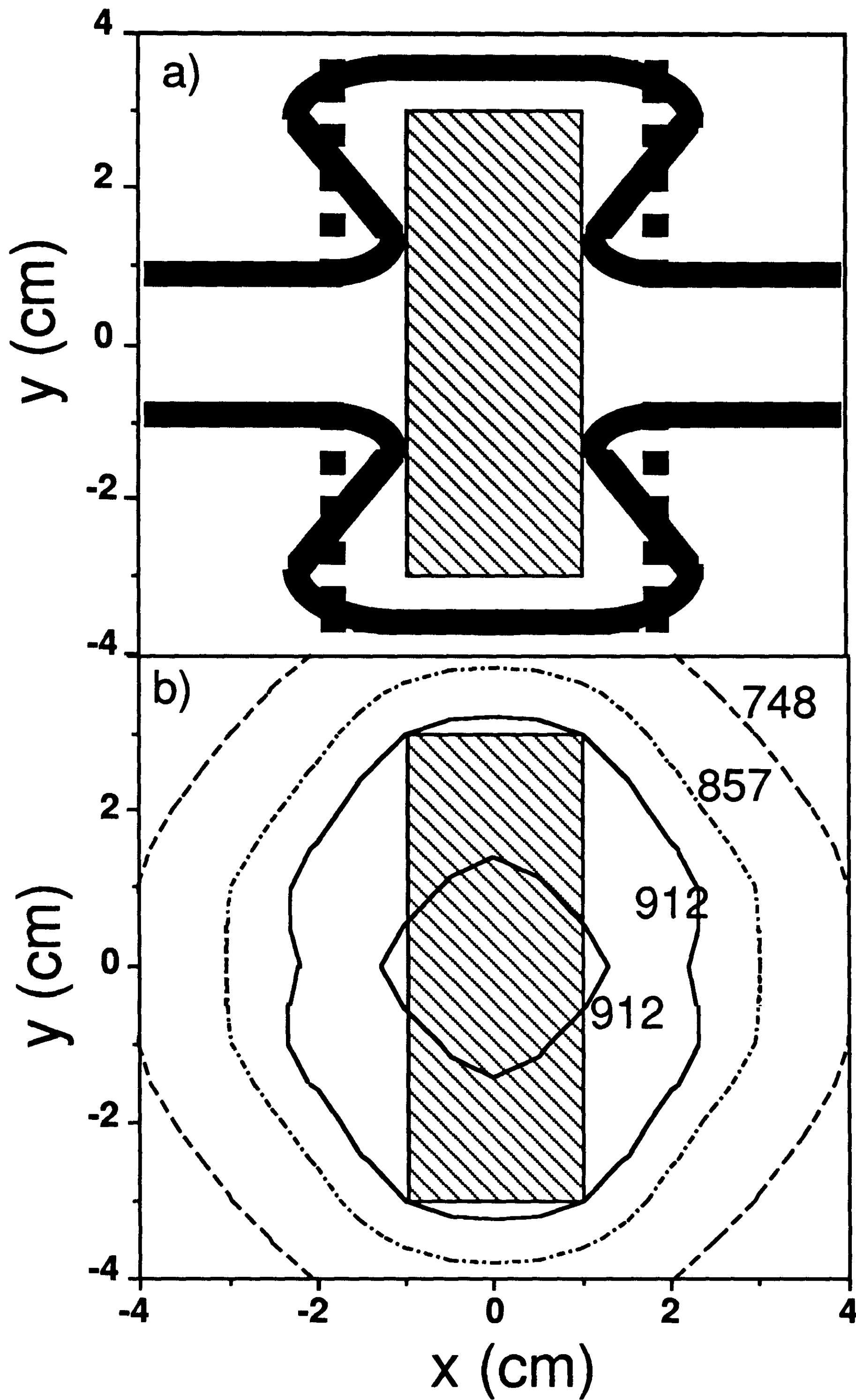

Figure 3-9. Comparison of (a) 2 filament geometry (solid line) and area of measured temperature uniformity, and (b) calculated temperature contours for straight filament approximation (dashed line). Other parameters : d_f = 1.27 mm, h_f = 1 cm.

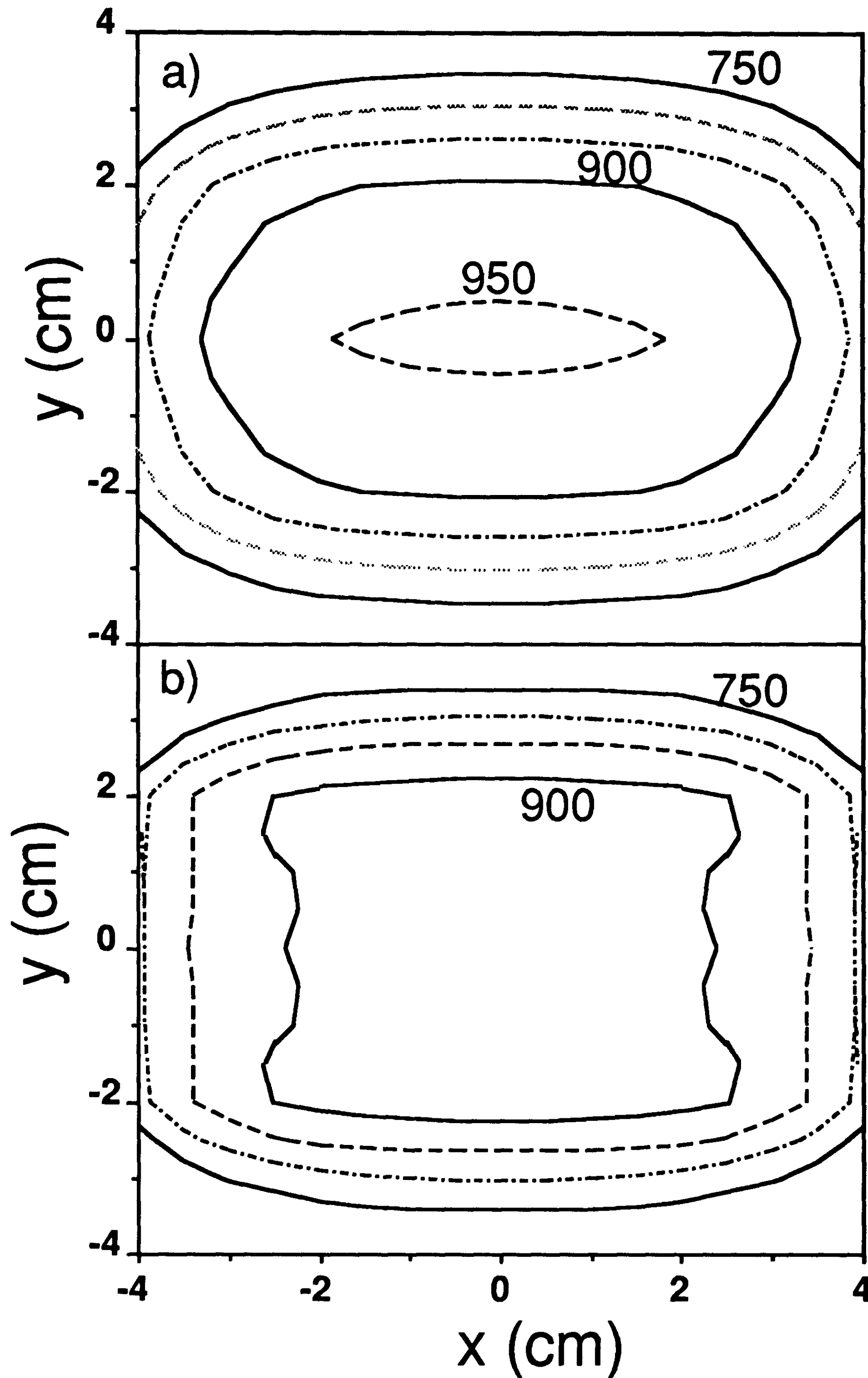

Figure 3-10. Comparison of calculated temperature profiles for (a) 3 filaments at y = 0, ±2 cm: d_f = 1.5 mm, h_f =1 cm, T_f = 2600 K; (b) 1 filament at y = 0 cm: d_f = 1.2 mm, h_f =1 cm, 2 filaments at y = ±2 cm: d_f = 1.5 mm, h_f = 0.7 cm. All filaments 10 cm long, T_f = 2600 K.

To investigate another method of achieving substrate temperature uniformity the calculations were used to analyze the effect of rotating the substrate. Eqns. 1-4 were used to compute the shape factor for points at radius R and angular position Ø. The average shape factor for a given radius is given by,

$$F(R)_{avg} = \frac{1}{2\pi} \int_{0}^{2\pi} F_{fs}(R,\varnothing)\, d\varnothing \qquad (11)$$

The averaged shape factor was used in conjunction with Eqns. 5-9 to generate temperature profiles as before. Fig. 3-11 shows a comparison between a stationary and rotating substrate for 3 parallel filaments. In addition to gaining symmetry, the temperature gradients are much smaller in the rotating case. Rotation decreases the maximum temperature difference across the substrate from 220 K to 140 K. The reason for this improvement is that the entire substrate comes in close proximity to the filaments at some point during rotation.

E. Relationship to Growth Rates

Jansen and coworkers[22] have studied diamond deposition rates for various filament geometries. Film thickness were measured at different distances perpendicular to the middle of the filament(s) and found to be a strong function of position and filament geometry. Our normalized radiation flux profiles calculated from Eqns. 1-2 were compared with their reported normalized film thickness profiles (Fig. 3-12). Since the deposition time for these films was kept constant, it is clear that the growth rate profiles closely follow the variations in radiation flux. The maximum growth rate (on an absolute scale) for both case A and B was found to be the same, in agreement with the fact that the substrate was held at constant temperature. Thus, the consistently higher growth rates observed away from the center for the longer filament is due solely to geometry. Though the substrate was held at a nominal temperature of 900°C by external heating, temperature variations across the substrate may remain due to radiation flux from the filament. In addition, the authors found that the deposition rate was independent of filament diameter.[22] The normalized radiation flux is also independent of the filament diameter, depending solely on the filament position and length.

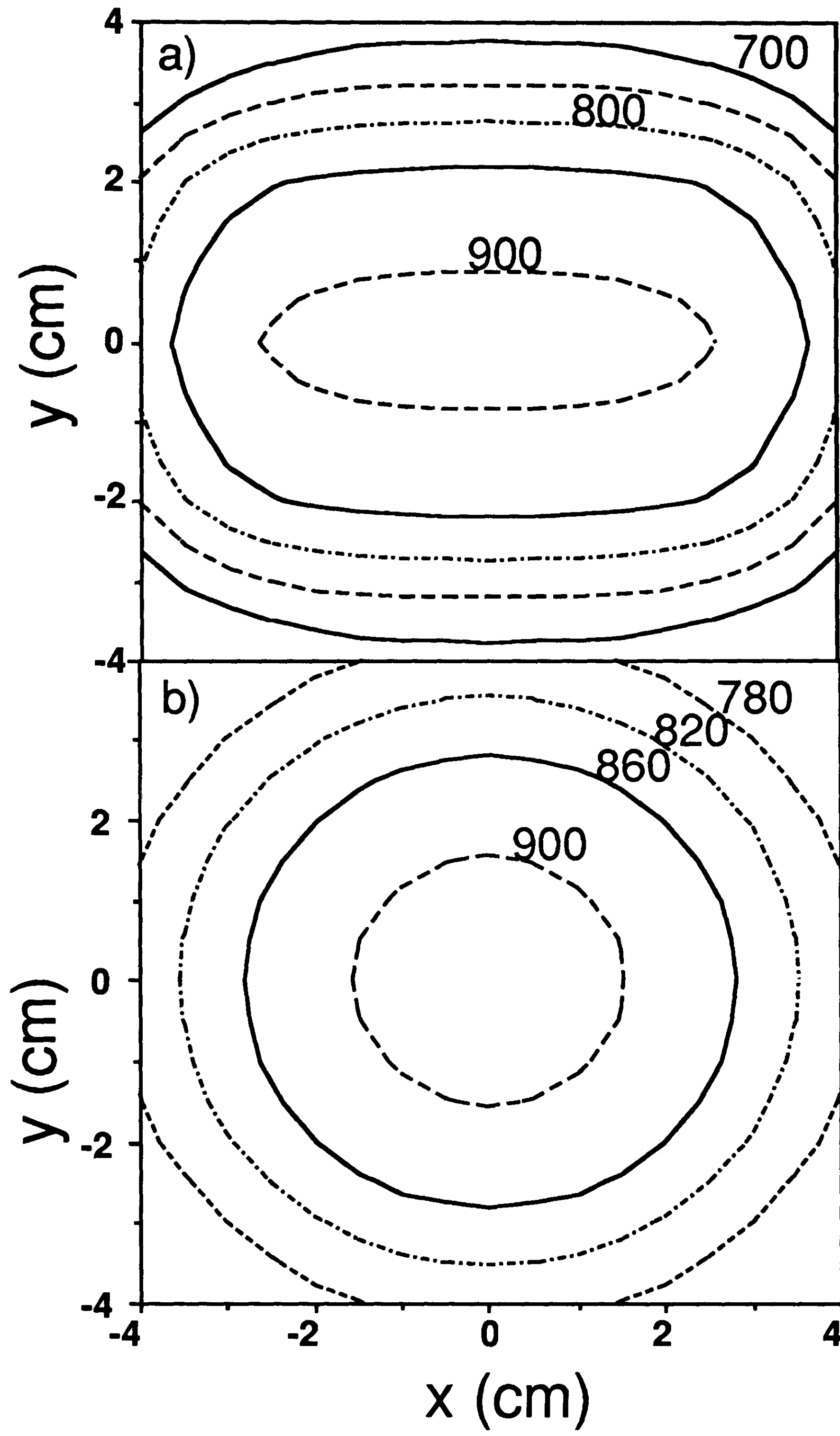

Figure 3-11: Comparison of calculated temperature profiles for (a) stationary, and (b) rotating substrates. Three 10 cm filaments separated by 2 cm. Other parameters are d_f = 1.0 mm, h_f = 1.0 cm, T_f = 2600 K.

Another explanation is that the variations in growth rate may result from a spatial distribution in the flux of gaseous precursors and/or the H atom. As previously discussed, the H atom flux may have a similar dependence on filament geometry as radiation.

There is, however, a marked departure from this linear relationship for case D (two 4" filaments separated by 20 mm) where the growth rate at the center of the substrate deviates from the radiation flux profile. An explanation for this deviation may be depletion of gas-phase diamond precursors due to Soret diffusion.[25] In this case a hot zone between the two filaments is created where the relatively heavy carbon containing molecules are displaced by hydrogen molecules and atoms. In case C (two 4" filaments separated by 9 mm) this zone is much smaller and enough precursors can diffuse in from the sides so as not to limit the growth rate.

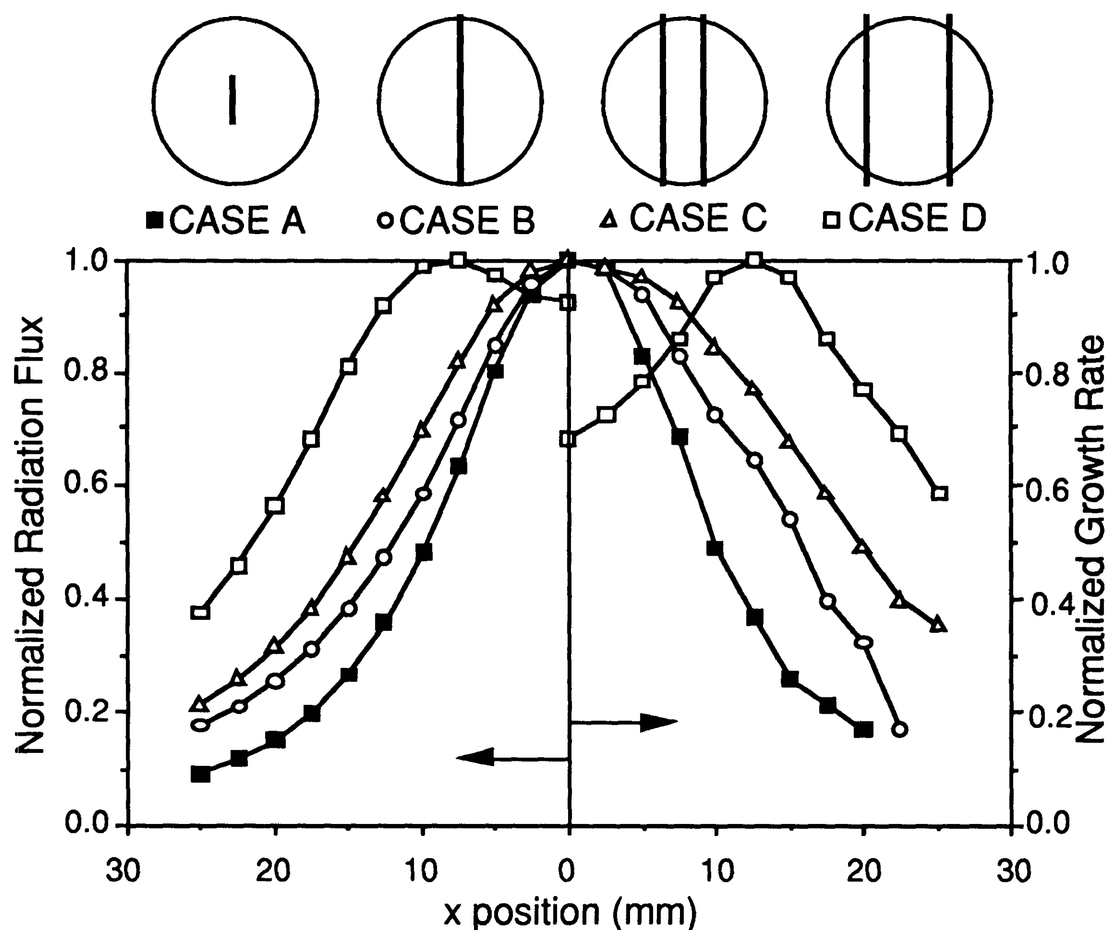

Figure 3-12. A comparison between the normalized growth profiles as measured by Jansen and coworkers (Ref. 22) and normalized radiation flux profiles. Case A: one 0.5 in. filament, Case B: one 4 in. filament, Case C: two 4 in. filaments 9 mm apart, Case D: two 4 in. filaments 20 mm apart. All cases $d_f = 1.016$ mm, $h_f = 1.2$ cm.

V. Conclusions

An ability to grow uniform diamond films over a large area requires that the substrate temperature be held constant. Even in the presence of external heating, temperature gradients across the substrate may remain due to the proximity of the filament to the substrate. Heat transfer calculations were used to predict temperature profiles across the substrate as a function of filament shape and geometry. These calculations gave reasonable agreement with experimental measurements. It is evident that hydrogen recombination makes a significant contribution to the substrate temperature, but uniformity is determined by the geometric dependence of the radiation flux. We developed a two-filament geometry based on the calculations that yielded uniform substrate temperatures over a relatively large area. The effect of other deposition parameters was also discussed. We have demonstrated that for a number of filament geometries, a close match exists between the normalized radiation flux profiles and the growth rates. Currently, an effort is under way to use these results to develop filament geometries capable of depositing diamond films over large areas.

List of References

1. R. C. DeVries, Annu. Rev. Mat. Sci. **17**, 161 (1987).
2. J. C. Angus and C. C. Hayman, Science, **241**, 913 (1988)
3. B. V. Spitsyn, L. L. Bouilov and B. V. Deriyaguin, J. Cryst. Growth **52**, 219 (1981).
4. K. Kobashi, K. Nishimura, Y. Kawate and T Horuchi, Phys. Rev. B. **38**, 4067 (1988).
5. Y. Hirose and N. Kondo, Program and Book of Abstracts, 35th Japan Society of Applied Physics Spring Meeting, pg 434, (1988).
6. Y. Hirose and Y. Terasawa, Jpn. J. Appl. Phys. **25**, L619 (1981).
7. K. A. Snail, D. B. Oakes, J. E. Butler and L. M. Hanssen, pg 503, Proc. of the Second International Conference, eds. R. Messier, J. T. Glass, J. E. Butler and R. Roy, MRS, Pittsburgh, PA.
8. Y. Tzeng, C. C. Tiu, R. Phillips, T. Srivinyunon, and Y. Chen, Appl. Phys. Lett. **57**, 789, 1990.
9. F. Akatsuka and F. Shimura, Applications of Diamond Films and Related Materials, eds. Y. Tzeng, M. Yoshikawa, M. Murakawa and A. Feldman, pg 379, Elsevier Science Publisher B. V. 1991. (Substrate effects)
10. S. Matsumoto, Y. Sato, M. Kamo and N. Setaka, Jpn. J. Appl. Phys. **21**, L183 (1982).
11. P. K. Bachmann, D. Leers and H. Lydtin, Diamond and Related Materials **1**, 1 (1991).
12. L. Schafer, M Sattler, and C. -P. Klages, Applications of Diamond Films and

Related Materials, eds Y. Tzeng, M. Yoshikawa, M. Murakawa and A. Feldman, pg 453 Elsevier Science Publisher B. V. (1991).
13. J. Nulman, SPIE Proceedings on Rapid Isothermal Processing, Vol.1189, p.72 (1989).
14. F. Kreith and M. S. Bohn, *Principles of Heat Transfer* (Harper and Row, New York, 1986).
15. M. Sommer and F.W. Smith, J. Mater. Res. **5**, 2433 (1990).
16. S. Benson, *Thermochemiical Kinetics* (Wiley, New York, 1976).
17. W.L. Hsu, Appl. Phys. Lett. **59**, 1427 (1991).
18. M. Frenklach, J. Appl. Phys. **65**, 5142 (1989).
19. F. Jansen, I. Chen, and M. A. Machonkin, J. Appl. Phys. **66**, 5749, (1989).
20. U. Meier, K. Kohse-Hoinghaus, L. Schafer and C. P. Klages, Appl. Phys. Lett. **58**, 571 (1991).
21. Y. S. Touloukian, Thermophysical Properties of High Temperature Solid Materials, Vol. 1, 1038 (MacMillan Company, New York)
22. F. Jansen, M. A. Machonkin and D. E. Kuhman, J. Vac. Sci. Tech. **A(8)** 3785, (1990).
23. T. Debroy, K. Yankala, W. A. Yarbourgh and R. Messier, J. Appl. Phys. **68**, 2424 (1990).
24. D.G. Goodwin and G. G. Gavillet, J. Appl. Phys. **68**, 6393, (1990).
25. S.J. Harris and A. M. Weiner, J. Appl. Phys. **67**, 6520, (1990).

CHAPTER FOUR

TRANSPORT PHENOMENA IN HOT-FILAMENT DIAMOND DEPOSITION

(Published in Proceedings of the Electrochemical Society, Volume **93**, Number (17) p. 236, (1993) as "Impact of Transport Phenomena on Hot-filament Reactor Design", C. A. Wolden and K. K. Gleason)

Abstract

Hot-filament chemical vapor deposition is a common method employed for diamond deposition. Two dimensional finite element solutions to the conservation equations of mass, momentum, and energy were solved to calculate the fluid flow and temperature profiles in a hot -filament systems. Natural convection is identified as an important force controlling flow profiles, and its importance to mass transport, growth rates, and film uniformity is discussed. The effects of operating conditions and reactor geometry on flow patterns and temperature profiles were analyzed. The model was used to identify operating regimes which reduced the effects of natural convection. The simulations show that appropriate reactor orientation and design can be used to minimize recirculation cells.

INTRODUCTION

Hot-filament chemical vapor deposition(CVD) has been widely used to produce diamond films at low-pressure[1]. Uniform temperature and concentration profiles are requisite for the deposition of high quality large area films. Despite the experimental simplicity of hot-filament CVD, modeling the system is challenging due to the presence of steep temperature gradients, radiative heating, and heterogeneous chemistry.

In previous efforts we have demonstrated how filament design can be manipulated to achieve substrate temperature uniformity [2]. Modeling work has shown that atomic hydrogen production is controlled by heterogeneous chemistry at the filament[3]. Isotopic labeling studies show that rapid heterogeneous reactions are important for hydrocarbon species as well[4]. Furthermore, the gas-phase chemistry is controlled by a limited set of well-known reactions[5].

Here we present fluid flow and temperature profiles to provide insight into the design and operation of hot-filament systems. Particularly, we focus on natural convection and show how appropriate reactor design and operating conditions can be used to minimize this phenomena. Natural convection has been shown to adversely effect film uniformity in other CVD systems when the growth rate is controlled by transport to the growing surface [6,7]. In hot-filament systems we are concerned with transport to the

chemically active zone at and near the filaments.

Previously, DebRoy and coworkers at Penn State analyzed the heat transfer and fluid dynamics in a 2 dimensional reactor [8]. The fluid dynamics are reported for a single condition at 30 torr. Angus et al. [9] performed a similar simulation for a two-dimensional horizontal reactor operated at 20 torr and 760 torr, identifying the importance of natural convection at the higher pressure. We examine the effects of natural convection over a wide range of reactor conditions and orientation in order to provide a guideline for reactor design.

MODEL FORMULATION

We have developed a two-dimensional finite element model of a typical hot-filament reactor [2,3,10]. Three filaments (diameter = 1 mm) separated by 1 cm are suspended 1 cm away from a substrate that is 8 cm across (Figs. 4-1, 4-2). The temperature of the 2 cm thick substrate temperature is controlled at 1073 K, and the filaments are maintained at 2600 K. The reactor is 12 cm across, 12 cm in length, and the reactor walls are maintained at 330 K by water-cooling.

The simulations were performed using FIDAP [11], a commercial code which employs the finite element method. The ideal gas equation of state was assumed, and the transport properties of pure hydrogen were used[12]. Since all surface temperatures are fixed and the gas-phase is transparent, radiative heat transfer does not impact calculation of the temperature profiles in the reactor. The equations of mass, momentum, and energy conservation are simultaneously solved for the temperature and flow fields. All calculations were performed on the MIT Cray X-MP and required ≈ 60 s/iteration. In this study we examine the effects of varying reactor orientation, flow rate , and operating pressure on natural convection.

RESULTS AND DISCUSSION

First we examined the effect of reactor orientation. Three configurations are examined: vertical upflow, vertical downflow, and horizontal. Heating at the hot filaments and substrate results in density gradients which are the driving force for natural convection.

Fig. 4-1 compares the streamlines of (a) a vertical reactor with gas inlet at the bottom and flowing upward, (b) a vertical reactor with inlet at the top and flowing downward, and (c) a horizontal reactor. Natural convection is present in all reactors at these conditions: P = 20 torr and the superficial inlet velocity, defined as the volumetric flow rate corrected for pressure divided by the reactor cross sectional area, U_∞ = 0.1 cm/s. In the upflow reactor (1a) the majority of the gases flow up past the filaments. In contrast the downflow reactor (1b), the presence of the recirculation cell diverts the flow to the outside of the reactor, bypassing the reactive zone near the filaments. In the case of the horizontal reactor(1c) buoyancy effects destroy the reactor symmetry. The temperature profiles are almost identical for the three cases, consistent with the Peclet number $\approx 10^{-3}$ [13], which indicates that conduction rather than convection dominates heat transfer. Thus the gas phase temperature profiles are controlled by the surface temperatures as shown previously [3]. Having demonstrated that the vertical upflow configuration is best for minimizing natural convection, we now examine the effects of flow rate and pressure for this system.

The results of increasing the flow rate are shown in Fig. 4-2. The recirculation cell is reduced as the superficial velocity is increased to 1 cm/s (compare Fig. 4-1a with Fig. 4-2a), and finally eliminated for U_∞ = 10 cm/s (Fig. 4-2b). Next we keep the flow rate of Fig. 2b constant, but increase the reactor pressure to 100 torr. The inlet velocity is reduced by a factor of five, and the recirculation cells return (Fig. 4-2c). By increasing the flowrate another 5X the flow returns to a forced convection profile, although a small recirculation cell remains (Fig. 4-2d). Thus, by manipulating either pressure and flow rate, a flow dominated by forced convection may be attained. However a significant advantage of operating at lower pressure is increased diffusive transport, which is inversely proportional to pressure.

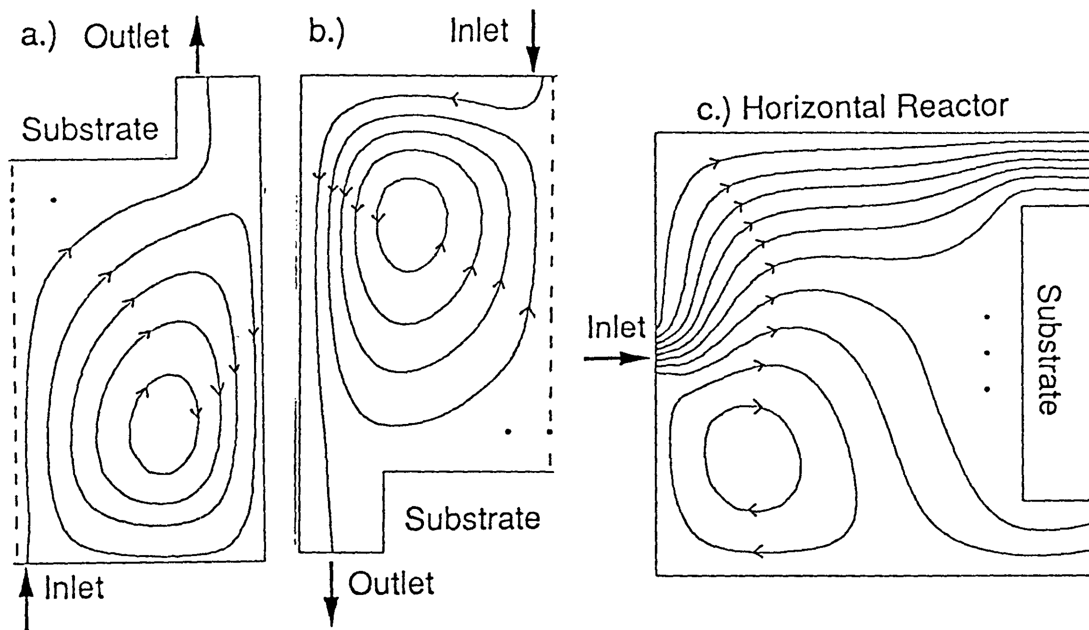

Figure 4-1: Predicted streamlines for (a) a vertical upflow reactor, (b) vertical downflow reactor, and (c) a horizontal reactor. All cases P = 20 torr, inlet velocity is $U_\infty = 0.1$ cm/s.

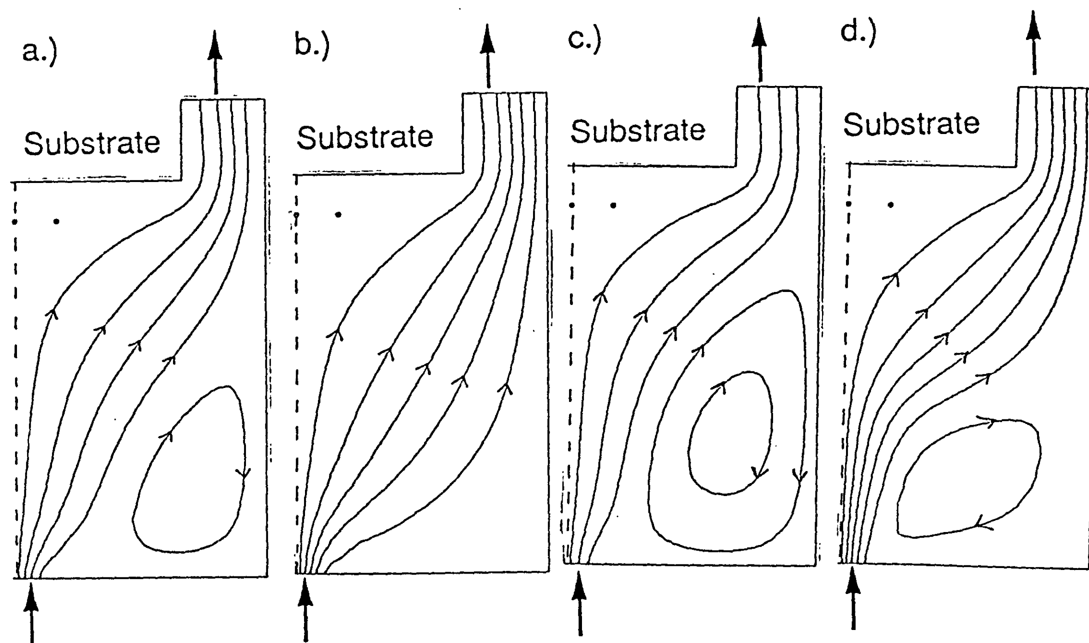

Figure 4-2: The impact of pressure and flowrate in vertical uplfow reatcor. a.) $U_\infty = 1$ cm/s, P = 20 torr; b.) $U_\infty = 10$ cm/s, P = 20 torr; c.) $U_\infty = 2$ cm/s, P = 100 torr; d.) $U_\infty =$ 10 cm/s, P = 100 torr.

The relative importance of natural and forced convection may be analyzed through the dimensionless parameter, Gr/Re^2, where Gr and Re are the Grashof and Reynolds numbers[13],

$$\frac{Gr}{Re^2} = \frac{gL(T_o - T_\infty)}{T_\infty U_\infty^2} \qquad (1)$$

where g = acceleration of gravity, L = characteristic length (reactor radius), T_o = characteristic "hot" temperature ($\approx$ 2000 K), T_∞ = inlet temperature, and U_∞ = superficial inlet velocity. Natural convection effects are important for values of Gr/Re^2 much larger than 1. For a given reactor, all of the parameters in Eq. 1 are fixed except for U_∞, which may be manipulated by flowrate and pressure. For our vertical upflow reactor we found that a forced convection profile is achieved for values of $Gr/Re^2 < 100$.

Lastly, it has been shown in microwave systems that diamond morphology and quality is residence time dependent [15,16]. The concept of residence time is only appropriate under conditions of forced convection flow (case 2b). In the presence of natural convection, the residence times of molecules bypassing the convection cell will be much shorter than the nominal value, while molecules in the cell will remain much longer. Recirculation cells can cause depletion of necessary precursors and accumulation of deposition byproducts, which may lead to a decrease in quality as seen in other CVD systems [6,7]. By providing a uniform residence time, a forced convection profile improves the uniformity of the species reaching growing substrate. We removed the filaments and repeated the flow simulations and found very similar profiles to those shown in Figs. 4-1 and 4-2. Therefore, the guidelines outlined for the hot-filament system should be useful for microwave reactors as well.

CONCLUSIONS

The fluid flow and temperature profiles have been solved in two dimensions for an extensive range of reactor configurations, orientations, and operating conditions. Natural convection is an important driving force in hot-filament reactors, arising from the large

thermal gradients present. The effects of natural convection was demonstrated, and its implications for mass transport, growth rate, and uniformity are discussed. The results demonstrate that natural convection effects can be reduced by increasing the flow rate, decreasing the pressure, and operating in a vertical upflow orientation. For vertical upflow reactors, the effects of natural convection are minimized for values of $Gr/Re^2 < 100$. In addition, the implications of this work are also applicable to microwave systems. By operating reactors as described, improved species flux uniformity should be attained.

REFERENCES

1. J. C. Angus and C. C. Hayman, Science, **241**, 913 (1988).
2. C. Wolden, S. Mitra, and K. K. Gleason, J. Appl. Phys. **72**, 3750 (1992).
3. C. Wolden and K. K. Gleason, Appl. Phys. Lett. **62** 2329, (1993).
4. K. M. McNamara and K. K. Gleason, J. Electrochem. Soc. **140**, L22 (1993).
5. C. Wolden, K. K. Gleason, and J. B. Howard, submitted to Combust. Flame, March 1993.
6. D. I. Fotiadis, S. Kieda, and K. F. Jensen, J. Crystal Growth **102**, 441, (1990).
7. M. E. Coltrin, R. J. Kee, and G.H. Evans, J. Electrochem. Soc. **136**, 819, (1989).
8. T. Debroy, K. Tankala, W. A. Yarbourgh and R. Messier, J. Appl. Phys. **68**, 2424, (1990).
9. M. A. Kuczmarski, P. A. Washlock and J. C. Angus, at The Applied Diamond Conference, Auburn, AL, (Aug. 1991).
10. W.L. Hsu, Appl. Phys. Lett. **59**, 1427 (1991).
11. FIDAP User's Manual, Version 6.0, Fluid Dynamics International, June 1991.
12. *Physical and Thermodynamic Properties of Pure Chemicals: Data Compilation*, eds. T. E. Daubert and R. P. Danner, (Hemisphere, New York, 1989).
13. F. Kreith and M. S. Bohn, *Principles of Heat Transfer* (Harper and Row, New York, 1986).
14. F. G. Celii, D. White and A. J. Purdes, J. Appl. Phys. **70**, 5636, (1991).
15. W. Zhu, R. Messier, and A. R. Badzian, in *Proceedings of the !st International Symposium on Diamond and Diamond-Like Films*, Edited by J. P. Dismukes, A. J. Purdes, B. S. Meyerson, T. D. Moustakas, K. E. Spear, K. V. Ravi and M. Yoder (Electrochemical Society, New York, 1989), Vol. 89-12, p.296.

CHAPTER FIVE

HETEROGENEOUS REACTIONS IN HOT-FILAMENT DIAMOND CVD

(Published in Applied Physics Letters, Volume **62**, p. 2329, (1993) as "Heterogeneous Formation of Atomic Hydrogen in Hot-filament Diamond Deposition", C. A. Wolden and K. K. Gleason)

Abstract

Hot-filament reactors are one of the simplest apparati for the chemical vapor deposition of diamond films, and have been the subject of extensive modeling efforts. However, most previous efforts have neglected the impact of the filament on both chemistry and fluid flow. As a result these models fail to explain some experimental observations, such as the dramatic drop in atomic hydrogen with increasing carbon fraction. A two-dimensional finite element model has been developed for the reactor of W. L. Hsu [Appl. Phys. Lett. **59**, 1427 (1991)], focusing on the relative importance of heterogenous and homogenous chemistry in the production of atomic hydrogen. Our calculations show that catalytic activity is responsible for at least 95% of the atomic hydrogen production. In addition, the concentration of atomic hydrogen at the filament is far below thermal equilibrium values. The effect of recombination of hydrogen atoms at the growing surface was examined. An analysis of experimental data reveals an activation energy of 150 kJ/mol for the filament-catalyzed reaction. From these measurements, a kinetic expression is developed to explain catalytic production of atomic hydrogen at the surface.

Hot-filament chemical vapor deposition (HFCVD) is a common method for the production of diamond films.[1,2] As a result HFCVD kinetics have been the focus of many experimental[3-12] and modeling efforts.[4,8,13-16] However, with one exception[16], these HFCVD models have neglected the influence of the filaments on both chemistry and fluid flow, and thus have been forced to adopt unrealistic residence times and geometries to account for measured species production. In addition, these simulations fail to predict the fall off in atomic hydrogen that is observed with increasing carbon fraction.[5,9-11]

In this letter, we use a 2-D finite element model to interpret the experiments of Hsu.[9,11] We focus on experiments where the only reactant was hydrogen[11], to discern the relative importance of gas-phase and filament catalyzed production of atomic hydrogen. The importance of atomic hydrogen for the deposition of diamond is well recognized.[1,2,13] Postulated roles include stabilization of the growing surface, creation of surface radicals, preferential etching of graphitic carbon, and promotion of the gas-phase chemistry. In addition, hydrogen incorporation has been correlated to adsorption in the IR region[17], and

multiple quantum NMR results indicate that hydrogen is located at defects and grain boundaries.[18] Here we examine each of the three phenomena that control the production/consumption of atomic hydrogen in the hot-filament system: (1) gas-phase chemistry, (2) filament catalysis, and (3) consumption at the growing surface.

Figure 5-1 shows the two-dimensional representation of Hsu's reactor that was modeled. A molecular beam mass spectroscopy system provided quantitative concentrations of both stable and radical species at the growing surface which we compare directly to our modeling results. For the experiments in hydrogen a single straight filament of diameter 0.25 mm was held 13 mm below the substrate at 1073 K.[11] In another set of experiments, Hsu used 3 straight filaments separated by 0.5 cm to simulate a planar geometry.[9] The filament temperature was varied from 2000-2700 K and the pressure was maintained at 20.25 torr. Water-cooling maintained the reactor walls at approximately 328 K.[19]

The simulations were performed using FIDAP[20], a commercial code which employs the finite element method.[21] The bulk of the reactor was modeled with quadratic elements while triangular elements were employed to capture the cylindrical geometry of the filament(s). The ideal gas equation of state was assumed, and the temperature dependence of transport properties was included.[22] Since all surface temperatures are fixed and the gas-phase is transparent, radiative heat transfer does not impact these calculations. Molecular hydrogen enters through two inlets at the bottom of the reactor at a flow rate of 170.6 Pa * l / s. The equations of mass, momentum , and energy conservation are simultaneously solved for the temperature and flow fields. All calculations were performed on the MIT Cray X-MP and required ≈ 45 s/iteration.

First, only gas phase chemistry was examined, and the lone reaction considered was:

$$H + H + H_2 = H_2 + H_2 \quad (1)$$

whose forward rate coefficient is $k_f = 9.7 \times 10^{16} T^{-0.6}$ ($cm^6 / mol^2 s$)[23], where T is in Kelvin, and the reverse rate coefficient was determined from the thermodynamic equilibrium coefficient.[24] The temperature of the inlet is 300 K, and it is assumed that the concentration of atomic hydrogen in the feed and at the cold reactor walls is negligible.

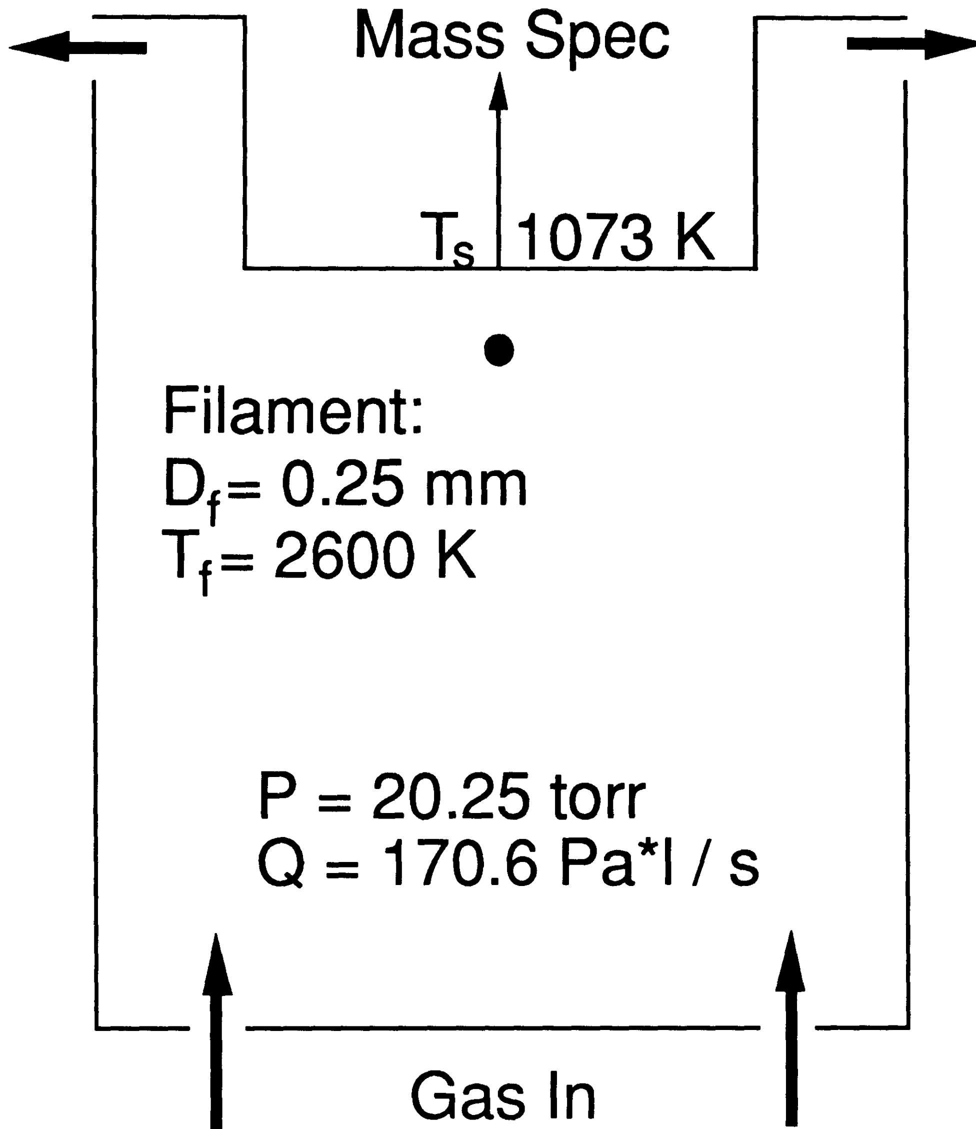

Figure 5-1. Cross section of the reactor that was modeled from Refs. 9,11, and 19.

For a filament temperature of 2600 K, the atomic hydrogen concentration at the growing surface, $[H]_{surf}$, is only 0.4% of the experimentally measured mole fraction x_H = 0.002. For the three filament arrangement, our calculated value of $[H]_{surf}$ rose to ≈ 3% of Hsu's measured value. The temperature profile between the filament and substrate drops off more slowly for the 3 filament case (Fig.5-2), accounting for the increased concentration. The calculations are insensitive to the velocity field as doubling the inlet flow rate or cutting it in half altered $[H]_{surf}$ by < 1%. Thus 3-D flow patterns should not

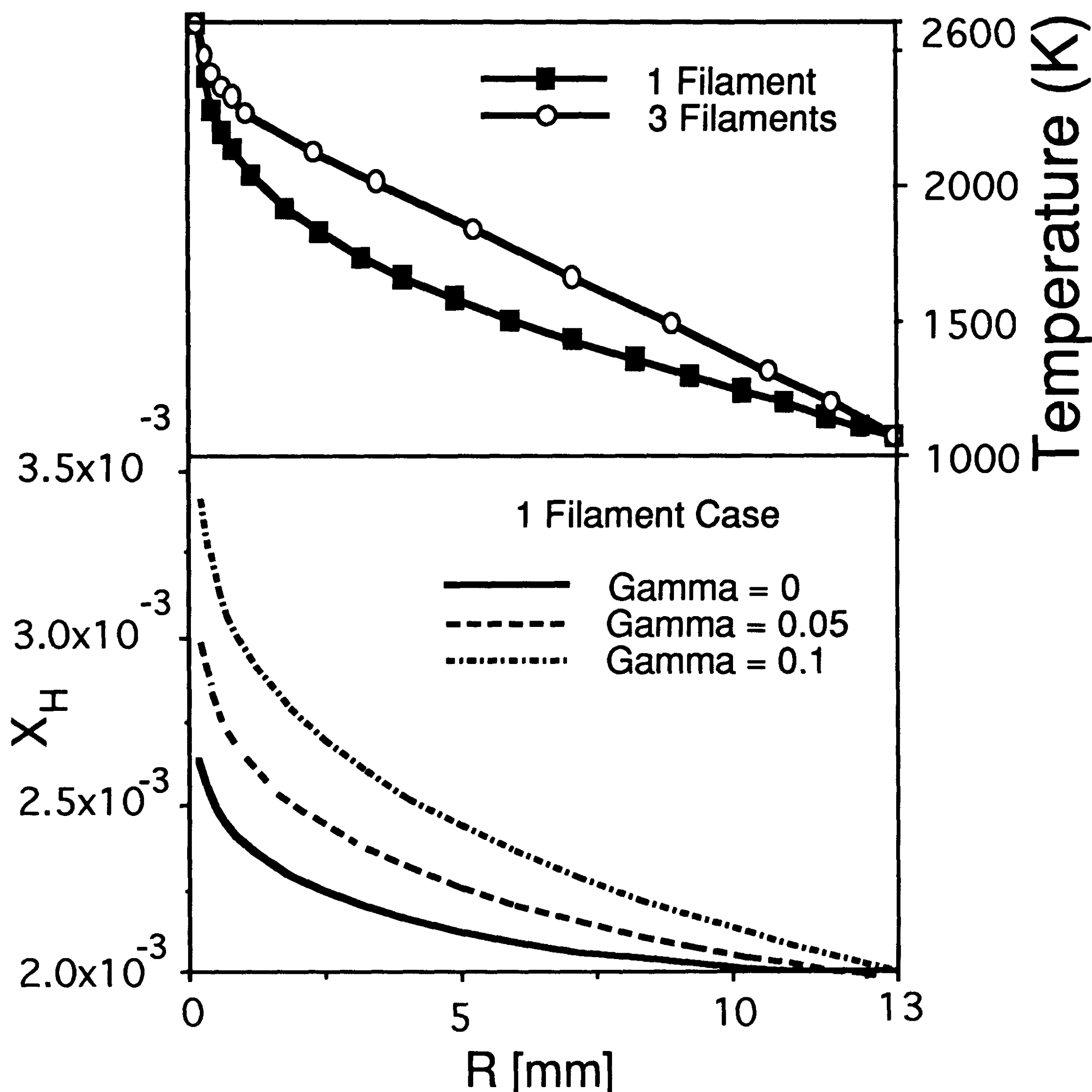

Figure 5-2. Top: Temperature profiles between the filament (R = 0.125 mm) and the substrate (R=13 mm) for the 1 filament (squares), and 3 filament (circles) cases. Bottom: Atomic hydrogen profile between a single filament and substrate for $\gamma = 0$ (solid line), $\gamma = 0.4$ (dashed line), and $\gamma = 0.83$ (dash-dot line).

appreciably effect our results. Varying the filament temperature by ±100 K altered the predicted concentrations by only 25%. Thus, gas-phase chemistry cannot account for the measured concentration of H radicals.

Next, catalytic chemistry at the filament was added to the analysis. It is difficult to model the chemistry of gas-surface reactions due to the scarcity and uncertainty of kinetic

parameters. Therefore as an initial approach, we impose the additional boundary condition that the H atom concentration at the filament, $[H]_{fil}$, be fixed. This constant value of $[H]_{fil}$ was varied until the H atom concentration at the substrate, $[H]_{surf}$, matched the experimental value of Hsu. For a filament temperature of 2575 K, $[H]_{fil}$ is only 30% greater than the value at the substrate, $[H]_{surf}$, indicating that the gas-phase recombination reaction (Eq.1) is slow relative to the time required for diffusive transport to the surface (< 0.001 s).

Proposed models for diamond growth begin with the following two reactions between gas phase atomic hydrogen and the growing surface[25-27]:

$C_D\text{-}H + H_{(gas)} \rightarrow C_D\text{-}* + H_2(gas)$ Abstraction (2)

$C_D\text{-}* + H_{(gas)} \rightarrow C_D\text{-}H$ Addition (3)

where C_D-H and C_D-* are a hydrogen terminated surface site and a surface radical site, respectively. These reactions are expected to be much faster than the addition of carbon species to the surface. Thus the fraction of surface radical sites is controlled by the ratio of these rates.[28] The sum of these two reactions is the exothermic (ΔH_r = -444 kJ / mol H_2) recombination of atomic hydrogen at the growing surface which has been recognized as a major means of heat transfer to the substrate by a number of researchers[12,29-31]. As with chemistry at the filament, the kinetics of reactions (2) and (3) are not well known. Assuming a first order reaction for the destruction of H atoms at the growing surface, the rate may be described using kinetic theory[32] and a sticking coefficient γ:

$$r_{des} = \gamma [H]_{surf} \sqrt{\frac{RT}{2\pi M}} \qquad (4)$$

where R is the universal gas constant and M is the molecular weight of H. Experimental measurements of heat transfer[30] in hot-filament reactors yield estimates of γ between 0.3 and 0.5. Assuming H recombination is the only means of heat transfer to the substrate, an upper bound for γ is estimated to be 0.83.[30] The importance of surface recombination was investigated by varying γ and observing its effect on the$[H]_{fil}$ (Fig. 5-2). All three cases shown have the characteristic concentration profile of diffusion in cylindrical coordinates,

in agreement with experimentally observed profiles.[10,12] Surface recombination increases $[H]_{fil}$ by as much as 30 % in the case of the upper bound. Thus, our results demonstrate that heterogenous chemistry at the filament is the source of atomic hydrogen, and that the growing surface is a heterogeneous sink. Gas-phase chemistry, the source for atomic hydrogen generation in previous models, plays a negligible role in the hot-filament system.

The concentration of H at the substrate is in superequilibrium with respect to the substrate temperature.[9] In previous efforts the value of $[H]_{fil}$ has been assumed to be at or near thermal equilibrium.[13,33] Our calculated $[H]_{fil}$ using γ=0.4 as a function of filament temperature is shown in Fig. 5-3 along with the equilibrium values.[34] A difference of two orders of magnitude is observed over the entire range. Thus, atomic hydrogen production is a kinetically controlled process far from equilibrium.

The data of Celii and Butler[5] was used to develop a kinetic expression for catalytic production of atomic hydrogen. These authors used the resonance-enhanced multiphoton ionization (REMPI) technique to detect atomic hydrogen in a tungsten filament system at 25 torr, where the methane fraction was varied from 0 to 3%. Replotting their data in an Arrhenius format in Fig. 5-4 reveals two distinct regimes of atomic hydrogen production. The regressed slope from the high temperature (>2250 K) data gives an apparent activation energy (E_A) of 150±10 kJ/mol, while at lower temperatures (<2100 K), E_A has a substantially greater value of 330±15 kJ/mol. 330 kJ/mol is typical of values measured for the homogenous reaction in combustion flames.[23] We interpret the value of 150 kJ/mol as the activation energy of a chemical reaction at the filament. Diffusion of species to the filament produce a substantially smaller apparent activation energy (20-40 kJ/mol).[35]

Both activation energies are independent of methane concentration. However, poisoning of the filaments is evidenced by the decreasing value of the y intercept with methane fraction. At typical operating conditions (T_{fil} = 2300-2700 K), the production of atomic hydrogen is dominated by the catalytic process, consistent with our simulations. In addition, an Arrhenius plot of the calculated $[H]_{fil}$ values in Fig. 5-3 yields a similar activation energy of 155 kJ/mol.

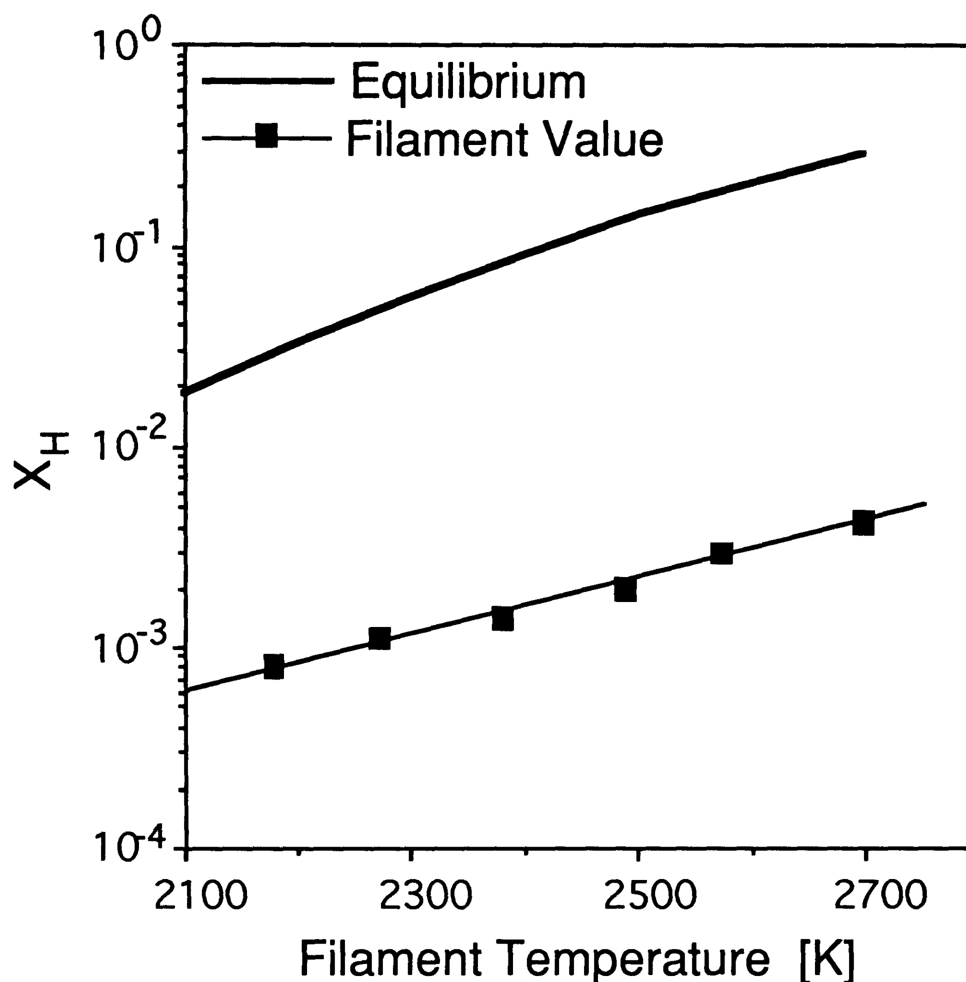

Figure 5-3. Comparison of calculated [H]fil (squares), and equilibrium values (solid lines) as a function of filament temperature. The difference of two orders of magnitude indicates that H atom production is a kinetically controlled process.

We have formed a kinetic expression for the filament-catalyzed production of atomic hydrogen using the Langmuir-Hinshelwood formalism.[35] The three elementary reactions used are reversible, dissociative adsorption of hydrogen on 2 filament surface sites *, reversible adsorption of a hydrocarbon species C_xH_y on a filament site, and desorption of atomic hydrogen. Recent isotopic labeling studies have shown that CxHy species are indeed very reactive on the filament.

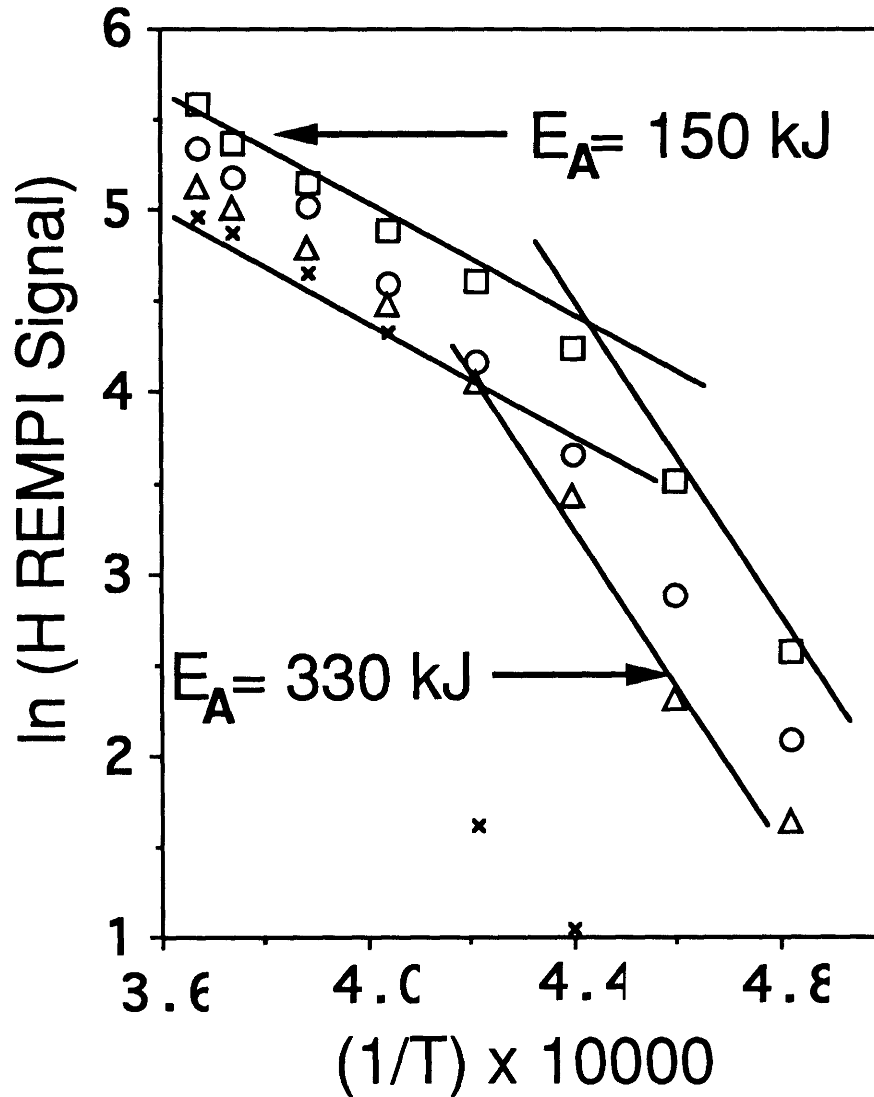

Figure 5-4. Arrhenius plot of atomic hydrogen REMPI signal from Ref. 5 as a function of methane concentration: squares = 0%, circles = 0.5%, triangles = 1%, crosses = 3%. The lines are regressed from data in the two temperature regimes to yield the activation energies.

Assuming hydrogen desorption is the rate limiting step, we obtain the following expression for steady state production of atomic hydrogen,

$$\frac{d[H]}{dt} = \frac{k_{des} \sqrt{K_{H2} P_{H2}}}{(1 + \sqrt{K_{H2} P_{H2}} + K_C P_C)} \qquad (5)$$

where k_{des} is the rate coefficient for desorption, K_{H2}, K_C, P_{H2}, and P_C are the adsorption equilibrium constants and partial pressures of H_2 and hydrocarbons, respectively.

In the absence of methane, Eq. (5) suggests that the production of atomic hydrogen should become saturated above a critical pressure. Indeed, Meier et al.[10] experimentally verified that the hydrogen atom concentration becomes saturated at hydrogen partial pressures greater than 7 torr. Most importantly, Eq. (5) predicts the competitive inhibition phenomena that is observed when hydrocarbons are added to the system.[5,9,11] By fitting Eq. (5) to experimental data[5,11] we obtain a value for $K_C / \sqrt{K_{H2}}$ of 15±5. This ratio is an expression of the relative energies of adsorption of hydrocarbons and hydrogen on the tungsten filament. From our model of Hsu's reactor in the absence of methane, we estimate the atomic hydrogen production rate, $k_{des} = 0.088e^{(-E/RT)}$ [mol / cm^2 s] where the activation energy E is 150 kJ and T is the filament temperature [K].

We have investigated the production and destruction of atomic hydrogen in hot-filament systems. We found that production was controlled by catalysis at the filament, and that recombination on the substrate has an appreciable effect on the gas concentrations. The production at the filament is a kinetically controlled process, far from equilibrium. Analysis of experimental data yielded an activation energy of 150 kJ/mol, and an expression for the production of atomic hydrogen was developed which we will incorporate as we extend our efforts to include methane pyrolysis chemistry.

REFERENCES

1. J. C. Angus and C. C. Hayman, Science **241**, 913 (1988).
2. W. A. Yarbourgh and R. Messier, Science **247**, 688, (1990).
3. F. G. Celii, P. E. Pehrsson, H.-t. Wang, And J. E. Butler, Appl. Phys. Lett. **52**, 2045, (1988).
4. S. J. Harris, A. M. Weiner and T. A. Perry, Appl. Phys. Lett. **53**, 1605, (1988).
5. F. G. Celii and J. E. Butler, Appl. Phys. Lett. **54**, 1031, (1989).
6. S. J. Harris, A. M. Weiner, D. N. Belton and S. J. Schmieg, J. Appl. Phys. **66**, 5353, (1989).
7. F. Jansen, I. Chen, and M. A. Machonkin, J. Appl. Phys. **66**, 5749, (1989).
8. S. J. Harris and A. M. Weiner, J. Appl. Phys. **67**, 6520, (1990).
9. W. L. Hsu, in *Proceedings of the Second International Symposium on Diamond Materials*, edited by A. J. Purdes, B. M. Meyerson, J. C. Angus, K. E. Spear, R. F. Davis and M. Yoder, (The Electochemical Society, Pennington, NJ, 1991), p. 217.
10. U. Meier, K. Kohse-Hoinghaus, L. Schafer and C. P. Klages, Appl. Phys. Lett.

58, 571, (1991).
11. W. L. Hsu, Appl. Phys. Lett. **59**, 1427, (1991).
12. K. Tankala and T. DebRoy, J. Appl. Phys. **72**, 712, (1992).
13. M. Frenklach, J. Appl. Phys. **65**, 5142 (1989).
14. D. G. Goodwin and G. Gavillet, J. Appl. Phys. **68**, 6393, (1990).
15. M. Frenklach and H. Wang, Physical Review B **43**, 1520, (1991).
16. M. A. Kuczmarski, P. A. Washlock and J. C. Angus, at The Applied Diamond Conference, Auburn, AL, (Aug. 1991).
17. K. M. McNamara, C. J. Robinson and K. K. Gleason, J. Vac. Sci. & Tech. A **10**, 3143, (1992).
18. D. H. Levy and K. K. Gleason, J. Phys. Chem. **96**, 8125, (1992).
19. W. L. Hsu, personal communication, (1992).
20 FIDAP User's Manual, Version 6.0, Fluid Dynamics International, (Evanston, IL, June 1991.)
21. G. Strang and G. Fix, *An Analysis of the Finite Element Method* (Prentice-Hall, New York, 1973).
22. *Physical and Thermodynamic Properties of Pure Chemicals: Data Compilation* , eds. T. E. Daubert and R. P. Danner, (Hemisphere, New York, 1989).
23. J. Warnatz, in *Combustion Chemistry*, ed. W. C. Gardiner Jr. , (Springer-Verlag, New York, 1984).
24. R. J. Kee, F. M. Rupley, and J. A. Miller, *Sandia Report* SAND87-8215, (1987).
25. M. Frenklach and K. Spear, J. Mater. Res. **3**, 133 (1988)
26. S. J. Harris, J. Appl. Phys. Lett. **56**, 2298 (1990).
27. M. Frenklach, J. Phys. Chem. **97**, 5794, (1992).
27. W. A. Yarbrough, K. Tankala, M. Mecray and T. DebRoy, Appl. Phys. Lett, **60**, 2068 (1992).
29. C. Wolden, S. Mitra, and K. K. Gleason, J. Appl. Phys. **72**, 3750, (1992).
30. R. Gat and J. C. Angus, submitted to J. Appl. Phys., (August 1992).
31. I. Levine, *Physical Chemistry, Second Edition*, (McGraw-Hill, New York, 1983).
32. T. DebRoy, K. Tankala, W. A. Yarbrough and R. Messier, J. Appl. Phys.**68**, 2424, (1990).
33. STANJAN, Version 3, © Stanford University, (1987).
34. G. F. Froment and K. B. Bischoff, *Chemical Reactor Analysis and Design, Second Edition*, (Wiley, New York, 1990).
35. K. M. McNamara and K. K. Gleason, J. Electrochem. Soc. **L22**, 140 (1993).

CHAPTER SIX

GAS-PHASE REACTIONS IN DIAMOND CVD

(Published in Combustion & Flame, Volume **96**, p. 75, (1994) as "A Reduced Reaction Mechanism for Diamond Deposition Modeling", C. A. Wolden, K. K. Gleason, and J. B. Howard)

ABSTRACT

A brute force sensitivity analysis was used to identify the key gas-phase reactions and species in conditions typical of hot-filament diamond reactors. The model reduction is accomplished by comparing the concentrations of important species (H, CH_3, and C_2H_2) with values calculated using "full" mechanisms in an idealized hot-filament environment. Two proposed mechanisms, containing 24 and 89 reactions, were both reduced to an identical simplified model consisting of 9 species and 9 elementary reactions. Some of these reactions may be grouped into two net reactions, further reducing the mechanism to 6 species and 6 reactions The reduced number of species and reactions will significantly reduce the computational requirements of two and three dimensional simulations.

INTRODUCTION

Reactor modeling has become a powerful tool for investigating complex processes such as combustion[1] and microelectronics processing[2]. Applying this technique to novel processes is an especially useful method to elucidate the underlying phenomena that control these processes. The relatively young field of diamond deposition is an example where reactor modeling can provide insight into a mechanism that is not well understood. Recently detailed kinetic modeling has been used to investigate diamond deposition in premixed flames[3]. Hot-filament chemical vapor deposition is a common method for the production of diamond films, and has been the subject of numerous modeling efforts[4-11].

Most earlier work has focused on chemistry, simulating extensive reaction mechanisms in simplified zero or one-dimensional flow models[4-9]. These efforts have elucidated many concepts involved in diamond deposition, but a more detailed understanding of the problem requires the full treatment of time-temperature history, which is a three-dimensional problem due to the presence of the filaments[12]. In addition, two and three-dimensional simulations provide a tool for achieving film uniformity over large areas and complex geometries. However, simulating the full fluid dynamics with mechanisms containing as many as 50 species becomes computationally restrictive. In two-dimensional simulations the Case Western group[10] used five gas-phase reactions, neglecting the production of acetylene. Our previous two-dimensional simulations focused on the reactions of atomic hydrogen[11].

In this paper, we use a sensitivity analysis to reduce two previously proposed reaction mechanisms. One of the objectives of this paper is to identify the species and reactions which are critically important, information that can be obscured by the inclusion of an excessive number of reactions. Second, the reduction provides a mechanism for two and three dimensional calculations which accurately represents the chemical dynamics, while significantly reducing computational burdens.

MODEL REDUCTION

Several reduction strategies have been developed[1], we follow the approach of using a brute-force sensitivity analysis to identify non-contributing reactions[13]. Reaction reduction has been demonstrated for problems in detonation [14], methane ignition[15], and flame simulations[16].

We have applied model reduction to the two gas-phase mechanisms most often cited in diamond growth. For a reactant mixture of methane and hydrogen, Harris and Weiner proposed a 24-reaction, 12-species reaction mechanism. We use the parameters of ref. [5] and updated in ref. [9]. In addition, Frenklach and Wang[8] proposed an 89-reaction, 39-species reaction mechanism. The most obvious difference between the mechanisms is their size. Harris only considers species up to C_2, while Frenklach includes species as large as naphthalene. Both mechanisms draw extensively from the combustion literature[17].

The most important step in reducing a mechanism is deciding the specific model response(s)[1]. In this work the responses are the concentrations of methyl radical, acetylene, and atomic hydrogen. The first two species are the most commonly cited gas-phase precursors to diamond growth[18,19]. Atomic hydrogen has a critical role in the formation of surface sites, heat transfer, and etching of sp^2 carbon[6,11]. These three species, along with methane and hydrogen which can be determined by completing the carbon and hydrogen inventories, represent all of the major species that are observed in hot-filament systems by molecular beam mass spectrometry[20]. In addition, these are the only species abundant enough to directly participate in diamond deposition[7]. Therefore if a species does not effect the concentration of these selected species, it will not significantly effect diamond growth.

In determining whether a reaction was important we used the following criteria:

$$\left|1 - \frac{[C]}{[C]_{full}}\right| < \varepsilon \qquad (1)$$

where [C] and $[C]_{full}$ are the concentrations calculated by the reduced and full mechanisms, respectively, and ε is an arbitrarily small constant. Choosing $\varepsilon = 0.05$ ensures that deviations caused by mechanism reduction are less than 5%.

Temperature or enthalpic effects were not considered as response variables since the reactive mixture is diluted in excess hydrogen(99%). The Peclet number for heat transfer is very small(10^{-3}), thus conduction dominates. The gas-phase temperature is controlled by the temperature of the reactor surfaces, most importantly the filament and growing surface[11].

The second step of the reduction is choosing the conditions for simulation. We adopt the postulate that the computations used to reduce the mechanism can be achieved using a representative, but greatly simplified geometry and conditions[21]. We have chosen to study the isothermal (T = 2000 K, P = 20 torr) evolution of a methane-hydrogen mixture in a well-stirred reactor. This is the same model that has been used by other researchers[4,5,7] to estimate the concentrations near the filament. At a residence time of $\tau_{res} = 0.1$ s, the mole fractions predicted by these models are similar to those measured experimentally[4,20].

At temperatures is below 1800 K the kinetics are slow relative to the residence time of diamond reactors. Thus, essentially all the gas-phase chemistry happens at or near the filament, and the reactive mixture is rapidly(< 0.001 s) transported to the substrate located approximately 1 cm away. The calculations are carried out using the Sandia perfectly-stirred reactor code[22], and the reverse reaction rates were calculated from the thermodynamic properties from Sandia[23] using the Chemkin package[24].

RESULTS

For $\varepsilon = 0.05$, both mechanisms reduced to the identical 9 species, 9 reaction mechanism presented in Table 6-1. The mechanism can be divided into three parts. First, the production of atomic hydrogen (reaction 1). Second, the interconversion of methane

and methyl radical (reactions 2-4). Finally, methyl radical combines with another methyl or the methylene radical to form C_2H_5 or C_2H_4 followed by hydrogen abstractions which reduce these molecules to acetylene. (reactions 5-9).

TABLE 6-1: Reduced Reaction Mechanism: Comparison of kinetic parameters. Units are cm^3, K, mol, and s.

	Harris[a]	Frenklach[b]
(1) $H_2 + H + H = H_2 + H_2$	$9.7 \times 10^{16}\ T^{-0.6}$	$9.7 \times 10^{16}\ T^{-0.6}$
	$k_{2000} = 1.0 \times 10^{15}$	$k_{2000} = 1.0 \times 10^{15}$
(2) $CH_4 = CH_3 + H$	$9.0 \times 10^{13}\ T^{1.1} e^{-45000/T}$	$1.34 \times 10^{33}\ T^{-6.18}\ e^{-54,366/T}$
	$k_{2000} = 3.6$	$k_{2000} = 8.3$
(3) $CH_4 + H = CH_3 + H_2$	$2.2 \times 10^{4}\ T^{3.0}\ e^{-4430/T}$	$8.6 \times 10^{5}\ T^{2.5}\ e^{-4400/T}$
	$k_{2000} = 1.9 \times 10^{13}$	$k_{2000} = 1.7 \times 10^{13}$
(4) $CH_3 + H = CH_2 + H_2$	$7.2 \times 10^{14}\ e^{-7600/T}$	$1.8 \times 10^{14}\ e^{-7600/T}$
	$k_{2000} = 1.6 \times 10^{13}$	$k_{2000} = 4.0 \times 10^{12}$
(5) $CH_3 + CH_3 = C_2H_5 + H$	$2.8 \times 10^{13}\ e^{-6850/T}$	$4.64 \times 10^{12} T^{0.11}\ e^{-5376/T}$
	$k_{2000} = 9.1 \times 10^{11}$	$k_{2000} = 7.3 \times 10^{11}$
6) $CH_3 + CH_2 = C_2H_4 + H$	2.0×10^{13}	5.0×10^{13}
	$k_{2000} = 2.0 \times 10^{13}$	$k_{2000} = 5.0 \times 10^{13}$
(7) $C_2H_5 = C_2H_4 + H$	$2.0 \times 10^{19}\ T^{-2.6}\ e^{-18,000/T}$	$6.28 \times 10^{37}\ T^{-8.24}\ e^{-22,480/T}$
	$k_{2000} = 6.5 \times 10^{6}$	$k_{2000} = 5.2 \times 10^{5}$
(8) $C_2H_4 + H = C_2H_3 + H_2$	$1.5 \times 10^{14}\ e^{-5133/T}$	$3.16 \times 10^{11}\ T^{0.7}\ e^{-4029/T}$
	$k_{2000} = 1.2 \times 10^{13}$	$k_{2000} = 8.6 \times 10^{12}$
(9) $C_2H_3 = C_2H_2 + H$	$4.0 \times 10^{24}\ T^{-4.7}\ e^{-20,000/T}$	$2.3 \times 10^{24}\ T^{-4.0}\ e^{-25,000/T}$
	$k_{2000} = 5.5 \times 10^{4}$	$k_{2000} = 5.4 \times 10^{5}$

[a]Parameters from references [5], except reactions 2, 7, and 9 are from reference [9].
[b]Parameters from reference [8], except reactions 3 and 9 which are determined from thermodynamics[23] and the reverse rate coefficients provided in reference [8].

Comparison of the reduced and full mechanisms is shown in Figure 6-1 for both models. Both reduced mechanisms reproduce the results of the full model very well over 4 orders of concentration, which includes values measured in hot-filament systems[20]. The

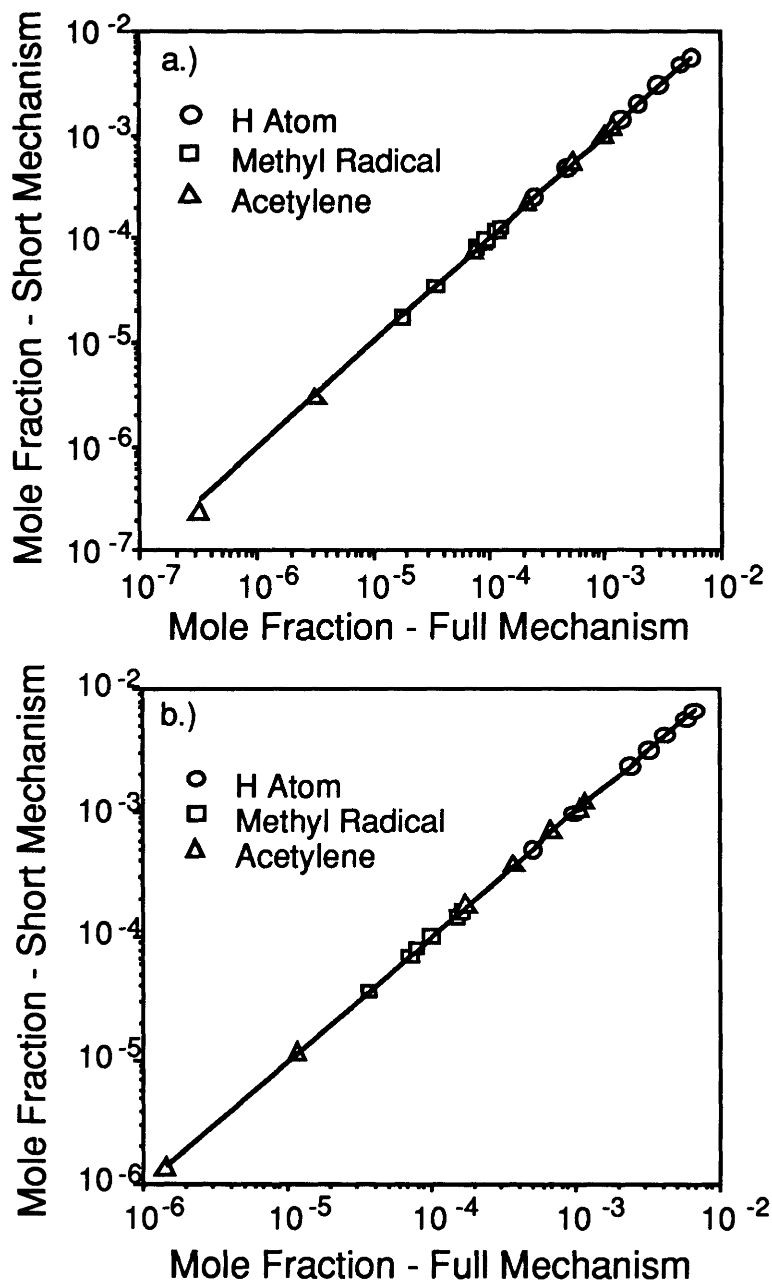

Fig. 6-1: Concentrations of atomic hydrogen, methyl radical, and acetylene calculated from the reduced mechanism versus the values from the complete mechanisms of a.) Harris and Weiner [5 ,9], and b.) Frenklach and Wang [8]. The solid line represents an exact one to one relationship. Conditions: P = 20 torr, T = 2000 K, 0.01 s $\leq \tau_{res} \leq$ 0.1 s.

results correspond to residence times ranging from 0.01 to 1 s. For τ_{res} < 0.01 s the composition is essentially unreacted, and for τ_{res} > 1 s the values approach equilibrium. The results are not sensitive to pressure as simulations repeated at 50 and 100 torr yielded identical results.

DISCUSSION

The reduction of two competing models to the same 9 reaction mechanism raises the question of how they compare to each other. Figure 2 shows the ratio of the three species as calculated using the parameters of Harris and Frenklach. Over the range examined, the predictions of Harris are 0 to 50 % less than Frenklach for each of the three species, a small difference for quantities that are typically evaluated on a logarithmic scale. Neither model is "tuned" in favor of a particular species, however the parameters of Frenklach are slightly

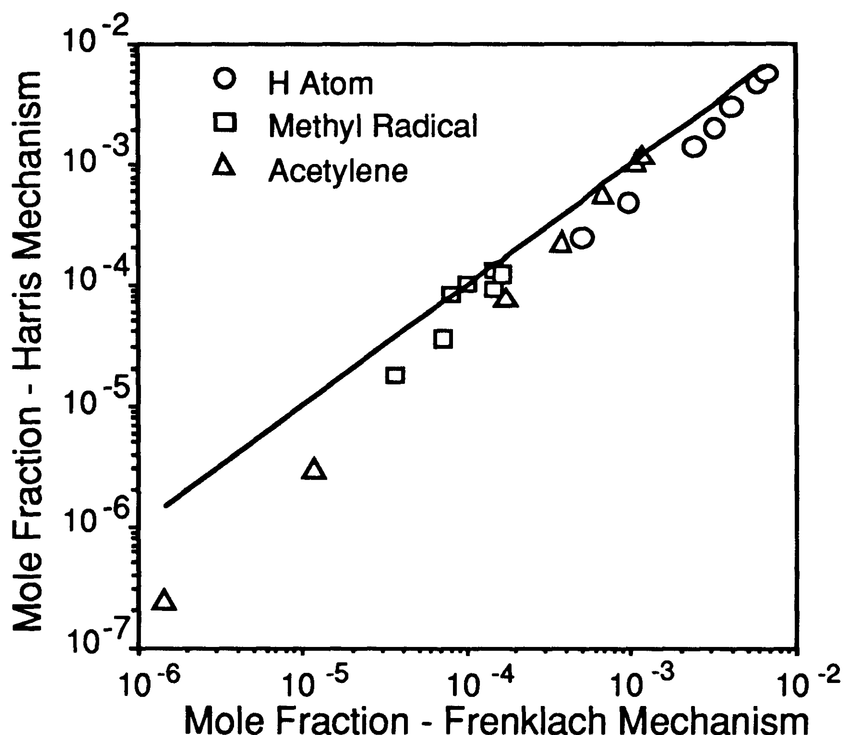

Figure. 6-2: Concentrations of atomic hydrogen, methyl radical, and acetylene calculated from the Harris mechanism [5,9] versus values calculated from the Frenklach [8] mechanism. The solid line represents an exact one to one relationship. Conditions: P = 20 torr, T = 2000 K, 0.01 s $\leq \tau_{res} \leq$ 0.1 s.

"faster". The similarity was somewhat unexpected since an inspection of the kinetic parameters of both groups revealed a number of discrepancies (for example, the rate coefficient for the unimolecular decomposition of ethane into two methyl radicals differed by 3 orders of magnitude at 2000 K). However, of the reactions where coefficients differed significantly, none had a substantial impact on the important species.

Performing a sensitivity analysis of the kinetic parameters in Table 1 reveals that the mechanism is very sensitive to the rate coefficient of reaction 2, the unimolecular decomposition of methane. In fact, the discrepancies observed in Fig. 2 may be almost entirely rectified by simply using the same kinetics for reaction 2, even though the authors only differ by a factor of 2 at T = 2000 K (Table 1).

In addition, the analysis revealed that the mechanism is insensitive to the parameters of reactions 7-9. Once methyl and methylene combine they are rapidly converted to acetylene. These reactions are nearly irreversible since at these conditions 99% of the carbon will be converted to acetylene at equilibrium[23]. Summing the elementary reactions 5 and 7-9 yields the net reaction,

$$CH_3 + CH_3 \Rightarrow C_2H_2 + H_2 + 2H \qquad \text{(Reaction 5*)}$$

Similarly, adding reactions 6, 8, and 9 yield the net reaction,

$$CH_3 + CH_2 \Rightarrow C_2H_2 + H_2 + H \qquad \text{(Reaction 6*)}$$

The forward rate coefficients for reactions 5* and 6* are the same as for reactions 5 and 6(Table 1), and these are treated as irreversible reactions. To demonstrate the speed and irreversible nature of these reactions the simulations were repeated replacing elementary reactions 5-9 with net reactions 5* and 6*. The resulting concentrations are within 1% of the values predicted by the elementary reaction scheme(Fig. 1). Therefore, reactions 1-4 generates a mixture of methyl radical and atomic hydrogen, and reactions 5* and 6* control the conversion to acetylene.

A significant number of species have been eliminated in the reduction. First, the inclusion of species containing more than two carbon atoms is unwarranted. The residence times of hot-filament reactors are simply too short to produce larger aromatic compounds. Small hydrocarbon species that were eliminated during the reduction include C, CH, $CH_2^{(1)}$, C_2H_6, and C_2H. Frenklach includes both the singlet and triplet state of the

methylene radical, but including just the triplet state appears satisfactory.

The resulting 9 species, 9 reaction mechanism will significantly reduce the computational burden of 2 and 3-dimensional simulations. Use of the the global reactions 5* and 6* further reduces the mechanism to a 6 reaction, 6 species mechanism. We reiterate that the mechanism reported here is only applicable to a hot filament reactor using methane as the reactants under quality growth conditions ($\leq$ 1% CH_4). Although this work is directed at hot-filament systems, it is expected that the chemistry discussed here will also be critical in DC arc and microwave systems. However at higher temperatures and greater fraction of atomic hydrogen in these systems, one would suspect that some species eliminated here, particularly CH, C, and C_2H, may be important as well.

CONCLUSIONS

We found that both of the gas-phase mechanisms most commonly employed for the modeling hot-filament reactors could be reduced to the identical 9 reaction scheme. The elementary reaction set may be further condensed to a scheme that contains only 6 reactions and 6 species. The reduced mechanism accurately predicts the concentrations of all the major species in an idealized hot-filament environment. A comparison of the two models shows that they are very similar. Employing the model will lead to significant reductions in computational time for two and three-dimensional simulations. We are currently implementing the reduce model into a two-dimensional model of Hsu's reactor at Sandia[20].

REFERENCES

1. M. Frenklach, in *Numerical Approaches to Combustion Modeling*, (E. S. Oran, and J. P. Boris, Eds.), AIAA, 1991, Chapter 5.
2. K. F. Jensen, *J. Crystal Growth* 98:148-166 (1989).
3. E. Meeks, R. J. Kee, D. S. Dandy, and M. E. Coltrin, *Combust. Flame* 92:144-160 (1993).
4. S. J. Harris, A. M. Weiner and T. A. Perry, *Appl. Phys. Lett.* 53:1605-1607 (1988).
5. S. J. Harris and A. M. Weiner, *J. Appl. Phys.* 67:6520-6526 (1990).
6. M. Frenklach, *J. Appl. Phys.* 65:5142-5149 (1989).
7. D. G. Goodwin and G. Gavillet, *J. Appl. Phys.* 68:6393-6400 (1990).
8. M. Frenklach and H. Wang, *Physical Review B* 43:1520-1545 (1991).
9. S. J. Harris, A. M. Weiner and T. A. Perry, *J. Appl. Phys.* 70:1385-1391 (1991).
10. M. A. Kuczmarski, P. A. Washlock and J. C. Angus, in *The Applied Diamond Conference*, Auburn, AL, 1991.

11. C. Wolden and K. K. Gleason, *Appl. Phys. Lett.* 62:2329-2331, (1993).
12. C. Wolden, S. Mitra, and K. K. Gleason, *J. Appl. Phys.* 72:3750-3758 (1992).
13. M. Frenklach, in *Combustion Chemistry*, (W. C. Gardiner Jr., Ed.), Springer-Verlag, New York, 1984, Chapter 7.
14. E. S. Oran, J. P. Boris, T. R. Young, M. Flanigan, T. Burks and M. Picone, *Eighteenth Symposium (International) on Combustion* , The Combustion Institute, Pittsburgh, 1981, p. 1641.
15. M. Frenklach, in *Complex Chemical Reaction Systems, Mathematical Modeling and Simulations*, (J. Warnatz and W. Jager, Eds.), Springer-Verlag, Berlin, 1987, Vol. 47, p. 2.
16. H. Wang and M. Frenklach, *Combust. and Flame* 87:365-370 (1991).
17. J. Warnatz in *Combustion Chemistry*, (W. C. Gardiner Jr., Ed.), Springer-Verlag, New York, 1984, Chapter 5.
18. S. J. Harris, Appl. Phys. Lett. 56:2298-2300 (1990).
19. M. Frenklach and K. Spear, *J. Mater. Res.* 3:133-140 (1988).
20. W. L. Hsu, *Appl. Phys. Lett.* 59:1427-1429 (1991).
21. M. Frenklach, K. Kailasanath, and E. S. Oran, *Prog. Astronaut. Aeronaut.* 105:365-376 (1986).
22. P. Glarborg, R. J. Kee, J. F. Grcar and J. A. Miller, Sandia Report No. SAND86-8209, 1986.
23. R. J. Kee, F. M. Rupley, and J. A. Miller, Sandia Report No. SAND87-8215, 1987.
24. R. J. Kee, J. A. Miller, and T. H. Jefferson, Sandia Report No. SAND80-8003, 1980.

CHAPTER SEVEN

MOLECULAR BEAM REACTOR FOR THE STUDY OF DIAMOND SURFACE KINETICS

(Portions of this Chapter were published previously in Materials Research Society Symposium Proceedings, Volume **334**, p. 123, 1994 as "A Novel Molecular Beam Reactor for the Study of Diamond Surface Chemistry", C. A. Wolden, G. Zau, W. T. Conner, H. H. Sawin, and K. K. Gleason)

ABSTRACT

A novel reactor has been constructed to investigate the fundamental surface kinetics of diamond chemical vapor deposition(CVD). The molecular beam reactor permits independent control of the atomic hydrogen flux, the methyl radical flux and the substrate temperature. The low pressure in the growth chamber (≈ 1 mTorr) minimizes the impact of gas-phase chemistry. The reactive mixture impinging the substrate is sampled through an orifice and analyzed by molecular beam mass spectroscopy. Differential pumping in the two adjacent chambers quenches the beam, allowing quantitative analysis of radical species such as H and CH_3. Deposition was achieved onto seeded molybdenum and silicon substrates.

INTRODUCTION

In previous chapters we have analyzed the heat transfer, mass transfer, and the gas-phase kinetics. The remaining piece of the puzzle is surface kinetics. We have demonstrated that the reaction between atomic hydrogen and the growing surface is very important [1]. Surface kinetic models of diamond growth have impliedthat there are three requisites for diamond growth: a sufficient supply of atomic hydrogen, methyl radical, and the proper substrate temperature [2,3]. The hypothesis has been confirmed experimentally by Chen's group at Harvard [4] who grew crystals from supersonic beams of H atoms and methyl radicals. However, the species flux could not be quantified, and hence no kinetic information was obtained. For models, estimates of surface kinetics have been made by comparison to analogous gas-phase reactions [2] and by Monte-Carlo simulations [3]. However, experimental measurement of the surface kinetics of diamond growth and defect formation remain unknown. As discussed previously, deducing surface reactions from complex conventional reactors is nearly intractable.

To address the situatuation we have designed a reactor that permits independent control of the atomic hydrogen flux, the flux of reactive carbon precursors, and the substrate temperature. By successfully decoupling these variables, we have a unique tool to quantitatively investigate the impact of each parameter on the critical processes of diamond nucleation, growth, and defect formation.

EXPERIMENTAL

The molecular beam reactor is shown schematically in Figure 7-1. The system is housed in a six inch stainless steel tube partitioned into three chambers which are differentially pumped. Deposition occurs in the first chamber which is evacuated by a 1200 l/s diffusion pump. Two different substrates have been used; molybdenum foil mounted on a heater block and heavily doped 1 inch silicon wafers which were heated resistively. In either case, gases impinging on the substrate are withdrawn through a small (≈0.5 mm) orifice into a second chamber which is differentially pumped with a 500 l/s turbo pump. Gas molecules on the center line pass through a skimmer and into the third chamber which contains a mechanical chopper and a quadrapole mass spectrometer (UTI Model 100c). The mass spectrometer is pumped by a 50 l/s turbo, backed by a 200 l/s diffusion pump. The entire system is backed by a Alcatel rotary vein pump.

Under typical operating conditions the total flow rates are ≈10 sccm, with resulting pressures in the reactor being P_1 = 0-3 mTorr, $P_2 \leq 10^{-5}$ torr, $P_3 \leq 10^{-7}$ torr. The mean free path in the last two chambers is such that any molecule sampled though the substrate will pass the skimmer to the mass spectrometer without a collision. This allows quantitative detection of radicals as well as stable species. The output of the mass spectrometer is sent to a lock-in amplifier. The signal was tuned to match the chopper frequency, which allowed the beam signal to be distinguished from the background signal. The disappearance of the lock-in signal when a blocking flag was introduced confirms that the signal originates from the sampling beam.

Substrates preparation involves immersion for 20 minutes in an ultrasonic bath containing a mixture of acetone and submicron diamond powder. Substrate are removed, rinsed with acetone, rinsed with distilled water, and blown dry with filtered air. The procedure does not leave residual powder on the substrate as observed with Scanning Electron Microscopy and results in high nucleation densities and short induction times in a hot filament reactor [5]. Substrate temperature is monitored by a Type J thermocouple clamped on the substrate holder. The actual substrate temperature is hotter and was determined by removing the beams and calibrating the thermocouple with a pyrometer. Stable temperatures between 650 - 950 °C are easily achieved as shown in Figure. 7-2. Radiative heating from the substrate necessitates water-cooling of the reactor walls.

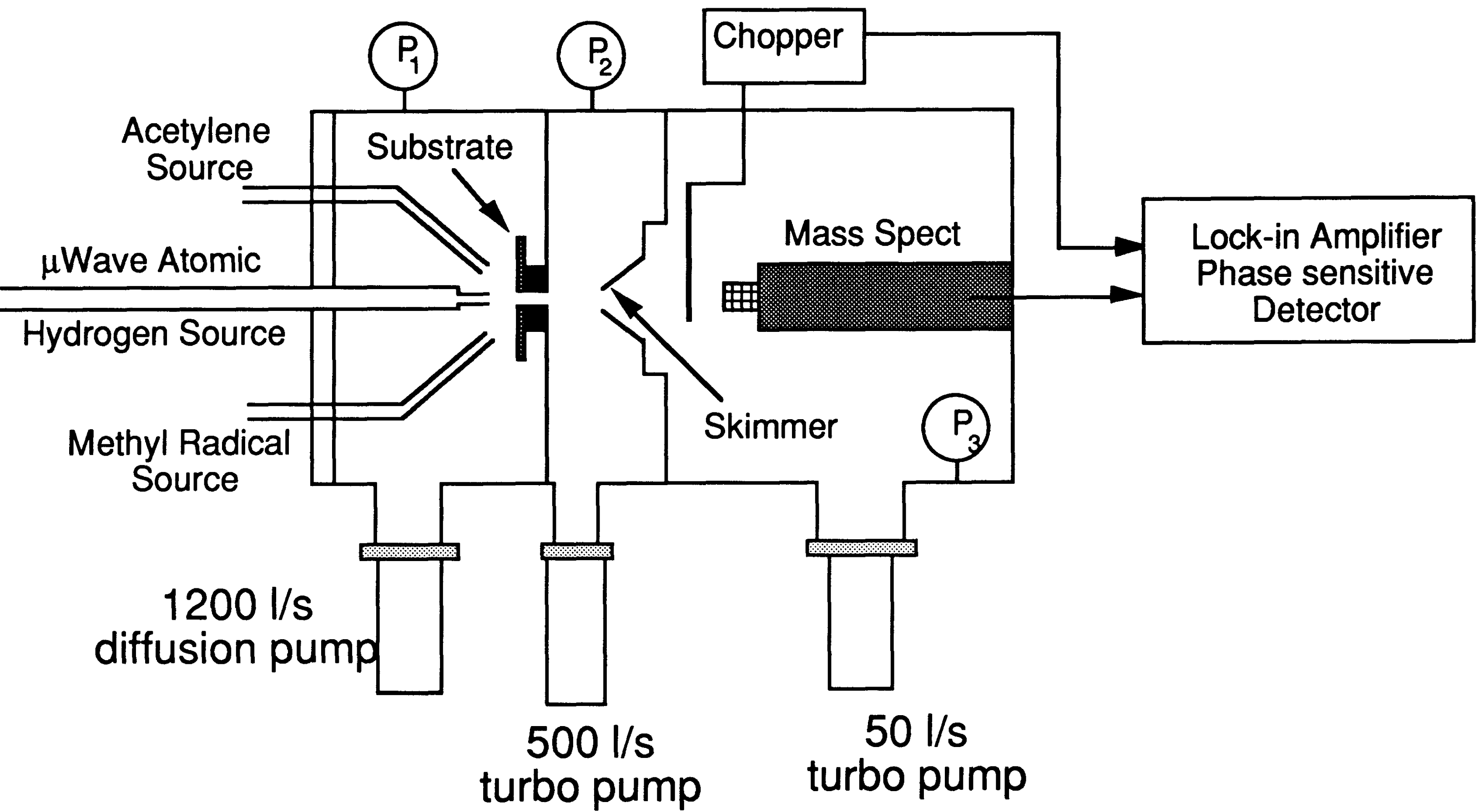

Figure 1: Schematic Drawing of Molecular Beam Reactor

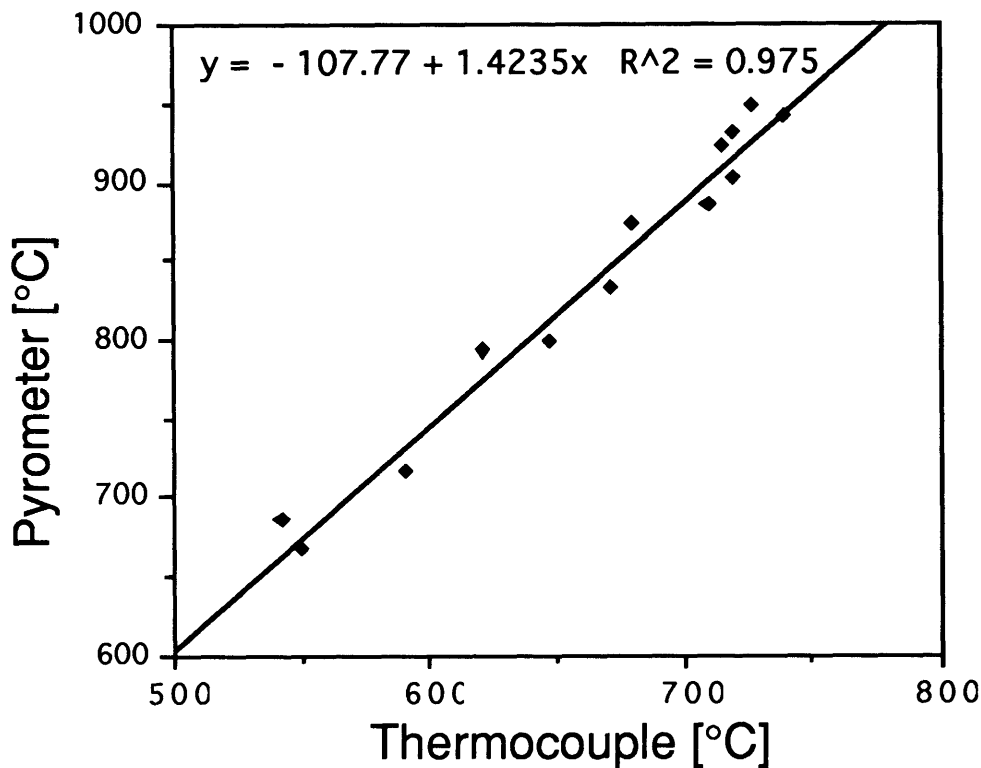

Fig. 7-2: Substrate temperature calibration of thermocouple using optical pyrometry.

The apparatus used to generate the beams is built onto an eight inch Conflat flange that is mounted on the end of the first chamber. The center beam is the remote microwave discharge source for the production of atomic hydrogen. This source is a unique feature of this reactor, generating a stable, high flux of hydrogen atoms inside the vacuum chamber.

The hydrogen atom source is a unique design employing a coaxial microwave waveguide. Microwaves and molecular hydrogen enter on the air-side, are transported into the reactor to a quartz vessel where a glow discharge is ignited. High power densities of >100 W/cm^3 have been achieved, creating near unity dissociation of hydrogen.

A schematic drawing of the coaxial waveguide microwave source developed at MIT [6] is shown in Fig. 7-3. Microwave power from an ASTEX S200 supply is introduced through a coupler (A). Sliding the microwave coupler allows the cavity to be impedance matched to the microwave source used. A threaded tuning slug (B) is positioned so the

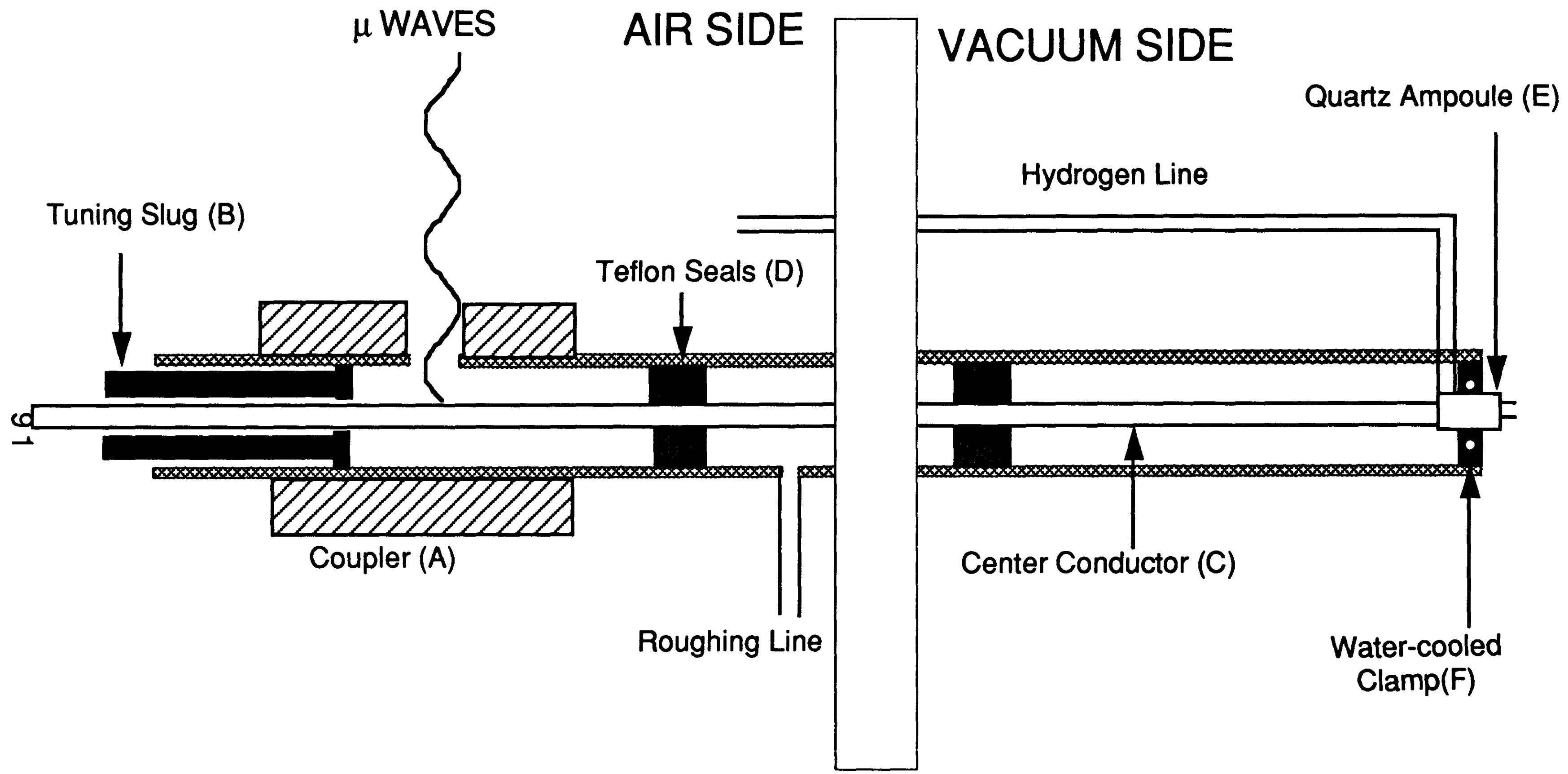

Figure 3: Schematic of remote microwave discharge source

length of the cavity is in resonance. Microwaves are transported along the center conductor (C) which performs as the waveguide. The center conductor is held in place by two teflon seals (D) which also act as vacuum seals. An additional roughing line between the two seals maintains the high vacuum environment.

At the end of the center conductor is a quartz ampoule (E) into which the process gas is introduced. Here the discharge is ignited using a high voltage arc. The ampoule is held flush to the conductor by water-cooled clamps (F). The microwaves are conducted through the plasma, extending the center conductor to the grounded end of the cavity, completing the microwave circuit. The use of the plasma to form the grounded end of the coaxial cavity makes this atom source extremely compact.

Atomic hydrogen is emitted from the nozzle of the glass vessel and transported to the substrate without recombination since the 3 body gas-phase recombination reaction is extremely slow [1]. The design eliminates the worries of wall recombination that occur in flow tubes. By varying the design of the glass vessel we can accommodate a wide range of flow rates. Since the tuning is controlled by the coupler and the tuning slug which are external to the vacuum, complex vacuum motion feedthroughs are not needed. Under typical operating conditions hydrogen is diluted with argon. The presence of argon stabilizes the plasma and by adjusting the volume fraction one can control the discharge characteristics.

Acetylene and methyl radicals are delivered to the substrate through two 3 mm I.D. quartz tubes which are mounted on either side of the atomic hydrogen source at 38° relative to the substrate normal. A number of organic precursors were used to generate methyl radicals by thermal pyrolysis, including di-tertiary butyl peroxide or DTBP $[(CH_3)_3COOC(CH_3)_3]$, methyl amine $[CH_3NH_2]$, iodomethane $[CH_3I]$, acetone, and methane. The last inch of the quartz tube is wrapped with heater wire held in place by ceramic paste. The tube may be heated to a nominal temperature of 600° C as measured by a thermocouple in the ceramic. Acetylene flows through the other tube unheated. All three sources are mounted approximately 1-2 cm from the substrate. The mean free paths at operating conditions are ≥5 cm so gas-phase scrambling is minimized.

For each condition the following procedure was used to search the parameter space for conditions suitable for diamond deposition. First, for a given flow rate the hydrogen plasma was optimized and kept constant. Then two substrate temperatures, typically 700°C and 850°C, were explored by varying the hydrocarbon flow rate. Deposits were analyzed by scanning electron microscopy (SEM) and micro-Raman spectroscopy. The conditons

explored are summarized in Table 7-1

Table 7-1: Experimental conditions explored in the molecular beam reactor. Substrate temperatures varied from 700-900°C in all cases. Micowave power was typically 80 W forward.

Hydrocarbon	Flowrate[sccm]	H2 [sccm]	Argon[sccm]
DTBP[a]	1-5	2-40	2-10
Acetone	1-5	3-5	2-10
Acetylene	2-10	3-40	2-10
Methane	1-8	5-40	2-10
Iodomethane	4-12	10-30	5-10
Methyl Amine	3	30	10

[a] Di-tertiary Butyl Peroxide: $(CH_3)_3COOC(CH_3)_3$

RESULTS

The hydrogen dissociation fraction is characterized using molecular beam mass spectroscopy by monitoring the lock-in signal at 1 and 2 atomic mass units (amu). When running the plasma with hydrogen alone the 2 amu peak decreased by less than 20%. The dissociation was dramatically improved by diluting hydrogen to 10-30% in argon. Under these conditions the amu 1 signal increased 120X when the plasma was ignited. In addition, the discharge was much brighter by visual inspection. However, at these conditions a significant fraction of the molecules are ionized, such that the background noise the 2 AMU signal also increases when the plasma is ignited. Characterization of the ionized fraction is required to fully quantify the dissociation fraction .

When DTBP pyrolyses, 90% decomposes into two methyl radicals and two acetones. The source appears to be operating satisfactorily. The 15 amu (methyl radical) and 43 amu (acetone) increase sharply as the quartz tube is heated above 300 °C. The signals continues to increas euntil it level out at 500°C (Fig. 7-4). For the other precursors there was little decomposition up to the maximum source temperature of 600°C.

Mass spectroscopy confirms the absence of gas-phase chemistry. Monitoring the mass spectra between 12 and 30 amu revealed no observable conversion of methyl radical to methylene or C2 hydrocarbons such as acetylene or ethane when both sources are on. Similarly, the absence of gas phase chemistry is observed when acetylene is the carbon source.

Despite the low absolute pressure, the high dissociation fraction directed nature of the

beams should allow respectable deposition rates. By introducing a gas through the directed beam and comparing the mass spectrometer signal to the case when the gas enters a side port, an enhancement factor between 5 and 15 is observed. Thus, although the base pressure is ≈ 1 mTorr, the effective partial pressures of atomic hydrogen and methyl radical is between 5 and 15 mtorr. These values are similar to fluxes reported for hot-filament systems, which are 40 mTorr and 4 mTorr for atomic hydrogen and methyl radical, respectively [7].

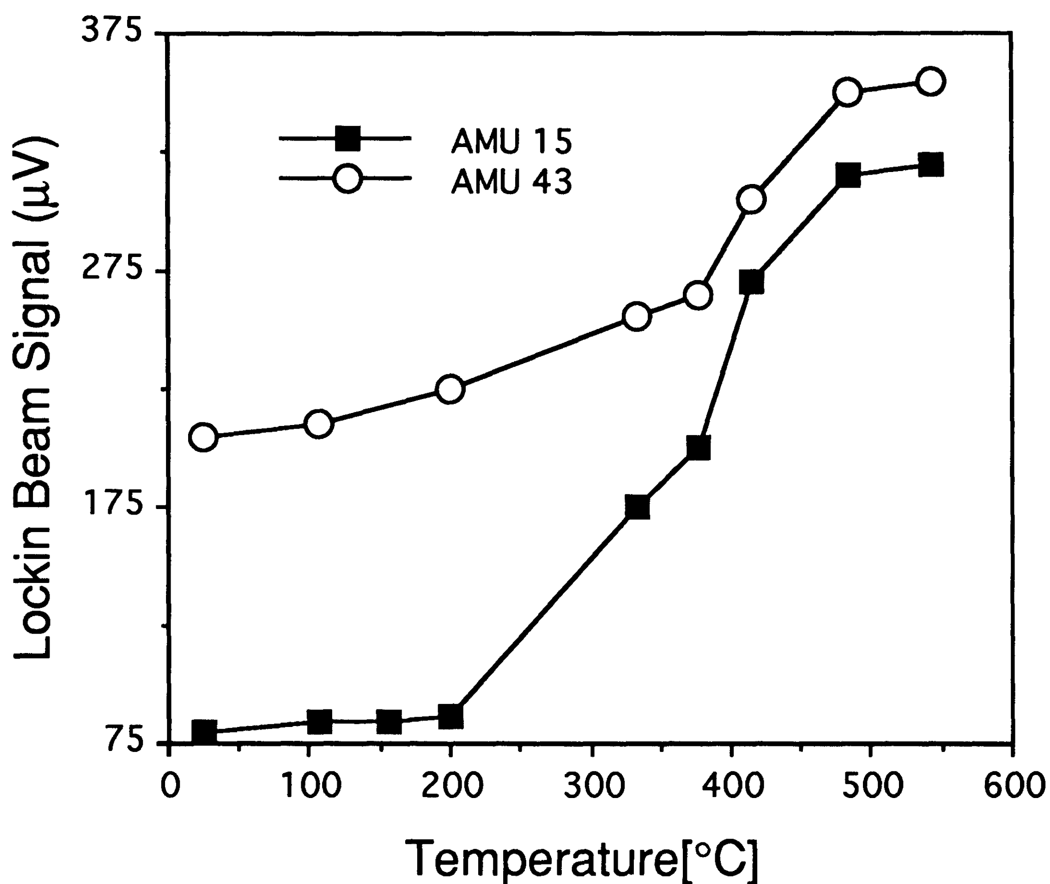

Fig. 7-4: Lock-in mass spectrometer signal for amu 15, 43 as a function of quartz temperature for 2 sccm DTBP.

The deposits have been analyzed by SEM (Fig. 7-5) and show some faceting and structure, although they are not clearly diamond. Samples have also been evaluated by Micro-raman spectroscopy and show spectras characteristic of amorphous carbon and microcrystalline graphite with peaks at 1350 and 1550 cm^{-1} (Figure 7-6). Raman is about 50 times more sensitive to sp^2 carbon [8], so although the films may be highly sp^3 bonded, high quality material has not been obtained in the reactor.

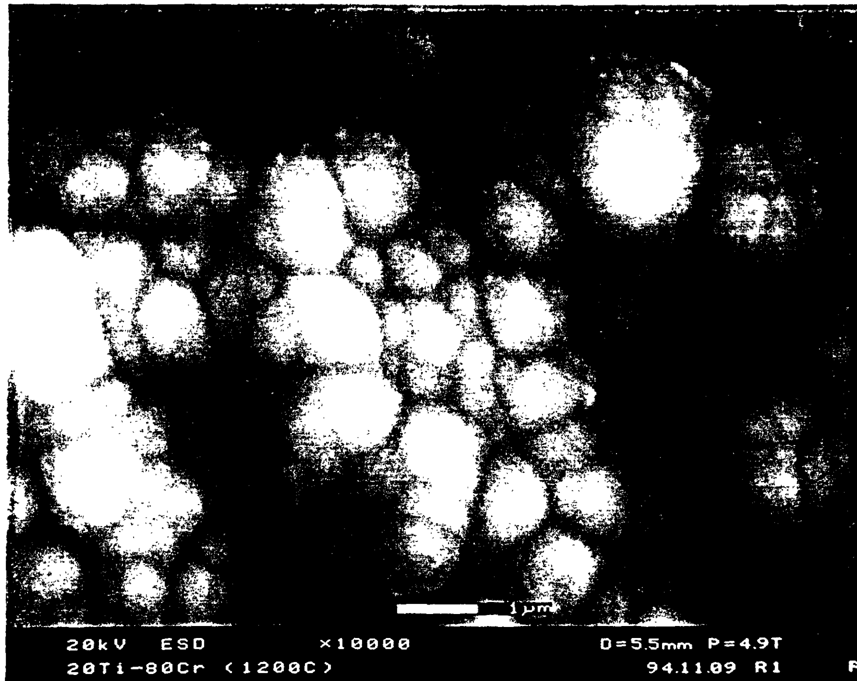

Figure. 7-5: SEM of material deposited under following conditions; Deposition time = 3.5 hours, substrate temperature = 800°C, CH_4 flow = 3 sccm, H_2 flow =30 sccm, Ar flow =8 sccm. Pressure = 2.9 mtorr.

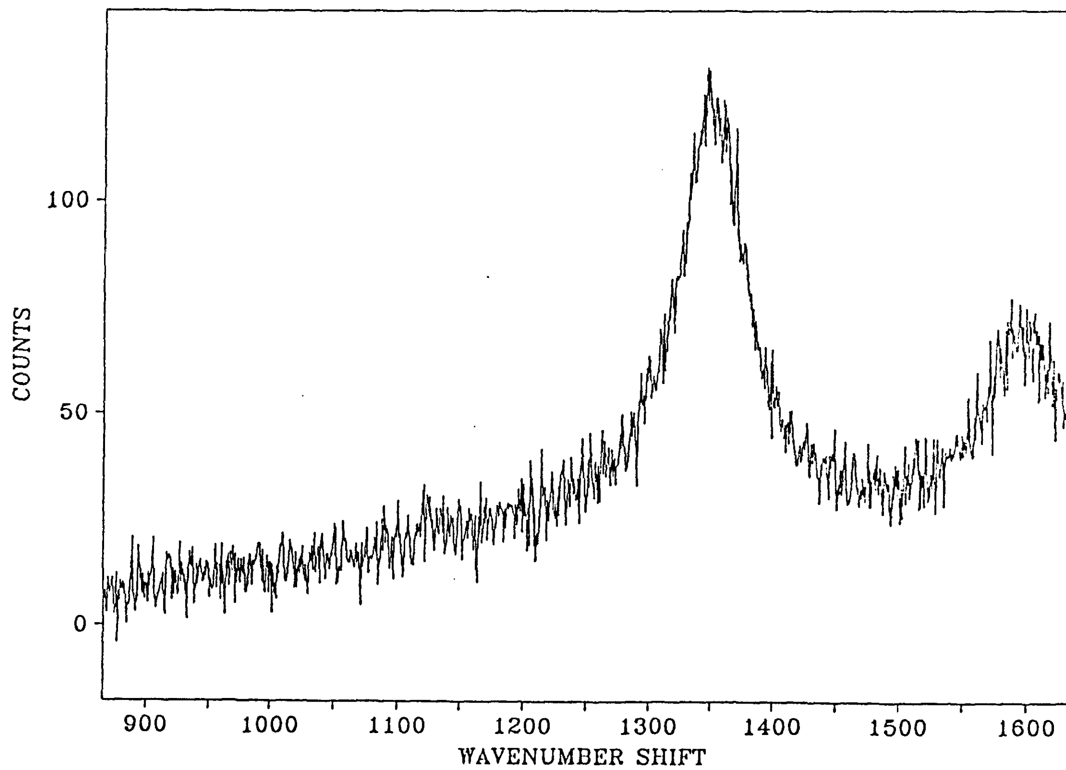

Figure 7-6: Typical micro-raman spectra of material deposited in molecular beam reactor.

DISCUSSION

Direct evidence of the high fraction of atomic hydrogen dissociation is the fraction of carbon necessary to achieve deposition. Figure 7-7 show the region where deposition occurred. In typical systems there is a finite region of concentration space between no growth and amorphous carbon deposition where diamond growth is achieved. In the beam reactor, as carbon fraction is increased conditions switch from no growth to amorphous carbon without a region of diamond growth. The existence of the diamond domain has been argued on thermodymanic grounds [9]. However the fact that the deposition region is shifted significantly up and to the right in Figure 7-7 indicates that carbon deposition is controlled by kinetics rather than thermodynamics. The kinetic basis for this observation is discussed in detail in the following chapter.

A consequence of the high carbon fractions created another experimental difficulty. It was observed that if the hydrocarbon partial pressure in the reaction chamber was greater than 0.2 mTorr, significant amounts of carbon diffused into and deposited on the interior walls of the quartz ampoule. Deposition occurs preferentially on hotter parts of the ampoule that are not in direct contact with the water cooled-clamp. Once formed it was difficult to remove as it is impervious to hydrogen plasma or sulfuric acid treatment, leading me to speculate that it may be SiC. The coating proves very detrimental to the performance of the atom source, thus there is a limit on the hydrocarbon partial pressure that can be explored. In a different system where the hydrogen atom source is used to reduce carbon incorporation in copper films deposited from organometallic precursors, the operating pressure is $\leq 10^{-5}$ and no such films are observed [10].

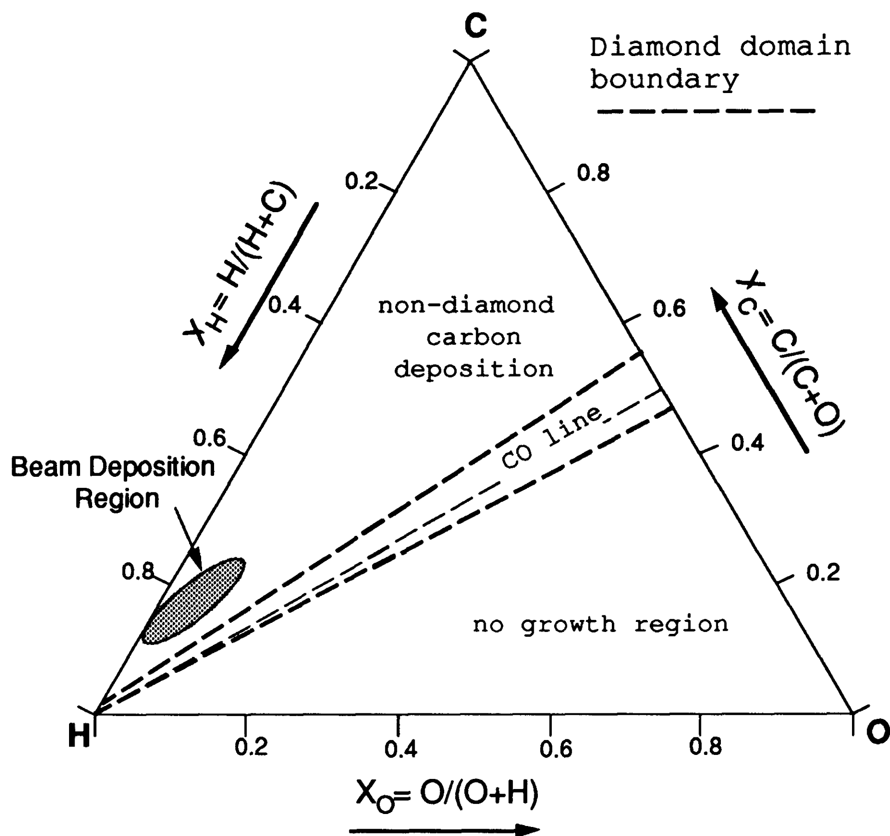

Figure 7-7: Bachmann triangle showing region of carbon deposition in beam system.

CONCLUSIONS

A novel reactor has been constructed that will allow diamond surface chemistry to be studied where all the major variables have been decoupled. Low operating pressures eliminate gas-phase chemistry. Deposition has been achieved from a directed beam of highly dissociated atomic hydrogen and a directed flux of methyl radicals. Although crystals have been formed, the quality is not that of good CVD diamond.

REFERENCES

1. C. Wolden and K. K. Gleason, Appl. Phys. Lett. **62**, 2329 (1993).
2. S. J. Harris and D. G. Goodwin, J. Phys. Chem. **97**, 23 (1993).
3. S. Skokov, B. Weiner, and M. Frenklach, J. Phys. Chem. **98**, 7073 (1994).
4. S. S. Lee, D. W. Minsk, D. J. Vestyck, and P. Chen, Science **263**, 1596, (1994).
5. M. Kwan, personal communication (1994).
6. G. Zau, G. Gibson, H. H. Sawin, Patent Pending (1993).
7. W. L. Hsu, Appl. Phys. Lett. **59**, 1427, (1991).
8. K. M. McNamara and K. K. Gleason, Diamond and Related Mat. **1**, 1145, (1992).
9. N. A. Prijaya, P. K. Bachmann, and J. C. Angus, Diamond and Related Mat. **3**, 129 (1994).
10. T. Chiang, personal communication, (1994).

CHAPTER EIGHT

SURFACE KINETICS: HYDROGEN RECOMBINATION AND METHYL DESORPTION

ABSTRACT

Attempts to deposit high quality diamond in the molecular beam reactor discussed in the previous chapter have been unsuccessful. The major difference between this experiment and conventional systems is the reduced pressure ≈ 10 mTorr. A surface kinetic model was developed in order to analyze the results from the molecular beam reactor. Numerical results indicate two growth regimes. At conventional conditions the growth rate is limited by the rate of hydrogen abstractions, whereas at lower pressures methyl desorption limits growth, causing a dramatic falloff in growth rates as pressure is reduced. Second, the rate of H abstraction is the key reaction underlying all diamond surface kinetic models. An analytical model is developed to predict H atom profiles between filament and substrate. Comparison between the model and recent experimental profiles is used to estimate the overall sticking probability, γ. An analysis of current kinetic models indicates is performed, and the general conclusion is that these models significantly overpredict the rate of abstraction in view of experimental profiles and energy balance considerations. The implications in terms of optimum mixture is discussed.

INTRODUCTION

One of the advantages of the molecular beam system is that it is an ideal case to model as the gas and surface reactions are decoupled. For a specified gas-phase species flux and temperature, one integrates the surface kinetics and obtains the growth rate from the surface concentrations at steady state. We build upon the model developed by Coltrin and Dandy to study diamond growth in DC plasma torches [1] and combustion flame synthesis [2]. The input to the model is substrate temperature, total pressure(flux), and species mole fractions. One of the goals is to identify a kinetic explanation(s) for the lack of growth observed in the molecular beam system. In addition, the model can be used to evaluate the impact of each input parameters of the above. In addition, sensitivity analysis is performed to determine which surface reactions are controlling. Upon identification of these reactions, the kinetics are critiqued with respect to experimental concentration profiles and energy balance considerations.

MODEL FORMULATION

The modeling approach is similar to that used in SURFACE CHEMKIN [3], which was developed by Dandy and Coltrin for use in diamond growing environments [1]. The surface reaction mechanism used for modeling is shown in Table 8-1. As a base case we adopt the mechanism of Coltrin and Dandy which is listed in Table 8-1. The reactions only considers growth from methyl radical and is derived from previously proposed mechanisms [4]. The species designated by (S) indicate the surface species which are shown pictorially in Fig. 8-1. The mechanism is not truly elementary, as the species shown in Fig. 8-1 are not necessarily the exact moieties that are going to be present on the growing surface, but the 6 species represent all the possible configurations of an sp3 hybridized surface species. The goal of the modeling is not quantitative prediction, but to accurately predict trends and identify rate limiting steps [1]. Inspection of the reaction in Table 8-1 show that nearly all reactions involve interaction of a gas-phase molecule and a

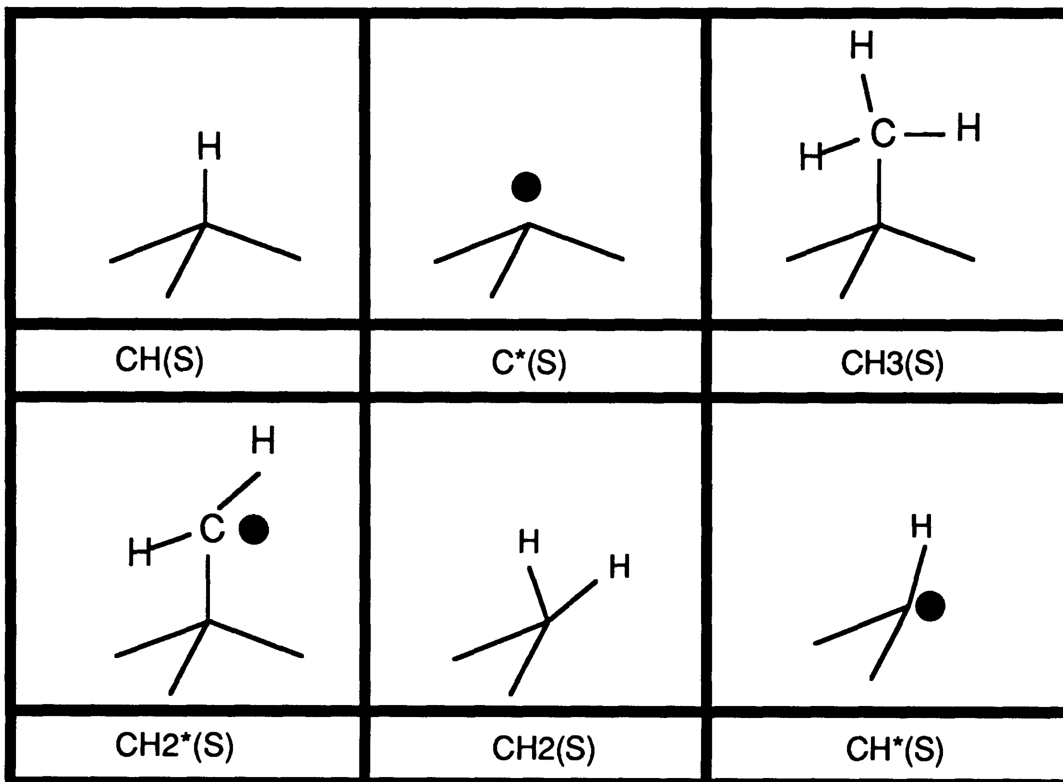

Figure 8-1: Schematic drawing of the surface species considered.

TABLE 8-1: Surface Reaction Mechanism. All reactions reversible.

(S1)	CH(S) + H <-> C*(S) + H2	H abstraction
(S2)	C*(S) + H <-> CH(S)	H addition
(S3)	C*(S) + CH3 <-> C(D) + CH3(S)	Methyl addition
(S4)	CH3(S) + H <-> CH2*(S) + H2	H Abstraction
(S5)	CH2*(S) + H <-> CH3(S)	H Addition
(S6)	CH2*(S) + CH*(S) <-> CH2(S) + CH(S)	Surface Recombination
(S7)	CH2(S) + H <-> CH*(S) + H2	H Abstraction
(S8)	CH*(S) + H <-> CH2(S)	H Addition

surface species. The emphasis is that these reactions control diamond growth in accord with the experimental observations that small changes in gas composition can dramatically effect the characteristics of the films. The analysis is only for the regime of high quality growth as no sp^2 bonded species are included. There are no reactions of methyl radical with a methyl surface species, which would lead to hydrogen incorporation. This is consistent with the ratio of high H atoms to methyl radical that is observed experimentally.[7]

The kinetic parameters used are those presented in reference [1]. A surface species becomes bulk diamond when its is bonded to 4 other carbon atoms. This is accomplished by reaction S3. The reverse of reaction S3, methyl desorption, results in the loss of a bulk diamond carbon (i.e. etching). After solving for the steady state concentrations, the growth rate is calculated by,

$$\text{Growth Rate} = 1.23 \times 10^8 * \{k_{3f}\,[C^*(S)][CH3] - k_{3r}\,[CH3(S)]\} \quad [\mu m/hr] \qquad (1)$$

The factor in Eq. (1) converts from reaction units of [mol cm^{-2} s^{-1}] to the linear growth rate.

The only gas phase species considered are H, H_2, and CH_3. In the molecular beam reactor the fluxes are specified, and no gas phase reactions in accordance with the conditions of the molecular beam reactor. The model can also be used to study real reactors by coupling the surface model to gas-phase chemistry. Alternatively, if species measurements are available, the species flux may be determined from gas theory [5],

$$\text{Flux} = \frac{P_i}{(2\pi RT\, MW_i)^{0.5}} \qquad \left[\frac{mol}{cm^2\ s}\right] \qquad (2)$$

The majority of quantitative species measurements are from hot-filament reactors [6-10]. At the time the molecular beam reactor was constructed, the only *in situ* measurements of both radicals in a diamond CVD system were by molecular beam mass spectrometry [6]. Hsu reported concentrations of 4 x 10^{14} cm^{-3} and 4 x 10^{13} cm^{-3} for atomic hydrogen and methyl radical, respectively. However, recent measurements using high sensitivity absorption spectroscopy report significantly higher values for atomic hydrogen ranging from 1 to 3 x 10^{15} cm^{-3} [7]. These values are similar to those measured using laser induced fluorescence (LIF), although no substrate was present in that study [8]. The presence of the substrate would alter the measured values of H atom if rapid heterogeneous recombination reduces the surface relative to the bulk. Concentration measurements of H and CH_3 are summarized in Table 8-2.

Table 8-2: Summary of H atom and methyl radical concentration measurements. Measurements made between filament and diamond covered substrate. Reactor conditions P = 20 torr, filament diameter was 0.25 mm, filament temperature = 2500 K, 1% methane in hydrogen except where noted.

Worker	Technique	[H] cm^{-3}	[CH_3] cm^{-3}
Childs et al [7][a]	UV Absorption Spectroscopy	1-4 x 10^{15}	2-4 x 10^{13}
Hsu [6][b]	Molecular Beam MS	4.2 x 10^{14}	1.65 x 10^{13}
Celii et al [9][c]	IR Absorption Spectroscopy	n/a	5 x 10^{13}
Harris & Weiner [10][d]	Sampling MS	2-5 x 10^{14}	1.8 x 10^{13}
Schafer et al [8][e]	Laser-Induced Fluorescence	1-5 x 10^{15}	n/a

[a] Range of values due to spatial variations measured. CH_3 and CH measured, H deduced assuming partial equilibrium.

[b] Sampled through 150 μm orifice in substrate.

[c] T_f = 2300-2500°C. Coiled filament, diameter = 0.33 mm. P = 20-30 torr.

[d] 0.75 % methane. H atom measured by recombination enthalpy technique, CH_3 determined using H atom concentrations, mass spectral measurements of CH_4, and using assumption of partial equilibrium. T_f =2400 K.

[e] Range represents a number of filament, temperatures, and carbon fractions configuration. P = 22.8 torr.

The agreement in methyl radical concentration is remarkable considering the differences in reactor configurations and measurement techniques. However, the H atom measurements vary over an order of magnitude. Of the work summarized in Table 8-2, the LIF study [8] directly measures [H], and it is the only procedure calibrated by a controlled flowtube study[11]. Hsu [6] measured atoms impinging upon the growing surface with molecular beam mass spectrometry. Whether this low value may be explained by rapid

heterogeneous recombination is analyzed in detail later in the chapter. The values of Harris and Weiner [10], are more suspect for two reasons. First, the data rely on a enthalpic technique that requires knowledge of γ, the reaction probability of H with diamond. The error in this parameter is value 100% [12]. In addition, the reported values are further complicated by a transport analysis [12]. The data of Childs et al [7] is deduced from direct measurements of CH and CH_3 and well known equilibrium constant, with an absolute error of 40%. We note that the required H atom concentration for a hot filament system may be 10 times as great as originally believed, which may partially explain the low growth rates observed in the molecular beam reactor.

For our base case we use the data of Childs et al [7]. The reactor pressure is 20 torr, $T_s = 1100$ K, $x_H = 0.02$, $x_{CH3} = 0.0005$ and the balance H_2 after converting their data into mole fractions. The ratio of H:CH_3 measured is about 40, compared with a value of 10 assumed in current modeling efforts [13,14].

RESULTS

Integrating the surface kinetics for the base case one obtains a growth rate of 0.74 μm/hr, which is in a factor of 2 of growth rates measured in our hot-filament CVD reactor. The species fractions at steady state are shown in Table 8-2. The H terminated site, CH(s), and the radical C*(s) account for the majority of the sites.

Table 8-3: Surface species fractions calculated for the base case conditions.

Species	Surface Mole Fraction
CH(S)	0.778
C*(S)	0.221
CH3(S)	3.7×10^{-4}
CH2*(S)	7.7×10^{-7}
CH2(S)	9.5×10^{-4}
CH*(S)	4.8×10^{-5}

The model is examined with respect to total pressure, atomic hydrogen mole fraction, and methyl radical mole fraction. Figure 8-2(a) shows the dependence on total pressure for the case of a constant ratio of hydrogen to methyl radical. The plain line in Fig. 8-2(a) shows the slope representing a 1 to 1 relationship. As shown the falloff in

growth rates with decreasing pressure is much steeper. Thus the model predicts that decreasing the total flux by a factor of 10 will result in a 100 fold reduction in growth rates.

The impact of atomic hydrogen is shown in Fig. 8-2(b). The slope is very close to the 1:1 relationship. This is in contrast to a similar simplified model that predicts the 1:1 relationship for low atomic hydrogen concentrations (< 0.5 % atomic hydrogen), but leveling off and becoming independent of atomic hydrogen above 20% [15]. The model predictions for variations in methyl radical mole fraction fall on top of the 1:1 line, in agreement with other models [15] and experiment [16].

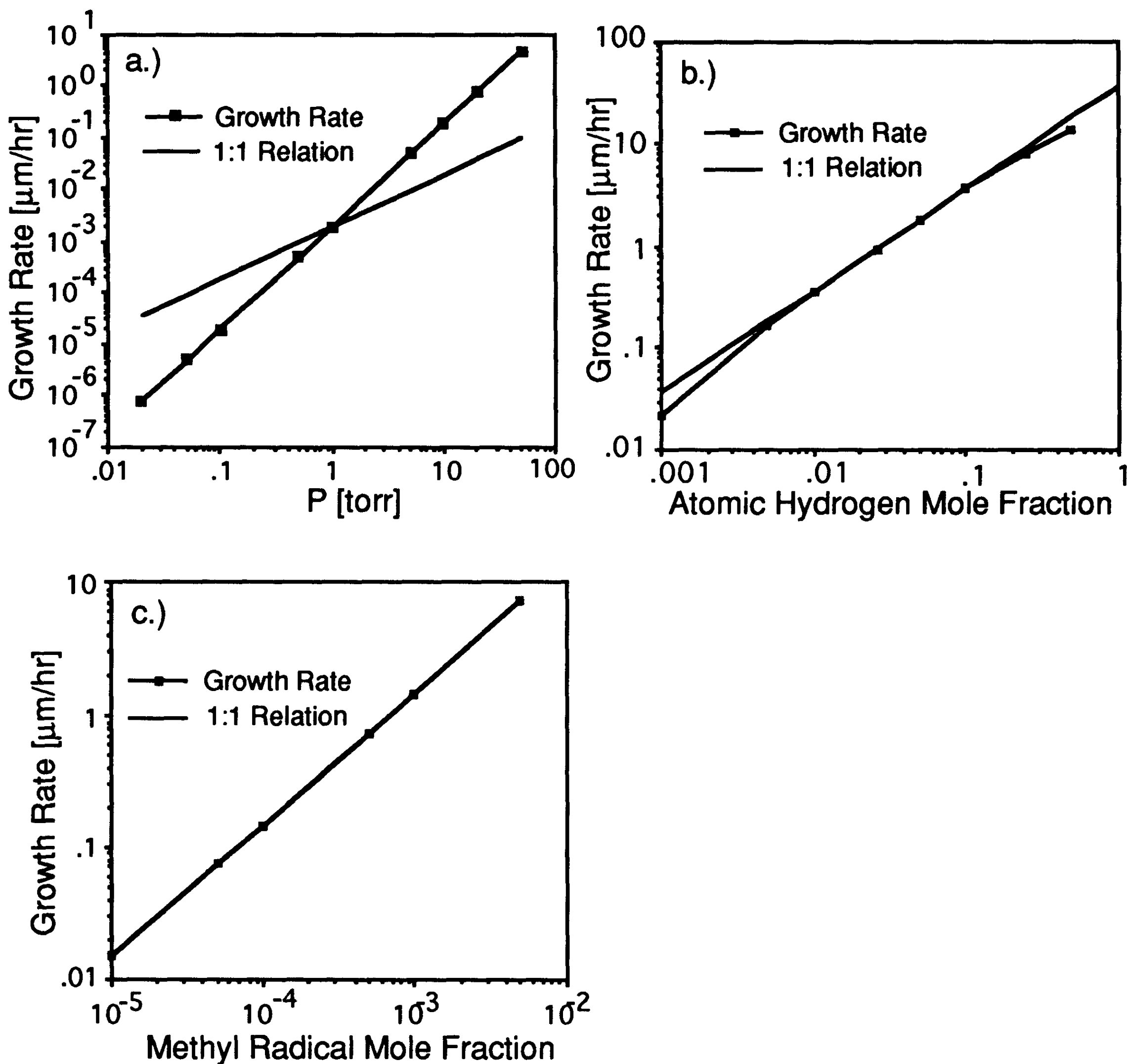

Figure 8-2: Dependence of growth rate on a.) Total Pressure(flux), b.) Atomic Hydrogen Mole Fraction, and c.) Methyl Radical Mole Fraction.

A sensitivity analysis was performed in order to determine the controlling reactions in Table 8-1 that are responsible for the trends presented in Fig. 8-2. The results are very sensitive to the first four reactions, and almost independent of the kinetic parameters used for reactions S5 - S8. The first two reactions are discussed later in more detail, but their impact is basically to control the fraction of open sites, which is directly proportional to the growth rate (Eq. 1). The importance of reactions S3 and S4 both are related methyl radical desorption. In the case of reaction S3 the kinetic parameters are not so important, but rather the equilibrium constant. The radical-radical recombination, k_{3f}, is a facile reaction, while k_{3r} is determined through the equilibrium constant.

The importance of k_{3r} is related to the residence time of an absorbed methyl radical. A variety of methods have been used to estimate K_{eq} for reaction S3, a survey of the literature indicates that $K_{eq} \geq 2 \times 10^9$ cm^3 mol^{-1}[1,13,14]. Using reasonable kinetic parameters for methyl absorption one estimates a lower bound of $k_{3r} \approx 2 \times 10^3$ s^{-1}. The upshot is that an adsorbed methyl radical has a surface residence time of $\tau_{CH3} = 0.5$ ms ($1/k_{3r}$), during which it must react with atomic hydrogen in order to become incorporated into the lattice or it will just thermally desorb. Figure 8-3 plots the total number of collisions with H atoms an absorbed methyl radical will experience during its surface residence time as a function of atomic hydrogen partial pressure.

At typical hot-filament conditions there will be ≈40 such collisions as compared to <5 at the conditions of the molecular beam reactor. This offers an explanation why such slow growth was observed and explains why the dramatic falloff predicted in Fig. 8-2(a) is observed. The forward reaction of S3 is proportional to pressure while the reverse is constant. In addition, it explains why the model predicts the near linear relationship with atomic hydrogen and the sensitivity to S4. Increases in [H] or k_{4f} directly increase the rate at which absorbed methyl radicals react, increasing there opportunity to be incorporated in the lattice.

There is experimental support for Fig 8-2(a) as well. The data of Kondoh et al [26] is reproduced in Figure 8-4. Their reactor was a specialized hot-filament system in which each operating parameter could be varied independently. Above 10 torr the growth rates is essential constant, while it falls off dramatically as P is reduced below 5 torr. This consistent with the hot-filament LIF measurements of Schafer et al. [8], who observed that radical concentration saturates above 8 torr, and becomes proportional to P at lower pressures. It has been proposed that methyl desorption is also responsible for the decline

in growth rates in hot -filament systems at substrate temperatures > 900°C [27].

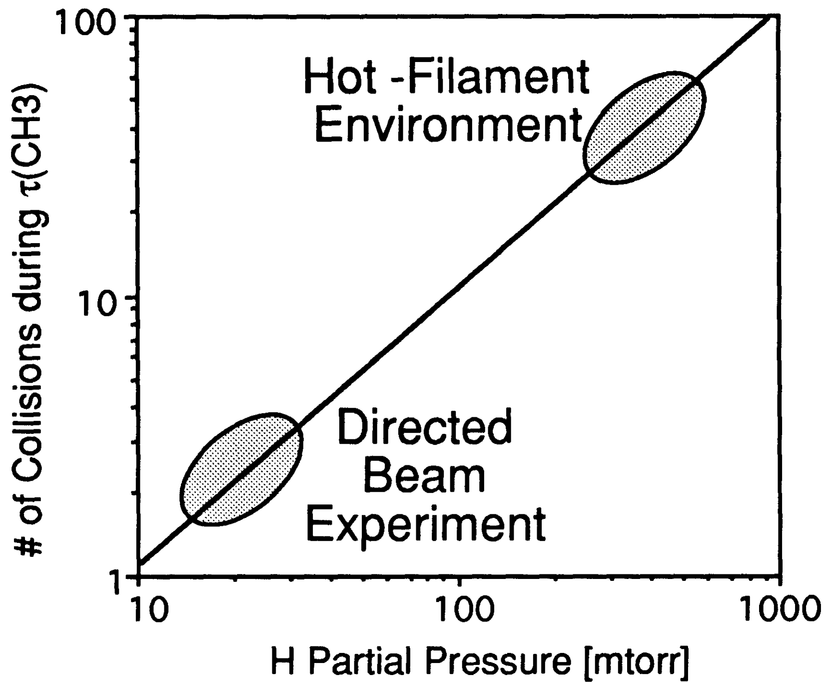

Figure 8-3: Plot of number of collisions between atomic hydrogen and an absorbed methyl radical during it's lifetime as a function of atomic hydrogen partial pressure.

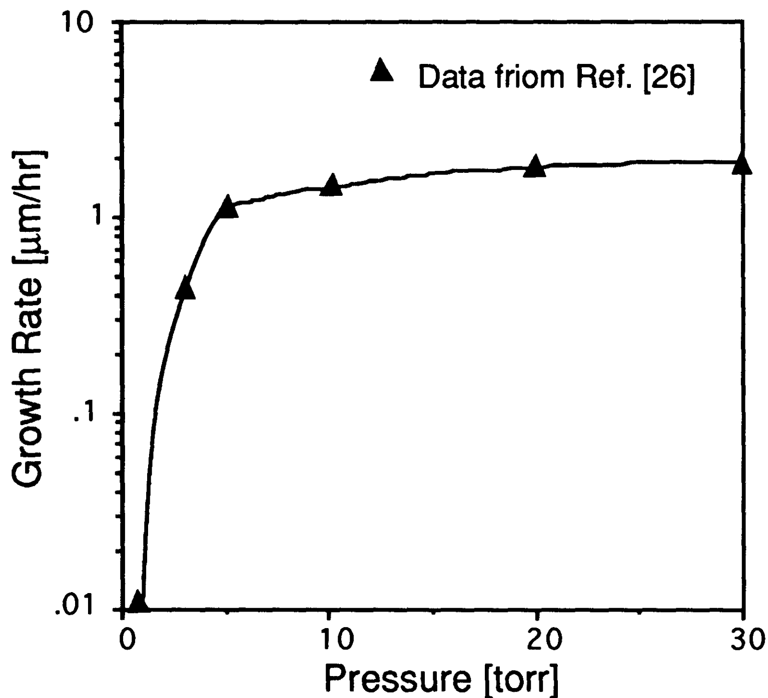

Figure 8-4: Experimental observation of falloff in growth rate with pressure. Ref. [26]

Although the model is sensitive to reaction S1 and S2, it is important to clarify that these reactions do not contribute to the phenomena shown in Figs. 8-2 and 8-4. The variations with operating conditions are due to S3 and S4, while S1 and S2 only impact the absolute rate that is predicted. The conclusion of the sensitivity analysis is that predicted growth rate is directly proportional to k_{1f} and inversely proportional to k_{2f}. Since 99% of surface sites are either CH(s) or C*(s) (Table 8-3), and reactions 1 and 2 are much faster than the other reactions, the kinetics of these two reactions control the fraction of radical sites according to the relation,

$$\text{Fraction C*(s)} = \frac{k_{1f}\,[H] + k_{2r}}{k_{1f}\,[H] + k_{1r}\,[H_2] + k_{2f}\,[H] + k_{2r}} \qquad (3)$$

As long as the concentration of atomic hydrogen is large enough, the reverse of reactions S1 and S2 are relatively slow and the above relationship simplifies to,

$$\text{Fraction C*(s)} = \frac{k_{1f}}{k_{1f} + k_{2f}} \qquad (4)$$

In all diamond deposition systems, the value of [H] is large enough such that Eq. 4 holds. Since the growth rate calculated by Eq. 2 is directly proportional to [C*(s)], Eq. 4 explains the results of the sensitivity analysis. Most atomic hydrogen reacts through reactions S1 and S2, thus k_{1f} and k_{2f} determine the reaction probability of H on diamond, γ. The parameter γ is one of the surface reactions that has been recently measured [12], [27]. An analytical model is developed in the next section to predict H atom profiles which are compared with experimental profiles, and estimates of γ are presented.

ANALYTICAL SOLUTION

Let us consider the reaction and transport of hydrogen in a hot-filament reactor as the idealization situation framed in cylindrical coordinates as shown in Figure. 8-5. It has been shown previously [18-20] that it is very appropriate to ignore convective flow and gas-phase reactions in these reactors. Thus, the problem is defined by heterogeneous reactions and nonisothermal diffusion. Hydrogen atoms are produced at a filament of radius R_f held at a temperature T_f. Atomic hydrogen is then transported via diffusion to a substrate

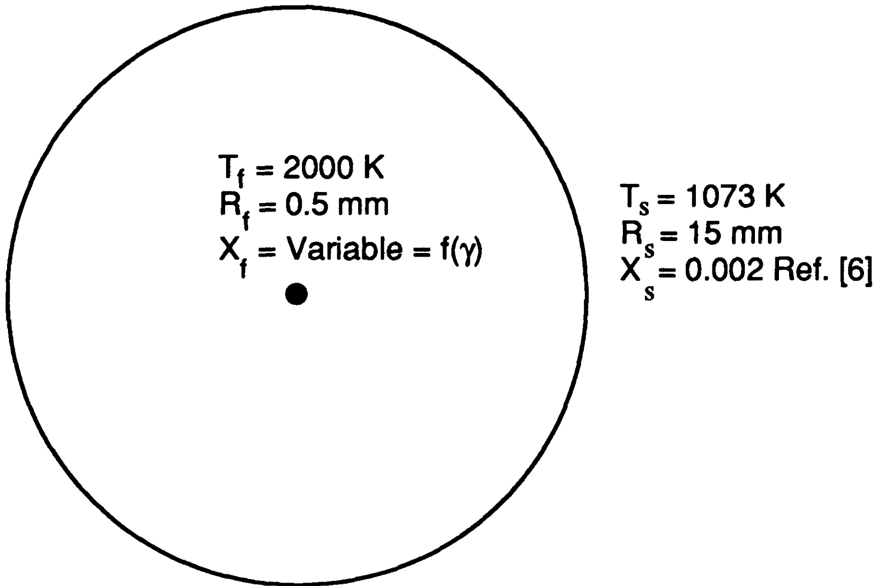

Figure 8-5: Geometry used to solve for atomic hydrogen heterogeneous reaction - nonisothermal diffusion, boundary conditions set in accordance with experimental conditions in Refs. [6, 7].

located at $r = R_s$, and fixed temperature T_s where it reacts with the growing surface. The conservation equation for atomic hydrogen in radial coordinates then simplifies to,

$$\frac{d}{dr}\left(\frac{rcD}{1-x}\frac{dx}{dr}\right) = 0 \tag{5}$$

where
c = concentration [mol/cm^3]
D = H atom diffusivity in hydrogen [cm^2/s]
x = H atom mole fraction

wit the following boundary conditions at the filament and substrate,

$T_f = 2000$ K	$T_s = 1100$ K
$R_f = 0.5$ mm	$R_s = 15$ mm
x_f = Variable = f(γ)	$x_s = 0.002$ (from Ref. [6])

The boundary conditions are adapted from the experimental conditions of Refs.[7], where hydrogen dissociation measurements were made between a 0.25 mm filament at 2500 K and a substrate at 800°C located 15 mm away. Reactor pressure is 20 torr and methane fraction was 1%. The filament boundary conditions reflect the observation that there is a 500° discontinuity between the filament temperature and the gas temperature

within ≈0.5 mm of the filament [17]. The experimental conditions are the same as Hsu [6], except that the filament - substrate separation was 13 mm in that case. The mole fraction at the substrate is fixed at $x_s = 0.002$ in accordance with the molecular beam measurement of Ref. [6]. The mole fraction at the filament is varied, and reflects the reaction probability at the substrate, γ, as discussed below.

The geometry is obviously simplified since there is a substrate on only one side of the filament. However, it is a minor simplification as long as the presence of the substrate doesn't radically influence the gas-phase concentrations. Evidence supporting the simplification was provided by Celii and Butler [18], who observed similar H atom REMPI signals when the laser was placed above the filament and when it was between the filament and substrate.

Solving the analogous energy equation yields a logarithmic temperature profile which may be very well approximated using a power law expression as shown in Figure 8-6.

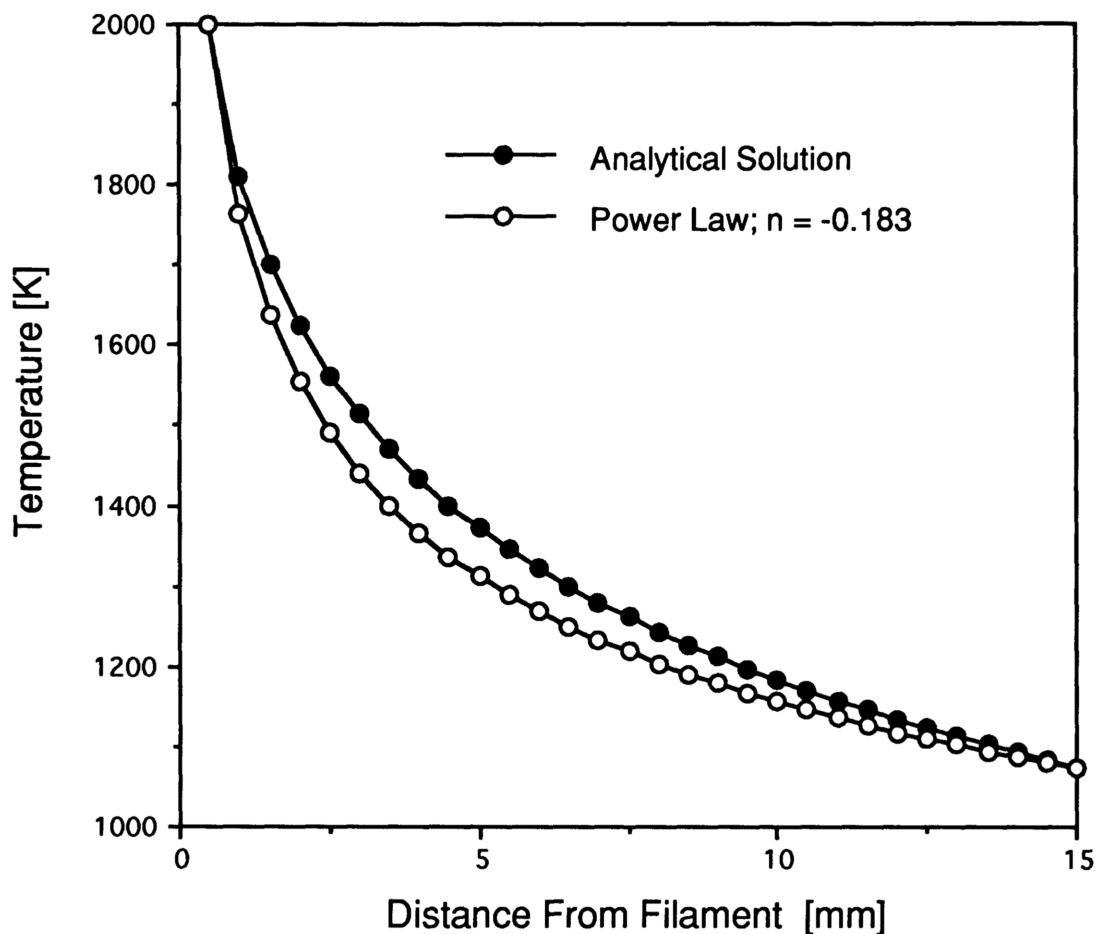

Figure 8-6: Comparison of analytical solution and power law formulation used.

Using this expression for the temperature profile the temperature dependence of the diffusivity and concentration may be recast in terms of r.

$$T = T_f \left(\frac{r}{r_f}\right)^{-0.183} \tag{6}$$

$$D = D_o \left(\frac{T}{T_o}\right)^{1.65} = C_D \, r^{-0.30195} \tag{7}$$

$$c = \frac{P}{RT} = C_c \, r^{0.183} \tag{8}$$

Substituting Eqns. (7) and (8) into Eq. (5), pulling out the constants to obtain,

$$\frac{d}{dr}\left(\frac{r^{0.88105}}{1 - x}\frac{dx}{dr}\right) = 0 \tag{9}$$

Integrating twice, and rearranging for mole fraction, x,

$$x = 1 - \exp(C_1 \, r^{0.11895} + C_2) \tag{10}$$

The constants C_1 and C_2 are evaluated by applying the boundary conditions,

$$C_1 = \frac{[\ln(1 - x_s) - \ln(1 - x_f)]}{0.3492} \tag{11}$$

$$C_2 = \ln(1 - x_s) - C_1 \, r_s^{0.11895} \tag{12}$$

Since x_s is fixed, inspection of Eq. (5) shows that the H atom profile is controlled by the value of x_f which represents production at the filament. The sticking probability, γ, is the fraction of H atoms hitting the surface that react as given by,

$$\gamma = \frac{\text{Flux reacting at Substrate}}{\text{Background Flux at Substrate}} = \frac{\left[\frac{cD}{1 - x}\frac{dx}{dr}\right]_{r = R_s}}{\left[\frac{cvx_s}{4}\right]} \tag{13}$$

In the above equation c and D are defined above, v is the thermal velocity of an H atom, and the gradient dx/dr is obtained by differentiating Eq. (10),

$$\frac{dx}{dr} = -0.11895\ C_1\, r^{(-0.88105)} \exp(C_2) \exp(C_1\, r^{(0.11895)}) \tag{14}$$

The mole fraction at the filament is directly related to the value of γ, i.e. specifying the x_f fixes the value of γ and vice versa as related through equations (10) and (13).

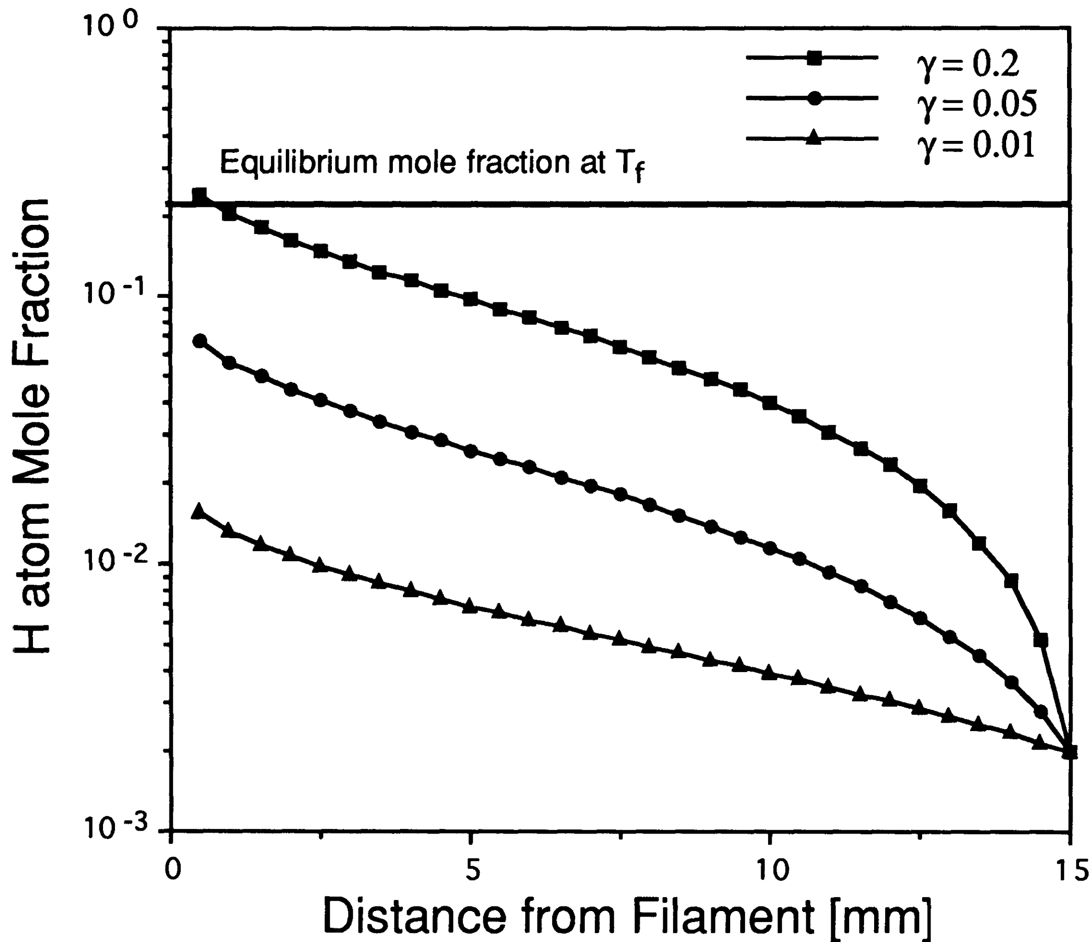

Figure 8-7: Atomic hydrogen profiles as a function of sticking probability.

The atomic hydrogen profiles were calculated by selection of x_f, but are recast as functions of γ in Figure 8-7 since that is the variable of interest. The horizontal line in Fig. 8-7 corresponds to the equilibrium mole fraction of atomic hydrogen at $T_f \approx 2600$ K. Thus, $\gamma = 0.2$ is upper bound for the sticking probability. The impact of γ is reflected in the magnitude of x_f, and the concentration gradient at the substrate.

The calculation of γ is a function of both x_f and x_s (Eq. 10). The dependence of γ was evaluated by using two different choices of x_s. In addition to the value of Hsu, we examine a value 4x greater, which Childs et al[7] obtained when they fitting their concentration profile data. Figure 8-8 plots the filament mole fraction as a function of γ for the two values of x_s.

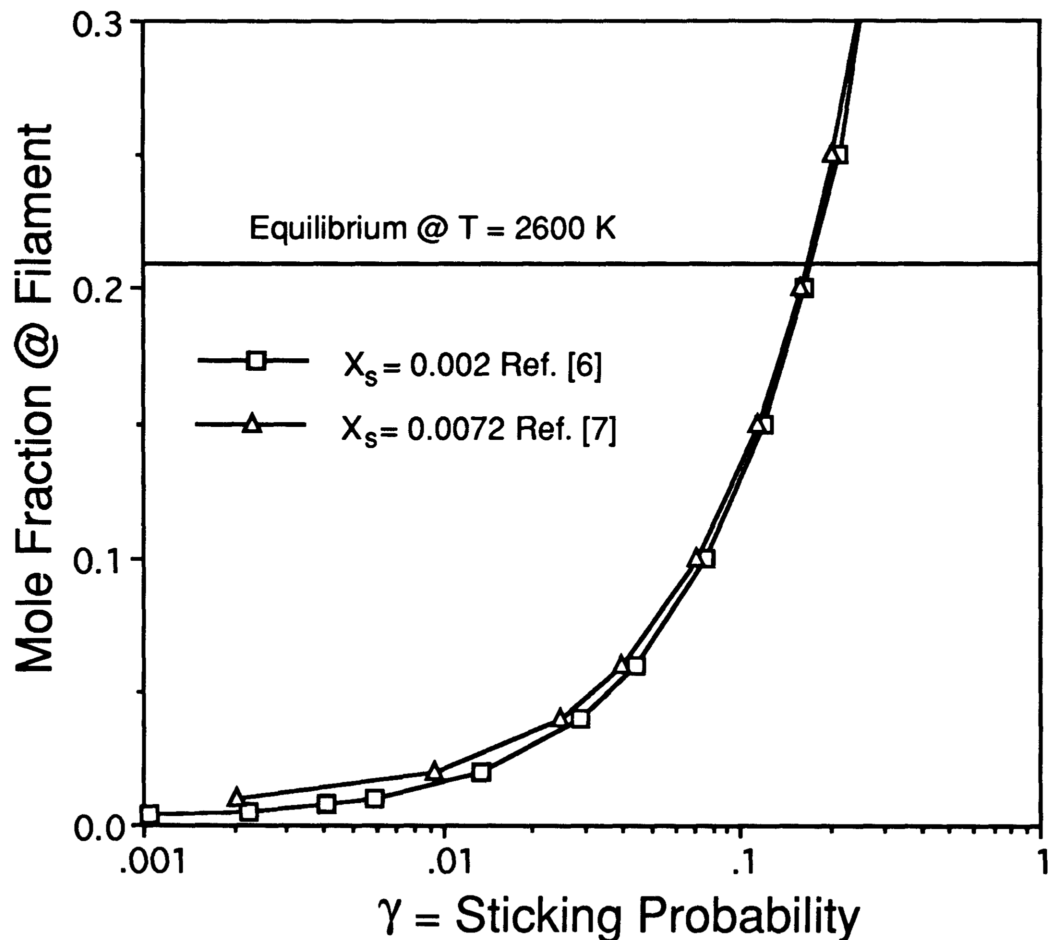

Figure 8-8: Filament mole fraction as a function of γ for two substrate mole fractions.

The first point of Fig. 8-8 is that γ is essentially independent of specification of x_s, at least in the range of interest. The second conclusion is that γ is strongly dependent on x_f and vice versa. Harris's enthalpic technique [12] placed the recombination probability in the range of $0.06 \leq \gamma \leq 0.24$. As Fig. 8-8 shows, the corresponding filament concentrations would vary by more than an order of magnitude. To estimate γ, the predicted atomic hydrogen profiles are plotted along with the experimental profiles of Ref. [7] in Figure 8-9. As before, the 2 plots in Fig. 8-9 represent two different substrate concentrations that we have examined; (a) $x_s = 0.002$, (b) $x_s = 0.0072$. The profiles are consistent with values of $\gamma \approx 0.02$-0.04, significantly less than reported values [12],[27]. In Harris' analysis [12], energy transfer other than H atom recombination (radiation, conduction) is neglected, resulting in an overprediction of γ.

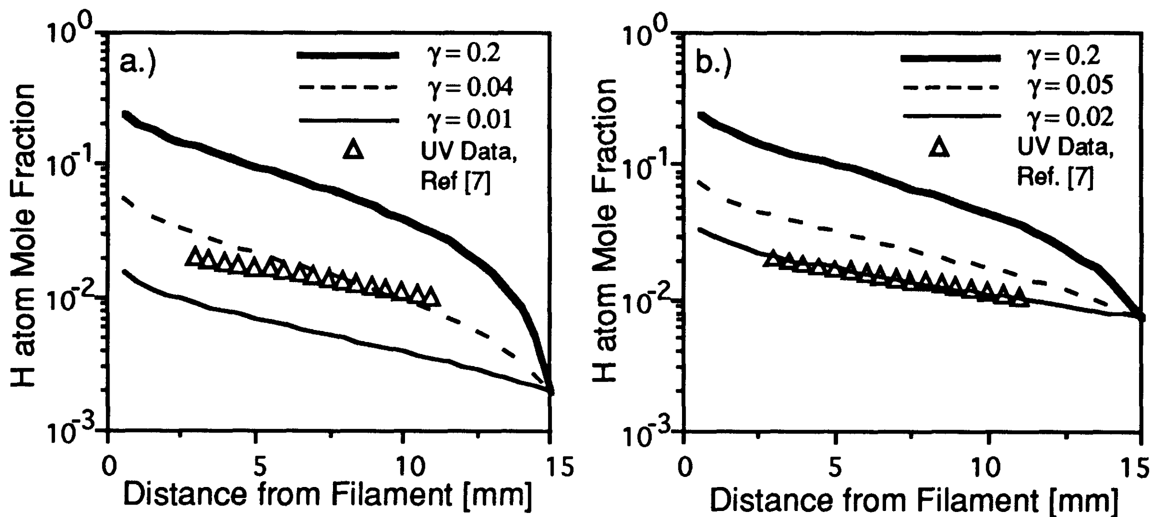

Figure 8-9: Comparison of data of Childs et. al. [7] and 3 profiles controlled by different sticking probabilities, γ. (a) is for a substrate mole fraction $x_s = 0.002$ [6]; (b) is for a substrate mole fraction $x_s = 0.0072$ [7]. Good agreement for $\gamma = 0.04$, $\gamma = 0.02$ respectively.

Although the fitting of γ relies more on the absolute value of [H] than the gradient, the estimated value is also consistent with the measurements Connel et al [17]. In their experiments laser spectroscopy to measure gas-phase temperature and relative H atom concentration with a spatial resolution of 250 μm. They observed no detectable falloff in

the signal in the 2 mm above the substrate, which is a signature for small values of γ (see Fig. 8-6). Since γ is a reflection of the kinetics of reactions S1 and S2, our estimates are compared with values that are obtained using the kinetics of the current surface modeling efforts in the last section.

COMPARISON WITH PROPOSED KINETICS

The value of γ reflects the net effect of reactions S1and S2 through the relation [1],

$$\gamma = \frac{8\, k_{1f}\; k_{2f}}{v\,(k_{1f} + k_{2f})}\,\Gamma \tag{15}$$

where v is the thermal velocity of hydrogen and Γ is the average surface density =5.22×10^{-9} mol cm^{-2}.

As discussed above, surface models are sensitive to these reactions, and their impact on the fraction of open sites. Inspection of the literature places γ in the range from 0.001[21] to 0.26 [13]. For our simulation conditions (20 torr, x_H = 0.02), the surface kinetic formulation described above has been used to evaluate γ using the kinetic parameters of recently proposed models of growth in order to compare with our estimates. As eluded to earlier, recombination of atomic hydrogen is very exothermic (ΔH_r = -104 kcal/mol H_2), playing an important role in substrate heating [22, 23]. One way of monitoring the rate of recombination is by noting the associated heat flux [12]. The associated heat released is simply,

$$\frac{Q_H}{A} = \frac{\Delta H_r\, \gamma\, Flux_H}{2} \qquad [W / cm^2] \tag{16}$$

where the expression for the flux is given in Eq. 1. At diamond growth temperatures heat loss from the substrate is predominantly through radiation. Thus, a physical appreciation of γ is made by converting the associated heat flux to the blackbody temperature required to dissipate the energy assuming the substrate radiates from both sides with unity emissivity,

$$T_B = \left(\frac{Q_H}{2A\sigma}\right)^{0.25} \qquad [K] \qquad (17)$$

where σ is the Stefan-Boltzman constant, 5.67 x 10^{-12} [W / cm^2 K^4]. Allowing radiation from both sides and setting σ = 1 makes the value obtained from Eq. 17 a lower bound. In Table 8-4, the proposed kinetics of various workers are converted into γ, heat flux, and the associated blackbody temperature. Assuming these conditions yield a growth rates of 2 μm/hr (typical for hot-filament systems), the number of H atoms that react per incorporated C atom incorporated is determined and included in Table 8-4.

Table 8-4: A comparison of kinetics by evaluating γ, associated heat flux (Q_H/A), equivalent blackbody substrate temperature T_B, and the number of H atoms required per carbon atom incorporated into the lattice assuming a growth rate of 2 μm/h. Conditions: P =20 torr, T_s = 1200 K, x_H = 0.02, x_{CH3} = 5 x 10^{-4}.

Worker	γ	Q/A [W/cm2]	T_B [K]	H atoms/C
This Work	0.04	6.0	852	1,116
Coltrin,Dandy [1]	0.16	23.9	1205	4,464
Harris, Goodwin [13]	0.26	38.9	1361	7,254
Frenklach et al [14]	0.22	32.9	1305	6,138

A general observation is that all values of γ now used are much higher than the value predicted our analysis of measured H atom profiles, reflected in significant heat load. Examining the blackbody temperatures, the kinetics of all proposed models would result in values above the substrate temperature of 1100 K. This conflicts with the experimental setup used in the concentration measurements, which required electrical heating to maintain the substrate at this temperature [24]. The fraction of open sites varies greatly from model to model, significantly effecting growth rates as the dominant reaction pathway in one mechanism requires 2 adjacent radical sites [13]. In all cases, a very large number of H atoms (~10^3) must react before a single carbon is completely incorporated into the lattice.

As important as the absolute values of the two parameters are for it is the ratio of the two that controls the fraction of free sites where carbon species can add to the surface. For example, Harris and Frenklach use similar values for k_{1f}, and their values for k_{2f} only

differ by a factor of 3, 1 vs. 3 x 10^{13} [cm^3 mol^{-1} s^{-1}]. Usually a difference this small is insignificant, but since reactions S1 and S2 are dominant, tone mechanism predicts 10% radical sites and the other almost 30%. The fraction of open sites may be related to gamma. In Figure 8-10 the fraction of open sites is calculated as a function of γ, assuming the radical recombination reaction k_{2f} = 2 x 10^{13} [cm^3 mol^{-1} s^{-1}]. As mentioned before the fraction of open sites is critical. At high percentage radical sites, the fraction of diradical sites becomes significant, possibly allowing for new growth mechanisms since the stability of absorbed hydrocarbons increases dramatically at diradical sites[13], due to reductions in steric repulsion.

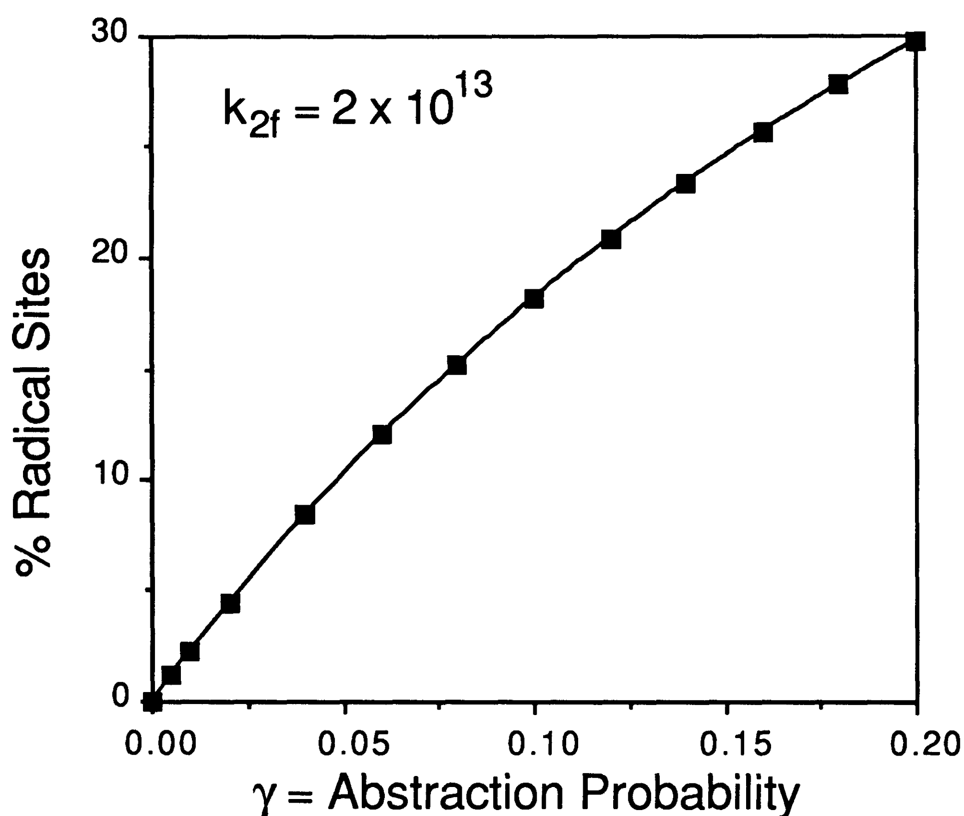

Figure 8-10: Percentage of radical sites as a function of γ assuming k_{2f} = 2 x 10^{13}.

CONCLUSIONS

To summarize, a surface kinetic model was used to evaluate the surface kinetics in the molecular beam reactor. Methyl radical desorption is identified as the rate limiting step and is consistent with experimental evidence. In addition, a sensitivity analysis indicated that the surface model is very sensitive to the hydrogen abstraction and recombination reactions, S1 and S2. These two reactions are responsible for γ, the overall reaction probability of atomic hydrogen and diamond surface. An analytical model of H atom transport and heterogeneous reaction was developed. The predicted gas-phase H atom profiles and maximum concentration are very strong functions of γ. By matching predicted and experimental H atom profiles, γ was estimated to be $\approx$ 0.02 - 0.04. A survey of current kinetic models indicates that proposed values of γ are all > 0.15, which are in conflict with observed concentration measurement, thermodynamics, and energy balance considerations. Since this reaction forms the basis of current growth models, significant re-evaluation may be required.

REFERENCES

1. M. E. Coltrin and D. S. Dandy, J. Appl. Phys. **74**, 5803, (1993).
2. E. Meeks, R. J. Kee, D. S. Dandy, and M. E. Coltrin, Combust. Flame **92**, 144 (1993).
3. M. E. Coltrin, R. J. Kee and F. M. Rupley, Sandia National Laboratory Report, SAND 90-8003, 1990.
4. S. J. Harris, Appl. Phys. Lett. **56**, 2298, (1990).
5. I. N. Levine, *Physical Chemistry, 2nd Edition*, McGraw-Hill, New York (1983).
6. W. L. Hsu, Appl. Phys. Lett. **59**, 1427, (1991).
7. M. A. Childs, K. L. Menningen, H. Toyoda, Y. Ueda, L. W. Anderson, and J. E. Lawler, Phys. Lett. A , **194**, 119, (1995).
8. L. Schafer, C. P. Klages, U. Meier, and K. Kohse-Hoinghaus, Appl. Phys. Lett. **58**, 571, (1991).
9. F. G. Celii, P. E. Pehrsson, H. T. Wang, and J. E. Butler, Appl. Phys. Lett. **52**, 2043, (1988).
10. S. J. Harris and A. M. Weiner, J. Appl. Phys. **75**, (1994).
11. U. Meier, K. Kohse-Hoinghaus, L. Schafer, and C. P. Klages, Appl. Optics **29**, 4993, (1990).
12. S. J. Harris and A. M. Weiner, J. Appl. Phys. **74**, 1022 (1993).
13. S. J. Harris and D. G. Goodwin, J. Phys. Chem. **97**, 23 (1993).
14. S. Skokov, B. Weiner, and M. Frenklach, J. Phys. Chem. **98**, 7073 (1994).
15. D. G. Goodwin, J. Appl. Phys. **74**, 6888, (1993).
16. S. J. Harris, A. M. Weiner, and T. A. Perry, J. Appl. Phys. **70**, 1385, (1991).

17. L.L. Connel, J. W. Fleming, H. N. Chu, D. J. Vestyck, and J. E. Butler, submitted to J. Appl. Phys. (January, 1995).
18. F. G. Celii and J. E. Butler, Appl. Phys. Lett. **54**, 1031, (1989).
19. C. A. Wolden and K. K. Gleason, *Proceedings of the Electrochemical Society*, **93** (17), 236, (1993).
20. C. A. Wolden and K. K. Gleason, Appl. Phys. Lett. **62**, 2329 (1993).
21. M. Frenklach and H. Wang, Physical Review B **43**, 1520, (1991).
22. C. A. Wolden, S. Mitra, and K. K. Gleason, J. Appl. Phys. **72**, 3750, (1992).
23. K. Tankala, M. Mecray, T. DebRoy ans W. A. Yarborough, Appl. Phys. Lett. **60**, 2068, (1992).
24. K. L. Menningen, M. A. Childs, P. Chevako, H. Toyoda, L. W. Anderson, and J. E. Lawler, Chem. Phys. Lett. **204**, 543, (1993).
25. J. Warnatz, in *Combustion Chemistry*, ed. W. C. Gardiner Jr., (Springer-Verlag, New York, 1984).
26. E. Kondoh, T. Ohta, T. Mitomo, and K. Ohtsuka, J. Appl. Phys. **72**, 705, (1992).
27. L. N. Krasnoperov, I. J. Kalinovski, H-N. Chu, and D. Gutman, J. Phys. Chem. **97**, 11787, (1993).

APPENDIX I

RADIATIVE HEAT TRANSFER CALCULATIONS

In this Appendix the m-files are listed that were used in Matlab to calculate shape factors and solve for substrate temperature. The calculations were performed on a DECStation.

```
% Program hb4.m
% Program to predict surface temperatures based on radiative heat flux and
% conduction thru the wafer.Includes hb.sub don't lose heat.

Tf=2600;
%Tf=input('Enter the temperature of the filament: ');
%alpha=input('enter the emissivity of TaC: ')
alpha=.5;
dr=.5;
%dr=input('Enter spacing on grid in cm(<= 1): ');
R=5+dr;                          % Cover the wafer + a border
[x,y]=meshdom(-R:dr:R, -R:dr:R);     % create mesh for cyl

cyl       % Program calc. shape factor F for filament geometry

pret      % Program gives first guess at T profile - Tfr

Tm=Tfr;           % Assume no big gradient in z direction

p=max(size(x)); % Dimension of matrices

% Iterative process for finding T profile

res=200     % so loop starts
conv=20;    % convergence criteria= 0.25K per surface grid point

while res>conv,
%for k2=1:10,  % 10 loops

% Calculate important parameters

em=-2.8324+1.0379e-2*Tm-9.653e-6*Tm.^2+2.963e-9*Tm.^3;   %wafer emissivity
% I=5.67E-12*.45*Tf^4-em.*5.67E-12*Tm.^4;                 %Eb1-Eb2
qr=alpha*em.*F.*Tf.^4;                  % Rad Dist+IxF(shape factor)
qrb=em*2;     % Radiation away from back side


% Recalulate temperature using energy balance-No conduction
res=0;      % start addition from 0
 for i=1:p,
  for j=1:p,
    if (x(i,j)^2+y(i,j)^2)<25.1,   % 25 is edge of wafer
      Tm2(i,j)=(qr(i,j)/qrb(i,j))^.25;              % rad balance
      Tm2(i,j)=(Tm2(i,j)+Tm(i,j))/2;                 % New T
    else
      Tm2(i,j)=Tm(i,j);
    end
```

```
    end
  dT=abs(Tm2(i,j)-Tm(i,j));
  res=res+dT;                    % add residual
  end
 end

% rename new Temps
 for i=1:p,
  for j=1:p,
   Tm(i,j)=Tm2(i,j);            % Rename Tm
  end
 end

res                      % Monitor loop progress
Tm(12,12)                    % Monitor center temperature

end
Tmr=Tm(4:20, 4:20);
('Now include conduction in the wafer')
% Now include conduction balance

res=250       % so loop starts
conv=160;      % convergence criteria= 0.5K per surface grid point

t=.05;        % Thickness of wafer in cm

while res>conv,
%for k2=1:1,  % 10 loops

% Calculate important parameters

k=2.4408-5.1269e-3*Tm+4.2304e-6*Tm.^2-1.2292e-9*Tm.^3;      % k(Si) W/cmK
em=-2.8324+1.0379e-2*Tm-9.653e-6*Tm.^2+2.963e-9*Tm.^3;    %wafer emissivity
qr=alpha*em.*F.*Tf.^4*5.67e-12*dr^2;                    % Rad from filament
qrb=2*5.67e-12*(Tm.^4)*(dr^2).*em;      % Radiation away from both sides

% Routine for setting T off wafer = lowest temp

% Find lowest temp
Tmin=Tmax;
 for i=1:p,
  for j=1:p,
    if (x(i,j)^2+y(i,j)^2)<25.1,    % 25 is edge of wafer
     if Tm(i,j)<Tmin,
        Tmin=Tm(i,j);          % Lowest temp on wafer
     end
    end
  end
 end

% Substitute Tmin for off wafer spots
```

```
 for i=1:p,
   for j=1:p,
      if (x(i,j)^2+y(i,j)^2)>25.1,    % 25 is edge of wafer
        Tm(i,j)=Tmin;
      end
   end
 end

% Recalulate temperature using energy balance + conduction
res=0;        % start addition from 0
 for i=1:p,
   for j=1:p,
      if (x(i,j)^2+y(i,j)^2)<25.1,    % 25 is edge of wafer
        qc(i,j)=k(i,j)*t*(Tm(i,j+1)+Tm(i,j-1)+Tm(i+1,j)+Tm(i-1,j));
        Tm2(i,j)=(qr(i,j)-qrb(i,j)+qc(i,j))/(4*k(i,j)*t);    %Energy balance

        Tm2(i,j)=(Tm2(i,j)+Tm(i,j))/2;                    % New T
      else
        Tm2(i,j)=Tm(i,j);
      end
%    dT=abs(Tm2(i,j)-Tm(i,j));
%    res=res+dT;                    % add residual

   end
 end

hbsub                          % Don't lose heat

% convergence criteria,rename temps
 for i=1:p,
   for j=1:p,
    dT=abs(Tm2(i,j)-Tm(i,j));        % residual T
    res=res+dT;                   % add residuals
    Tm(i,j)=Tm2(i,j);               % Rename Tm
   end
 end

res                      % Monitor loop progress
%Tm(12,12)                    % Monitor center temperature

end
e=max(Tm);e=e';e=max(e);
TMAX=e                       % Print out Tmax
alpha                    % print out TaC emmissivity
Tmg=Tm(4:20,4:20);            % Match up with matrix
clg
axis('square')
cs=contour(Tmg, -4:.5:4, -4:.5:4);
axis('square')
%clabel(cs, 'manual')
```

```
% PROGRAM cyl.m
% Program for cylindrical filaments: Calculates the flux of radiation from
% any combination of horizontal and vertical filaments.
% This is for cylinders with diameter Df and height h.
% Before calling this program in Matlab first use meshdom() to
% create the grid that you will calculate the radiation to.
% Also use the grid axis when entering the positions of the filaments

n=input('Enter the number of horizontal filaments')

%Initialize qr
z=size(x);
F=zeros(z(1,1),z(1,2));

for i=1:n

% All lengths given in cm;

y0=input('Enter y position of horizontal filament ');
%h=input('Enter filament/substrate separation:  ');
h=1;
%Df=input('Enter filament diameter:  ');
Df=0.1;

L1=2;
%L1=input('Enter the starting position of the filament ')
L2=-L1;
%L2=input('Enter the final position of the filament ')
Y=y-y0;

C1=Df*h*(h^2+Y.^2).^.5;

C2=(Y.^2+h^2).^.5;

C=C1./(2*pi*C2.^2);

I1=(L1-x)./(C2.^2+(L1-x).^2)+C2.^(-1).*atan((L1-x)./C2);

I2=(L2-x)./(C2.^2+(L2-x).^2)+C2.^(-1).*atan((L2-x)./C2);

qh=abs(C.*(I1-I2));
 F=F+qh;
end

% Verticall cylidrical filament section

m=0
%m=input('Enter the number of vertical filaments')

for j=1:m
```

```
x0=input('Enter the x  position of the vertical filaments ')
L1=input('Enter the starting position of the filament ')
%L2=L1-1
L2=input('Enter the final position of the filament ')
X=x-x0;

C1=Df*h*(h^2+X.^2).^.5;

C2=(X.^2+h^2).^.5;

C=C1./(2*pi*C2.^2);

I1=(L1-y)./(C2.^2+(L1-y).^2)+C2.^(-1).*atan((L1-y)./C2);

I2=(L2-y)./(C2.^2+(L2-y).^2)+C2.^(-1).*atan((L2-y)./C2);

qv=abs(C.*(I1-I2));
 F=F+qv;
end

F;

('F is th matrix to use with mesh, contour etc in matlab')

F(12,12)

% PROGRAM pred.m
% Program to provide initil guess for hb.m

%Tmax=input('Guess the maximum surface temperature on the substrate: ');
Tmax=1000;
%Tmin=input('Guess the minimum surface temperature on the substrate:');
Tmin=700;

qz=F;
a=max(qz);
a=a';
a=max(a);
z=qz/a;
b=min(z);
b=b';
b=min(b);
dt=(Tmax-Tmin)/(1-b);
% Calculate the front side temperature

Tfr=Tmin+(z-b)*dt;

% PROGRAM hbsub.m
% Sub Make sure everything balances
Qin=0;
Qout=0;            % Initialize variables
```

```
n2=0;               % counter

qr=alpha*F.*Tf.^4*5.67e-12*dr^2;          % Rad from filament
qrb=2*5.67e-12*(Tm2.^4)*(dr^2).*em;        % Radiation away from back side

  for i=1:p,
   for j=1:p,
      if (x(i,j)^2+y(i,j)^2)<25.1,    % 25 is edge of wafer
       Qin=Qin+qr(i,j);             % Heat radiated to wafer
       Qout=Qout+qrb(i,j);            % Heat radiated away from the wafer
       n2=n2+1;                     % # of spots on wafer
      end
   end
  end

dQ=Qin-Qout;                        % Total gain/loss of wafer in Joules
mass=2.33*25*t*pi;                     % Mass of wafer - density=2.33
cp=.703;                            % Heat Capacity J/g K
rt=dQ/(cp*mass*n2);                    % Temp raise per spot on wafer

Tm2=Tm2+rt;                         % Adjust temperature across board
```

APPENDIX II

FIDAP CODES FOR SOLUTION OF MASS TRANSPORT AND ATOMIC HYDROGEN PRODUCTION

This Appendix contains the codes used to calculate the velocity and temperature fields, FLOW.FIINP, and the chemistry of atomit hydrogen, FIL.FIINP. The simulations were carried out on the MIT Cray and at the Pittsburgh Supercomputing Center.

FLOW.FIINP: Input file used to calculate temperature, flow profiles.

```
/     Contains accurate physical properties
/     2-dimensional model
/     3 filaments @ 0, +/- 0.5
/     D=15 cm, H=18 cm, off center: center = 9.3
/
/     Redone 10/5/93 - less grid points
/     Parameters for Geometric Space [cm]
/
*PARAMETER
R1 8.685
R2 8.71
R3 8.735
R4 8.755
R5 8.775
R6 8.785
R7 8.7911612
R8 8.8088388
R9 8.815
R10 8.825
R11 8.845
R12 8.865
R13 8.89
R14 8.915
/
R21 9.185
R22 9.21
R23 9.235
R24 9.255
R25 9.275
R26 9.285
R27 9.2911612
R28 9.3088388
R29 9.315
R30 9.325
R31 9.345
R32 9.365
R33 9.39
R34 9.415
/
R41 9.685
R42 9.71
R43 9.735
R44 9.755
R45 9.775
```

```
R46 9.785
R47 9.7911612
R48 9.8088388
R49 9.815
R50 9.825
R51 9.845
R52 9.865
R53 9.89
R54 9.915
/
RT 1.8
RI1 3.6
RTS 4.0
RBS 14.6
RI2 15.0
RB 16.8
RF1 8.8
RF2 9.3
RF3 9.8
/
H1 11.485
H2 11.51
H3 11.535
H4 11.555
H5 11.575
H6 11.585
H7 11.5911612
H8 11.6088388
H9 11.615
H10 11.625
H11 11.645
H12 11.665
H13 11.69
H14 11.715
/
HI 1
HF 11.6
HS 12.9
HO 16.3
HR 18.0
/
*FIMESH(2-D,IMAX=27,JMAX=23)
EXPI
1 2 3 4 5 6 7 8 9 10 11 12 13 14 15 16 17 18 19 20 21 22 44 46 56 62 68
EXPJ
1 0 0 0 9 11 0 0 17 0 0 0 25 27 29 0 33 35 39 41 57 59 67
/
POINT
/#   I   J   K   X   Y
/    GEOMETRY FOR FILAMENT #1
1 1 1 1 H7 R7
```

```
2 1 5 1 H7 R8
3 1 9 1 H8 R8
4 1 13 1 H8 R7
5 1 17 1 H7 R7
/
6 2 1 1 H6 R6
7 2 5 1 H6 R9
8 2 9 1 H9 R9
9 2 13 1 H9 R6
10 2 17 1 H6 R6
/
11 3 1 1 H5 R5
12 3 5 1 H5 R10
13 3 9 1 H10 R10
14 3 13 1 H10 R5
15 3 17 1 H5 R5
/
16 4 1 1 H4 R4
17 4 5 1 H4 R11
18 4 9 1 H11 R11
19 4 13 1 H11 R4
20 4 17 1 H4 R4
/
21 5 1 1 H3 R3
22 5 5 1 H3 R12
23 5 9 1 H12 R12
24 5 13 1 H12 R3
25 5 17 1 H3 R3
/
26 6 1 1 H2 R2
27 6 5 1 H2 R13
28 6 9 1 H13 R13
29 6 13 1 H13 R2
30 6 17 1 H2 R2
/
31 7 1 1 H1 R1
32 7 5 1 H1 R14
33 7 9 1 H14 R14
34 7 13 1 H14 R1
35 7 17 1 H1 R1
/
38 0 0 0 HF RF1
/
/    GEOMETRY FOR FILAMENT #2
41 8 1 1 H7 R27
42 8 5 1 H7 R28
43 8 9 1 H8 R28
44 8 13 1 H8 R27
45 8 17 1 H7 R27
/
46 9 1 1 H6 R26
```

47 9 5 1 H6 R29
48 9 9 1 H9 R29
49 9 13 1 H9 R26
50 9 17 1 H6 R26
/
51 10 1 1 H5 R25
52 10 5 1 H5 R30
53 10 9 1 H10 R30
54 10 13 1 H10 R25
55 10 17 1 H5 R25
/
56 11 1 1 H4 R24
57 11 5 1 H4 R31
58 11 9 1 H11 R31
59 11 13 1 H11 R24
60 11 17 1 H4 R24
/
61 12 1 1 H3 R23
62 12 5 1 H3 R32
63 12 9 1 H12 R32
64 12 13 1 H12 R23
65 12 17 1 H3 R23
/
66 13 1 1 H2 R22
67 13 5 1 H2 R33
68 13 9 1 H13 R33
69 13 13 1 H13 R22
70 13 17 1 H2 R22
/
71 14 1 1 H1 R21
72 14 5 1 H1 R34
73 14 9 1 H14 R34
74 14 13 1 H14 R21
75 14 17 1 H1 R21
/
78 0 0 0 HF RF2
/
/ GEOMETRY FOR FILAMENT #3
81 15 1 1 H7 R47
82 15 5 1 H7 R48
83 15 9 1 H8 R48
84 15 13 1 H8 R47
85 15 17 1 H7 R47
/
86 16 1 1 H6 R46
87 16 5 1 H6 R49
88 16 9 1 H9 R49
89 16 13 1 H9 R46
90 16 17 1 H6 R46
/
91 17 1 1 H5 R45

```
92 17 5 1 H5 R50
93 17 9 1 H10 R50
94 17 13 1 H10 R45
95 17 17 1 H5 R45
/
96 18 1 1 H4 R44
97 18 5 1 H4 R51
98 18 9 1 H11 R51
99 18 13 1 H11 R44
100 18 17 1 H4 R44
/
101 19 1 1 H3 R43
102 19 5 1 H3 R52
103 19 9 1 H12 R52
104 19 13 1 H12 R43
105 19 17 1 H3 R43
/
106 20 1 1 H2 R42
107 20 5 1 H2 R53
108 20 9 1 H13 R53
109 20 13 1 H13 R42
110 20 17 1 H2 R42
/
111 21 1 1 H1 R41
112 21 5 1 H1 R54
113 21 9 1 H14 R54
114 21 13 1 H14 R41
115 21 17 1 H1 R41
/
118 0 0 0 HF RF3
/
/     geometry for rest of reactor-5 levels
201 22 1 1 0 RT
202 22 5 1 0 RI1
203 22 6 1 0 RTS
206 22 14 1 0 R1
207 22 15 1 0 R14
209 22 17 1 0 R21
210 22 18 1 0 R34
212 22 19 1 0 R41
213 22 20 1 0 R54
216 22 21 1 0 RBS
217 22 22 1 0 RI2
218 22 23 1 0 RB
/
221 23 1 1 H1 RT
222 23 5 1 H1 RI1
223 23 6 1 H1 RTS
226 23 14 1 H1 R1
227 23 15 1 H1 R14
229 23 17 1 H1 R21
```

230 23 18 1 H1 R34
232 23 19 1 H1 R41
233 23 20 1 H1 R54
236 23 21 1 H1 RBS
237 23 22 1 H1 RI2
238 23 23 1 H1 RB
/
241 24 1 1 H14 RT
242 24 5 1 H14 RI1
243 24 6 1 H14 RTS
246 24 14 1 H14 R1
247 24 15 1 H14 R14
249 24 17 1 H14 R21
250 24 18 1 H14 R34
252 24 19 1 H14 R41
253 24 20 1 H14 R54
256 24 21 1 H14 RBS
257 24 22 1 H14 RI2
258 24 23 1 H14 RB
/
261 25 1 1 HS RT
262 25 5 1 HS RI1
263 25 6 1 HS RTS
266 25 14 1 HS R1
267 25 15 1 HS R14
269 25 17 1 HS R21
270 25 18 1 HS R34
272 25 19 1 HS R41
273 25 20 1 HS R54
276 25 21 1 HS RBS
277 25 22 1 HS RI2
278 25 23 1 HS RB
/
281 26 1 1 HO RT
282 26 5 1 HO RI1
283 26 6 1 HO RTS
296 26 21 1 HO RBS
297 26 22 1 HO RI2
298 26 23 1 HO RB
/
181 27 1 1 HR RT
182 27 5 1 HR RI1
183 27 6 1 HR RTS
196 27 21 1 HR RBS
197 27 22 1 HR RI2
198 27 23 1 HR RB
/
LINE
/ for first filament
31 32
32 33

```
33 34
34 35
/
1 31
2 32
3 33
4 34
5 35
/     for second filament
71 72
72 73
73 74
74 75
/
41 71
42 72
43 73
44 74
45 75
/     for third filament
111 112
112 113
113 114
114 115
/
81 111
82 112
83 113
84 114
85 115
/
/     LINES FOR REST OF REACTOR
/ips ipf RATIO IRAT
201 221 5. 3 5.
202 222 5. 3 5.
203 223 5. 3 5.
206 226 5. 3 5.
207 227 5. 3 5.
209 229 5. 3 5.
210 230 5. 3 5.
212 232 5. 3 5.
213 233 5. 3 5.
216 236 5. 3 5.
217 237 5. 3 5.
218 238 5. 3 5.
/
241 261 2. 3 2.
242 262 2. 3 2.
243 263 2. 3 2.
246 266 2. 3 2.
247 267 2. 3 2.
```

249 269 2. 3 2.
250 270 2. 3 2.
252 272 2. 3 2.
253 273 2. 3 2.
256 276 2. 3 2.
257 277 2. 3 2.
258 278 2. 3 2.
/
221 241
222 242
223 243
226 246
227 247
229 249
230 250
232 252
233 253
236 256
237 257
238 258
/
261 281
262 282
263 283
276 296
277 297
278 298
/
281 181
282 182
283 183
296 196
297 197
298 198
/
/ horizontal groups
/ 2 sides
201 202
202 203
221 222
222 223
241 242
242 243
261 262
262 263
281 282
282 283
181 182
182 183
/
216 217

217 218
236 237
237 238
256 257
257 258
276 277
277 278
296 297
297 298
196 197
197 198
/ from edge to filament
203 206 2. 4
223 226 2. 4
243 246 2. 4
263 266 2. 4
/
213 216 2. 3
233 236 2. 3
253 256 2. 3
273 276 2. 3
/ filament 1
206 207
226 227
246 247
266 267
/ between 1 and 2
207 209 2. 3 2.
227 229 2. 3 2.
247 249 2. 3 2.
267 269 2. 3 2.
/ filament 2
209 210
229 230
249 250
269 270
/ between 2 and 3
210 212 2. 3 2.
230 232 2. 3 2.
250 252 2. 3 2.
270 272 2. 3 2.
/ filament 3
212 213
232 233
252 253
272 273
/
ARC
1 2 38
2 3 38
3 4 38

```
4 5 38
/
41 42 78
42 43 78
43 44 78
44 45 78
/
81 82 118
82 83 118
83 84 118
84 85 118
/
SURFACE
1 35
41 75
81 115
/
CDRIVE
201 218 218 198
/     delete susceptor
DELETE
183 276
183 196
/     delete filament areas
226 247
229 250
232 253
/     eliminate duplicate nodes
MERGE
1 35 1 35
41 75 41 75
81 115 81 115
/
1 35 201 198
41 75 201 198
81 115 201 198
/
ELEMENTS(TRANSITION,TRIANGLE,NODES=6)
11 12 1 2 0 6 7
12 13 2 3 0 7 8
13 14 3 4 0 8 9
14 15 4 5 0 9 10
/
51 52 41 42 0 46 47
52 53 42 43 0 47 48
53 54 43 44 0 48 49
54 55 44 45 0 49 50
/
91 92 81 82 0 86 87
92 93 82 83 0 87 88
93 94 83 84 0 88 89
```

```
94 95 84 85 0 89 90
/
ELEMENTS(TRANSITION,TRIANGLE,NODES=6,INC1=2)
21 22 11 12 0 16 17
22 23 12 13 0 17 18
23 24 13 14 0 18 19
24 25 14 15 0 19 20
/
61 62 51 52 0 56 57
62 63 52 53 0 57 58
63 64 53 54 0 58 59
64 65 54 55 0 59 60
/
101 102 91 92 0 96 97
102 103 92 93 0 97 98
103 104 93 94 0 98 99
104 105 94 95 0 99 100
/
ELEMENTS(TRANSITION,TRIANGLE,NODES=6,INC1=4,INC2=2)
31 32 21 22 0 26 27
32 33 22 23 0 27 28
33 34 23 24 0 28 29
34 35 24 25 0 29 30
/
71 72 61 62 0 66 67
72 73 62 63 0 67 68
73 74 63 64 0 68 69
74 75 64 65 0 69 70
/
111 112 101 102 0 106 107
112 113 102 103 0 107 108
113 114 103 104 0 108 109
114 115 104 105 0 109 110
/
ELEMENTS(QUADRILATERAL,NODES=9)
201 198
/
ELEMENTS(BOUNDARY,NODES=3)
281 181
298 198
/
BCNODE(UX)
202 203 7.215
216 217 7.215
BCNODE(UX)
201 202
203 216
217 218
218 298
201 281
181 183
```

```
183 263
263 276
276 196
196 198
/    FILAMENTS
1 2
2 3
3 4
4 5
/
41 42
42 43
43 44
44 45
/
81 82
82 83
83 84
84 85
/
BCNODE(UY)
201 218
218 298
201 281
181 183
183 263
263 276
276 196
196 198
/    FILAMENTS
1 2
2 3
3 4
4 5
/
41 42
42 43
43 44
44 45
/
81 82
82 83
83 84
84 85
/
BCNODE(TEMPERATURE)
202 203 300
216 217 300
201 202 328
203 216 328
217 218 328
```

```
218 298 328
201 281 328
181 183 328
196 198 328
183 263 1073
263 276 1073
276 196 1073
/     FILAMENTS
1 2 2600
2 3 2600
3 4 2600
4 5 2600
/
41 42 2600
42 43 2600
43 44 2600
44 45 2600
/
81 82 2600
82 83 2600
83 84 2600
84 85 2600
/
END
/
*FIPREP
PROBLEM(NONLINEAR,STRONGLY)
EXECUTION(NEWJOB)
PRESSURE(MIXED,DISCONTINUOUS)
SOLUTION(S.S.=8)
/STRATEGY(S.S.=4)
ICNODE(TEMP=1500)
ICNODE(VELO,STOKES)
DATAPRINT(CONTROL)
PRINTOUT(NONE)
POSTPROCESS(ALL)
NODES(FIMESH)
DENSITY(VARIABLE=0.0010615,TEMPERATURE)
BODYFORCE
-980 0
/     elements
ELEMENTS(TRIANGLE,NODES=6,FIMESH)
ELEMENTS(TRIANGLE,NODES=6,FIMESH)
ELEMENTS(TRIANGLE,NODES=6,FIMESH)
ELEMENTS(TRIANGLE,NODES=6,FIMESH)
ELEMENTS(TRIANGLE,NODES=6,FIMESH)
ELEMENTS(TRIANGLE,NODES=6,FIMESH)
ELEMENTS(TRIANGLE,NODES=6,FIMESH)
ELEMENTS(TRIANGLE,NODES=6,FIMESH)
ELEMENTS(TRIANGLE,NODES=6,FIMESH)
ELEMENTS(TRIANGLE,NODES=6,FIMESH)
```

```
ELEMENTS(TRIANGLE,NODES=6,FIMESH)
ELEMENTS(TRIANGLE,NODES=6,FIMESH)
ELEMENTS(TRIANGLE,NODES=6,FIMESH)
ELEMENTS(TRIANGLE,NODES=6,FIMESH)
ELEMENTS(TRIANGLE,NODES=6,FIMESH)
ELEMENTS(TRIANGLE,NODES=6,FIMESH)
ELEMENTS(TRIANGLE,NODES=6,FIMESH)
ELEMENTS(TRIANGLE,NODES=6,FIMESH)
ELEMENTS(TRIANGLE,NODES=6,FIMESH)
ELEMENTS(TRIANGLE,NODES=6,FIMESH)
ELEMENTS(TRIANGLE,NODES=6,FIMESH)
ELEMENTS(TRIANGLE,NODES=6,FIMESH)
ELEMENTS(TRIANGLE,NODES=6,FIMESH)
ELEMENTS(TRIANGLE,NODES=6,FIMESH)
ELEMENTS(TRIANGLE,NODES=6,FIMESH)
ELEMENTS(TRIANGLE,NODES=6,FIMESH)
ELEMENTS(TRIANGLE,NODES=6,FIMESH)
ELEMENTS(TRIANGLE,NODES=6,FIMESH)
ELEMENTS(TRIANGLE,NODES=6,FIMESH)
ELEMENTS(TRIANGLE,NODES=6,FIMESH)
ELEMENTS(TRIANGLE,NODES=6,FIMESH)
ELEMENTS(TRIANGLE,NODES=6,FIMESH)
ELEMENTS(TRIANGLE,NODES=6,FIMESH)
ELEMENTS(TRIANGLE,NODES=6,FIMESH)
ELEMENTS(TRIANGLE,NODES=6,FIMESH)
ELEMENTS(TRIANGLE,NODES=6,FIMESH)
ELEMENTS(QUADRILATERAL,NODES=9,FIMESH)
ELEMENTS(OUTFLOW,NODES=3,FIMESH)
ELEMENTS(OUTFLOW,NODES=3,FIMESH)
/
/    PHYSICAL PROPERTIES
VOLUMEXPANSION(CURVE=11,REFTEMP=1450)
-1000 300 700 1000 1225 1450 1675 1900 2200 2600 2800
.003 .00333 .00143 .001 .000816 0. .000597 .000526 .000455 .000385 .000385
VISCOSITY(CURVE=11)
-1000 300 500 700 1000 1450 1900 2200 2400 2600 2800
0.091 0.091 0.131 0.166 0.213 0.276 0.333 0.369 0.392 0.414 0.414
CONDUCTIVITY(CURVE=11)
-1000 300 500 700 1000 1450 1900 2200 2400 2600 2800
1.52 1.52 2.26 2.91 3.82 5.04 6.17 6.88 7.34 7.79 7.79
SPECIFICHEAT(CURVE=11)
-1000 300 500 700 1000 1450 1900 2200 2400 2600 2800
5.84 5.84 6.02 6.13 6.36 6.74 7.02 7.15 7.22 7.27 7.27
RENUMBER
END
*END
```

CHEMISTRY PART: this contains the lines from FIL1.FIINP that differ from the flow problem.

```
BCNODE(SPEC=2)
201 218
218 298
201 281
181 183
196 198
183 263
276 196
/    FILAMENTS
1 2 0.00269
2 3 0.00269
3 4 0.00269
4 5 0.00269
/
41 42 0.00269
42 43 0.00269
43 44 0.00269
44 45 0.00269
/
81 82 0.00269
82 83 0.00269
83 84 0.00269
84 85 0.00269
/
END
/
*FIPREP
PROBLEM(NONLINEAR,NOMO,WEAKLY,WEAK=2)
EXECUTION(NEWJOB)
SOLUTION(S.S.=5)
ICNODE(TEMP,READ))
ICNODE(UX,READ)
ICNODE(UY,READ)
/ICNODE(SPEC=1,CONSTANT=0.928)
ICNODE(SPEC=2,CONSTANT=0.0002)
/ICNODE(SPEC=3,CONSTANT=0.072)
DATAPRINT(CONTROL)
PRINTOUT(NONE)
POSTPROCESS(ALL)
NODES(FIMESH)
DENSITY(constant=0.0010615)
/    elements
ELEMENTS(TRIANGLE,NODES=6,FIMESH)
ELEMENTS(TRIANGLE,NODES=6,FIMESH)
ELEMENTS(TRIANGLE,NODES=6,FIMESH)
ELEMENTS(TRIANGLE,NODES=6,FIMESH)
ELEMENTS(TRIANGLE,NODES=6,FIMESH)
ELEMENTS(TRIANGLE,NODES=6,FIMESH)
ELEMENTS(TRIANGLE,NODES=6,FIMESH)
ELEMENTS(TRIANGLE,NODES=6,FIMESH)
ELEMENTS(TRIANGLE,NODES=6,FIMESH)
```

```
ELEMENTS(TRIANGLE,NODES=6,FIMESH)
ELEMENTS(TRIANGLE,NODES=6,FIMESH)
ELEMENTS(TRIANGLE,NODES=6,FIMESH)
ELEMENTS(TRIANGLE,NODES=6,FIMESH)
ELEMENTS(TRIANGLE,NODES=6,FIMESH)
ELEMENTS(TRIANGLE,NODES=6,FIMESH)
ELEMENTS(TRIANGLE,NODES=6,FIMESH)
ELEMENTS(TRIANGLE,NODES=6,FIMESH)
ELEMENTS(TRIANGLE,NODES=6,FIMESH)
ELEMENTS(TRIANGLE,NODES=6,FIMESH)
ELEMENTS(TRIANGLE,NODES=6,FIMESH)
ELEMENTS(TRIANGLE,NODES=6,FIMESH)
ELEMENTS(TRIANGLE,NODES=6,FIMESH)
ELEMENTS(TRIANGLE,NODES=6,FIMESH)
ELEMENTS(TRIANGLE,NODES=6,FIMESH)
ELEMENTS(TRIANGLE,NODES=6,FIMESH)
ELEMENTS(TRIANGLE,NODES=6,FIMESH)
ELEMENTS(TRIANGLE,NODES=6,FIMESH)
ELEMENTS(TRIANGLE,NODES=6,FIMESH)
ELEMENTS(TRIANGLE,NODES=6,FIMESH)
ELEMENTS(TRIANGLE,NODES=6,FIMESH)
ELEMENTS(TRIANGLE,NODES=6,FIMESH)
ELEMENTS(TRIANGLE,NODES=6,FIMESH)
ELEMENTS(TRIANGLE,NODES=6,FIMESH)
ELEMENTS(TRIANGLE,NODES=6,FIMESH)
ELEMENTS(TRIANGLE,NODES=6,FIMESH)
ELEMENTS(TRIANGLE,NODES=6,FIMESH)
ELEMENTS(QUADRILATERAL,NODES=9,FIMESH)
ELEMENTS(OUTFLOW,NODES=3,FIMESH)
ELEMENTS(OUTFLOW,NODES=3,FIMESH)
/
/    PHYSICAL PROPERTIES
CONDUCTIVITY(CURVE=11)
-1000 300 500 700 1000 1450 1900 2200 2400 2600 2800
1.52 1.52 2.26 2.91 3.82 5.04 6.17 6.88 7.34 7.79 7.79
SPECIFICHEAT(CURVE=11)
-1000 300 500 700 1000 1450 1900 2200 2400 2600 2800
5.84 5.84 6.02 6.13 6.36 6.74 7.02 7.15 7.22 7.27 7.27
/
MATE(SPEC=2,MDIF=2,MREA=2)
/    HYDROGEN ATOM
DIFFUSIVITY(SET=2,CURVE=11)
-1000 300 500 700 1000 1450 1900 2200 2400 2600 2800
79.4 79.4 189 335 615 1156 1831 2349 2723 3120 3120
/
/    REACTIONS
/    terms for H
REACTION(SET=2,TERMS=4,CONSTANT)
2.519E+15 51118.6 -3 0 0 0 0 0 0 0 0 0 0 0 0 0 0 0 0 0
-2.1126E+13 0 -4.6 0 2 0 0 0 0 0 0 0 0 0 0 0 0 0 0
4.3417E+13 50396.9 -3 0 0 0 0 0 0 0 0 0 0 0 0 0 0 0 0
```

```
-1.082E+13 0 -5 0 2 0 0 0 0 0 0 0 0 0 0 0 0 0 0 0
SPTRANSFER(CONSTANT=0,POWER=1)
ELEMENTS(SPECIES=2,NODES=3,FIMESH)
/
RENUMBER
END
*END
```

APPENDIX III

MOLECULAR BEAM EQUIPMENT DRAWINGS

This appendix contains detailed mechanical drawings pertaining to the microwave discharge source.

List of Drawings — Page

Figure i: Cross-section of beam source in reactor.. 147
Figure 0: Assembly.. 148
Figure 1: Flange.. 149
Figure 2: Overall view of outer tube.. 150
Figure 2A: Outer Tube... 151
Figure 2B: Slot Dimensions.. 152
Figure 2C: Outer Tube Vacuum End.. 153
Figure 2D: Outer Tube Air End... 154
Figure 2E: Rough Line.. 155
Figure 2F: Outer Tube and Flange... 156
Figure 3: Tuning Slug.. 157
Figure 4: Collar.. 158
Figure 5: Inner Conductor... 159
Figure 6: Inner Conductor Tip... 160
Figure 7A: Outer Conductor Tip.. 161
Figure 7B: Outer Conductor Clamp.. 162
Figure 8: Teflon Seals... 163
Figure 9: Quartz Ampoule.. 164
Figure 10: Water Lines.. 165
Figure 11: H2 lines.. 166
Figure 12: H2 line cross section... 167
Figure 13: Hydrocarbon gas line1... 168
Figure 14: Power Feedthrough... 169
Figure 15: Hydrocarbon gas line 2.. 170

Design: Reactor X-Section
Date: 10/18/93
Material: Stainless Steel
Unit: Inch

CROSS SECTION APPARATUS INSTALLED IN REACTOR

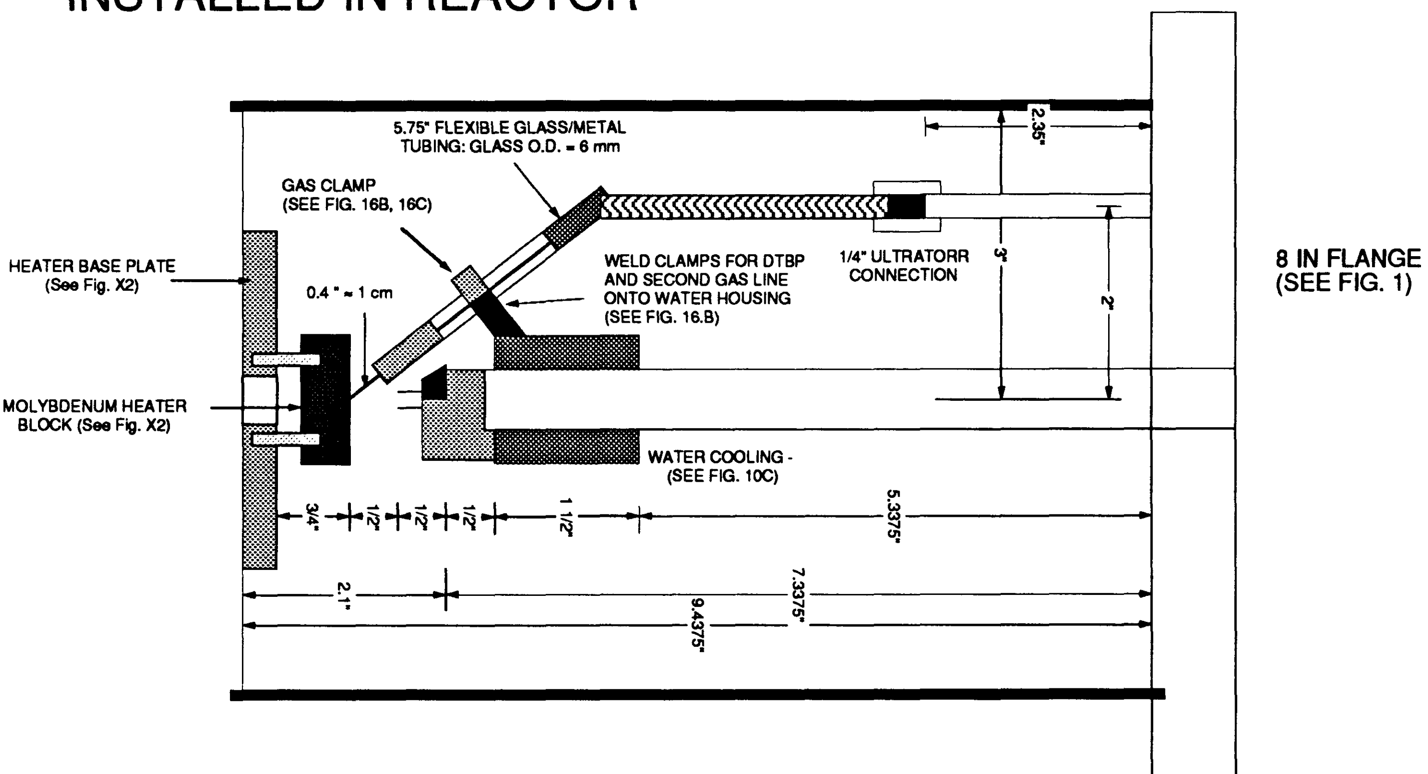

FIGURE 0: ASSEMBLY

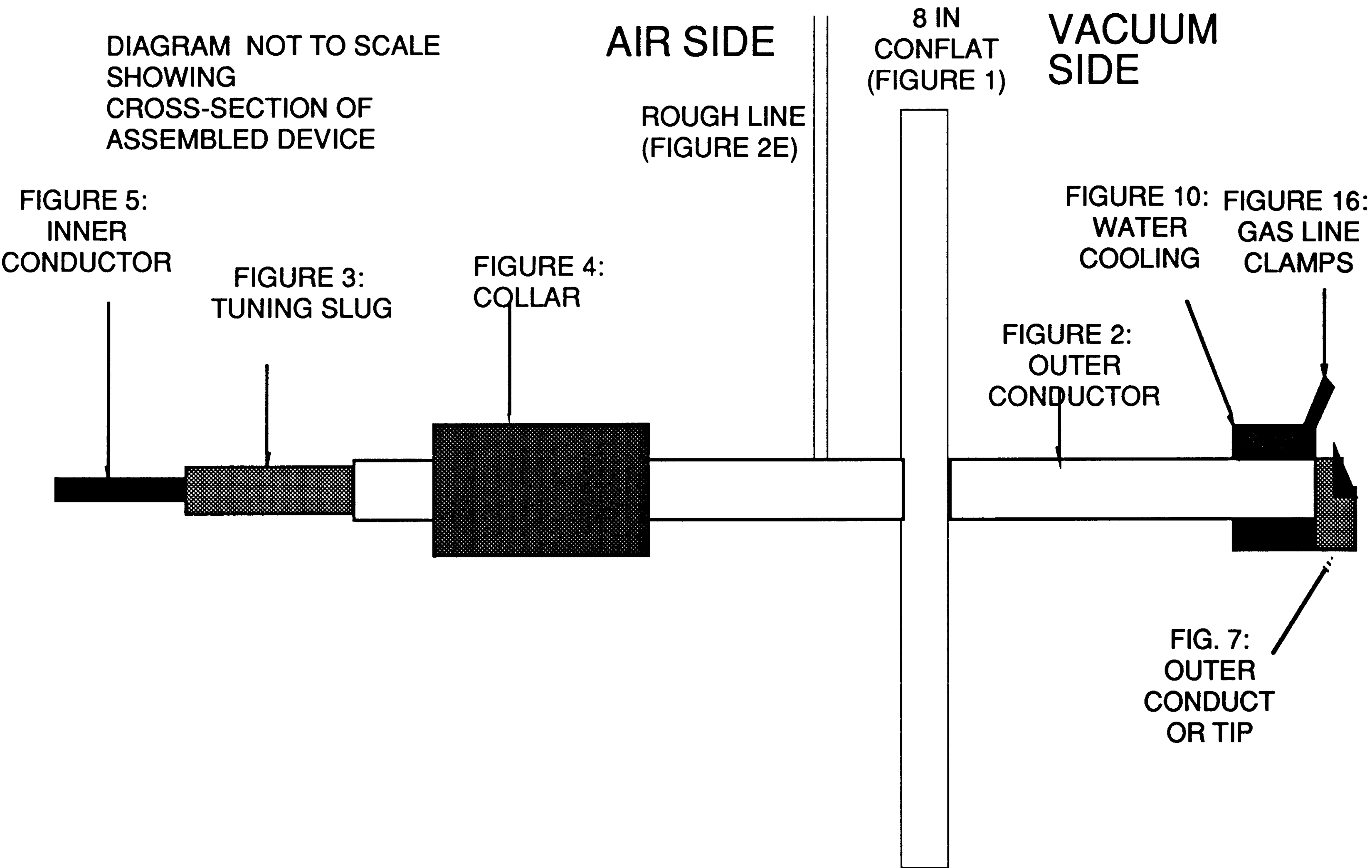

FIGURE 1: FLANGE

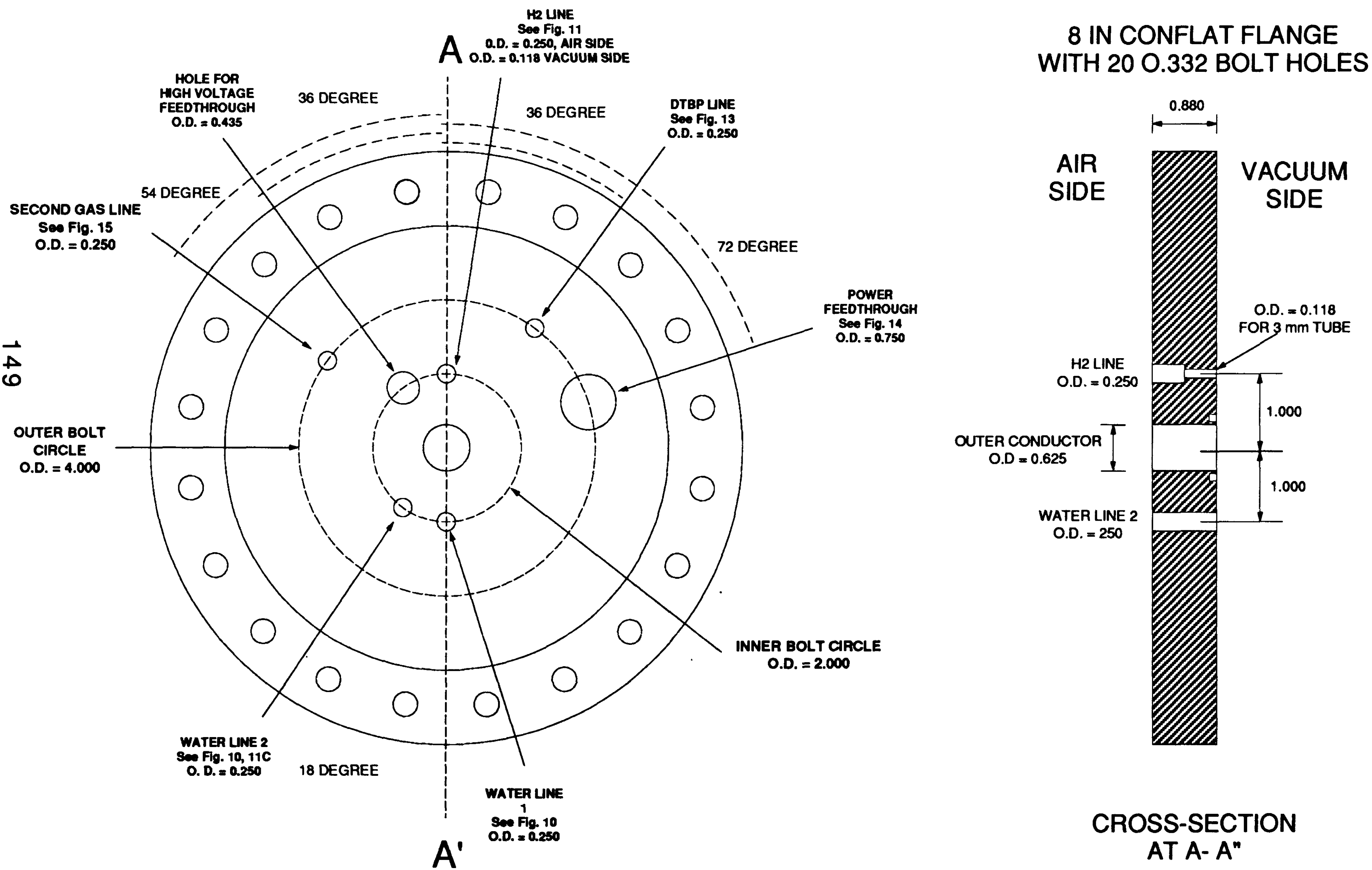

FIGURE 2: OUTER TUBE VIEWS

Colin Wolden
MIT Rm. 66-419
Cambridge, MA 02139
(617) 253-6480

Design: Outer Tube Views
Date: 10/17/93
Material: Stainless Steel
Unit: Inch

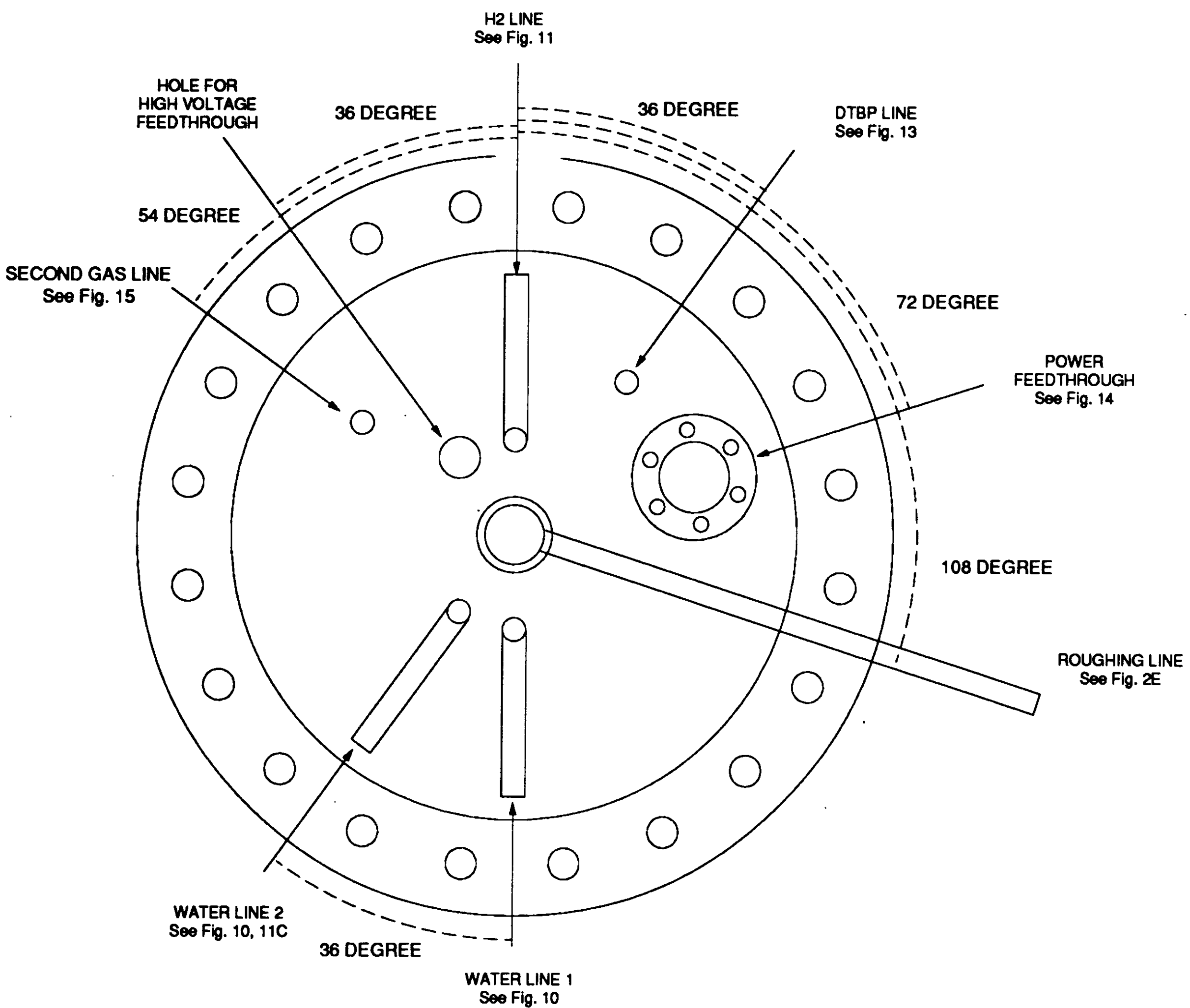

FIGURE 2A: OUTER CONDUCTOR

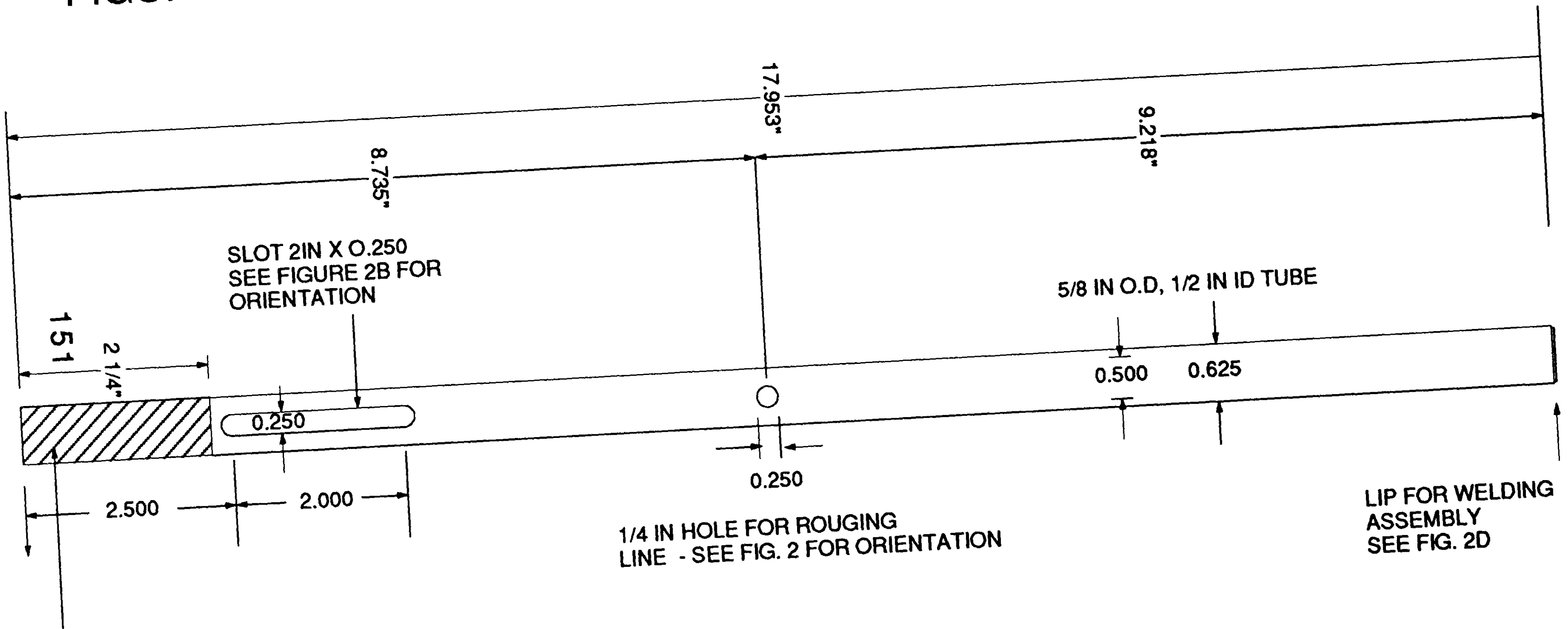

FIGURE 2B: SLOT DETAIL

Colin Wolden
MIT Rm. 66-419
Cambridge, MA 02139
(617) 253-6480

Design: Slot Detail
Date: 10/17/93
Material: Stainless Steel
Unit: Inch

VIEW FROM ABOVE SLOT

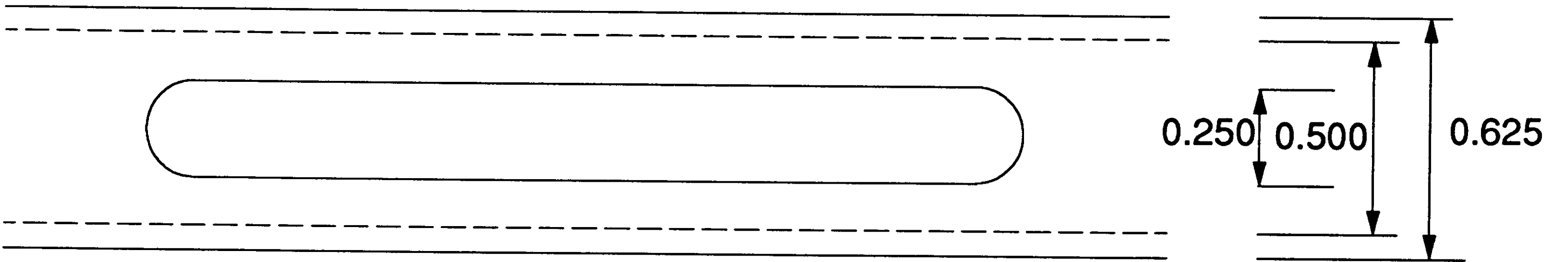

ANGULAR POSITIONS OF SLOT AND ROUGHING LINE - SEE FIG 2A FOR LINEAR POSITIONS ON TUBE.

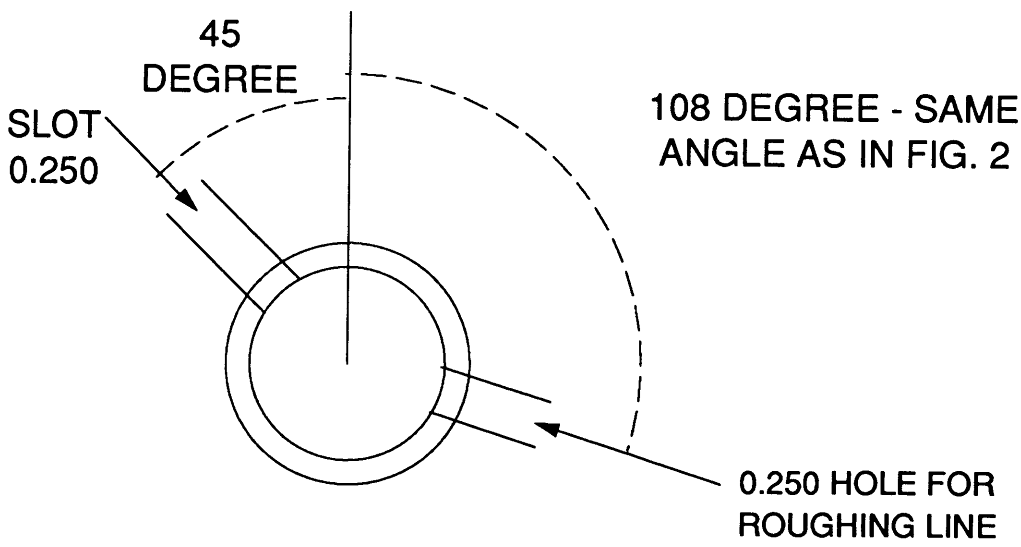

FIGURE 2C: OUTER CONDUCTOR - AIR END

Colin Wolden
MIT Rm. 66-419
Cambridge, MA 02139
(617) 253-6480

Design: Outer Tube - Air End
Date: 10/17/93
Material: Stainless Steel
Unit: Inch

AIR SIDE END
CROSS-SECTION

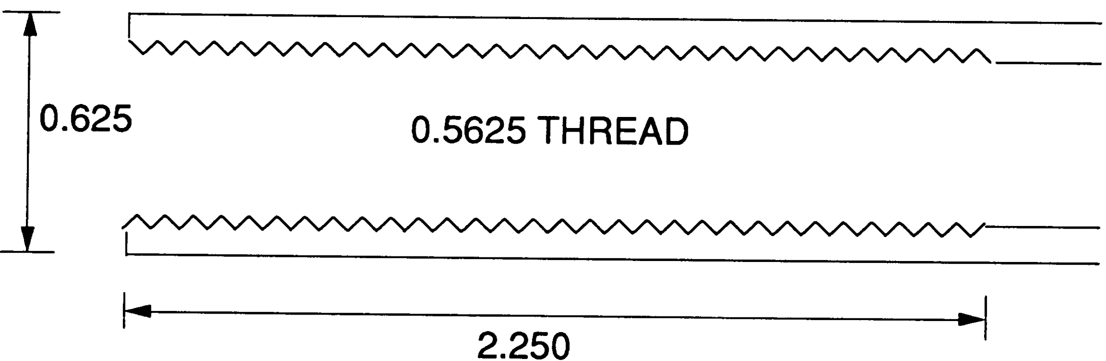

Threaded on the inside to fit outside
of TUNING SLUG (FIg. 3)

FIGURE 2D: OUTER CONDUCTOR - VACCUM END

Colin Wolden
MIT Rm. 66-419
Cambridge, MA 02139
(617) 253-6480

Design: Outer Tube - Air End
Date: 10/17/93
Material: Stainless Steel
Unit: Inch

VACCUUM SIDE END
CROSS-SECTION

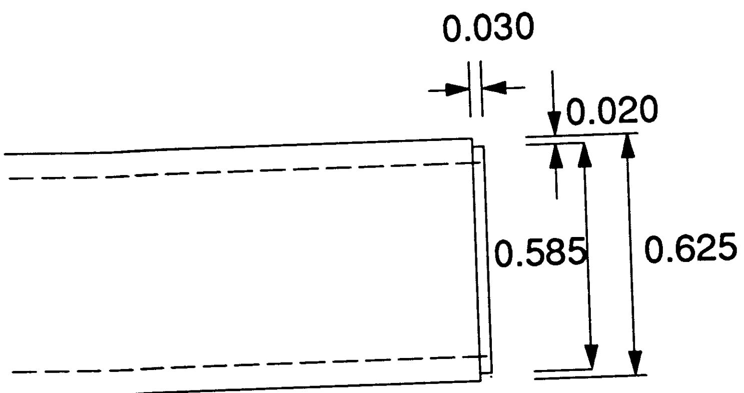

VACCUUM SIDE END
CROSS-SECTION

FIGURE 2E: ROUGH LINE

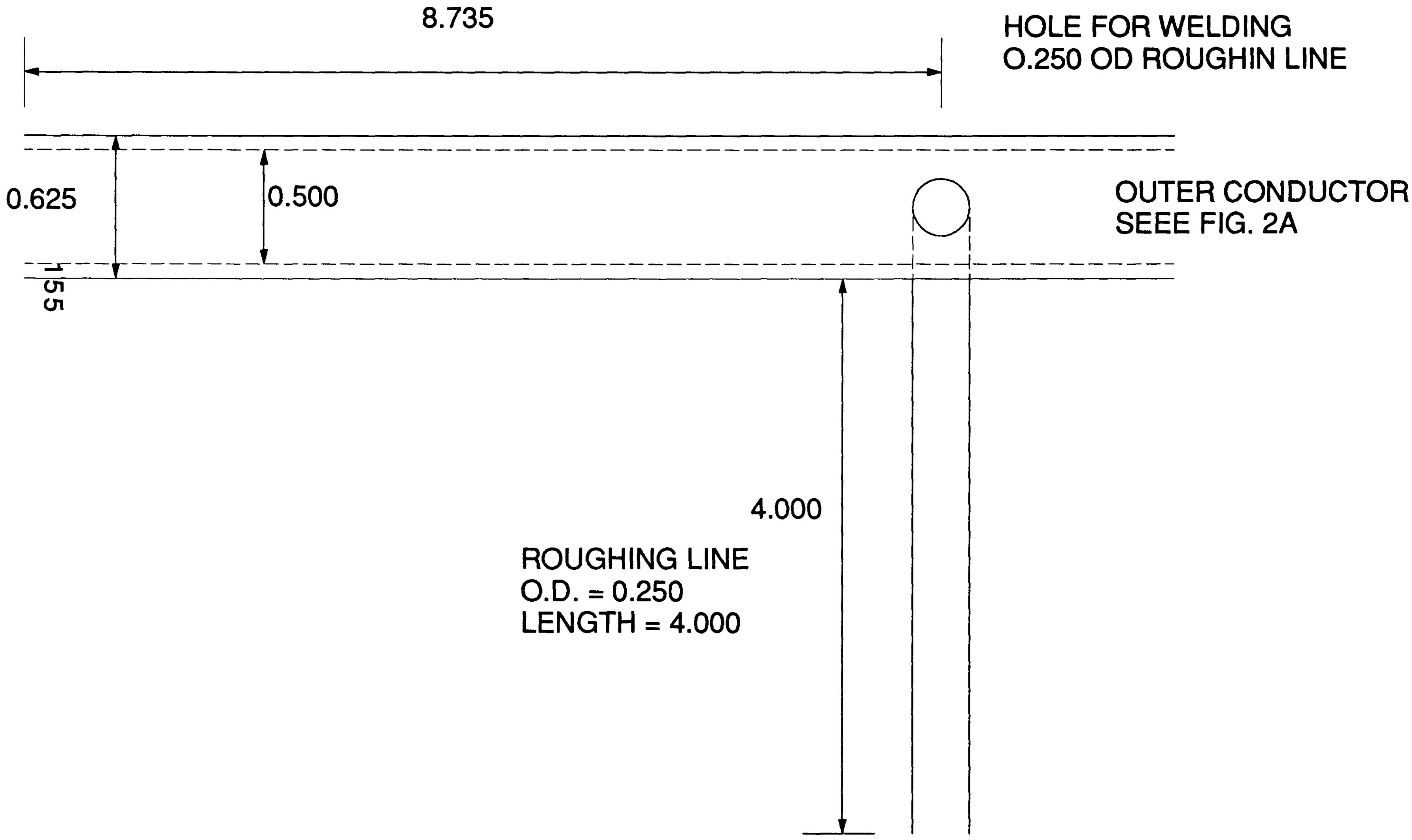

FIGURE 2F: OUTER TUBE & FLANGE

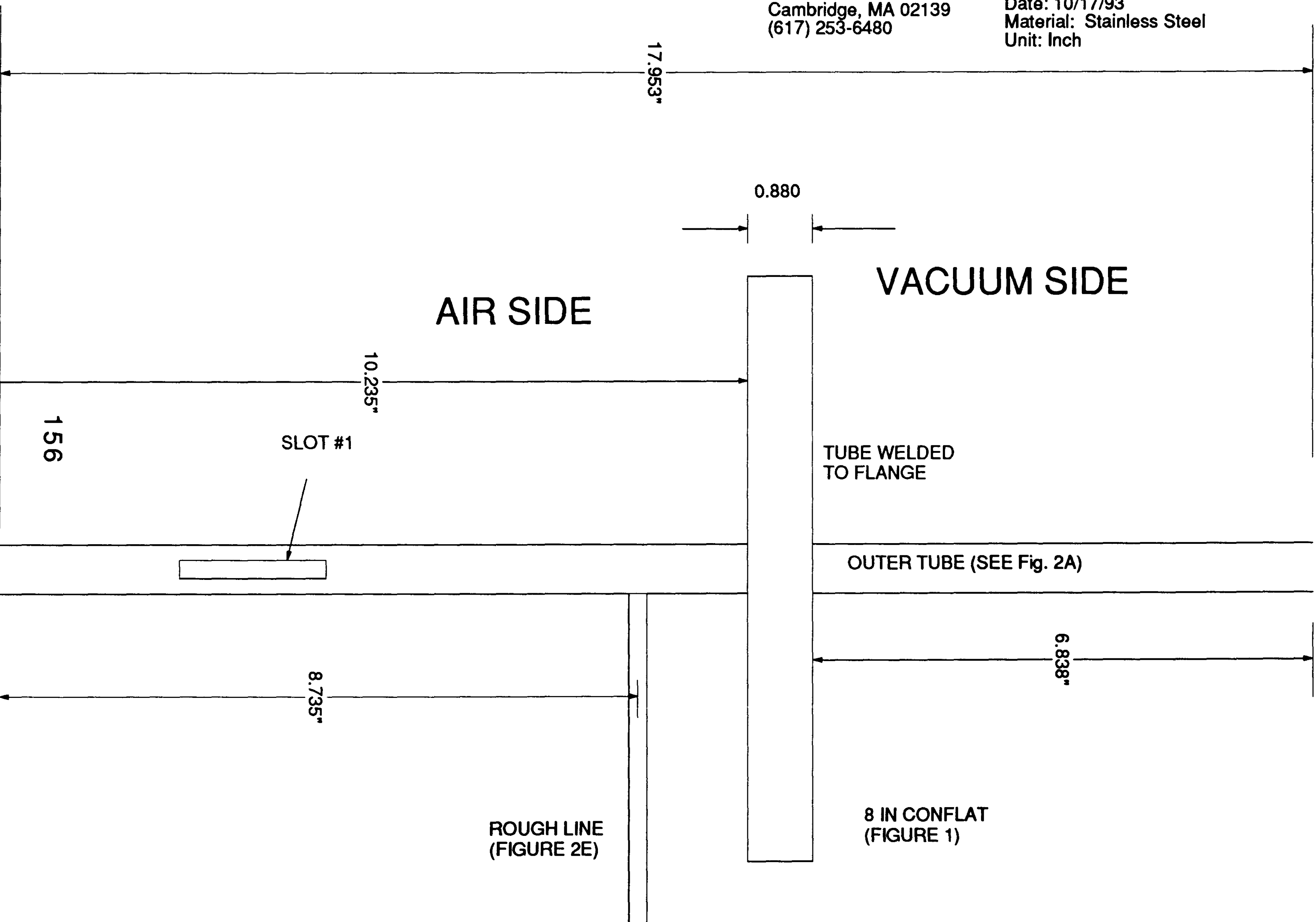

FIGURE 3: TUNING SLUG

Colin Wolden
MIT Rm. 66-419
Cambridge, MA 02139
(617) 253-6480

Design: Tuning Slug
Date: 10/17/93
Material: Brass
Unit: Inch

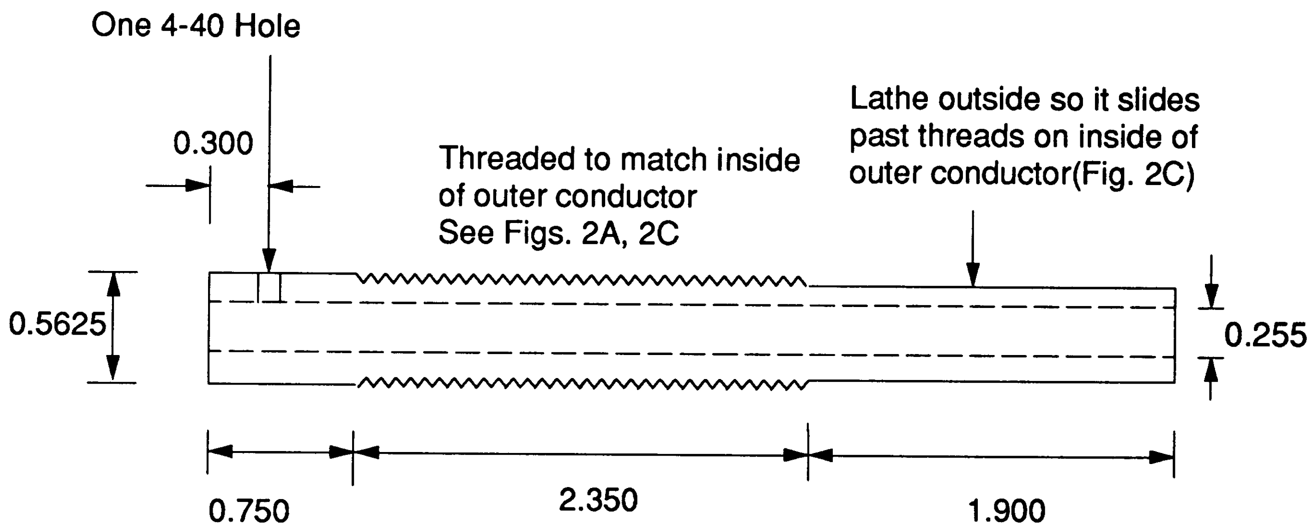

FIGURE 4: COLLAR

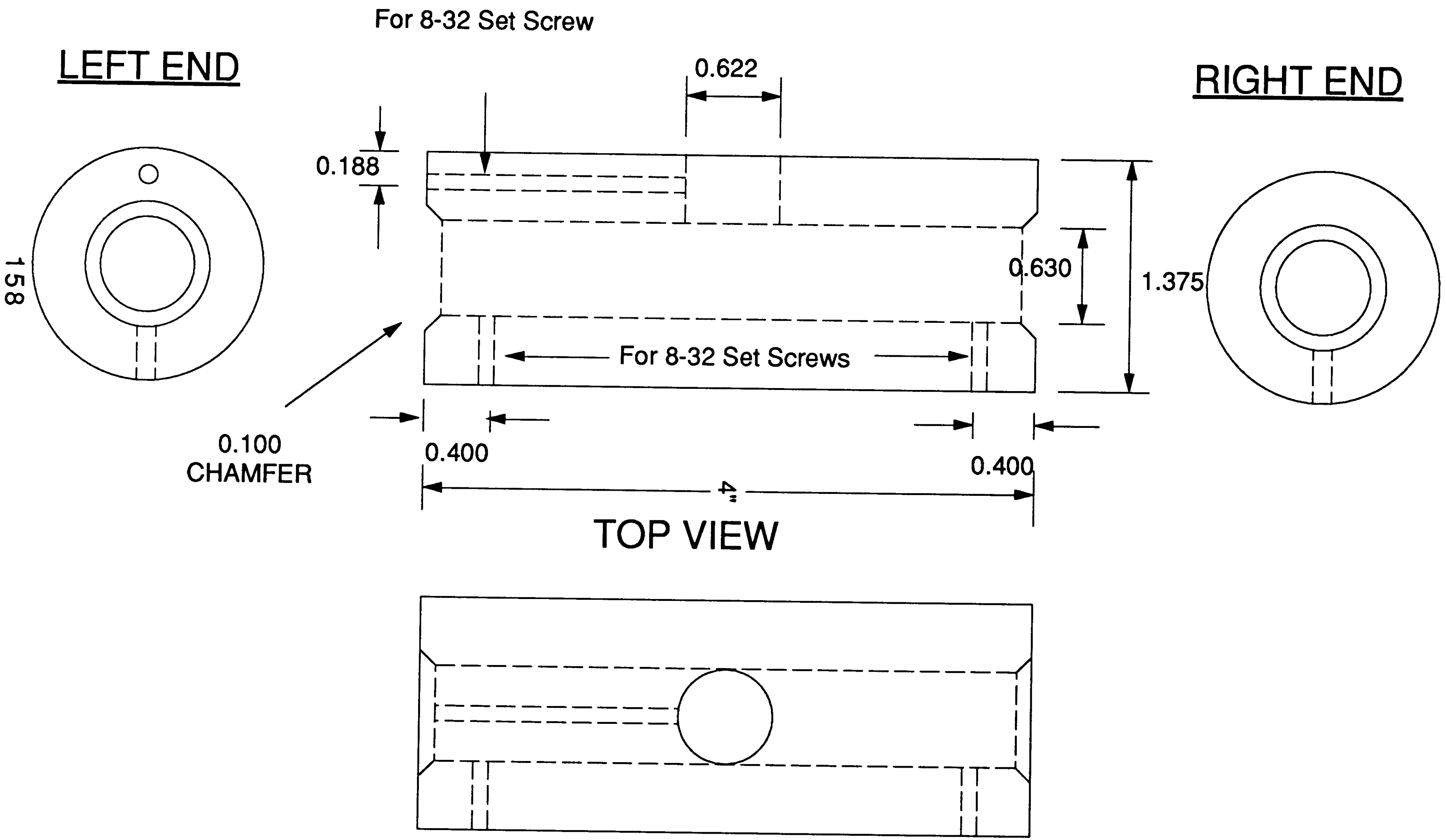

FIGURE 5: CONDUCTOR TUBE

Colin Wolden
MIT Rm. 66-419
Cambridge, MA 02139
(617) 253-6480

Design: Conductor Tube
Date: 10/17/93
Material: Silver Plated Stainless Steel
Unit: Inch

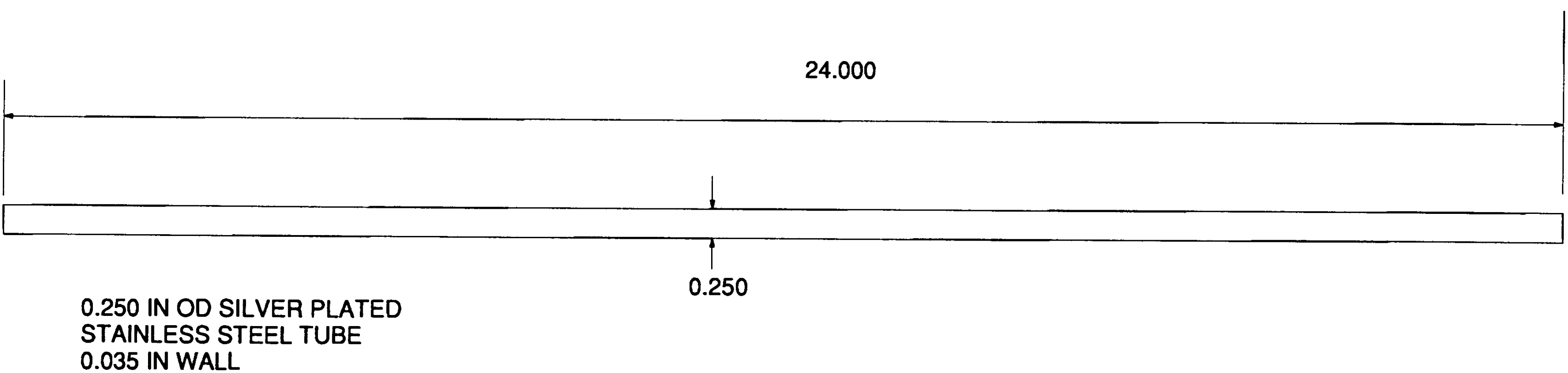

0.250 IN OD SILVER PLATED
STAINLESS STEEL TUBE
0.035 IN WALL

FIGURE 6: CONDUCTOR TUBE TIP

Colin Wolden
MIT Rm. 66-419
Cambridge, MA 02139
(617) 253-6480

Design: Conductor Tube Tip
Date: 10/17/93
Material: Copper
Unit: Inch

PIECE IS BRAZED TO ONE END OF CONDUCTOR TUBE (FIGURE 5)

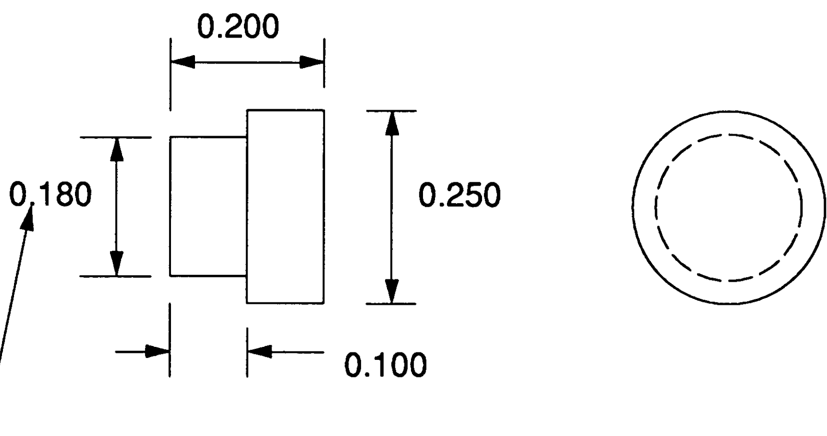

FIGURE 7A: OUTER CONDUCTOR TIP

Colin Wolden
MIT Rm. 66-419
Cambridge, MA 02139
(617) 253-6480

Design: Outer Conductor Tip
Date: 10/17/93
Material: Stainless Steel
Unit: Inch

TOP VIEW

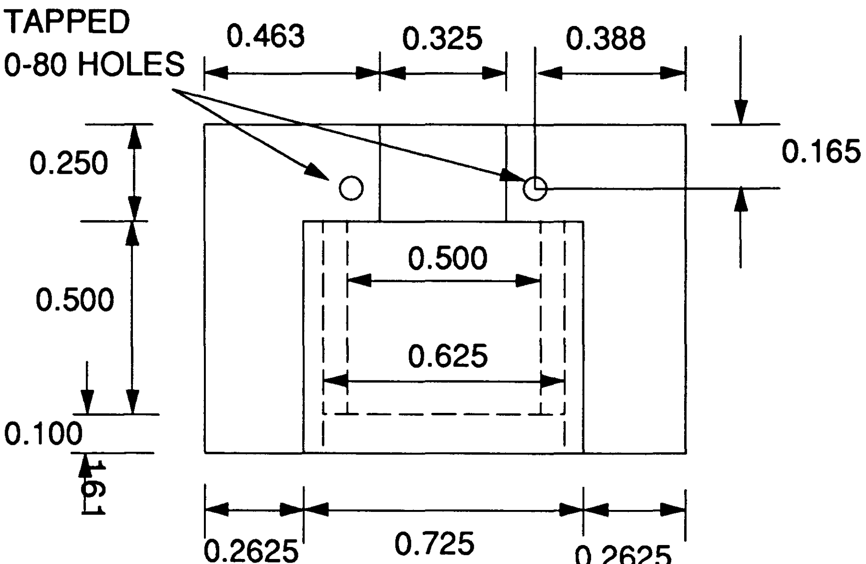

SIDE VIEW

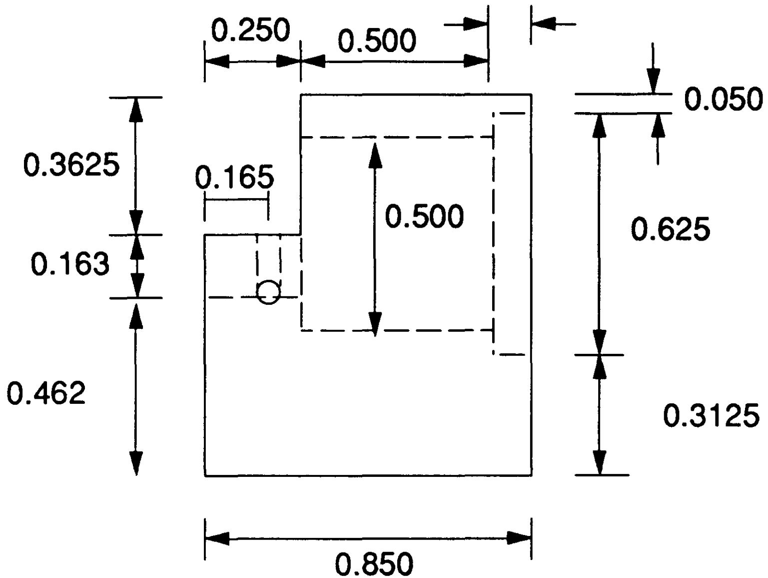

AXIAL VIEW

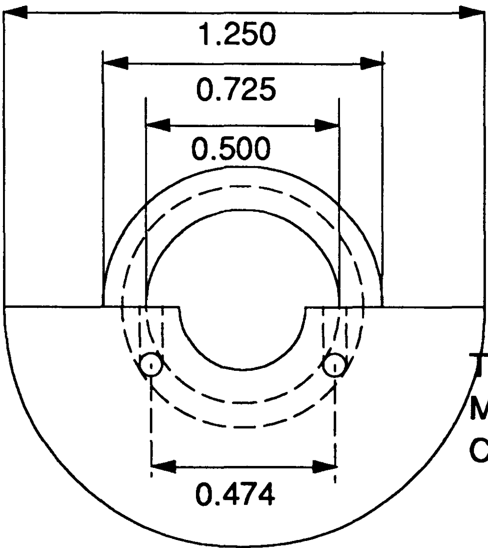

TAPPED 0-80 HOLES MUST MATCH WITH HOLES ON CLAMP (FIG. 7B)

TIP FITS AROUND OUTER CONDUCTOR AND WELDED ON TO WATER HOUSING

SEE FIGURE 16 FOR VIEW OF ASSEMBLY ONTO OUTER CONDUCTOR

FIGURE 7B: OUTER CONDUCTOR CLAMP

Colin Wolden
MIT Rm. 66-419
Cambridge, MA 02139
(617) 253-6480

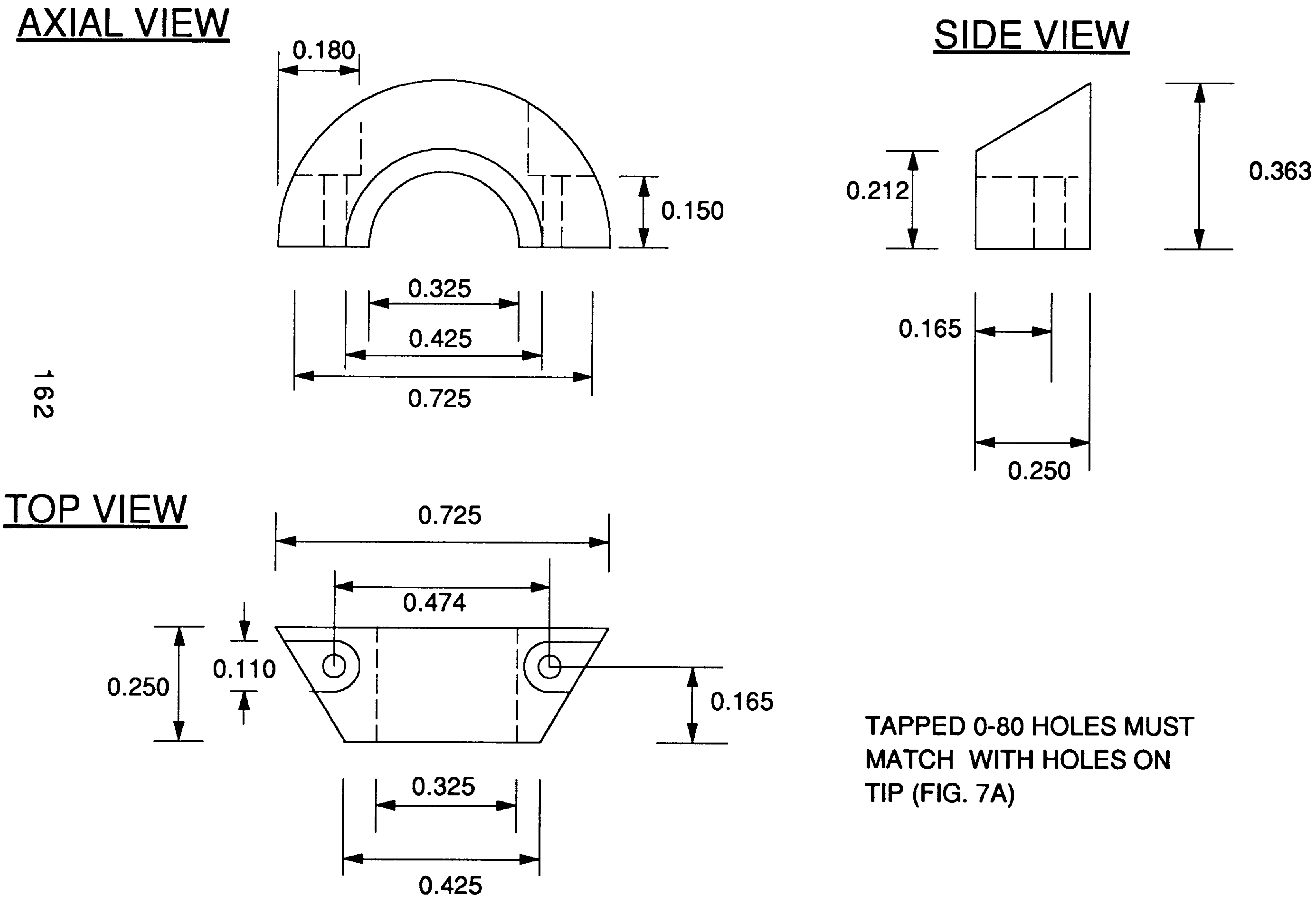

TAPPED 0-80 HOLES MUST MATCH WITH HOLES ON TIP (FIG. 7A)

FIGURE 8: TEFLON SEALS

Colin Wolden
MIT Rm. 66-419
Cambridge, MA 02139
(617) 253-6480

Design: Teflon Seals
Date: 10/17/93
Material: Teflon
Unit: Inch

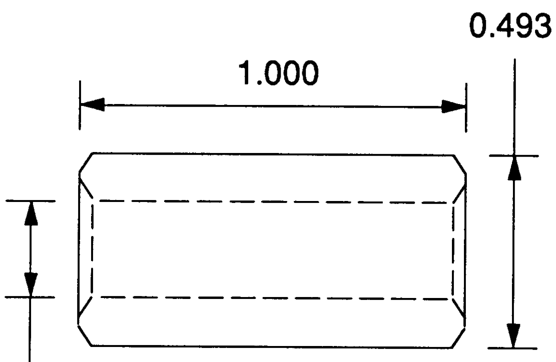

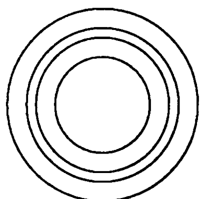

FIGURE 9: QUARTZ CHAMBER

3.0 mm x 3.0 mm diameter nozzle

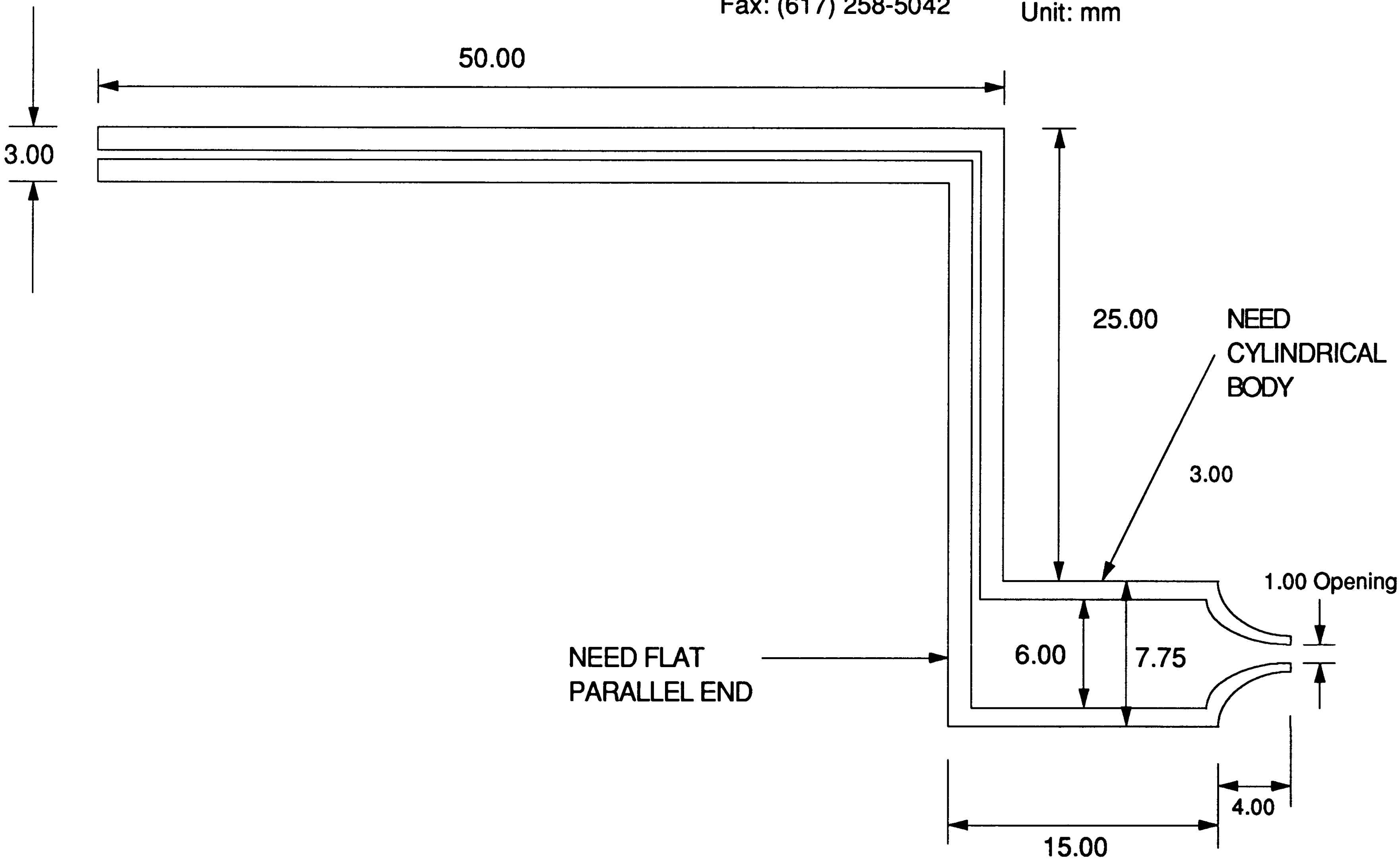

FIGURE 10: WATER LINE 1

Colin Wolden
MIT Rm 66-419
Cambridge, MA 02139
(617) 253-6480

Design: Water line Cross-section
Sate: 10/17/93
Material: Stainless Steel
Unit: Inch

THE CROSS - SECTION OF
WATER LINE 1:
WATER LINE 2 IS IDENTICAL

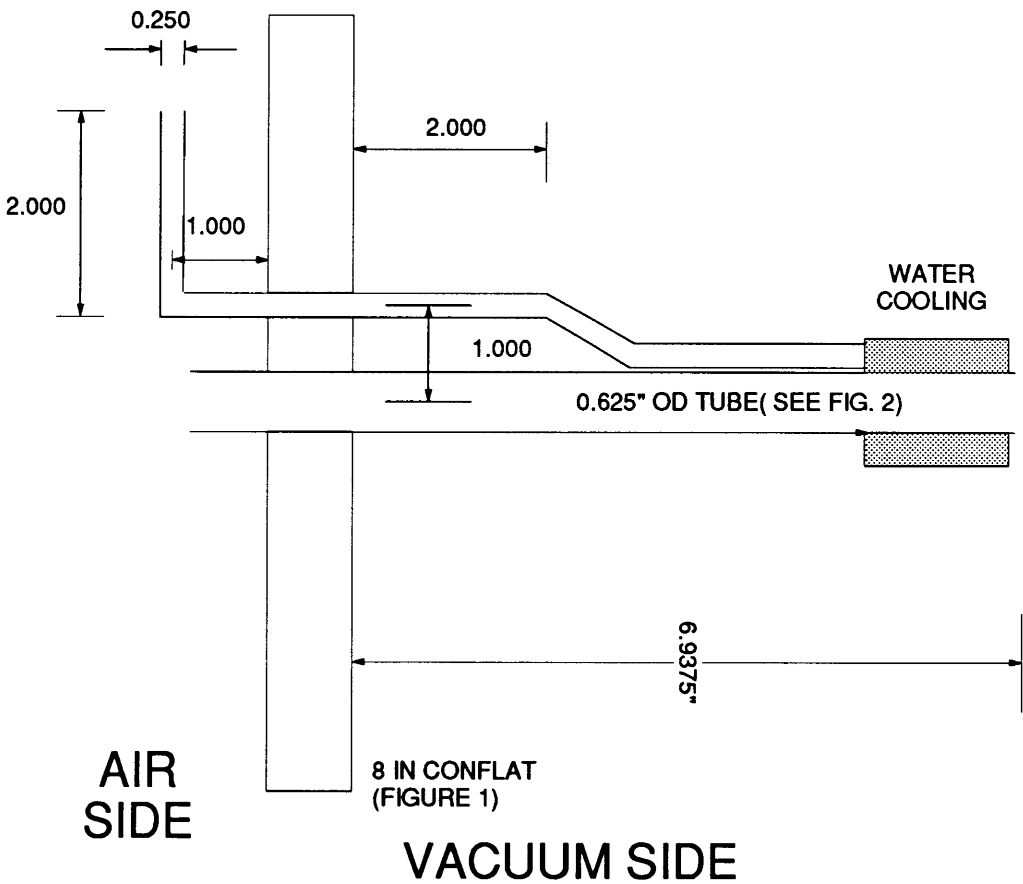

WATER HOUSING

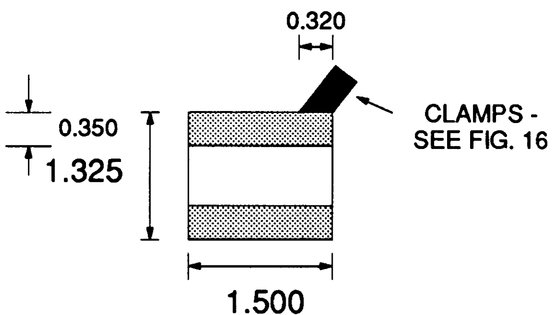

FIGURE 11: H2 LINE

Colin Wolden
MIT Rm. 66-419
Cambridge, MA 02139
(617) 253-6480

Design: H2 Line
Date: 10/17/93
Material: Stainless Steel
Unit: Inch

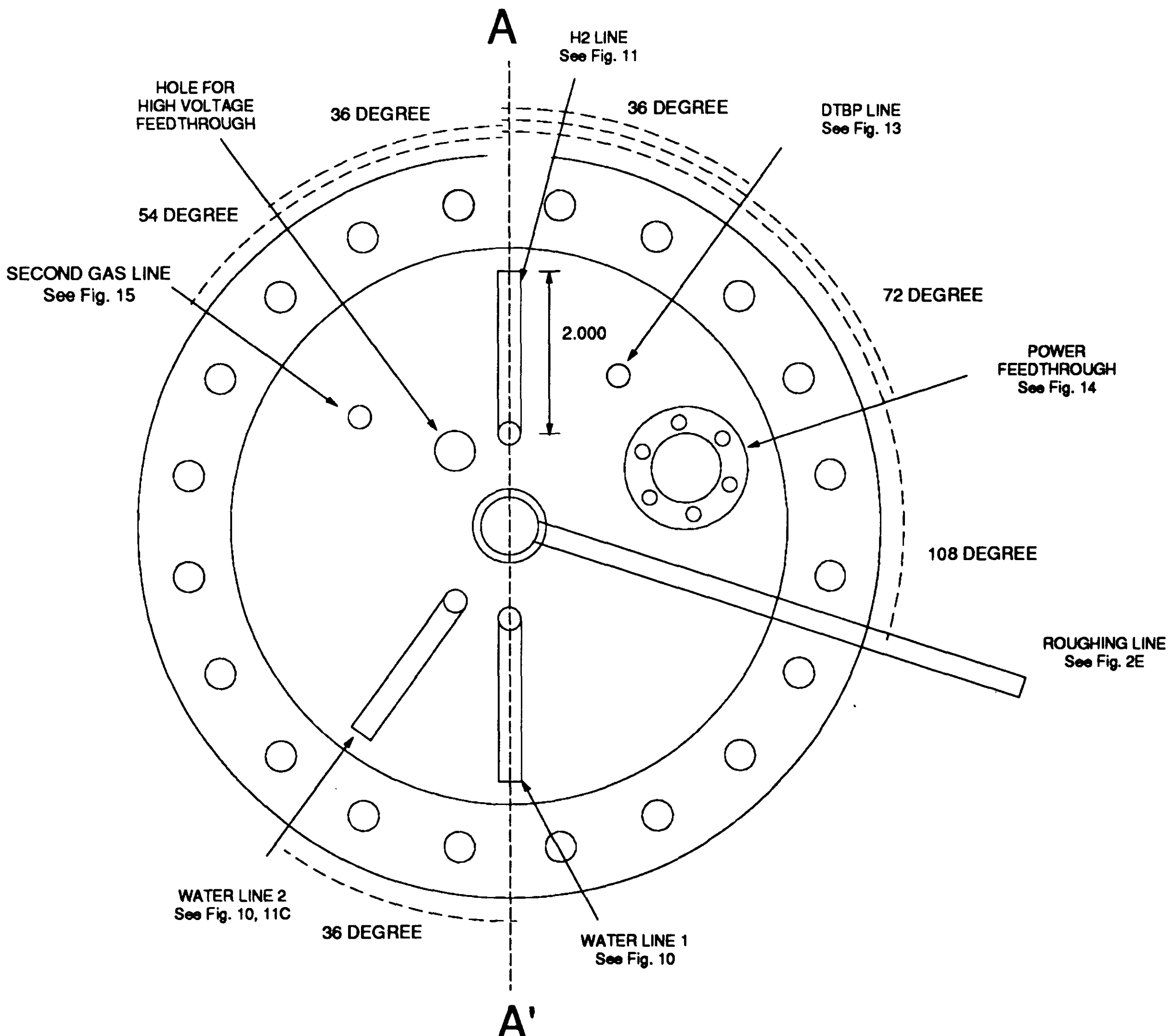

FIGURE 12 : H2 LINE - CROSS-SECTION

Colin Wolden
MIT Rm. 66-419
Cambridge, MA 02139
(617) 253-6480

Design: H2 Line along A-A'
Cross-section
Date: 10/17/93
Material: Stainless Steel
Unit: Inch

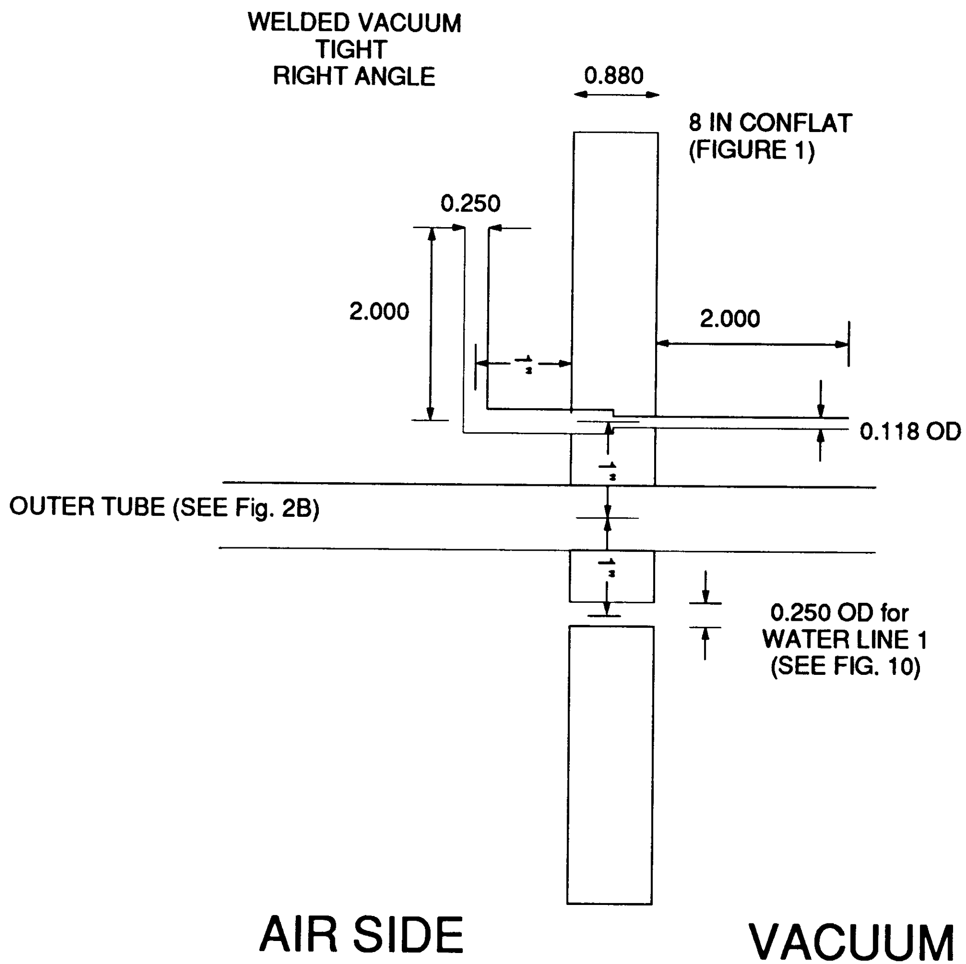

FIGURE 13: DTBP LINE

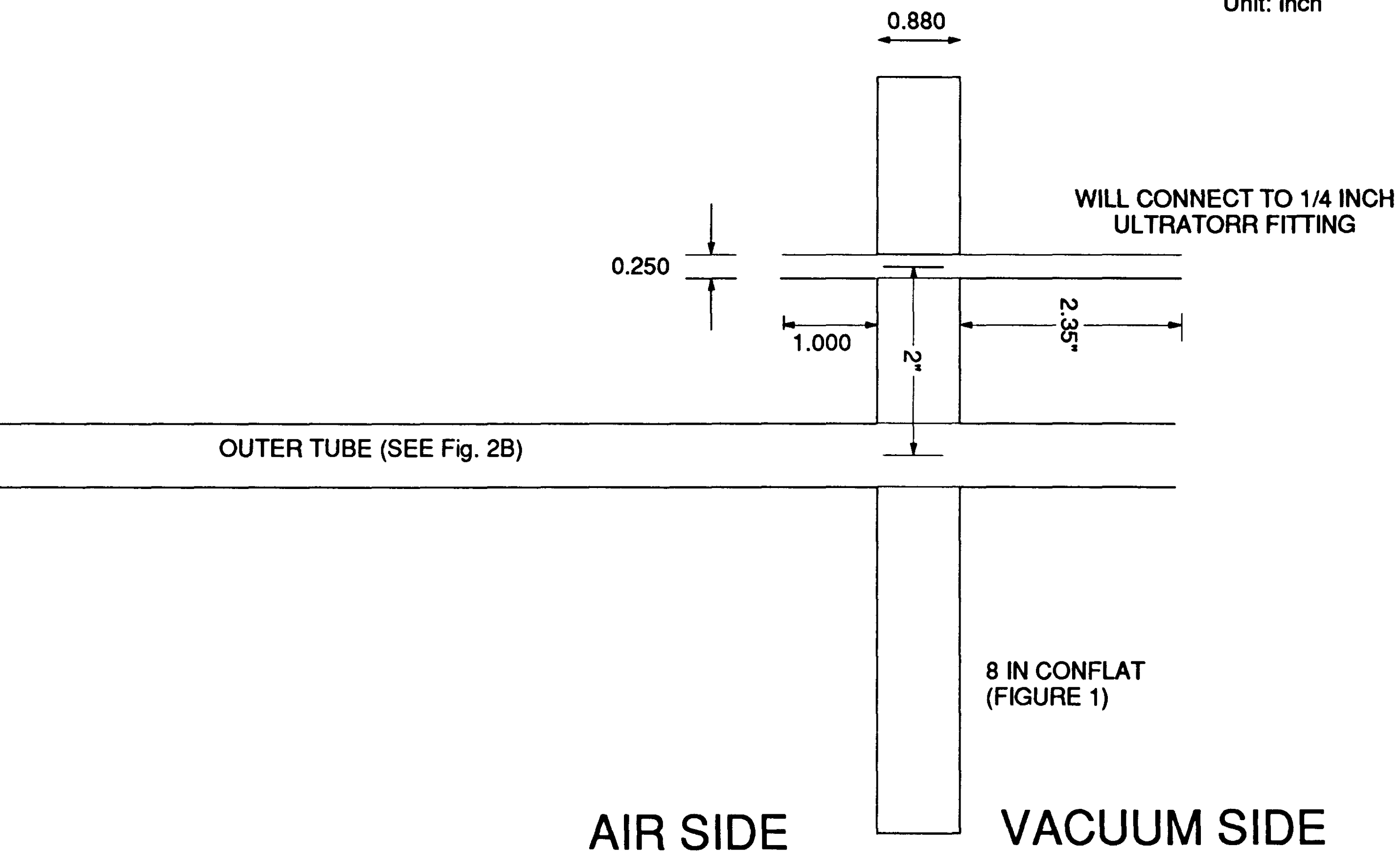

FIGURE 14B: POWER FEEDTHROUGH CROSS-SECTION

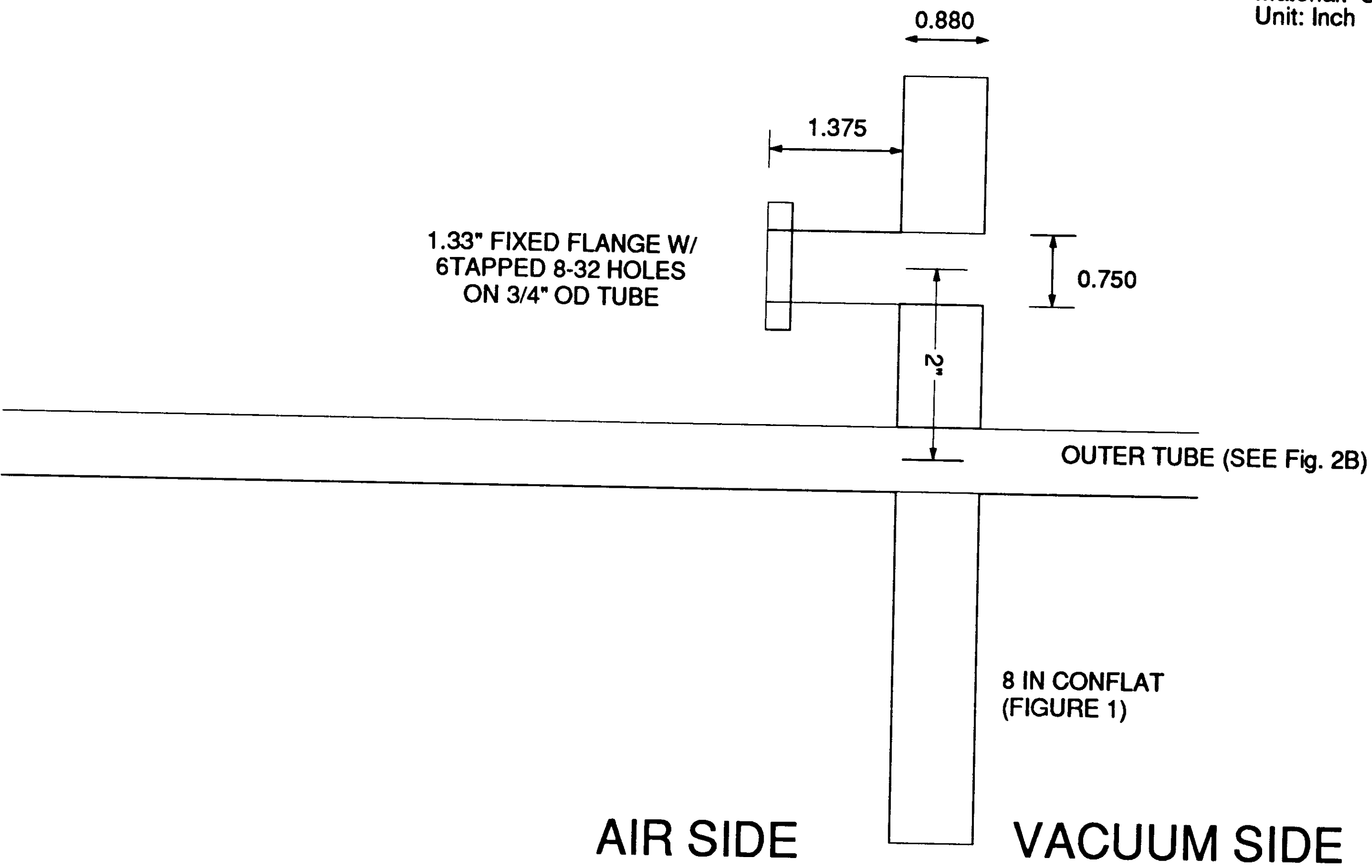

FIGURE 15: GAS LINE #2

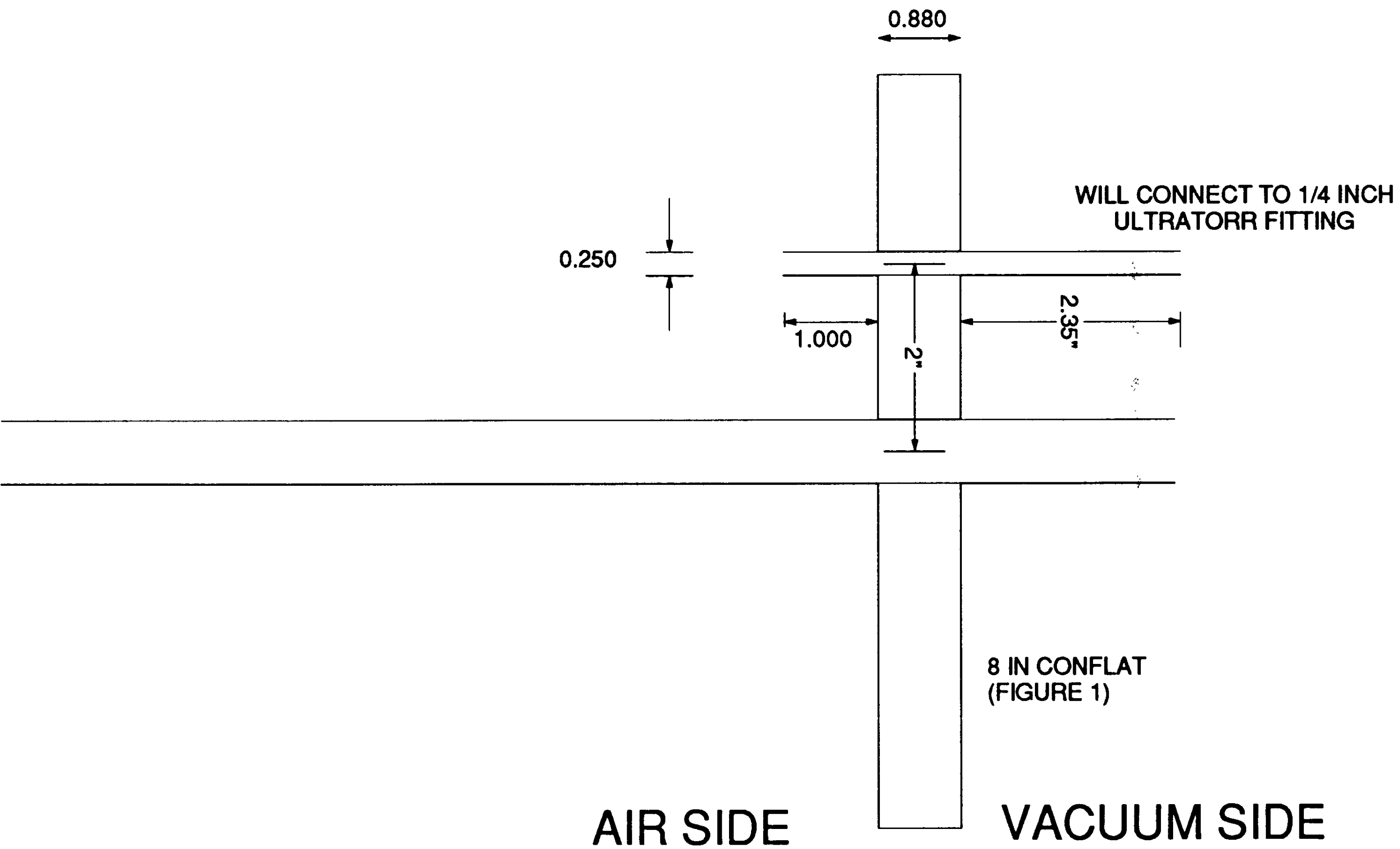

APPENDIX IV

FORTRAN CODES FOR ANALYSIS AND EVALUATION OF SURFACE KINETICS

Fortran programs used to analyze the surface chemistry. The subroutine rates includes the surface and gas-phase thermochenmistry. It uses an approach similar to the CHEMKIN package. The program surface it a modified 4th order runga kutta integrator.

```
SUBROUTINE rates(ktemp,k1f,k1r,k2f,k2r,k3f,k3r,k4f,k4r,
    &     k5f,k5r,k6f,k6r,k7f,k7r,k8f,k8r,k9f,k9r,k10f,k10r)
c   last update 2/2/95 - contains new thermo - FRENKLACH et. al.
c   Calculate kinetic parameters-calc initial surface fractions
c
c   *****************************************************
c   * DEFINE VARIABLES                                  *
c   *                                                   *
c   * amat(8,14): Thermo data for 8 gas species         *
c   * sa(10,7): Thermo data for 10 surface sites        *
c   * temp:  Temperature [K]                            *
c   * sd:  Surface site density [mol/cm2]               *
c   * delth:  Change enthalpy of reaction [cal/mol]     *
c   * deltst: Change in entropy xtemp of raction [cal/mol] *
c   * deltg:  Gibbs free energy change of reaction [cal/mol] *
c   * kp: Pressure equilibrium constant [atm]           *
c   * kc: Concentration equlibrium constant             *
c   * k1f, k1r, k2f, etc.: Individual rate constants    *
c   * g1f, g2f, etc:  reaction probability              *
c   *                                                   *
c   *****************************************************
c
c
    implicit double precision (a-h,o-z)
    implicit real (k)
c
c   14 parameters: 1-7 T > 1000, 8-14 300 < T < 1000
    double precision amat(8,14), sa(10,7), hrt(8), sr(8), st(8)
    double precision hg(30), stg(30), hs(30), sts(30)
c
c
    temp=ktemp
    ngas=8
    nsurf=10
c
c   GAS THERMODYNAMIC DATA FROM THRM$(GRI-Mech)
c
c   data - species #1 = H
    amat(1,1)=2.50000001E+00
    amat(1,2)=-2.30842973E-11
    amat(1,3)=1.61561948E-14
    amat(1,4)=-4.73515235E-18
    amat(1,5)=4.98197357E-22
    amat(1,6)=2.54736599E+04
    amat(1,7)=-4.46682914E-01
    amat(1,8)=2.50000000E+00
    amat(1,9)=7.05332819E-13
```

```
      amat(1,10)=-1.99591964E-15
      amat(1,11)=2.30081632E-18
      amat(1,12)=-9.27732332E-22
      amat(1,13)=2.54736599E+04
      amat(1,14)=-4.46682853E-01
c
c     data - species #2 = H2
      amat(2,1)=3.33727920E+00
      amat(2,2)=-4.94024731E-05
      amat(2,3)=4.99456778E-07
      amat(2,4)=-1.79566394E-10
      amat(2,5)=2.00255376E-14
      amat(2,6)=-9.50158922E+02
      amat(2,7)=-3.20502331E+00
      amat(2,8)=2.34433112E+00
      amat(2,9)=7.98052075E-03
      amat(2,10)=-1.94781510E-05
      amat(2,11)=2.01572094E-08
      amat(2,12)=-7.37611761E-12
      amat(2,13)=-9.17935173E+02
      amat(2,14)=6.83010238E-01
c
c     data - species #3 = CH3
      amat(3,1)=2.28571772E+00
      amat(3,2)=7.23990037E-03
      amat(3,3)=-2.98714348E-06
      amat(3,4)=5.95684644E-10
      amat(3,5)=-4.67154394E-14
      amat(3,6)=1.67755843E+04
      amat(3,7)=8.48007179E+00
      amat(3,8)=3.67359040E+00
      amat(3,9)=2.01095175E-03
      amat(3,10)=5.73021856E-06
      amat(3,11)=-6.87117425E-09
      amat(3,12)=2.54385734E-12
      amat(3,13)=1.64449988E+04
      amat(3,14)=1.60456433E+00
c
c     data - species #4 = CH4
      amat(4,1)=7.48514950E-02
      amat(4,2)=1.33909467E-02
      amat(4,3)=-5.73285809E-06
      amat(4,4)=1.22292535E-09
      amat(4,5)=-1.01815230E-13
      amat(4,6)=-9.46834459E+03
      amat(4,7)=1.84373180E+01
      amat(4,8)=5.14987613E+00
      amat(4,9)=-1.36709788E-02
      amat(4,10)=4.91800599E-05
      amat(4,11)=-4.84743026E-08
      amat(4,12)=1.66693956E-11
```

```
      amat(4,13)=-1.02466476E+04
      amat(4,14)=-4.64130376E+00
c
c     data - species #5 = C(GAS)
      amat(5,1)=2.49266888E+00
      amat(5,2)=4.79889284E-05
      amat(5,3)=-7.24335020E-08
      amat(5,4)=3.74291029E-11
      amat(5,5)=-4.87277893E-15
      amat(5,6)=8.54512953E+04
      amat(5,7)=4.80150373E+00
      amat(5,8)=2.55423955E+00
      amat(5,9)=-3.21537724E-04
      amat(5,10)=7.33792245E-07
      amat(5,11)=-7.32234889E-10
      amat(5,12)=2.66521446E-13
      amat(5,13)=8.54438832E+04
      amat(5,14)=4.53130848E+00
c
c     data - species #6 = CH2(triplet)
      amat(6,1)=2.87410113E+00
      amat(6,2)=3.65639292E-03
      amat(6,3)=-1.40894597E-06
      amat(6,4)=2.60179549E-10
      amat(6,5)=-1.87727567E-14
      amat(6,6)=4.62636040E+04
      amat(6,7)=6.17119324E+00
      amat(6,8)=3.76267867E+00
      amat(6,9)=9.68872143E-04
      amat(6,10)=2.79489841E-06
      amat(6,11)=-3.85091153E-09
      amat(6,12)=1.68741719E-12
      amat(6,13)=4.60040401E+04
      amat(6,14)=1.56253185E+00
c
c     data - species #7 = CH
      amat(7,1)=2.87846473E+00
      amat(7,2)=9.70913681E-04
      amat(7,3)=1.44445655E-07
      amat(7,4)=-1.30687849E-10
      amat(7,5)=1.76079383E-14
      amat(7,6)=7.10124364E+04
      amat(7,7)=5.48497999E+00
      amat(7,8)=3.48981665E+00
      amat(7,9)=3.23835541E-04
      amat(7,10)=-1.68899065E-06
      amat(7,11)=3.16217327E-09
      amat(7,12)=-1.40609067E-12
      amat(7,13)=7.07972934E+04
      amat(7,14)=2.08401108E+00
c
```

```
c     data - species #8 = C2H2
      amat(8,1)=4.14756964E+00
      amat(8,2)=5.96166664E-03
      amat(8,3)=-2.37294852E-06
      amat(8,4)=4.67412171E-10
      amat(8,5)=-3.61235213E-14
      amat(8,6)=2.59359992E+04
      amat(8,7)=-1.23028121E+00
      amat(8,8)=8.08681094E-01
      amat(8,9)=2.33615629E-02
      amat(8,10)=-3.55171815E-05
      amat(8,11)=2.80152437E-08
      amat(8,12)=-8.50072974E-12
      amat(8,13)=2.64289807E+04
      amat(8,14)=1.39397051E+01
c
c
c     SURFACE THERMOCHEMISTRY DATA [Coltrin & Dandy, JAP 74, 5803 (1993)]
c     Species 7, estimated based on given data
c
c     data - Surface Species #1: CH
      sa(1,1)=1.4872259E+00
      sa(1,2)=3.3000924E-03
      sa(1,3)=-2.8411702E-07
      sa(1,4)=-3.4383971E-10
      sa(1,5)=7.6660243E-14
      sa(1,6)=0.0
      sa(1,7)=0.4
c
c     data - Surface species #2: C*
      sa(2,1)=1.6900997E+00
      sa(2,2)=1.1069085E-03
      sa(2,3)=-1.2616481E-07
      sa(2,4)=-1.1996654E-10
      sa(2,5)=2.8811839E-14
      sa(2,6)=43400
      sa(2,7)=0.4
c
c     data - Surface species #3: CH3
      sa(3,1)=2.2271934E+00
      sa(3,2)=6.4840489E-03
      sa(3,3)=-5.0900690E-07
      sa(3,4)=-6.6263206E-10
      sa(3,5)=1.4445464E-13
      sa(3,6)=17300
      sa(3,7)=0.8
c
c     data - Surface species #4: CH2*
      sa(4,1)=1.7394471E+00
      sa(4,2)=5.1764320E-03
      sa(4,3)=-4.2153641E-07
```

```
      sa(4,4)=-5.3463645E-10
      sa(4,5)=1.1763388E-13
      sa(4,6)=50700
      sa(4,7)=0.5
c
c     data - Surface species #5: CH2
      sa(5,1)=1.7394471E+00
      sa(5,2)=5.1764320E-03
      sa(5,3)=-4.2153641E-07
      sa(5,4)=-5.3463645E-10
      sa(5,5)=1.1763388E-13
      sa(5,6)=-11500
      sa(5,7)=0.5
c
c     data - Surface species #6: CH*
      sa(6,1)=1.4872259E+00
      sa(6,2)=3.3000924E-03
      sa(6,3)=-2.8411702E-07
      sa(6,4)=-3.4383971E-10
      sa(6,5)=7.6660243E-14
      sa(6,6)=31900
      sa(6,7)=0.4
c
c     data - Surface species #7: C**
      sa(7,1)=1.6900997E+00
      sa(7,2)=1.1069085E-03
      sa(7,3)=-1.2616481E-07
      sa(7,4)=-1.1996654E-10
      sa(7,5)=2.88118239E-14
      sa(7,6)=90000
      sa(7,7)=0.4
c
c     data - Surface species #8: CH**
      sa(8,1)=1.4872259E+00
      sa(8,2)=3.3000924E-03
      sa(8,3)=-2.8411702E-07
      sa(8,4)=-3.4383971E-10
      sa(8,5)=7.6660243E-14
      sa(8,6)=89200
      sa(8,7)=0.4
c
c     data - Surface species #9: C***
      sa(9,1)=1.6900997E+00
      sa(9,2)=1.1069085E-03
      sa(9,3)=-1.2616481E-07
      sa(9,4)=-1.1996654E-10
      sa(9,5)=2.88118239E-14
      sa(9,6)=129100
      sa(9,7)=0.4
c
c     data - Surface species #10: C(D)
```

```
      sa(10,1)=1.6900997E+00
      sa(10,2)=1.1069085E-03
      sa(10,3)=-1.2616481E-07
      sa(10,4)=-1.1996654E-10
      sa(10,5)=2.88118239E-14
      sa(10,6)=500
      sa(10,7)=0.4
c
      temp=1200
c
c     Evaluate Gas Thermochemistry
c     loop over species
        do 20 j = 1, ngas
c
          if (temp .gt. 1000) then
            hrt(j)=enth(amat(j,1), amat(j,2), amat(j,3), amat(j,4),
     &           amat(j,5), amat(j,6), temp)
c
            sr(j)=entro(amat(j,1), amat(j,2), amat(j,3), amat(j,4),
     &           amat(j,5), amat(j,7), temp)
          else
            hrt(j)=enth(amat(j,8), amat(j,9), amat(j,10), amat(j,11),
     &           amat(j,12), amat(j,13), temp)
c
            sr(j)=entro(amat(j,8), amat(j,9), amat(j,10), amat(j,11),
     &           amat(j,12), amat(j,14), temp)
          end if
c
          hg(j)=hrt(j)*1.987*temp
          stg(j)=sr(j)*1.987*temp
c
 20     continue
c
c
c     Evaluate Surface Thermochemistry
c
        do 30 k = 1, nsurf
c
          hs(k)=senth(sa(k,1), sa(k,2), sa(k,3), sa(k,4),
     &         sa(k,5), sa(k,6), temp)
c
c      print 022, hs(k)
c
          sts(k)=sentro(sa(k,1), sa(k,2), sa(k,3), sa(k,4),
     &         sa(k,5), sa(k,7), temp)
c
c     print 022, sts(k)
c
 30     continue
c
c     SURFACE SITES DENSITY [mol/cm2]
```

```
      sd=5.22e-09
c
c   EVALUATE REACTIONS
c
c   REACTION 1: CH(S) + H <-> C*(S) + H2          [Coltrin s1]
c
      delth=hs(2)+hg(2)-hs(1)-hg(1)
      deltst=sts(2)+stg(2)-sts(1)-stg(1)
      deltg=(delth-deltst)
      kp=exp(-deltg/(1.987*temp))
c   kc=kp*(RT)^(-change in number of moles)
      kc=kp
      g1f=2.14*exp(-7300/(1.987*temp))
      k1f=100*((8.314*temp)/(2*3.14159*0.001))**(0.5)
      k1f=(k1f*(g1f/(1-g1f/2)))/sd
      k1r=k1f/kc
c
c   REACTION 2: C*(S) + H <-> CH(S)               [Coltrin s2]
c
      delth=hs(1)-hg(1)-hs(2)
      deltst=sts(1)-stg(1)-sts(2)
      deltg=(delth-deltst)
      kp=exp(-deltg/(1.987*temp))
c   kc=kp*(RT)^(-change in number of moles)
      kc=kp*(82.06*temp)
      g2f=0.3
      k2f=((g2f/(1-g2f/2))*100*(8.314*temp/(2*3.14159*0.001))**(0.5))
      k2f=k2f/sd
      k2r=k2f/kc
c
c   REACTION 3: C*(S) + CH3 <-> C(D) + CH3(S)        [Coltrin s3]
c
      delth=hs(3)+hs(10)-hs(2)-hg(3)
      deltst=sts(3)+sts(10)-sts(2)-stg(3)
      deltg=(delth-deltst)*2
      kp=exp(-deltg/(1.987*temp))
c   kc=kp*(RT)^(-change in number of moles)
      kc=kp*(82.06*temp)
      g3f=0.33
      k3f=((g3f/(1-g3f/2))*100*(8.314*temp/(2*3.14159*0.015))**(0.5))
      k3f=k3f/sd
      k3r=k3f/kc
c
c   REACTION 4: CH3(S) + H <-> CH2*(S) + H2          [Coltrin s5]
c
      delth=hs(4)+hg(2)-hs(3)-hg(1)
      deltst=sts(4)+stg(2)-sts(3)-stg(1)
      deltg=(delth-deltst)
      kp=exp(-deltg/(1.987*temp))
c   kc=kp*(RT)^(-change in number of moles)
      kc=kp
```

```
      g4f=4.28*exp(-7300/(1.987*temp))
      k4f=((g4f/(1-g4f/2))*100*(8.314*temp/(2*3.14159*0.001))**(0.5))
      k4f=k4f/sd
      k4r=k4f/kc
c
c    REACTION 5: CH2*(S) + H <-> CH3(S)              [Coltrin s18]
c
      delth=hs(3)-hs(4)-hg(1)
      deltst=sts(3)-sts(4)-stg(1)
      deltg=(delth-deltst)
      kp=exp(-deltg/(1.987*temp))
c    kc=kp*(RT)^(-change in number of moles)
      kc=kp*(82.06*temp)
      g5f=0.3
      k5f=((g5f/(1-g5f/2))*100*(8.314*temp/(2*3.14159*0.001))**(0.5))
      k5f=k5f/sd
      k5r=k5f/kc
c
c    REACTION 7: CH*(S) + CH2*(S) <-> CH(S) + CH2(S)   [From Coltrin s6]
c
      delth=hs(1)+hs(5)-hs(4)-hs(6)
      deltst=sts(1)+sts(5)-sts(4)-sts(6)
      deltg=(delth-deltst)
      kp=exp(-deltg/(1.987*temp))
c    kc=kp*(RT)^(-change in number of moles)
      kc=kp
      k7f=6e19
      k7r=k7f/kc
c
c    REACTION 8: CH2(S) + H <-> CH*(S) + H2            [Coltrin s4]
c
      delth=hs(6)+hg(2)-hs(5)-hg(1)
      deltst=sts(6)+stg(2)-sts(5)-stg(1)
      deltg=(delth-deltst)
      kp=exp(-deltg/(1.987*temp))
c    kc=kp*(RT)^(-change in number of moles)
      kc=kp
      g8f=2.14*exp(-7300/(1.987*temp))
      k8f=((g8f/(1-g8f/2))*100*(8.314*temp/(2*3.14159*0.001))**(0.5))
      k8f=k8f/sd
      k8r=k8f/kc
c
c    REACTION 9: CH*(S) + H <-> CH2(S)               [Coltrin s14]
c
      delth=hs(5)-hs(6)-hg(1)
      deltst=sts(5)-sts(6)-stg(1)
      deltg=(delth-deltst)
      kp=exp(-deltg/(1.987*temp))
c    kc=kp*(RT)^(-change in number of moles)
      kc=kp*(82.06*temp)
      g9f=.3
```

```
      k9f=(g9f/(1-g9f/2))*(8.314*temp/(2*3.14159*0.001))**(0.5)
      k9f=100*k9f
      k9f=k9f/sd
      k9r=k9f/kc
c
      k6f=0
      k6r=0
      k10f=0
      k10r=0
c
 031  format (1x, 6e11.3e2)
c     print 031, temp, k2f, k2r, ktf, ktr
c     print *
c     print 031, k1f, k1r, k3f, k3r, k4f, k4r
c     print *
c     print 031, k5f, k5r, k6f, k6r, k7f, k7r
c     print *
c     print 031, k8f, k8r, k9f, k9r, k10f, k10r
c     print *
c
      return
      end
c
c*****H/RT function*****************************************************
c
      function enth(a1, a2, a3, a4, a5, a6, temp)
c
      double precision enth, a1, a2, a3, a4, a5, a6, temp
      enth=a1+a2*temp/2+a3*temp**2/3+a4*temp**3/4+a5*temp**4/5+a6/temp
c
      end
c*****S/R FUNCTION*****************************************************
c     S/R function
c
      function entro(a1, a2, a3, a4, a5, a7, temp)
c
      double precision entro, a1, a2, a3, a4, a5, a7, temp
      entro=a1*log(temp)+a2*temp+a3*temp**2/2+a4*temp**3/3+a5*temp**4/4
     &    +a7
c
      end
c**********************************************************************
c
c*****SURFACE H function***********************************************
c
      function senth(a1, a2, a3, a4, a5, hf, temp)
c
      double precision senth, a1, a2, a3, a4, a5, hf, temp
c     senth=2.0
      senth=1.987*(a1*(temp-298)+a2*(temp**2-298**2)/2)
      senth=senth+1.987*(a3*(temp**3-298**3)/3+a4*(temp**4-298**4)/4)
```

```
      senth=senth+1.987*(a5*(temp**4*temp-298**4*298)/5)+hf
c
      end
c*****SURFACE ST function*********************************************
c
c
      function sentro(a1, a2, a3, a4, a5, sf, temp)
c
      double precision sentro, a1, a2, a3, a4, a5, sf, temp
      sentro=1.987*(a1*log(temp/298)+a2*(temp-298)
     &    +a3*(temp**2-298**2)/2)
      sentro=sentro+1.987*(a4*(temp**3-298**3)/3+a5*(temp**4-298**4)/4)
     &    +sf
c
      sentro=sentro*temp
c
      end
c*********************************************************************
```

Here is the program surface, the ODE solver used to integrate the equations.

```
c=====================================================================
      program surface
C
C   9 Basic Reactions, 6 species
C   This program calls a Runge-Kutta integration subroutine as
C   described in the handout. You have to enter the equations to
C   be integrated in subroutine DERIVS. You might also want to
C   customize this program if you want to change integration endpoints,
C   include more equations to be integrated, etc.
C   Description of the Runge Kutta parameters can be found in the
C    handout.
c
c
      PARAMETER (NMAX=50,KMAXX=10000)
      INTEGER nbad,nok,nvar
       REAL eps,h1,hmin,x1,x2,dydx(NMAX),y(NMAX),dxsav,
     &     yp(NMAX,KMAXX),xp(KMAXX),temp,press,xh,xch3
      INTEGER kmax,kount
      COMMON /path/ kmax,kount,dxsav,xp,yp
c
c   Initialize all vectors
      do 10 i=1,NMAX
        dydx(i)=0.0
        y(i)=0.0
        do 15 j=1,KMAXX
          yp(i,j)=0.0
 15     continue
```

```
 10  continue
     do 20 i=1,KMAXX
       xp(i)=0.0
 20  continue
c
c    Define the integration end-points (check your units!)
c    Here [x1, x2] represents the integration interval, note that
c    the independent variable is represented by x. Also note that
c    in this example x1 and x2 are given in units of seconds.
c    You have to use the corresponding units for the rate constants
c    in subroutine DERIVS later.
     x1=0.0
     x2=1.0
c
c    Define the number of ODEs to be solved
     nvar=6
c
c    Enter Initial Conditions
c     print *, 'Enter effective pressure [torr]:'
c     read *, press
     press=20
c     print *, 'Enter atomic hydrogen mole fraction:'
c     read *, xh
     xh=0.02
c     print *, 'Enter methyl radical mole fraction:'
c     read *, xch3
     xch3=0.0004
c     print *, 'Enter Surface Temperature [K]:'
c     read *, temp
     temp=1100
c
c    Define the Runge-Kutta integration parameters
     h1=1.0e-5
     hmin=1.0e-20
     eps=1.0e-5
c
c    Define some parameters for controlling output
     kmax=KMAXX
     dxsav=5e-6
c
c    Call the ODE solver
      CALL ODEINT(nvar,x1,x2,eps,h1,hmin,nok,nbad,
     &     temp,press,xh,xch3)
c       write(*,*) 'nok=',nok, ' nbad=',nbad
c
c    Save the results
     do 30 i=1,KMAXX
       if (xp(i).gt.9e-6) then
         iend=i
         go to 40
       endif
```

```
 30  continue
 40  continue
c    print 115, iend
c
c   A data file called results2.dat is created and has three columns
c   The first is the independent variable (here : time), the
c   rest are the species concentrations.
c     open(unit=11, file='results2.dat', status='new')
c    do 50 i=1,iend
c       write (11,100) xp(i), (yp(j,i),j=1,nvar)
c 50  continue
c    print *
c    do 60 i=1,iend
c       print 120, xp(i), (yp(j,i),j=1,nvar)
c 60  continue
c 100  format(f13.5,1x,5(e13.6,1x))
c
c
 110  format (1x, 7(a10,1x))
 115  format (1x, i5)
 120  format (1x, 7(e10.3,1x))
      stop
      end
c
c==========================================================
===========
       SUBROUTINE DERIVS(x,y,dydx,a1f,a1r,a2f,a2r,a3f,a3r,a4f,a4r,
      &     a5f,a5r,a6f,a6r,a7f,a7r,a8f,a8r,a9f,a9r,a10f,a10r)
      IMPLICIT REAL (a-h,k,o-z)
      PARAMETER (NMAX=50, NRXN=10)
      REAL dydx(NMAX),y(NMAX)
c
c   Here you have to provide the vector giving the derivatives
c   of each species, at any given time (here : x) and species
c   vector (here : y)
c
c   Reminder: Be careful to define your rate constants in units
c          that match with the above given integration interval.
c
c   Define rate constants (time unit is seconds).
c   Define gas info, kinetic parameters
c
c   Define rates of surface reactions
c
      r1f = a1f*y(1)
      r1r = a1r*y(2)
      r2f = a2f*y(2)
      r2r = a2r*y(1)
      r3f = a3f*y(2)
      r3r = a3r*y(3)
```

```
      r4f = a4f*y(3)
      r4r = a4r*y(4)
      r5f = a5f*y(4)
      r5r = a5r*y(3)
      r6f = a6f*y(2)*y(3)
      r6r = a6r*y(1)*y(4)
      r7f = a7f*y(4)*y(6)
      r7r = a7r*y(5)*y(1)
      r8f = a8f*y(5)
      r8r = a8r*y(6)
      r9f = a9f*y(6)
      r9r = a9r*y(5)
c
c     Define Surface ODEs.
c      y(1) = CH;   y(2) = C*;   y(3) = CH3;
c      y(4) = CH2*;  y(5) = CH2;  y(6) = CH*
c
      dydx(1) = r1r+r2f-r1f-r2r+r7f-r7r+r6f-r6r
      dydx(2) = r1f-r1r+r2r-r2f+r3r-r3f-r6f+r6r
      dydx(3) = r3f-r3r-r4f+r4r+r5f-r5r-r6f+r6r
      dydx(4) = r4f-r4r-r5f+r5r+r6f-r6r-r7f+r7r
      dydx(5) = r7f-r7r-r8f+r8r+r9f-r9r
      dydx(6) = -r7f+r7r+r8f-r8r-r9f+r9r
c
      return
      end
c
c=============================================================
===========
      SUBROUTINE odeint(nvar,x1,x2,eps,h1,hmin,nok,nbad,
     &     temp,press,xh,xch3)
      IMPLICIT REAL (a,k)
      DOUBLE PRECISION change
      INTEGER nbad,nok,nvar,KMAXX,MAXSTP,NMAX
      REAL eps,h1,hmin,x1,x2,TINY,temp,press,xh,xch3,gr
      REAL recomb,net,flux,eff,btemp,ph,gamma,tol,total
      REAL ctot,ch,cch3,ch2,fraction
      PARAMETER (MAXSTP=5000000,NMAX=50,KMAXX=10000,TINY=1.e-30)
C     USES derivs , rkqs
      INTEGER i,kmax,kount,nstp,klast
      REAL dxsav,h,hdid,hnext,x,xsav,dydx(NMAX),xp(KMAXX),y(NMAX),
     *yp(NMAX,KMAXX),yscal(NMAX),ystart(NMAX),check(NMAX),
     *yold(NMAX),diff(NMAX)
      COMMON /path/ kmax,kount,dxsav,xp,yp
c
      print *, 'Enter tolerance:'
      read *, tol
c      tol=1e-10
      do 10 i=1,NMAX
        ystart(i)=0.0
        yold(i)=1
```

```
 10  continue
c
     x=x1
     h=sign(h1,x2-x1)
     nok=0
     nbad=0
     kount=0
c
c    RIGHT HERE CALL SUBROUTINES RATES,INITIAL GUESS
c
     ctot=press/(760*82.06*temp)
     ch=ctot*xh
     cch3=ctot*xch3
     ch2=ctot*(1-xh-xch3)
c
      call rates(temp,k1f,k1r,k2f,k2r,k3f,k3r,k4f,k4r,
     &      k5f,k5r,k6f,k6r,k7f,k7r,k8f,k8r,k9f,k9r,k10f,k10r)
c
     a1f=k1f*ch
     a1r=k1r*ch2
     a2f=k2f*ch
     a2r=k2r
     a3f=k3f*cch3
     a3r=k3r
     a4f=k4f*ch
     a4r=k4r*ch2
     a5f=k5f*ch
     a5r=k5r
     a6f=k6f
     a6r=k6r
     a7f=k7f
     a7r=k7r
     a8f=k8f*ch
     a8r=k8r*ch2
     a9f=k9f*ch
     a9r=k9r
     a10f=k10f
     a10r=k10r
c
c     print 20, temp, k1f, k1r, k2f, k2r
 20   format (1x, 6(e11.4,1x))
c
c    Define the initial conditions for surface concentrations
c
c    Calculate initial Coverages
     xf1=(a2f+a1r)/(a1f+a1r+a2f+a2r)
     xf2=1-xf1
     xf3=(a9f+a8r)/(a8f+a8r+a9f+a9r)
     xf4=1-xf3
c
c    calculated from H only calculation at 1200
```

```
      ystart(1)=0.4778*5.22e-9
      ystart(2)=0.0222*5.22e-9
      ystart(3)=0*5.22e-9
      ystart(4)=0*5.22e-9
      ystart(5)=0.4859*5.22e-9
      ystart(6)=0.0141*5.22e-9
c
      do 11 i=1,nvar
        y(i)=ystart(i)
11    continue
      if (kmax.gt.0) xsav=x-2.*dxsav
      do 16 nstp=1,MAXSTP
        call derivs(x,y,dydx,a1f,a1r,a2f,a2r,a3f,a3r,a4f,a4r,
     &        a5f,a5r,a6f,a6r,a7f,a7r,a8f,a8r,a9f,a9r,a10f,a10r)
        do 12 i=1,nvar
          yscal(i)=abs(y(i))+abs(h*dydx(i))+TINY
12      continue
        if(kmax.gt.0)then
          if(abs(x-xsav).gt.abs(dxsav)) then
            if(kount.lt.kmax-1)then
              kount=kount+1
              klast=kount-1
              xp(kount)=x
              do 13 i=1,nvar
                yp(i,kount)=y(i)
                diff(i)=abs(yp(i,klast)-y(i))
13            continue
            change=1
            if(kount.gt.1)then
              change=0
              do 25 i=1,NMAX
                diff(i)=diff(i)/5.22e-9
                change=change+diff(i)
25            continue
              print 120, change, (y(j),j=1,nvar)
            endif
            xsav=x
          endif
        endif
      endif
        if((x+h-x2)*(x+h-x1).gt.0.) h=x2-x
        call rkqs(y,dydx,nvar,x,h,eps,yscal,hdid,hnext,
     &      a1f,a1r,a2f,a2r,a3f,a3r,a4f,a4r,
     &      a5f,a5r,a6f,a6r,a7f,a7r,a8f,a8r,a9f,a9r,a10f,a10r)
        if(hdid.eq.h)then
          nok=nok+1
        else
          nbad=nbad+1
        endif
        if((x-x2)*(x2-x1).ge.0.)then
          do 14 i=1,nvar
```

```
        ystart(i)=y(i)
14      continue
       if(kmax.ne.0)then
        kount=kount+1
        xp(kount)=x
        do 15 i=1,nvar
          yp(i,kount)=y(i)
15        continue
       endif
       return
      endif
c      CHECKS AND FINAL GROWTH CALCULATION
 120     format (1x, 7(e10.3,1x))
 121     format (1x, i5, 6(e10.3,1x))
 110     format (1x, 7(a10,1x))
 021     format(1x,a40,e11.4)
       fraction=(a3f*y(2)-a3r*y(3))/(a3f*y(2))
       gr=(a3f*y(2)-a3r*y(3))/5.22e-9
       gr=gr*3600/5606.7
c    UNITS: recomb, net[mol/cm2 s];flux [W/cm2];eff [mol H/mol D]
       recomb=a1f*y(1)+a2f*y(2)+a4f*y(3)+a5f*y(4)+a8f*y(5)+a9f*y(6)
       net=recomb-a1r*y(2)-a2r*y(1)-a4r*y(4)-a5r*y(3)
       net=net-a8r*y(6)-a9r*y(5)
       flux=(net*435000)/2
        btemp=((flux/(2*0.8*5.57e-12))**(0.25))-273.15
       eff=recomb/(a3f*y(2)-a3r*y(3))
c    Based on 2 um/hr
       eff=recomb/1.626e-8
       ph=recomb*82.06*760/((83140/(2*temp*3.14159*0.001))**(0.5))
       gamma=ph/(press*xh)
       total=(y(1)+y(2)+y(3)+y(4)+y(5)+y(6))/5.22e-9
c
       xs1=y(1)/5.22e-9
       xs2=y(2)/5.22e-9
       xs3=y(3)/5.22e-9
       xs4=y(4)/5.22e-9
       xs5=y(5)/5.22e-9
       xs6=y(6)/5.22e-9

c       if(x.gt.1e-5)then
       if(change.lt.tol)then
c
         print *
           write(*,*) 'nok=',nok, ' nbad=',nbad
         print 021, 'Steady State Growth Rate [micron/hr] = ', gr
         print *
         print *, 'Final Time, surface fractions'
           print 110, 'Time  ', '[CH]  ', '[C*]  ', '[CH3]  ',
     &          '[CH2*]  ', '[CH2]  ', '[CH*]  '
c
          print 120, x, xs1, xs2, xs3, xs4, xs5, xs6
```

```
        print *
         print 110, 'Total  ', 'reacomb ', ' Q [W/cm2]',
    &          ' T[rad] ', ' H/Diamond', '  Gamma ', 'Change '
        print 120, total, recomb, flux, btemp, eff, gamma, change
        return
c    endif
      endif
      if(abs(hnext).lt.hmin) pause
   *      'stepsize smaller than minimum in odeint'
      h=hnext
 16   continue
     write(*,*) 'nok=',nok, ' nbad=',nbad
     print 110, 'Time  ', '[CH]  ', '[C*]  ', '[CH3]  ',
    &     '[CH2*]  ', '[CH2]  ', '[CH*]  '
     print 120, x, xs1, xs2, xs3, xs4, xs5, xs6
    print *
     print 110, 'Total  ', 'reacomb ', ' Q [W/cm2]',
    &     ' T[rad] ', ' H/Diamond', '  Gamma ', 'Change '
     print 120, total, recomb, flux, btemp, eff, gamma, change
     pause 'too many steps in odeint'
    return
    END
c
c=============================================================
===========
     SUBROUTINE rkqs(y,dydx,n,x,htry,eps,yscal,hdid,hnext,
    &    a1f,a1r,a2f,a2r,a3f,a3r,a4f,a4r,
    &    a5f,a5r,a6f,a6r,a7f,a7r,a8f,a8r,a9f,a9r,a10f,a10r)
    IMPLICIT REAL (a)
    INTEGER n,NMAX
     REAL eps,hdid,hnext,htry,x,dydx(n),y(n),yscal(n)
    PARAMETER (NMAX=50)
C   USES derivs
    INTEGER i
    REAL errmax,h,htemp,xnew,yerr(NMAX),ytemp(NMAX),SAFETY,PGROW,
    *PSHRNK,ERRCON
     PARAMETER (SAFETY=0.9,PGROW=-.2,PSHRNK=-.25,ERRCON=1.89e-4)
    h=htry
1    call rkck(y,dydx,n,x,h,ytemp,yerr,
    &    a1f,a1r,a2f,a2r,a3f,a3r,a4f,a4r,
    &    a5f,a5r,a6f,a6r,a7f,a7r,a8f,a8r,a9f,a9r,a10f,a10r)
    errmax=0.
    do 11 i=1,n
     errmax=max(errmax,abs(yerr(i)/yscal(i)))
11   continue
    errmax=errmax/eps
    if(errmax.gt.1.)then
     htemp=SAFETY*h*(errmax**PSHRNK)
     h=sign(max(abs(htemp),0.1*abs(h)),h)
     xnew=x+h
     if(xnew.eq.x)pause 'stepsize underflow in rkqs'
```

```
      goto 1
     else
      if(errmax.gt.ERRCON)then
       hnext=SAFETY*h*(errmax**PGROW)
      else
       hnext=5.*h
      endif
      hdid=h
      x=x+h
      do 12 i=1,n
       y(i)=ytemp(i)
12     continue
      return
     endif
     END
c
c=====================================================================
===========
      SUBROUTINE rkck(y,dydx,n,x,h,yout,yerr,
     &      a1f,a1r,a2f,a2r,a3f,a3r,a4f,a4r,
     &      a5f,a5r,a6f,a6r,a7f,a7r,a8f,a8r,a9f,a9r,a10f,a10r)
     IMPLICIT REAL (a)
     INTEGER n,NMAX
      REAL h,x,dydx(n),y(n),yerr(n),yout(n)
     PARAMETER (NMAX=50)
C    USES derivs
     INTEGER i
     REAL ak2(NMAX),ak3(NMAX),ak4(NMAX),ak5(NMAX),ak6(NMAX),
      *ytemp(NMAX),A2,A3,A4,A5,A6,B21,B31,B32,B41,B42,B43,B51,B52,B53,
      *B54,B61,B62,B63,B64,B65,C1,C3,C4,C6,DC1,DC3,DC4,DC5,DC6
       PARAMETER (A2=.2,A3=.3,A4=.6,A5=1.,A6=.875,B21=.2,B31=3./40.,
       *B32=9./40.,B41=.3,B42=-.9,B43=1.2,B51=-11./54.,B52=2.5,
      *B53=-70./27.,B54=35./27.,B61=1631./55296.,B62=175./512.,
      *B63=575./13824.,B64=44275./110592.,B65=253./4096.,C1=37./378.,
      *C3=250./621.,C4=125./594.,C6=512./1771.,DC1=C1-2825./27648.,
     *DC3=C3-18575./48384.,DC4=C4-13525./55296.,DC5=-277./14336.,
     *DC6=C6-.25)
      do 11 i=1,n
       ytemp(i)=y(i)+B21*h*dydx(i)
11    continue
      call derivs(x+A2*h,ytemp,ak2,a1f,a1r,a2f,a2r,a3f,a3r,a4f,a4r,
     &      a5f,a5r,a6f,a6r,a7f,a7r,a8f,a8r,a9f,a9r,a10f,a10r)
      do 12 i=1,n
       ytemp(i)=y(i)+h*(B31*dydx(i)+B32*ak2(i))
12    continue
      call derivs(x+A3*h,ytemp,ak3,a1f,a1r,a2f,a2r,a3f,a3r,a4f,a4r,
     &      a5f,a5r,a6f,a6r,a7f,a7r,a8f,a8r,a9f,a9r,a10f,a10r)
      do 13 i=1,n
       ytemp(i)=y(i)+h*(B41*dydx(i)+B42*ak2(i)+B43*ak3(i))
13    continue
      call derivs(x+A4*h,ytemp,ak4,a1f,a1r,a2f,a2r,a3f,a3r,a4f,a4r,
```

```
    &     a5f,a5r,a6f,a6r,a7f,a7r,a8f,a8r,a9f,a9r,a10f,a10r)
    do 14 i=1,n
      ytemp(i)=y(i)+h*(B51*dydx(i)+B52*ak2(i)+B53*ak3(i)+B54*ak4(i))
14    continue
     call derivs(x+A5*h,ytemp,ak5,a1f,a1r,a2f,a2r,a3f,a3r,a4f,a4r,
    &     a5f,a5r,a6f,a6r,a7f,a7r,a8f,a8r,a9f,a9r,a10f,a10r)
    do 15 i=1,n
      ytemp(i)=y(i)+h*(B61*dydx(i)+B62*ak2(i)+B63*ak3(i)+B64*ak4(i)+
   *B65*ak5(i))
15    continue
     call derivs(x+A6*h,ytemp,ak6,a1f,a1r,a2f,a2r,a3f,a3r,a4f,a4r,
    &     a5f,a5r,a6f,a6r,a7f,a7r,a8f,a8r,a9f,a9r,a10f,a10r)
    do 16 i=1,n
      yout(i)=y(i)+h*(C1*dydx(i)+C3*ak3(i)+C4*ak4(i)+C6*ak6(i))
16    continue
    do 17 i=1,n
      yerr(i)=h*(DC1*dydx(i)+DC3*ak3(i)+DC4*ak4(i)+DC5*ak5(i)+DC6*
   *ak6(i))
17    continue
    return
    END
c
c=====================================================================
===========
```